Universidad Politécnica de Cartagena

ESCUELA INTERNACIONAL DE DOCTORADO

PROGRAMA DE DOCTORADO EN ENERGÍAS RENOVABLES Y EFICIENCIA ENERGÉTICA

TESIS DOCTORAL

APORTACIONES A LA MONITORIZACIÓN Y PREDICCIÓN DEL RECURSO SOLAR PARA LA INTEGRACIÓN DE FUENTES RENOVABLES EN SISTEMAS ELÉCTRICOS BASADAS EN INTERNET DE LAS COSAS

Presentada por Jose Miguel Paredes Parra para optar al grado de Doctor
por la Universidad Politécnica de Cartagena

Dirigida por:
Dr Ángel Molina García

Codirigida por:
Dra María del Carmen Bueso Sánchez

Cartagena, 2022

APORTACIONES A LA MONITORIZACIÓN Y PREDICCIÓN DEL RECURSO SOLAR PARA LA INTEGRACIÓN DE FUENTES RENOVABLES EN SISTEMAS ELÉCTRICOS BASADAS EN INTERNET DE LAS COSAS

Autor
JOSÉ MIGUEL PAREDES PARRA

Directores
Dr. ÁNGEL MOLINA GARCÍA
Dra. MARÍA DEL CARMEN BUESO SÁNCHEZ

Escuela Internacional de Doctorado
Universidad Politécnica de Cartagena

Cartagena, julio de 2022

Do...or do not. There is no try

(Yoda)

Agradecimientos

En primer lugar, a mis directores. Ángel y María del Carmen, sin vuestra motivación, guía y ayuda no hubiera podido completar esta tesis.

En segundo lugar a todos los colaboradores que han participado en las publicaciones, ya que sus aportaciones han resultado fundamentales para llevar a cabo estos trabajos.

En tercer lugar, a todas las personas que formamos parte de la familia de CETENMA, en especial a Gemma por su confianza y paciencia, y a Curro, Jorge y Dani por sus largas horas preparando el laboratorio solar.

Por último y más importante, a mis hijos Miguel y Carmen, por las horas que les he robado y que espero poder compensarles.

RESUMEN

La necesidad de lograr una economía descarbonizada para evitar los efectos del cambio climático ha derivado en una serie de compromisos internacionales que obligan a España y Europa a reducir paulatinamente sus emisiones de gases de efecto invernadero hasta alcanzar la neutralidad climática en 2050.

Este objetivo solo se puede alcanzar con un nuevo modelo energético basado en una integración masiva de energías renovables. Entre las tecnologías llamadas a convertirse en uno de los pilares de esta descarbonización de la economía se encuentra la energía solar fotovoltaica como consecuencia de su propia madurez tecnológica y la significativa reducción de costes que ha experimentado en los últimos años. Dentro de las instalaciones fotovoltaicas, una de las tipologías que ha recibido un mayor impulso son las instalaciones de autoconsumo ubicadas cerca de los puntos de demanda eléctrica gestionadas por los consumidores que pasan a ser también proveedores de energía y servicios a la red convirtiéndose en los denominados “prosumers“.

Esta integración masiva de nuevas plantas de generación distribuida supone un desafío para la gestión de la red eléctrica que, tradicionalmente, ha respondido a un modelo de flujo de potencias unidireccional donde la potencia fluye desde grandes unidades de generación hacia los puntos de consumo, ajustando en todo momento la generación a la demanda y consiguiendo un balance de potencias que permitiese regular y controlar de manera efectiva los valores de tensión y frecuencia dentro de rangos admisibles. El nuevo modelo de generación distribuida basada en renovables requiere de nuevas herramientas y estrategias de gestión para hacer frente a la variabilidad que presentan estas energías renovables por su propia naturaleza y el gran número y dispersión geográfica de instalaciones que requieren una mayor flexibilidad ante nuevos retos en forma de flujo bidireccional de energía.

Estas nuevas estrategias de gestión están apoyadas por los grandes avances realizados por las tecnologías de la información y la comunicación (TICs), que se han ido incorporando de forma paulatina de la mano de los operadores de red de cara a recoger diversas variables relacionadas con los estados de las unidades de generación y de los usuarios con objeto de optimizar la distribución y el consumo.

En el caso de la fotovoltaica, hasta hace unos años, el coste y la complejidad de los sistemas de monitorización de las instalaciones fotovoltaicas limitaban su uso a las plantas fotovoltaicas de gran capacidad (a partir de 1 MW, tanto por motivos económicos como normativos), pero la aparición y la rápida evolución en el mercado del denominado Internet de las Cosas, IoT por sus siglas en inglés (Internet of Things), ha causado una explosión en la cantidad y variedad de soluciones de bajo costo que podrían permitir la implementación a gran escala de los sistemas de monitorización de manera rentable.

Durante el desarrollo de esta tesis, de carácter eminentemente práctico, se ha trabajado en las tres capas que componen un sistema de IoT (percepción, comunicación y aplicación) para proponer un nuevo prototipo de gestión y comunicación de instalaciones fotovoltaicas de autoconsumo basado en estándares abiertos y soluciones de

bajo coste.

En la **capa de percepción** se han desarrollado y evaluado varios prototipos de sistemas de monitorización de acuerdo con los requisitos de la norma EC–61724, que describe las pautas generales para monitorizar y analizar el rendimiento de las plantas de energía fotovoltaica.

Dentro de la **capa de comunicaciones** se ha trabajado en integración y evaluación de nuevos sistemas de comunicaciones de bajo coste, gran cobertura y baja demanda de energía (LPWAN) como medio para el intercambio datos en un entorno de Internet de las cosas (IoT).

Por último, en la **capa de aplicaciones** se ha abordado el análisis de modelos de predicción de la generación de energía a corto plazo de estas instalaciones para proporcionar fiabilidad y estabilidad a la red, estudiándose tanto diferentes fuentes de datos de irradiancia para la aplicación de estos modelos como la influencia de los parámetros fundamentales de la red de comunicaciones en sus resultados.

ABSTRACT

The need to achieve a decarbonized economy to fight climate change has prompted several international commitments that oblige Spain and Europe to progressively reduce their greenhouse gas emissions until reaching climate neutrality in 2050. This goal can only be reached with a new energy model based on a massive integration of renewable energies. Among these technologies, photovoltaic solar energy is called to become one of the pillars to decarbonize the economy decarbonization thanks to its own technological maturity and the significant cost reduction, it has experienced in recent years.

Within the different types of photovoltaic installations, one of the fastest growing is that of self-consumption, which are installations located near the points of electricity demand managed by the consumers themselves who also become providers of energy and services to the network, becoming the so-called prosumers.

This massive integration of new distributed generation plants poses a challenge for the management of the electricity grid, which has traditionally responded to a unidirectional power flow model. In this unidirectional model, the power flows from the large generation units to the consumption points, adjusting the generation to achieve a power balance that allows effective regulation and control of the voltage and frequency values within the admissible ranges.

The new decentralized distributed model requires new tools and management strategies to deal with the variability that renewable energies present due to their very nature and the large number and the geographical dispersion of installations that require greater flexibility to ensure a constant supply to cover demand and meet new challenges in the form of bidirectional flow of power

These new management strategies are supported by the great advances made by information and communication technologies (ICTs) that have been gradually incorporated by the network operators in order to collect various variables related to generation units and consumer´s behavior in order to optimize distribution and consumption.

In the case of photovoltaics, until a few years ago, the cost and complexity of monitoring systems for photovoltaic installations limited their use to large-capacity photovoltaic plants (from 1 MW, both for economic and regulatory reasons), but the appearance and rapid evolution in the market of the so-called Internet of Things, IoT,

In this thesis, which has a practical approach, new contributions have been done to the three layers that make up an IoT system (perception, communication, and application) to propose a new management and communication prototype for self-consumption photovoltaic installations based on open standards and low-cost IoT solutions.

In the **perception layer**, several prototypes of monitoring systems have been developed and evaluated in accordance with the requirements of the EC–61724 standard,

which describes the general guidelines for monitoring and analyzing the performance of photovoltaic power plants.

Within the **communications layer**, work has been done on the integration and evaluation of new low-cost, high coverage, and low energy demand communications systems (LPWAN) to exchange data.

Finally, in the **applications layer**, the analysis of short-term power generation prediction models for these facilities has been addressed to provide reliability and stability to the network, studying both different sources of irradiance data for the application of these models such as the influence of the fundamental parameters of the communications network in their results. .

La presentación de esta tesis doctoral se realiza bajo la modalidad de "Compendio de Publicaciones", atendiendo a lo establecido en el artículo 20 del Reglamento de Estudios Oficiales de Doctorado de la Universidad Politécnica de Cartagena de 24 de marzo de 2021. Los trabajos han sido publicados con la autorización expresa del director y codirector de la presente tesis y se encuentran disponibles para su consulta en el capítulo 4. Dichos trabajos fueron preparados y publicados posteriormente al inicio de los estudios de doctorando y sus referencias se listan a continuación:

- *"PV Module Monitoring System Based on Low-Cost Solutions: Wireless Raspberry Application and Assessment". Paredes-Parra, J.M., Mateo-Aroca, A., Silvente-Niñirola, G., Bueso, M.C., Molina-García, A. 2018. Energies 11, no. 11: 3051.*
  https://doi.org/10.3390/en11113051
- *"An Alternative Internet-of-Things Solution Based on LoRa for PV Power Plants: Data Monitoring and Management". Paredes-Parra, J.M., García-Sánchez, A.J., Mateo-Aroca, A., Molina-García, A. 2019. Energies 12, no. 5: 881.*
  https://doi.org/10.3390/en12050881
- *"A Characterization of Metrics for Comparing Satellite-Based and Ground-Measured Global Horizontal Irradiance Data: A Principal Component Analysis Application'. Bueso, M.C., Paredes-Parra, J.M., Mateo-Aroca, A., Molina-García, A. 2020. Sustainability 12: 2454.*
  https://doi.org/10.3390/su12062454.
- *"Sensitive Parameter Analysis for Solar Irradiance Short-Term Forecasting: Application to LoRa-Based Monitoring Technology". Bueso, M.C., Paredes-Parra, J.M., Mateo-Aroca, A., Molina-García, A. 2022. Sensors (Basel) 22(4): 1499.*
  https://doi.org/10.3390/s22041499. PMID: 35214398; PMCID: PMC8874705.
- *"Democratization of PV micro–generation system monitoring via an open source IoT gateway based on NB–IoT". Paredes-Parra, J.M., Jiménez-Segura, R., Campos-Peñalver, D., Mateo-Aroca A., Ramallo-González, A.P., Molina-García, A. 2022. Sensors 22(13): 4966.*
  https://doi.org/10.3390/s22134966

En la mayoría de ellas, el doctorando ha sido autor principal.

ÍNDICE GENERAL

CAPÍTULO 1

MOTIVACIÓN Y OBJETIVOS

El Acuerdo del Clima de París de 2015 [1], ratificado por España, obliga a reducir las emisiones de gases de efecto invernadero un 40 % en 2030 sobre el nivel de 1990. En esta línea, la Unión Europea acordó en abril de 2021 su Ley del Clima que eleva el objetivo hasta el 55 % en 2030.

Por esta razón se han revisado las directivas de renovables, eficiencia energética y de edificios para adaptarlas al nuevo objetivo [2]. El gobierno de España publicó el pasado 31 de marzo en el BOE la versión final del Plan Nacional Integrado de Energía y Clima 2021-2030 (PNIEC) [3], y en abril el Congreso aprobó la Ley de Cambio Climático, confirmando el objetivo de reducción del 23 % de las emisiones en 2030 sobre el nivel de 1990.

Este plan prevé para el año 2030 una potencia total instalada en el sector eléctrico de 161 GW, de los que 50 GW serán energía eólica; 39 GW solar fotovoltaica; 27 GW ciclos combinados de gas; 15 GW hidráulica; 9 GW bombeo; 7 GW solar termoeléctrica; y 3 GW nuclear, así como cantidades menores de otras tecnologías.

En línea con esta estrategia de descarbonización de la economía, España ha desarrollado en los últimos años, una nueva legislación[4],[5],[6] que brinda apoyo y un buen escenario para el desarrollo de Fuentes de Energía Renovable (RES) especialmente la energía eólica y solar fotovoltaica (PV). De hecho, éstas han experimentado un enorme crecimiento como consecuencia de su propia madurez tecnológica. Específicamente, las instalaciones fotovoltaicas se han extendido ampliamente a diferentes niveles de voltaje gracias a la madurez de la tecnología y a una reducción significativa en el coste.

Dentro de las instalaciones fotovoltaicas, una de las tipologías que ha recibido un mayor impulso son las instalaciones de autoconsumo debido a un nuevo marco regulatorio que eliminaba trabas presentes en la legislación anterior junto que se ha extendido la aplicación de incentivos fiscales al autoconsumo en los impuestos locales y se

han introducido medidas específicas de promoción a nivel estatal y regional. Entre estas medidas especificas se puede destacar la reciente publicación de la Hoja de Ruta del Autoconsumo [7] o las medidas específicas dentro de las diferentes componentes del Plan de Recuperación y Resilencia [8].

Este impulso ha provocado un fuerte crecimiento de este tipo de instalaciones. Según los datos registrados por la Unión Española Fotovoltaica (UNEF) en 2021 en España se instalaron 1.203 MW de nueva potencia fotovoltaica en instalaciones de autoconsumo [9].

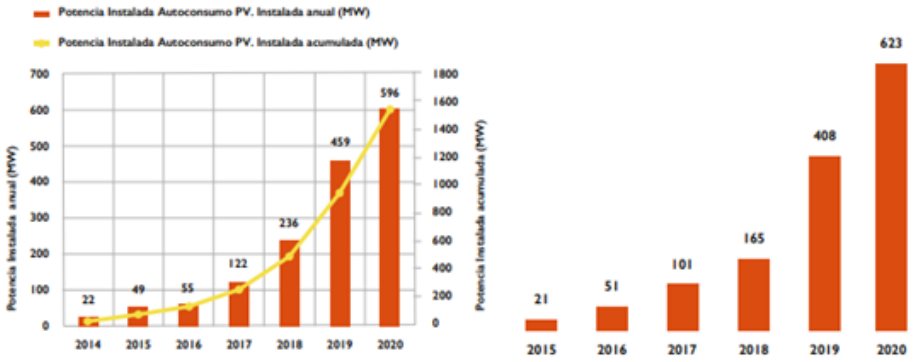

Figura 1.1: Evolución del autoconsumo. Fuente: Ministerio para la Transición Ecológica y el Reto Demográfico.[7]

Se prevé que este crecimiento seguirá constante en el periodo 2021 a 2030 alcanzando los 9 GW. Esta potencia podría aumentar hasta los 14 GW instalados de autoconsumo en 2030 en el caso de darse un escenario muy favorable de alta penetración como son los altos precios de la energía alcanzados en estos últimos meses debidos al incremento de los costes del gas natural por la guerra en Ucrania.

La integración masiva de este nuevo tipo de plantas de generación distribuida supone un desafío para la gestión de la red eléctrica que, tradicionalmente, ha respondido a un modelo de flujo de potencias unidireccional donde la potencia fluye desde grandes unidades de generación hacia los puntos de consumo, ajustando en todo momento la generación a la demanda y consiguiendo un balance de potencias que permite regular y controlar de manera efectiva los valores de tensión y frecuencia dentro de rangos admisibles. El nuevo modelo de generación distribuida basada en renovables requiere de nuevas herramientas y estrategias de gestión para hacer frente a la variabilidad que presentan estas energías renovables por su propia naturaleza y el gran número y dispersión geográfica de instalaciones que requieren una mayor flexibilidad ante nuevos retos en forma de flujo bidireccional de energía Estas instalaciones de autoconsumo están ubicadas cerca de los puntos de demanda eléctrica y son gestionadas por los consumidores que están adoptando un papel cada vez más activo, pasando de meros elementos pasivos y demandantes de recursos a agentes implicados en servicios a la red eléctrica, como el control de frecuencia o tensión, o la modificación de sus perfiles de demanda a través de las unidades de generación conectadas a red los denominados 'prosumers' [10].

Este cambio de rol de los consumidores está apoyado por los grandes avances realizados por las tecnologías de la información y la comunicación (TICs) que se han ido

incorporando de forma paulatina de la mano de los operadores de red de cara a recoger diversas variables relacionadas con los estados de las unidades de generación y de los usuarios con objeto de optimizar la distribución y el consumo.

La incorporación de este estas nuevas herramientas se ha ido realizando comenzando desde las grandes plantas de generación implementándose en plantas de menor potencia a medida que se iban desarrollando nuevas tecnologías que reducían los costes.

En el caso de la fotovoltaica, hasta hace unos años, el coste y la complejidad de los sistemas de monitorización de las instalaciones fotovoltaicas limitaban su uso a las plantas fotovoltaicas de gran capacidad (a partir de 1 MW, tanto por motivos económicos como normativos), pero la aparición y la rápida evolución en el mercado del denominado Internet de las Cosas, IoT por sus siglas en inglés (Internet of Things) [11] ha causado una explosión en la cantidad y variedad de soluciones de bajo costo que podrían permitir la implementación a gran escala de los sistemas de monitorización de manera rentable.

El concepto de internet de las cosas [12] se refiere a la interconexión digital de objetos cotidianos, como electrodomésticos, sistemas de salud, sistemas de seguridad y vigilancia, sistemas industriales, sistemas de transporte...empleando como soporte de comunicaciones internet. Su objetivo es automatizar el funcionamiento de éstos sin necesidad de intervención humana, favoreciendo un intercambio de información y una toma de decisiones en base a los datos intercambiados a los algoritmos implementados. Este tipo de soluciones implican una serie de requerimientos hardware sobre los que basar las comunicaciones, por lo que los dispositivos deben estar equipados con microcontroladores, transceptores y protocolos que faciliten y estandaricen la comunicación entre ellos y con entidades externas.

De acuerdo con la arquitectura recogida de estándares internacionales (IEEE P2413) un sistema de IoT se compone de tres capas: capa de percepción, capa de red y capa de aplicación IEEE P2413 [13].

- La capa de percepción incluye un conjunto de dispositivos habilitados para su conexión a Internet que tienen capacidad para la percepción y detección de objetos. Además, incluye sistemas de recogida de información así como el intercambio de información con otros dispositivos a través de la comunicación por Internet. Contadores, Sensores, sistemas de posicionamiento global (GPS), cámaras y dispositivos de identificación de radiofrecuencia (RFID) son ejemplos de dispositivos que existen en la capa de percepción.
- La capa de red es responsable del envío de los datos de la capa de percepción a la capa de aplicaciones, por tanto actúa como intermediaria entre ambas capas y facilita el envío y recepción de información. Habitualmente, y dependiendo de las aplicaciones y los equipos involucrados, los sistemas de IoT suelen utilizar una combinación de Internet y redes de corto alcance para el envío de la información desde dispositivos de percepción. Para ello hacen uso de pasarelas y otras tecnologías que permiten este tipo de interconexiones para largas distancias y donde los equipos pueden no tener una conexión directa o física a Internet.
- La capa superior es la capa de aplicación, donde la información entrante se proce-

sa para crear las estrategias de gestión. Las aplicaciones tienen un amplio rango de objetivos, entre los que podemos destacar la promoción y gestión de hogares inteligentes, ciudades inteligentes, la monitorización del sistema de energía, gestión de la demanda de energía, o la integración de recursos renovables que es el caso que aborda esta tesis.

Debido al carácter eminentemente práctico de esta tesis, en este trabajo se han realizado contribuciones en las tres capas de la arquitectura para proponer un nuevo prototipo de gestión y comunicación de instalaciones fotovoltaicas de autoconsumo (en la franja 15-100 kW) basado en estándares abiertos y soluciones de IoT de bajo coste.

En el capítulo siguiente se presenta un breve estado del arte de las diferentes tecnologías con el fin de explicar el contexto en el que se enmarca esta tesis, así como facilitar la comprensión de sus objetivos y contribuciones.

CAPÍTULO 2

ESTADO DEL ARTE

El objetivo de este capítulo es resumir brevemente el estado del arte de las tecnologías involucradas en cada una de las capas de la solución de IoT propuesta para la monitorización de instalaciones de autoconsumo para su operación y mantenimiento (O&M) a costes razonables para asegurar su rendimiento, su disponibilidad y su rentabilidad.

2.1. Capa de percepción

La capa de percepción o capa física es la encargada de recopilar y procesar la información y los datos procedentes de las instalaciones fotovoltaicas siendo uno de los objetivos de este trabajo hacerlo con soluciones basadas en estándares abiertos y de bajo coste para minimizar la inversión en este sistema y adecuarlo al coste de la instalación facilitando su implantación.

Este esfuerzo ha sido una prioridad en la última década pudiendo encontrarse diferentes soluciones en la literatura específica para monitorizar plantas de energía fotovoltaica. Más específicamente, algunas de estas contribuciones se centran en la monitorización local de datos PV.

De esta manera, Fuentes et al. describen un registrador de datos portátil basado en instrumentos independientes [14]. En otros trabajos se usa LabVIEW para monitorizar y comunicar varios dispositivos simultáneamente []. Bayrak et al. usan una tarjeta de adquisición de datos Labview (DAQ) para monitorizar la medición eléctrica de un sistema FV [15]. Chouder et al. también presentan una caracterización detallada del rendimiento y el comportamiento dinámico de las instalaciones fotovoltaicas a través del sistema de interfaz en tiempo real de LabVIEW [16]. Otros autores han propuesto soluciones inalámbricas para monitorizar instalaciones fotovoltaicas a nivel de panel. Como ejemplo, Ando et al. describen una conexión inalámbrica completa a nivel de panel para estimar las pérdidas de eficiencia y el envejecimiento anómalo de las instalaciones fotovoltaicas [17].

Contribuciones similares para la monitorización individual de paneles basados en tecnología inalámbrica se pueden encontrar en Prieto et al. [18], y Papageorgas et al. propusieron y evaluaron soluciones de monitorización in situ para paneles fotovoltaicos [19]. Moreno-García et al. presentan una arquitectura de dispositivos de adquisición, incluidos sensores inalámbricos distribuidos, para monitorizar y supervisar todos los dispositivos distribuidos en la planta [20]. Fanourakis et al. presentan un sistema de adquisición de bajo costo para registrar datos en una tarjeta micro SD [21]. Con respecto a las propuestas de monitorización remota de instalaciones fotovoltaicas se pueden encontrar varios trabajos relacionados en la literatura. La tabla 2.1 presenta una comparación de algunas de las características técnicas de los sistemas disponibles en la literatura y el sistema propuesto en este trabajo. En el resto de esta sección, discutiremos las similitudes y diferencias entre el sistema propuesto y los relacionados.

El sistema de monitorización propuesto por Caruso et al. consta de dos tipos de dispositivos: medidor inteligente y unidad principal [22]. Los medidores inteligentes son los dispositivos responsables de monitorizar el voltaje y los datos de corriente del sistema fotovoltaico en tiempo real, mientras que la unidad principal es el centro donde se almacenarán los datos recopilados por los dispositivos del medidor inteligente. Ambos se basan en el MCU ATmega328P-PU y se comunican a través de una red inalámbrica de radiofrecuencia (RF) que funciona a 315 MHz. Se puede acceder a los datos mediante una aplicación móvil que se comunica con el centro principal a través de Bluetooth.

En el trabajo de Su et al. se desarrolló una red de sensores de dos niveles para mo-

Tabla 2.1: Resumen de sistemas similares al propuesto encontrados en la literatura

Referencia	**Parámetros registrados**	**SW libre**	**Transmisión de datos**	**Conexión a internet**	**Almacenamiento**	**Sensores dedicados**
Caruso et al. [22]	Idc,Vdc	SI	315 MHz RF	Sin conexón	Tarjeta SD	SI
Su et al. [23]	Ta, Tm, G, h, Idc, Vdc	No	RF and ZigBee	Sin conexón	Local computer	SI
Al-Naima and Hamad [24]	Ta, h, Idc, Vdc	SI	-	Wi-Fi	ThingSpeak cloud database	SI
Pereira et al. [25]	Ta, Tm, G, h, Ws, Idc, Vdc, Pdc	SI	-	Wi-Fi	Local flash memory and cloud database	No
Aghenta and Iqbal [26]	Idc, Vdc, Vb	SI	Serial	Ethernet	EmonCMS local server	SI
Zago and Fruett [27]	Idc,Vdc	SI	ZigBee	Wi-Fi	Local Raspberry Pi	SI
Erraissi et al. [28]	Ta, Tm, G, Ws, Wd, Idc, Vdc Pdc, Iac, Vac, Pac	SI	Bluetooth	Ethernet	Local SD card	No
Melo et al.32	Ta, Tm, G, h, rf, Ws, Wd, Idc, Vdc, Pac	SI	LoRa	Wi-Fi	Local SD card and cloud database	Si

nitorizar sistemas fotovoltaicos [23].

El primer nivel de la red consta de nodos sensores que controlan el voltaje y la temperatura de cada módulo fotovoltaico. El segundo nivel consta de nodos de sensores que monitorizan la irradiación, la temperatura ambiente, el voltaje y la corriente de cada string. Además, los nodos de segundo nivel fusionan sus datos monitorizados con los datos obtenidos por el primer nivel y los envían a un centro de datos.

La comunicación entre los niveles se realiza a través de una red inalámbrica de radiofrecuencia, y el segundo nivel utiliza ZigBee para enviar todos los datos recopilados al nodo central. En estos estudios, los datos solo están disponibles localmente, lo que dificultaría la integración futura de estos sistemas en una red inteligente.

La conexión a Internet es crucial para proporcionar monitorización en tiempo real de los datos y permitir el acceso remoto al sistema. Esta necesidad nos enlaza con la siguiente capa de la arquitectura propuesta.

2.2. Capa de comunicaciones

Entre los estudios consultados, los sistemas de monitorización conectados a Internet se pueden configurar en dos topologías diferentes: los dispositivos de registro de datos se conectan directamente a Internet o dispositivos intermedios entre Internet y los registradores de datos.

Al-Naima y Hamad desarrollaron una red de sensores inalámbricos basada en el MCU ESP8266 para monitorizar la energía fotovoltaica del sistema [24]. Cada nodo de la red monitoriza los datos de corriente y voltaje de un conjunto de módulos fotovoltaicos y se conecta a Internet a través de Wi-Fi para enviar los datos recopilados a una plataforma en la nube de IoT. El sistema también es capaz de monitorizar la humedad y temperatura de la planta solar.

Aghenta e Iqbal presentan un enfoque similar pero sin realizar la adquisición de datos meteorológicos [26]. Un Arduino realiza la adquisición de sensores para medir la generación fotovoltaica y se comunica con una Raspberry Py a través de un bus serie. La Raspberry Pi se conecta a Internet mediante un cable Ethernet a través del cual los datos recopilados se envían a una plataforma IoT basada en un servidor local, donde se almacenan y se puede acceder a ellos. En el estudio desarrollado por Pereira et al. [25], el sistema propuesto se basa en ESP32 y ESP8266, que se comunican con un sistema de nube no especificada a través de Wi-Fi. Los datos de temperatura, irradiancia, humedad, velocidad del viento y generación de DC se recopilan cada 47 s y están disponibles a través de una aplicación web. Inicialmente, los registradores de datos de la propuesta se configuraron para comunicarse con Internet a través de Wi-Fi. Sin embargo, este enfoque presentó una limitación en la ubicación de los dispositivos registradores de datos debido al rango de Wi-Fi, adoptando en la versión actual una segunda topología que combina LoRa y Wi-Fi.

El sistema propuesto en Zedak et al. monitoriza voltaje, corriente, temperatura e irradiancia [29]. Este sistema se basa en un Arduino y utiliza una Raspberry Py como puerta de enlace. Los dos dispositivos se comunican mediante el protocolo I2C, mientras que Raspberry Py se comunica con un servicio en la nube mediante el protocolo MQTT. Además de almacenar y hacer que los datos estén disponibles, el servicio en la nube también puede enviar comandos de configuración a los dispositivos. Al igual que el estudio anterior, la comunicación por cable de corta distancia limita la disposición de los dispositivos y hace más compleja la instalación.

El sistema presentado en Zago et al. tiene una estructura basada en redes de sensores inalámbricos (WSN), en la que cada nodo sensor monitoriza la corriente y la tensión generada por un módulo fotovoltaico individual [27]. Los nodos envían datos a través de ZigBee a una Raspberry Py que aloja una página web, lo que permite el acceso a los datos de forma local y a través de Internet a través de Wi-Fi.

En el estudio desarrollado por Xia et al. [30], los módulos ZigBee se utilizan para recopilar y transmitir datos obtenidos de los inversores de la planta fotovoltaica, creando una red de sensores local. Se utiliza una puerta de enlace 4G para conectar la red local a Internet, lo que permite el acceso remoto a datos. La verificación de la suma de

Tabla 2.2: Network schemes and communication technologies properties

Network schemes	Technologies	Data transfer rate	Typical coverage range	Latency
HAN	Ethernet, PLC, Zigbee, WLAN, Z–Wave	10 – 100 kbps	up to 500 m	10 ms – 1 s
BAN/IAN	Ethernet, PLC, Wimax, WLAN	100 kbps – 1 Mbps	up to 1 km	10 ms – 2 s
NAN	Ethernet, PLC, DSL, Fiber–Optics, WiMax, NB–IoT, LoRa	100 kbps – 10 Mbps	0.1 – 10 km	10 – 50 ms
WAN	PLC, Ethernet, Fiber–Optics, LoRa, WiMax	10 Mbps – 1 Gbps	10 – 100 km	10 μs – 20 ms

comprobación se utiliza para garantizar la estabilidad de la transmisión de datos y para verificar su integridad. La tecnología ZigBee ha sido propuesta por diferentes autores [31, 32, 33, 34] en los últimos años como solución para el desarrollo de soluciones de monitorización dentro del ámbito del internet de las cosas [35] debido a su bajo consumo de energía. Como inconveniente y como se expone en [36], la tecnología Zigbee se ha probado ineficiente para cubrir grandes distancias ya que su alcance abarca de e 10 a 100 metros. Como solución para estos casos, un sistema de bajo coste basado en sistemas embebidos de IoT es presentado por Kekre et al. [37]. Esta solución utiliza un módulo GPRS y un microcontrolador de bajo costo para enviar la energía generada por una planta de energía fotovoltaica. También se ha propuesto el canal de voz GSM para la comunicación de datos, ya que la red GSM está fácilmente disponible en áreas rurales [38]. Como inconvenientes, Pereira et al. afirman que esta solución requiere una tarjeta SIM con carga de transferencia de datos y puede instalarse solo en lugares con cobertura telefónica [39].

Una de las alternativas empleadas para aumentar este alcance es el empleo de redes tipo LPWAN (Low-PowerWide-Area Network). LPWA es un término genérico reciente que involucra diferentes tecnologías enfocadas en permitir comunicaciones de área amplia minimizando el consumo de energía y el coste del sistema y tasa de datos para para cumplir con este objetivo [40, 12]. El objetivo de estas tecnologías es adaptarse al nicho de productos que requieren una larga vida útil de la batería, tienen ciclos de trabajo bajos y requieren de medio a largo rango. La mayoría de las tecnologías LPWA desarrolladas han surgido tanto en mercados con licencia como sin licencia, como SigFox, LTE-M, NB-IoT y de largo alcance (LoRa). Entre ellos, Shina et al. [41] afirmaron que las soluciones NB-IoT y LoRa son las dos tecnologías emergentes líderes, a pesar de las importantes diferencias técnicas en términos de arquitectura de red, características físicas y protocolo MAC entre ellas [41]. La tabla 2.2 compara diferentes esquemas de red y tecnologías de comunicación.

Como se mencionará posteriormente, ambas alternativas han sido evaluadas dentro de los trabajos incluidos en esta tesis [42, 43].

2.3. Capa de aplicaciones

La capa de aplicaciones es en la que los datos se usan para dar servicios al usuario, desde las aplicaciones domésticas sobre uso de recursos (agua, gas, electricidad), hasta las aplicaciones logísticas para las empresas, que optimicen los recursos y el tiempo de procesado. Cualquier aplicación, doméstica o industrial, que haga uso de dispositivos conectados (IoT) se incluye en esta "capa" (por ejemplo, las que hacen posible la smart home, smart cities, eHealth,...).

Dentro del sector de la generación de energía por fuentes renovables, uno de los servicios más demandados es la predicción y medición con alta precisión de la producción de los sistemas fotovoltaicos individuales que se ve afectada por muchos factores desatancado, como era de esperar, la radiación solar recibida por el campo solar. En la bibliografía podemos encontrar un número relevante de metodologías para medir y predecir la irradiación solar global, considerándose esencial para el diseño, la evaluación económica y el análisis del rendimiento de las plantas de energía fotovoltaica (PV) y su integración en los sistemas eléctricos [44, 45].

En [46] podemos encontrar una revisión reciente de los modelos de predicción de energía para energías renovables. Al considerar los diferentes métodos y propuestas, sus validaciones se llevaron a cabo a través de una variedad de medidas de errores basadas en el criterio del autor y enfocadas principalmente en resultados de pruebas estadísticas promediadas. Notton et al. propusieron la aplicación de redes neuronales artificiales —evaluadas por el error cuadrático medio relativo (rRMSE) y el error absoluto medio relativo (rMAE)— para estimar la irradiancia solar en planos inclinados [47].

De manera similar, se usaron el error de sesgo medio relativo (rMBE), rRMSE, el coeficiente de determinación (R^2) y el índice de Willmott d para evaluar tanto las redes neuronales artificiales como las aplicaciones de máquinas de vectores de soporte [48]. Bouchouicha et al. usaron el error cuadrático medio (RMSE) y rRMSE para validar un modelo reajustado sobre el Gran Sur de Argelia [49]. Noorian et al. evaluaron doce modelos para estimar la radiación difusa horaria en superficies inclinadas mediante la determinación del rRMSE [50].

Teke et al. realizaron una comparación extensa —más de 90 contribuciones— de modelos estimados de radiación solar, para sugerir los modelos más precisos [51]. En esta revisión, y de acuerdo con los resultados de las pruebas estadísticas utilizadas con mayor frecuencia, se compararon el modelado lineal, el modelado no lineal, el modelado de inteligencia artificial y los enfoques borrosos.

De acuerdo con la literatura específica, se puede afirmar que la mayoría de las contribuciones se evalúan aplicando el rRMSE y el rMAE.

Durante los últimos años, se han propuesto diferentes aplicaciones para la irradiancia horizontal global (GHI) basadas en satélites geoestacionarios de nueva generación; muy apropiado para monitorizar áreas remotas y territorios a gran escala con una mínima inversión y costos operativos.

Posteriormente, un número creciente de soluciones y bases de datos están disponibles en línea para aprovechar la información generada, por ejemplo, PVWatts [52], PVGIS [53], Global Atlas [54] y SolarGIS [55]. Sin embargo, Piasecki et al. afirman en [56] que, según el conocimiento de los autores, los datos de satélite hasta el momento no se han comparado con las mediciones proporcionadas por el National Instituto de Meteorología y Gestión del Agua (Polonia) desde la perspectiva de las fuentes de energía renovables. Otras contribuciones se centran en el análisis de estos datos de los satélites.

Por ejemplo, Bodis et al. combinaron fuentes de datos estadísticos y basados en satélites con aprendizaje automático para proporcionar una evaluación fiable del potencial técnico para la producción de electricidad fotovoltaica en tejados con una resolución espacial de 100 m en toda la Unión Europea (UE) [57]. Psiloglou et al. han publicado recientemente una comparación entre conjuntos de datos procedentes de satélites y los analizaron frente a mediciones terrestres al considerar solo un área rural aislada [58]. Boca et al. evaluaron un modelo de enfoque de regresión múltiple para la estimación rápida de potenciales fotovoltaicos en Europa y África basado en la base de datos PVGIS y a través del error porcentual absoluto medio (MAPE) [59].

Los datos basados en el espectrorradiómetro de imágenes de resolución moderada (MODIS), junto con los datos meteorológicos convencionales, se utilizan en [60] para estimar la radiación solar global media diaria mensual. Se aplican dos estadísticos: desviación de sesgo medio general (gMBD) y desviación de sesgo medio general relativo (rgMBD) en [61] para validar el GHI estimado mediante el uso de datos de irradiancia espectral basados en satélites.

Pierro et al. proporcionaron una puntación RMSE para evaluar la estimación y las predicciones de generación de energía fotovoltaica a través de datos de satélite y de modelos numéricos de predicción meteorológica [62]. Además, Tang et al. utilizaron el error de sesgo medio (MBE), RMSE y rRMSE para evaluar si las estimaciones del GHI se pueden mejorar aumentando la frecuencia de las observaciones de los satélites. Recientemente, la desviación absoluta media (MAD) fue la métrica empleada en [63] para comparar la irradiación global de un modelo de estimación satelital y las mediciones terrestres.

Buffat et al. también utilizaron datos de radiación solar de satélites para estimar el potencial de irradiación solar en los techos en grandes regiones. Se aplicaron el coeficiente de correlación y un error relativo mensual mediano para estimar la precisión de dichas estimaciones [64].

Otros autores han propuesto métodos para estimar la irradiación normal directa a partir de imágenes del satélite geoestacionario GOES para sistemas solares de concentración. En este caso, se utilizan los valores promedio de MBE y RMSE para validar los métodos [65].

Pfenninger et al. usaron los resultados de RMSE para validar los patrones a largo plazo de la producción fotovoltaica europea por medio de análisis por hora de 30 años y datos de satélites [66]. Ernst et al. compararon los datos de irradiación terrestres y satélites mediante el uso de resultados de intervalos de confianza [67]. En este marco, esta revisión de la literatura demuestra que existe una falta de acuerdo en las estrate-

gias de validación para los datos de irradiancia solar derivado de satélites [68]. Por lo tanto, y debido a esta falta de acuerdo en las metodologías de validación de conjuntos de datos de irradiancia solar, el objetivo del trabajo presentado en [69] se centra en evaluar métricas para comparar los datos de de irradiancia obtenidos por satélites frente a datos medidos en tierra y analizarlas mediante la técnica de componentes principales.

Profundizando en los modelos de predicción de generación de aplicación en plantas fotovoltaicas, se pueden encontrar diferentes soluciones de predicción en la literatura específica [70]. El marco de tiempo de predicción, también llamado horizonte, se define de acuerdo con la operación de la red y bajo resoluciones tanto espaciales como temporales. Se pueden definir diferentes horizontes de predicción, que varían desde segundos hasta días o semanas de anticipación. Con respecto a los horizontes espaciales, también se pueden abarcar desde una única ubicación hasta predicciones a nivel regional.

En [71] se propone y evalúa un nuevo modelo basado en mediciones horarias. En [72], Oudjana *et al.* exploraron la aplicación de redes neuronales para desarrollar modelos de predicción de generación de energía fotovoltaica. Se pueden encontrar otras soluciones basadas en redes neuronales en la literatura específica [73, 74, 75, 76, 77].

Naveed Akhter *et al.* [78] presentan una revisión crítica y sistemática de los métodos de predicción de energía fotovoltaica (PV), principalmente centrados en el aprendizaje automático y en soluciones metaheurísticas. Se utiliza una técnica de machine learning para la previsión de energía fotovoltaica de un modelo en tiempo real [79]. En [80] se analiza una revisión de la irradiación solar y la previsión de energía fotovoltaica.

Barbieri *et al.* concluyen que la temperatura y la irradiancia de la celda/módulo pueden considerarse como los mejores enfoques para una predicción precisa de la energía fotovoltaica; principalmente en condiciones nubladas con fluctuaciones de generación de energía difícilmente predecibles [81]. En [82], se analiza y cuantifica una revisión de predicción probabilístico centrada en los errores inherentes de diferentes estrategias de predicción.

La previsión de generación de energía fotovoltaica a corto plazo también es una tarea importante en la planificación y operación de sistemas de energía renovable. De hecho, Kaur *et al* afirman que el mercado de electricidad a corto plazo para equilibrar la demanda y la generación ofrece una oportunidad económica notable para integrar mayores proporciones de vRES en futuras redes eléctricas [83].

Yang *et al.* proponen un novedoso modelo de predicción basado en datos a escala multitemporal para mejorar la precisión de la producción de energía fotovoltaica a corto plazo [84]. Dambreville *et al.* proponen un nuevo enfoque de predicción de la irradiancia horizontal global (GHI) a muy corto plazo mediante el uso de un modelo autorregresivo espacio-temporal [85].

En cuanto a las métricas utilizadas en la literatura específica para la evaluación del rendimiento de estos modelos, se realiza cuantificando las discrepancias entre dichas predicciones y las mediciones meteorológicas mediante el uso de métricas de errores estadísticos tradicionales, como el error de sesgo medio o el error cuadrático medio

(RMSE) [86]. Por ejemplo, los indicadores de error porcentual absoluto medio (MAPE) y error absoluto medio (MAE) se utilizan en [87] para evaluar el rendimiento de los modelos de predicción de energía fotovoltaica del día siguiente basados en redes neuronales de aprendizaje profundo.

El error cuadrático medio normalizado (nRMSE) se usa en [88] para evaluar los errores de predicción. De manera similar, Huang *et al.* describen un estudio comparativo de métodos de predicción de energía solar fotovoltaica basados en nRMSE [89]. Gigoni *et al.* realizan una comparación exhaustiva de metodologías de predicción simples con soluciones más sofisticadas en 32 plantas fotovoltaicas (PV) de diferentes tamaños y tecnologías durante todo un año [90].

Considerando las contribuciones discutidas previamente, y respecto a las métricas apropiadas, la mayoría de los autores proponen y utilizan las siguientes estrategias: RMSE, MBE, y las versiones relativas de cada uno (rRMSE y rMBE), el error absoluto medio (MAE), el coeficiente de correlación de Pearson (r), y la desviación estándar del residual (SD). Sin embargo, en este análisis bibliográfico se identifica la falta de contribuciones enfocadas a evaluar posibles errores de predicción y la menor precisión de los resultados derivados de las fallos inherentes a la red de comunicación como pueden ser pérdidas de paquetes, posibles colisiones de paquetes, etc.; así como la influencia de dicha precisión de predicción a corto plazo del GHI. De hecho, una posible falla en la comunicación puede afectar significativamente tanto la recopilación de datos como los resultados de los modelos de predicción [91].

Por ello y partiendo de la experiencia del empleo de la tecnología de Lora en trabajos previos de los autores [42], en otro de los trabajos de esta tesis [69] se analiza la influencia de la solución LoRa sobre el predicción a corto plazo de la GHI.

CAPÍTULO 3

CONTRIBUCIONES

El objetivo de este capítulo es presentar las principales contribuciones de los trabajos realizados en el marco de esta tesis para alcanzar los objetivos definidos en el capítulo 1.

3.1. Sistema inalámbrico de monitorización de módulos fotovoltaicos de bajo costo basado en soluciones de código abierto

Como se ha descrito en el apartado anterior existen multitud de enfoques y diseños para realizar la monitorización de instalaciones de fotovoltaicas Se describe y evalúa un sistema de monitorización alternativo para instalaciones fotovoltaicas. La solución se basa en un sistema de código abierto y de bajo costo de acuerdo con los requisitos de IEC–61724 [92].

Esta IEC describe las pautas generales para monitorizar y analizar el rendimiento de las plantas de energía fotovoltaica. Los parámetros a ser monitorizados con respecto a las plantas de energía fotovoltaica conectadas a la red se resumen en la Tabla

Tabla 3.1: IEC–61724 Standard Parameters

		Symbol	**Units**
Meteorological	Total irradiance (on the array)	GI	W/m^2
	Ambient temperature	T_{am}	^oC
	Wind speed and direction (optional)	VA	
Photovoltaic array	Output voltage	VA	V
	Output Current	IA	A
	Output power	PA	W
	Module temperture	T_m	^oC
Utility grid	Utility voltage	V_u	V
	Current to/from utility grid	I_{TU}	A
	Power to/from utiliy grid	P_{TU}	W

El sistema de monitorización propuesto recopila datos meteorológicos y eléctricos a nivel de módulo fotovoltaico, proporcionando una arquitectura flexible e inalámbrica que se puede implementar en la mayoría de las instalaciones fotovoltaicas.

La arquitectura del sistema propuesto también se dirige a cumplir con la flexibilidad y escalabilidad para diferentes tipos de instalaciones fotovoltaicas. De hecho, se puede implementar en módulos fotovoltaicos independientemente de su configuración. Además, la arquitectura distribuida inalámbrica seleccionada nos permite modificar los nodos de acuerdo con el diseño de los módulos fotovoltaicos sin ningún cableado adicional.

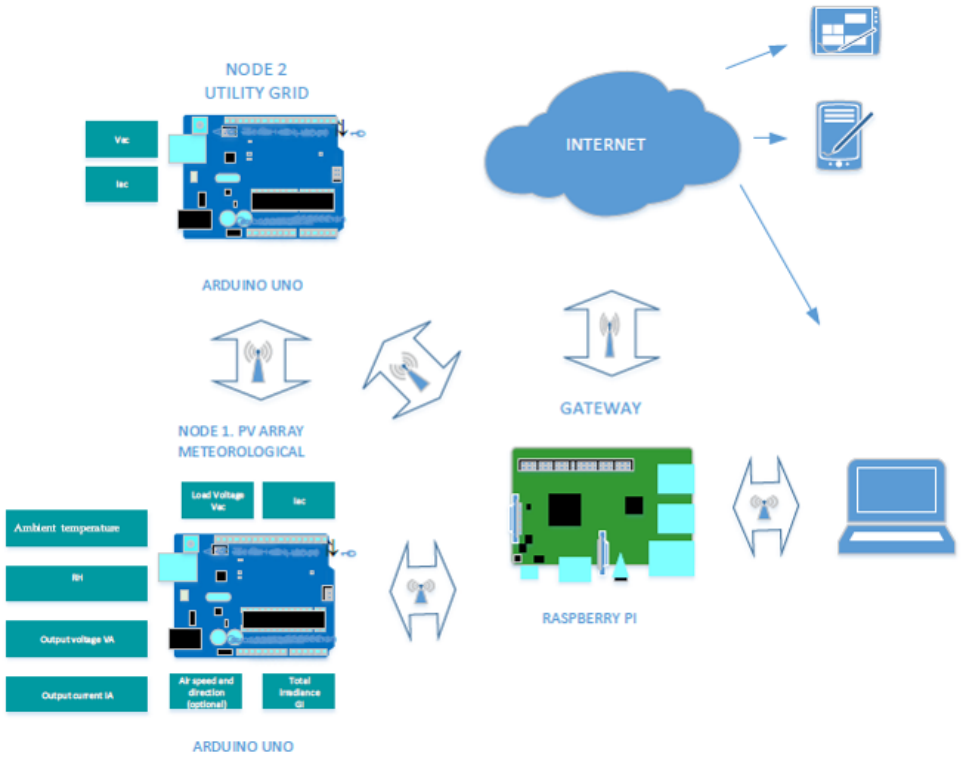

Figura 3.1: Arquitectura del sistema propuesto

Bajo esta topología inalámbrica flexible, el hardware seleccionado se basa en las plataformas Arduino y Raspberry Pi. Actualmente son conocidas soluciones de creación de prototipos extensibles, de código abierto y de bajo costo, lo que nos permite proporcionar un sistema de monitorización detallado a nivel de módulo fotovoltaico.

Los sensores han sido calibrados en un entorno de laboratorio y los resultados cumplen con los valores mínimos de precisión IEC-61724 en términos de corriente, voltaje y potencia. módulo fotovoltaico. La temperatura también está disponible a partir de la solución propuesta, con un error medio inferior al 4 %.

Se han realizado diferentes campañas de ensayos de campo en instalaciones fotovoltaicas españolas conectadas a red. Para evaluar la solución propuesta se han comparado los datos monitorizados con los datos recogidos de un equipo registrador de datos comercial, obteniendo errores inferiores al 2 % para variables meteorológicas y eléctricas. Los resultados extensos también se incluyen en el documento. Finalmente, también se ha incluido una interfaz de servidor web para proporcionar una conexión de cliente externo y un monitor. Se basa en *emoncms*, una aplicación web de código abierto para procesar, registrar y visualizar energía y otros datos ambientales

3.2. Solución alternativa de internet de las cosas basada en en LoRa para la monitorización y gestión de datos de plantas fotovoltaicas

El artículo 2 propone la utilización de una tecnología de código abierto de bajo coste y una red inalámbrica de baja potencia (LPWAN)[93] que combina las ventajas de cobertura de largo alcance y baja demanda de energía para ofrecer un sistema de monitorización para intercambio datos en un entorno de Internet de las cosas (IoT).

La arquitectura de red propuesta integra la infraestructura típica de una red LoRa-IoT[12] de manera similar a la 3.2

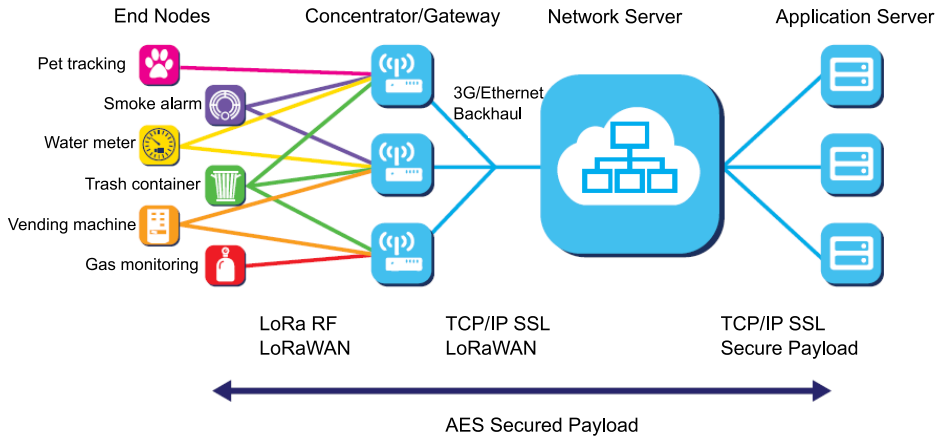

Figura 3.2: Arquitectura habitual de una red Lorawan (LoRa wireless area network)

Por lo tanto, para la evaluación de la solución propuesta se considera una topología en estrella que incluye dispositivos finales, puertas de enlace y un servidor de red central.

En la capa de percepción , todos los sensores seleccionados a cargo de monitorizar instalaciones fotovoltaicas se seleccionan para cumplir con los requisitos de IEC-61724. Los datos eléctricos de PV y los parámetros meteorológicos se recopilan para estimar las condiciones de funcionamiento de PV e intercambiar información de datos meteorológicos y eléctricos. Estos paquetes de datos se envían a un *gateway* desde las plantas de energía fotovoltaica correspondientes. Posteriormente, los datos recibidos por el gateway se reenvían a la capa de aplicación para su análisis y validación.

El diseño del sistema propuesto incluyó

- la selección de hardware del nodo final,
- desarrollo y configuración del software del nodo,
- el servidor de red LoRa

Según el mejor conocimiento de los autores, otras contribuciones en esta linea co-

mo [94, 95, 96] utilizan la tecnología LoRa como la forma de transmitir datos recopilados por sensores en una planta de energía fotovoltaica. En estas contribuciones, los autores instalaron un módulo de comunicación Lora para enviar paquetes a un *gateway* que incluye parámetros físicos como corriente o temperatura, sin entrar en detalles sobre problemas de comunicación.

A diferencia de estos trabajos, en nuestro trabajo se contribuye con una solución que aborda estas preocupaciones de manera más intensiva que utilizan la tecnología LoRa, asegurando el mejor rendimiento para transmitir información desde la instalación fotovoltaica al *gateway* y, en consecuencia, aumentando la fiabilidad del sistema. En este sentido, la velocidad de transmisión (bits por segundo) se ha ajustado a fondo para lograr un RSSI (Indicador de intensidad de la señal recibida) y unas cifras de Relación de señal y ruido (SNR) adecuados y aceptables para la solución propuesta.

3.3. Caracterización de métricas para la comparación de datos de satélite y terrestres basada en un análisis de componentes principales (PCA)

Entrando ya en la capa de aplicación de la solución propuesta, una de las aplicaciones más demandadas es la predicción y medición con alta precisión del rendimiento de las plantas de energía fotovoltaica (PV) de cara a una integración segura en los sistemas eléctricos[97].

Con este objetivo, recientemente tal y como se ha comentado en la sección correspondiente del estado del arte 2.3 se han propuesto diferentes estimaciones de irradiancia horizontal global (GHI) basadas en la información registrada por satélites geoestacionarios de nueva generación, proporcionando un número creciente de soluciones y bases de datos, en su mayoría disponibles en línea, además de las muchas instalaciones con datos de irradiancia medidos en tierra disponibles actualmente.

De acuerdo con la literatura específica, existe una falta de acuerdo en las estrategias de validación para un conjunto de datos de irradiancia derivados de satélites. Además, en contribuciones recientes se comparan diferentes fuentes de datos de irradiancia basadas en una diversidad de métricas arbitrarias.

Bajo este marco, el trabajo realizado para el artículo 3 describe una caracterización de métricas basada en una aplicación del análisis de componentes principales (PCA) para clasificar dichas métricas, con el objetivo de proporcionar información no redundante y complementaria. De esta forma, se identifican diferentes grupos de métricas aplicando el proceso PCA, lo que nos permite comparar diferentes fuentes de datos de irradiancia y explorar e identificar sus diferencias.

La metodología se ha evaluado utilizando datos de GHI medidos en tierra y por satélite recopilados durante un año en siete ubicaciones diferentes de España, con un tiempo de muestreo de una hora. La caracterización de los datos, los resultados y una discusión sobre la idoneidad de la metodología propuesta también se incluyen en este trabajo. documento.

3.4. Metodología para evaluar diferentes arquitecturas de monitorización de sistemas fotovoltaicos basadas en LoRaWan

Como se ha comentado en la sección anterior, una previsión precisa de generación de energía de estas instalaciones es crucial para proporcionar fiabilidad y estabilidad a las redes actuales. Al mismo tiempo, los requisitos de monitorización fotovoltaica son cada vez más demandados por diferentes agentes para proporcionar información fiable sobre rendimientos, eficiencias y posibles tareas de mantenimiento predictivo.

Bajo este marco, una de las contribuciones de este trabajo es la introducción de una metodología para evaluar diferentes arquitecturas de monitorización de instalaciones fotovoltaicas basadas en LoRa como las propuestas en términos de predicción de la generación de energía solar a corto plazo.

Se considera un análisis de ubicación de los nodos basado en la posible pérdida de datos, intervalos de tiempo a corto plazo y rangos de spreading factor para analizar su influencia en dichos propósitos de predicción de GHI a corto plazo.

Se propone como método de predicción un modelo de *Random Forest* lo que simplifica el problema de predicción, especialmente cuando la serie de tiempo presenta heterocedasticidad, no estacionariedad y múltiples ciclos estacionales.

Con este enfoque se proporciona un análisis de sensibilidad de los parámetros de las comunicaciones LoRa en términos de diseño de nodos, pérdida de datos, factor de dispersión e intervalos de tiempo cortos para evaluar su influencia en la precisión de la previsión de generación.

Las principales contribuciones de este documento se pueden resumir como

- una metodología para evaluar la precisión de la predicción a corto plazo de GHI para diferentes diseños de nodos y parámetros LoRa basados en un modelo de predicción *Random Forest*,
- un análisis de sensibilidad de los parámetros LoRa y los intervalos a corto plazo de los valores de predicción del GHI basados en una variedad de métricas,
- un estudio de caso a partir de mediciones de GHI en 2019 (tiempo de muestro de un minuto), área de 400 km^2, 289 nodos potenciales bajo consideración y un total de 13140 simulaciones.

Por lo tanto, esta metodología proporciona un análisis preliminar extenso de las posibles características de la red LoRa y el diseño de nodos en términos de precisión de datos, paquetes y posibilidades de predicción de GHI antes de que se complete la instalación.

3.5. Solución de monitorización aplicable para autoconsumo basada en NB-IoT

Tras la evaluación de la tecnología LoRA como base para la capa de comunicaciones del sistema de monitorización introducido se propone una solución alternativa basada en otra de las tecnologías de LPWAN, la tecnología NB-IoT para abordar las principales limitaciones de la tecnología de LoRA.

Además de la necesidad del despliegue de una red de *gateways* para la recogida de la información de las plantas fotovoltaicas, hay que tener en cuenta la influencia de la localización de estos en cuanto a distancia, obstáculos en linea visual, así como otros parámetros de influencia en la propagación de la señal como la limitación en el número de transmisiones permitidas siendo esta probablemente la mayor de las limitaciones.

Como se muestra en los trabajos realizados con la tecnología LoRa, esta solución solo permitía un número limitado de transmisiones, debido al tiempo en el aire de las transmisiones al trabajar con altos valores del factor de dispersión (SF11 y SF12) para asegurar una recepción precisa de paquetes de datos con un ciclo de trabajo restringido (1 %).

Como alternativa, en este trabajo, se propone el empleo de la tecnología NB-IoT para las comunicaciones. Esta tecnología, al presentar licencia, puede soportar comunicaciones masivas ya que no comparte espectro ni tiene restricciones en su ciclo de trabajo. Para su análisis y evaluación se desarrolla el hardware y el software de un nuevo sistema de monitorización basado en la plataforma desarrollo PyCom.

Toos los elementos que componen la solución propuesta, tanto los componentes de hardware como los sensores, fueron probados en un entorno de laboratorio, con el objetivo de evaluar su desempeño en diferentes condiciones. La solución se conectó y montó en condiciones exteriores en una instalación de autoconsumo fotovoltaico para evaluar la viabilidad de la solución para ser implementada en una variedad de situaciones y condiciones reales.

En cuanto a la calidad de comunicación de la solución propuesta, se han comparado los resultados usando las métricas adicionales utilizadas en trabajos anteriores de los autores [42].

Estas métricas son Tasa de entrega de paquetes, definida como la proporción entre los paquetes recibidos con éxito y el total de paquetes de datos enviados por los nodos finales, y los intervalos de tiempo entre diferentes paquetes de datos (tiempo entre llegadas) que está determinado por el valor del intervalo de tiempo correspondiente a cada paquete recibido. Los resultados obtenidos muestran que con tamaños de mensaje similares el sistema propuesto proporciona una conectividad fiable con un error de entrega de paquetes de alrededor del 4.6 % y un intervalo de tiempo estable entre paquetes de 60 segundos.

Estos resultados validan la viabilidad y fiabilidad de nuestra propuesta mejorando los resultados obtenidos en trabajos anteriores superando las limitaciones relacionadas con la falta de paquetes de datos y la frecuencia de los datos recibidos.

CAPÍTULO 4

ARTÍCULOS PUBLICADOS

En este capitulo se incluye una copia de los todos los articulos publicados que componen esta tesis.

4.1. PV module monitoring system based on low-cost solutions: a wireless Raspberry application and assessment

Información adicional:

- Revista: Energies 11, no. 11: 3051
- DOI: 10.3390/en11113051
- Fecha de publicación: Noviembre 2018
- Disponible en: `https://www.mdpi.com/1996-1073/11/11/3051`
- Referencia: [98]
  Paredes-Parra, J.M.; Mateo-Aroca, A.; Silvente-Niñirola, G.; Bueso, M.C.; Molina-García, Á. PV Module Monitoring System Based on Low-Cost Solutions: Wireless Raspberry Application and Assessment. Energies 2018, 11, 3051.
  `https://doi.org/10.3390/en11113051`

energies

MDPI

Article

PV Module Monitoring System Based on Low-Cost Solutions: Wireless Raspberry Application and Assessment

José Miguel Paredes-Parra [1], Antonio Mateo-Aroca [2], Guillermo Silvente-Niñirola [3], María C. Bueso [4] and Ángel Molina-García [3,*]

1 Technological Center for Energy and Environment (CETENMA), 30353 Cartagena, Spain; jmparedes@cetenma.es
2 Department of Electronic Technology, Universidad Politécnica de Cartagena, 30202 Cartagena, Spain; antonio.mateo@upct.es
3 Department of Electrical Engineering, Universidad Politécnica de Cartagena, 30202 Cartagena, Spain; silvente93@gmail.com
4 Department of Applied Mathematics and Statistics, Universidad Politécnica de Cartagena, 30202 Cartagena, Spain; mcarmen.bueso@upct.es
* Correspondence: angel.molina@upct.es; Tel.: +34-968-32-5462

Received: 20 September 2018 ; Accepted: 28 October 2018; Published: 6 November 2018

Abstract: The integration of renewables into power systems has led to multiple studies and analysis in terms of grid-power quality, reliability, and/or feasibility. Among different resources to be considered as alternative energy systems, wind and solar emerge as the most mature technologies. With regard to photovoltaic (PV) installations, monitoring problems requires detailed analysis, since solar-radiation fluctuations, soiling on solar panels, or deficiency of PV-panel performance can involve unexpected power-output oscillations and, subsequently, undesirable power-generation oscillations. Under this framework, this paper describes and assesses a wireless low-cost PV-module monitoring system based on open-source solutions. Our proposal allows us to monitor installations at the PV-module level, giving detailed information regarding PV power-plant performance. The proposed monitoring system is based on the IEC-61724 standard requirements, as a flexible and ad hoc solution with relevant connectivity options. Meteorological and electrical data are collected from the developed nodes and available for subsequent analysis. Detailed information of the solution, as well as extensive results collected in Spanish PV power plants connected to the grid, are also included in the paper.

Keywords: PV monitoring; low-cost solutions; renewable energy source integration

1. Introduction

Most developed countries have promoted policies and initiatives to achieve sustainability by reducing energy dependence and emissions. These initiatives aim to limit climate change and lead to a decarbonized energy system [1]. Indeed, the deployment of renewables and energy efficiency are considered key agents to fulfilling emission reductions and conforming to the Paris Agreement objectives [2]. In addition, this general situation, combined with the rapid cost decrease of renewable technologies (mainly photovoltaic (PV) installations—the price of solar PV modules was reduced by around 85% from 2010 to 2015 [3]), has promoted the rise of renewable-solution deployment and investment. As an example, the renewable sector globally added 167 GW of new generation capacity in 2017. This accounts for a growth of 8.3% over the previous year, maintaining similar rates since 2010, with 8–9% on average per year. This target has been mainly achieved as a result of new PV solar installations and wind power plants connected to the grid. In 2017, 94 GW were added from PV power plants and 47 GW from wind power plants, including 4 GW from offshore wind power plants [4].

Best et al. [5] affirms that solar and wind resources are on the upper rungs of the energy ladder, their integration being predominant in higher-income countries. Recent contributions, focused on future electricity systems, also assume that renewable assets can be considered a mix between wind- and solar-power generation [6]. In [7], and apart from wind and PV solar deployment, a slight increase has been estimated during the past few years for other renewable energy sources for electricity. In addition, Ellabban et al. [8] establishes a direct connection between technological maturity and economic barriers, mainly when the cost of a technology is above the cost of other competing alternatives. Therefore, wind and PV solar resources are currently the most integrated renewable energy sources into power systems, excluding hydropower-generation units. Nevertheless, there are no large-area power systems in the world where wind and solar power generate more than 50% of electricity [9].

The integration of wind and PV power plants into power systems involves certain technical problems, mainly focused on reliability, power quality, and stability [10]. The intermittent nature of such sources may increase grid stress, mainly due to undesirable oscillations on the supply side [11] that may affect voltage regulation of transmission systems [12]. At a low/medium-voltage level, different reactive power control strategies have also been proposed to facilitate renewables integration [13], including active power curtailment [14]. As an additional solution to guarantee a balance between generation and demand, with reduced capacity and costs of operating reserves [15], short-term forecasting of PV production emerges as a relevant topic of interest. In fact, several methods for forecasting PV power over a short-term horizon can be found in the specific literature [16–18]. These methods depend on weather conditions and previous PV power-production data. Therefore, updated weather and electric values would allow us to more accurately forecast short-term PV power production. Moreover, real-time monitoring technologies can provide relevant local and accurate information to ensure the control and reliability of the grid [19]. To achieve these goals, and according to Colak et al. [20], current power systems should be modernized in terms of sensing, communication, measurement, and automation technologies.

With regard to PV monitoring systems, prior efforts can be found in the specific literature. Low-cost solutions have been considered as a priority during the last decade, proposing different monitoring and communication systems. In [21], a low-cost microcontroller-based data-acquisition system (DAQS) for remote PV water-pumping systems is proposed. Communications are based on the GSM network and, in particular, on the Short text-Message Service (SMS). Contributions that focused on power-line communication (PLC) modules can be also found in the specific literature. In [22], a PLC compliant with HomePlug is proposed to monitor each PV module. Another example based on a PLC module is evaluated in [23], where four PV panels are simultaneously monitored. Nevertheless, recent contributions affirm that the level of noise in a power-line network is considered much higher than any other type of communication network [24]. A semiautomated solution for testing and monitoring PV-module performances is described in [25]. A modified rheostat is used to estimate the I-V characteristics of a PV module. Communication between nodes is carried out through a wired RS485 communication protocol, and a solution is built around wired/wireless devices and the Internet of Things (IoT), a concept that is described in [26]. PV installation is monitored at the inverter level. An extensive comparison of monitoring and transmission systems is also included in this contribution. Another solution based on wired/wireless sensor-network technologies for in situ solar-panel monitoring is discussed in [27]. The proposed architecture used low-cost open-source tools based on an Arduino platform, including wireless ZigBee connectivity. ZigBee-based wireless technology is also proposed in [28] to provide online monitoring systems for PV power plants connected to the grid. An overview of ZigBee devices and modules is described in [29], including a PV energy system belonging to a water treatment and distribution company. Evaluation of measurement accuracy is discussed in [30]. A recent review of PV monitoring systems can be found in [31], mainly focused on low-cost monitoring proposals. A detailed overview of PV monitoring-system components, such as sensors, controllers, data transmission, and storage solutions, is also included in this work.

According to previous works and contributions of the authors in PV monitoring [32], this paper proposes a flexible, low-cost, and user-friendly monitoring system based on open-source prototyping boards for PV power plants according to the IEC-61724 standard requirements. The main contributions of this paper are summarized as follows:

- PV installations are monitored at the PV-module level according to the current IEC-61724 standard, estimating PV-module performances and providing predictive maintenance.
- Low-cost and open-source wireless solutions are used to facilitate the integration of the proposed system in PV power plants.
- The wireless solution is flexible and can be adapted according to the layout and configuration of the PV modules.

The rest of the paper is structured as follows: Section 2 gives a detailed description about the proposed low-cost monitoring solution. Section 3 describes experimental field tests carried out in a Spanish PV installation connected to the grid. Extensive results and assessment of the proposed solution are also included in this section. Finally, the conclusion is given in Section 4.

2. Proposed Low-Cost Solution

2.1. Preliminaries

This monitoring system aims to collect electrical and environmental data at the PV-module level. In addition, it allows us to evaluate PV-module performance and identify abnormal behaviors. The proposed solution is in line with one of the most relevant references for PV system monitoring, standard IEC 61724: 'Photovoltaic system performance monitoring. Guidelines for measurement data exchange and analysis'. Recent contributions based on this IEC standard can be found in [33], where a battery monitoring system based on the IoT is proposed. This IEC describes the general guidelines for monitoring and analysis of PV power-plant performance. Parameters to be monitored concerning grid-connected PV power plants are summarized in Table 1. According to this standard, the proposed system architecture is also addressed to meet flexibility and scalability requirements for different types of PV installations. Indeed, it can be implemented on PV modules independent of their configuration. Additionally, the selected wireless-distributed architecture allows us to modify nodes according to the layout of the PV modules without any additional wiring. Under this flexible wireless topology, the selected hardware is based on the Arduino and Raspberry Pi platforms. They are well-known low-cost, open-source, and extensible-prototyping solutions, allowing us to provide a detailed monitoring system at PV-module level.

Table 1. IEC-61724 standard parameters.

		Symbol	Units
Meteorological	Total irradiance (on the array)	GI	W/m^2
	Ambient temperature	T_{am}	°C
	Wind speed (optional)	WS	m/s
	Wind direction (optional)	WD	degrees
Photovoltaic array	Output voltage	VA	V
	Output Current	IA	A
	Output power	PA	W
	Module temperature	T_m	°C
Utility grid	Utility voltage	V_u	V
	Current to/from utility grid	I_{TU}	A
	Power to/from utility grid	P_{TU}	W

Arduino was initially proposed for educational development and subsequently extended for commercial purposes. Arduino boards usually involve an onboard power supply, USB ports, and an ATMEL microcontroller chip. It provides communication and control support, avoiding sophisticated PCB design and implementation. A large variety of sensors and additional components can be integrated through custom library and drive support by the manufacturers. Arduino platforms have recently been proposed in other data-collection efforts, including embedding wireless sensor networks [34,35]. On the other hand, Raspberry Pi [36] is a credit card-sized ARM-based single-board computer (SBC). It was initially proposed by the Raspberry Pi Foundation [37] to support computer-programming learning. This initial objective was extended toward a great number of applications, mainly due to the advantages in terms of low cost, full customization, and excellent scalability. Nowadays, a relevant number of solutions can be found in the specific literature. Recent projects based on Raspberry Pi equipment and focused on real-time data-monitoring purposes are proposed in [38–40]. A recent review of energy-management systems for homes based on the current IoT era can be found in [41]. In addition, low cost, high accuracy, and great flexibility solutions for wireless industrial-energy monitoring platforms are presented in [42].

2.2. General Architecture

Figure 1 shows an example of the general architecture, where electrical and environmental nodes are schematically depicted. These nodes are based on Arduino UNO technology, including wireless communication. It is a flexible solution, adaptable under different PV module configurations and arrays. Both environmental and DC electrical data at the PV-module level are then collected and sent to the sink node, based on Raspberry Pi technology. This sink node allows us to collect parameters at the inverter level, depending on different PV power-plant configurations. These collected data are sent to a gateway, providing subsequent analysis and monitoring applications.

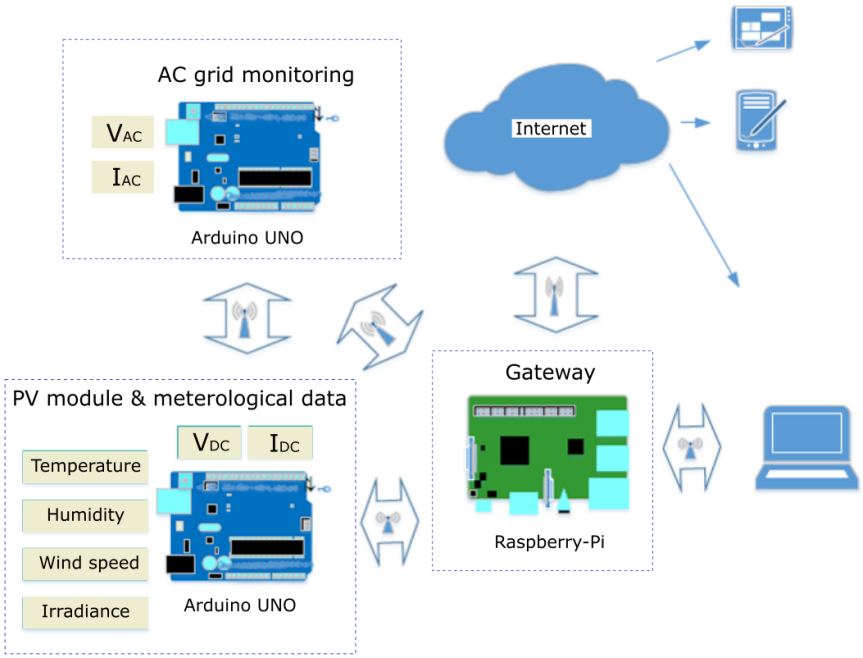

Figure 1. Proposed wireless architecture.

To offer an open-source and low-cost solution, the prototype was based on OpenEnergyMonitor equipment [43]. OpenEnergyMonitor is a recent open-source project with different solutions, mainly focused on home energy-monitoring applications. Designs and codes are available online, and they are supported by a relevant community of developers. This solution includes Arduino

technology for sensors and the data-collecting process, and Raspberry Pi equipment as a server for wireless communications (433 MHz RF). For RF data transmission, a HopeRF RFM69CW module is included [44]. This RF module offers low power demand and low transmission costs, and it is suitable for the proposed system where data exchanges between sensor nodes and the gateway are frequently required. Figure 2 shows examples of the assembled node and the corresponding gateway based on Raspberry-Pi solutions.

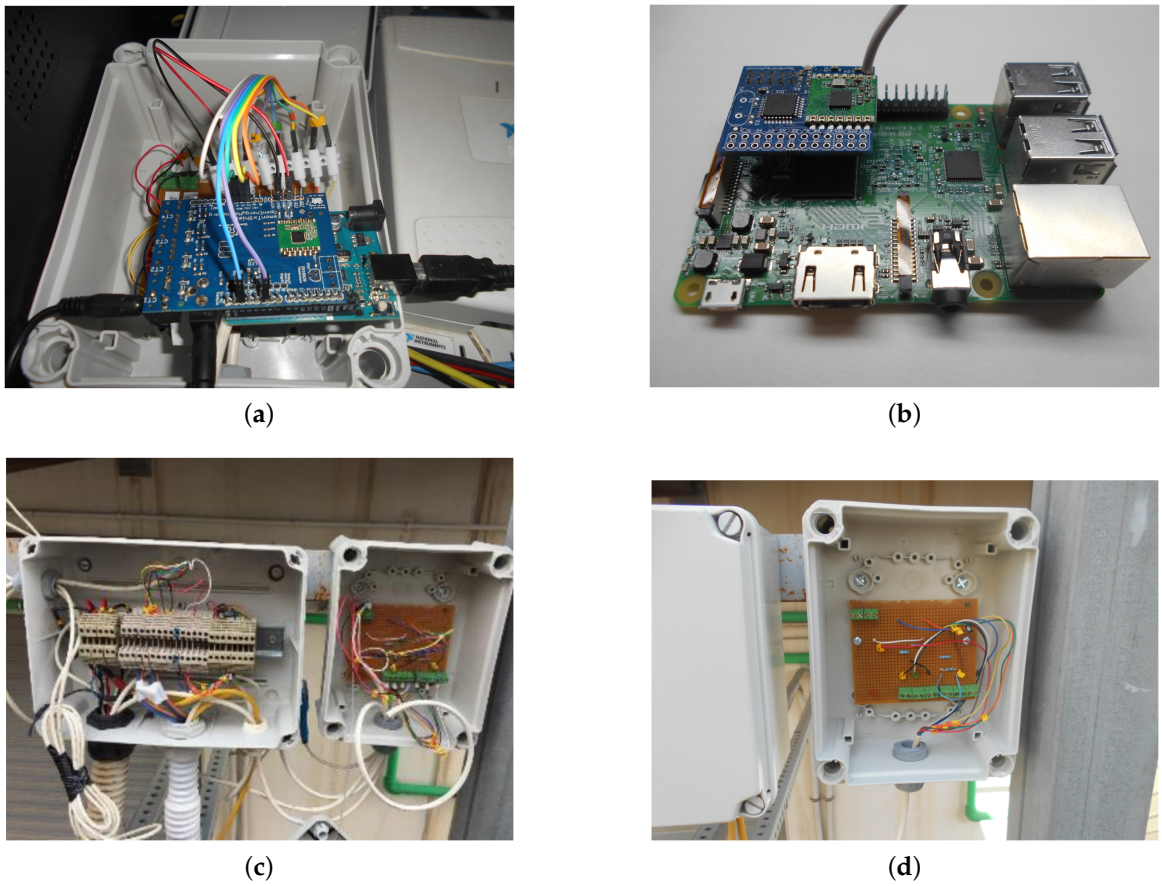

Figure 2. Examples of the prototype nodes and connections: (**a**) assembled node 1; (**b**) gateway Raspberry Pi; (**c**) external connections; and (**d**) detail of external connections.

2.3. Hardware Solution: Sensors

Nowadays, and under low-cost requirements, a wide range of sensors are currently available for electrical and environmental parameter monitoring [45]. Moreover, most of them provide additional characteristics based on the IoT [46,47] or they allow extensive connection with Arduino-based solutions [48,49]. Based on the IEC-61724 requirements [50], a set of low-cost sensors to measure and collect meteorological and electrical parameters is selected by the authors. With regard to environmental variables, recent contributions propose to monitor temperature and humidity by a wireless low-cost solution with PV microcells [51]. In our case, temperature is measured near PV modules as an attempt to more accurately estimate real-environmental PV-module conditions. A DHT-22 temperature/humidity sensor with digital output is selected for this application. The DHT sensor is directly supported by Arduino IDE technology and, according to Priya et el. [52], it provides very accurate results and refreshes very quickly. Other recent DTH22 applications can be found in [53,54]. Assuming that the short-circuit current (ISC) is nearly proportional to irradiance [55], solar irradiance (W/m^2) is measured by a 5 Wp short-circuit encapsulated polycrystalline silicon module. Shunt resistance is selected and implemented to give a voltage range suitable for Arduino

analog inputs. Calibration of this module was carried out by the authors through the CETENMA Solar TestBed, based on the global sunlight method available in [56]. This silicon module is installed outdoors, along with a CMP21 ISO secondary-standard pyranometer manufactured by Kipp and Zonen. Recent CMP21 applications to estimate diffuse and global horizontal irradiation can be found in [57]. Both signals, the encapsulated polycrystalline silicon module monitored by the Arduino and the pyranometer voltage outputs measured using an Agilent 34401A digital multimeter, were simultaneously and accordingly collected. The Agilent 34401A Digital multimeter has been widely used in PV and PV/thermal solar studies [58]. Figure 3 shows an example of a real PV installation and the reference pyranometer (CMP21). Calibration results are also included in this figure.

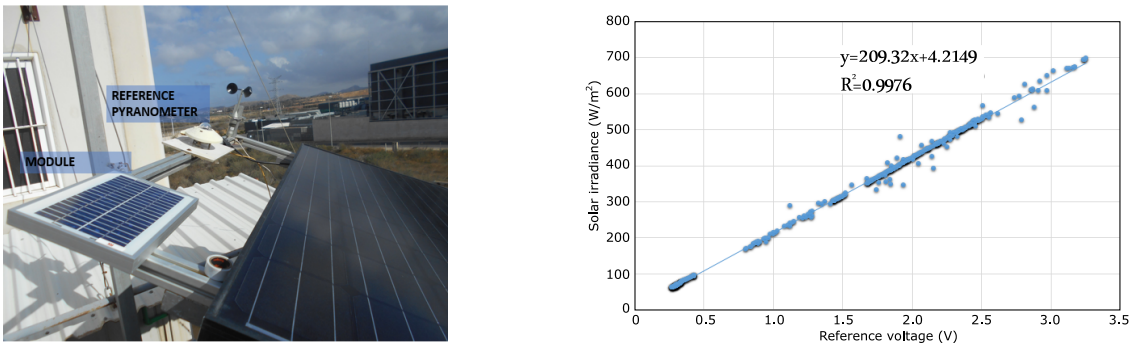

Figure 3. Pyranometer module calibration: (**a**) real PV installation; and (**b**) pyranometer calibration.

In general, commonly used standard approaches to model cell temperature do not include the influence of wind on cell temperature [59], limited only to ambient air and inplane irradiance measurements [60]. Moreover, according to Copper et al. [61], wind speed should be measured if the array is subjected to extreme weather conditions. Wind speed thus has less impact on PV-module performance than temperature. Nevertheless, it affects PV-system performance by increasing convective heat loss and reducing PV-module temperature [62]. For the proposed system and this case study, we monitored wind-speed data by using a hemispherical cup anemometer with a linear-frequency output variable. In line with IEC-61724, uncertainty including instrumentation should be lower than 0.5 m/s for wind speeds <5 m/s, and lower than 10% for monitored wind speeds >5 m/s.

Most correlations found in the specific literature for PV electrical power as a function of the cell/module operating temperature and basic environmental variables are linear [63]. Indeed, Dubey and Skoplaki et al. [64,65] affirm that the PV-module power output practically depends linearly but rather strongly on operating temperature. Module temperature should be collected at the center of the back surface of the PV module and in the center of the array field (location on module given in IEC 61829 method A) [66]. Nevertheless, where to measure the temperature of a PV is still debated by researchers [67]. In the proposed system, a low-cost solution based on analog sensors, such as probe LM35, is used with this aim. The LM35 series are precision integrated-circuit temperature sensors made by National Semiconductor [68]. The output voltage is linearly proportional to temperature (in Celsius), and this output does not require any external calibration [69]. For this specific application, output-voltage measurement was previously checked assuming that 0 V was proportional to 0 °C. In addition, several field-test campaign measurements were carried out by the authors to verify these temperature values. Estimated LM35 temperature values were compared to a calibrated RTD sensor, monitored by an Agilent Datalogger. Figure 4 shows the extensive results obtained in these field-test campaigns.

An STC-013-000 hall-effect sensor was used for the current measurements [70]. The inductive current sensor gives low-voltage output suitable to be collected by the Arduino. In line with [71], this sensor was chosen due to the extended work made available by the OpenEnergyMonitor Project [72],

and its accuracy and ease of use. Other STC-013 applications for residential smart-power management systems can be also found in the specific literature [73]. The same configuration was used at nodes 2 and 3 to measure grid parameters. Finally, voltage and current-sensor calibration was carried out by the authors at an electrical calibration laboratory. With this aim, a Transmille 3000A Series precision multiproduct calibrator was used (see Figure 5). Results are summarized in Table 2.

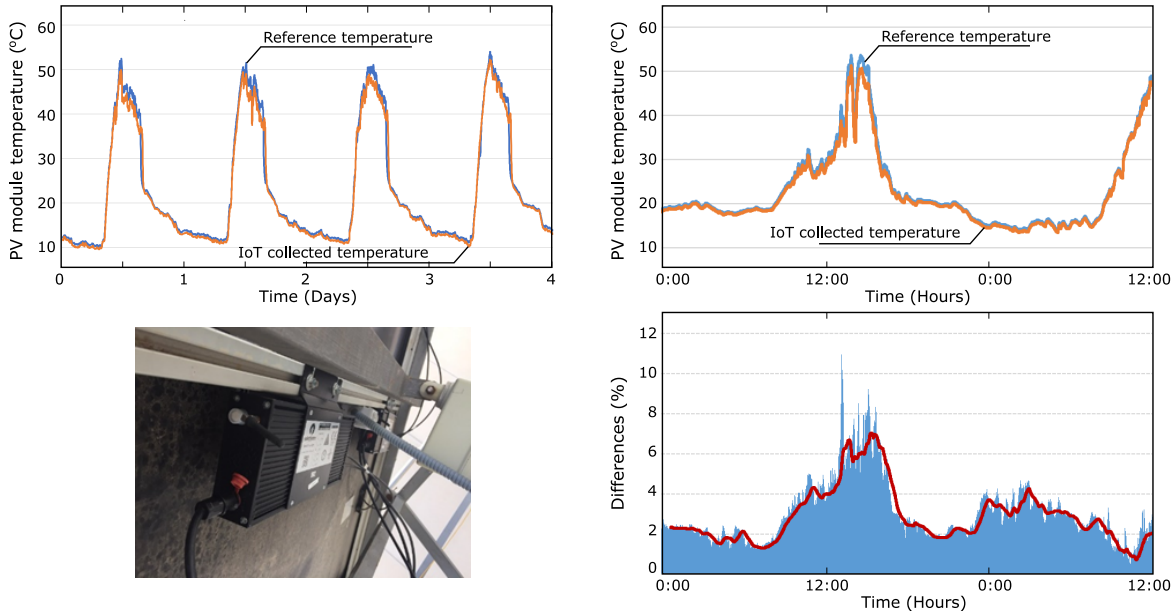

Figure 4. LM35 temperature validation. Example of field-test measurements.

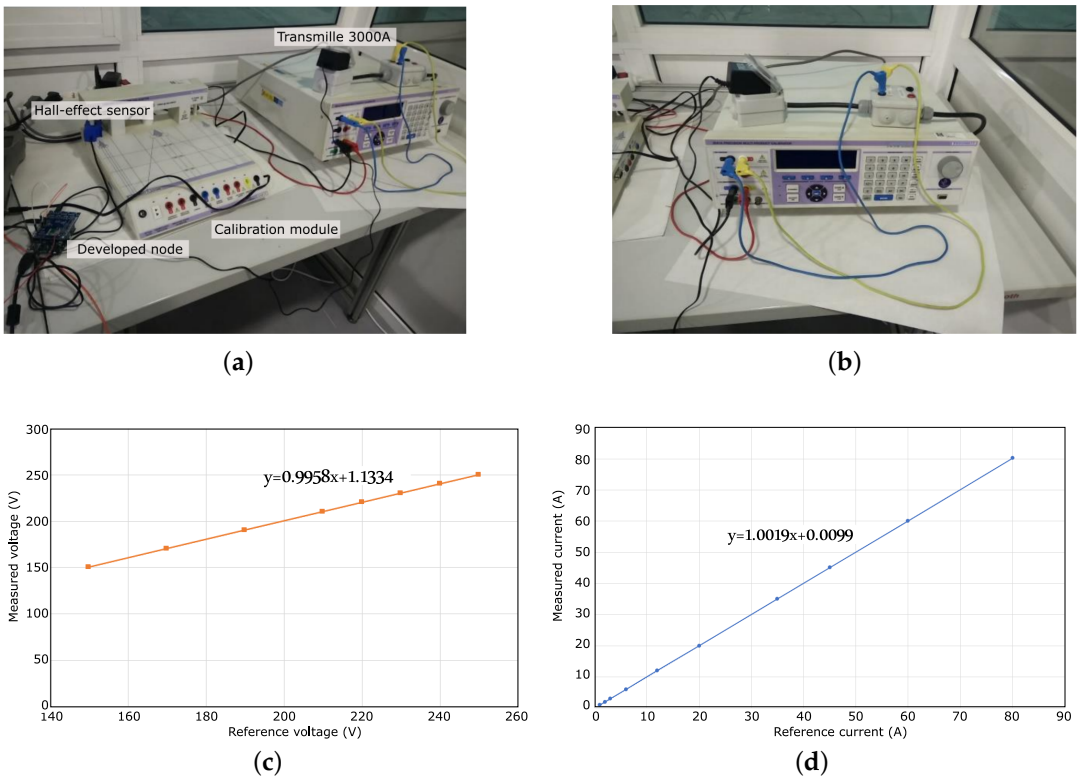

Figure 5. Voltage and current-sensor calibration: (**a**) calibration laboratory details; (**b**) multi-product calibrator equipment; (**c**) voltage calibration results; and (**d**) current calibration results.

Table 2. Calibration results.

Parameter	IEC-61724 Minimum Accuracy	Results
Current	1%	0.11%
Voltage	1%	0.04%
Power	2%	0.22%

2.4. Software Design

Layered architecture for IoT applications has usually been used to provide suitable frameworks for devices, data storage, and processing management. Under these requirements, several IoT architectures can be deployed at the device, gateway, and cloud layers [74]. Although there is no single consensus of IoT architecture, different contributions propose a three-layer architecture: perception, network, and application layers [75]. In our case, the first layer includes data-acquisition sensors according to IEC-61724 requirements. Access to the sensors and devices is coordinated by the device manager, which is responsible for maintaining a map of devices/sensors. Nodes collect electrical and environmental data with a 30 s sample-time interval. All data are then managed on a database, i.e., the network layer responsible for connecting to other servers or network devices. The connection from end units to the Internet or the Cloud is established at an edge system serving as communication gateway to bridge local networks with cloud systems [76]. Figure 6 summarizes the proposed global solution based on three-layer architecture.

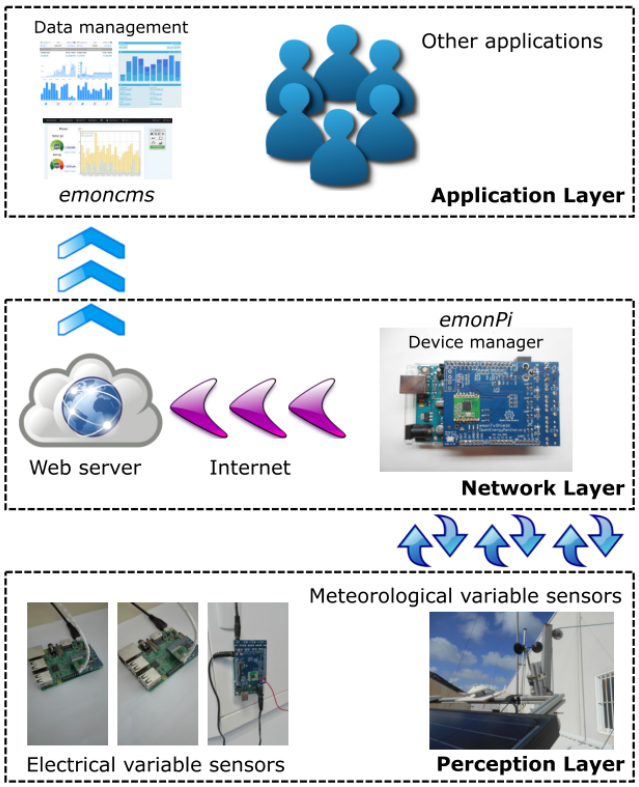

Figure 6. Three layers of Internet of Things architecture.

With regard to the application layer, OpenEnergyMonitor Project provides a popular low-cost energy and environmental monitoring solution based on *emonPi*. It has been recently used for the cost-saving potential of dynamic electricity rates [77], and for the management and administration of consumption records as well [78]. Under this framework, *emoncms* is an open-source web application for processing, logging, and visualizing energy and other environmental data [79]. A web-server

interface is included to provide external client connection and monitoring. Data management and visualization can also be suitable through smartphones, tablets, or devices supporting an Internet connection. This web application has thus been adapted and customized by the authors to process and visualize data collected from the nodes. Figure 7 gives some examples of the front-end web-application panel developed by the authors and available to users.

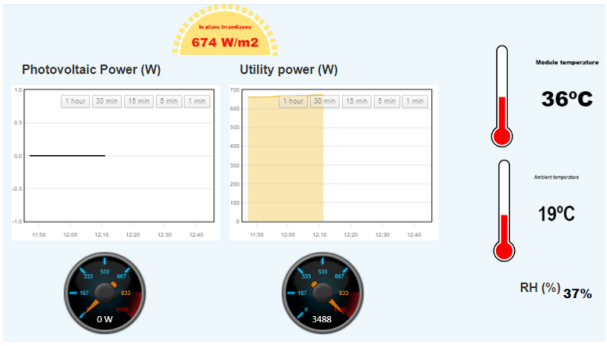

(**a**)

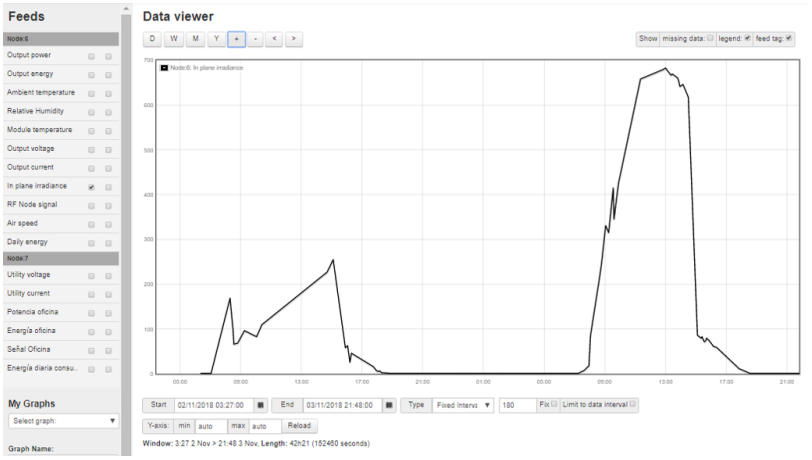

(**b**)

Figure 7. Customized *Emoncs* web application. Front-end example: (**a**) dashboard panel; and (**b**) PV data front-end.

2.5. Economic Evaluation: Cost-Effectiveness

According to the main objectives and characteristics discussed in Section 1, the proposed monitoring system is a flexible and low-cost solution. The flexibility is included through a distributed architecture, where the information is exchanged among nodes by means of a wireless protocol solution. To guarantee a low cost system, the selected hardware components are based on open-source projects with a relevant cost effectiveness threshold.

Table 3 summarizes the monitoring node cost. This node is in charge of collecting electrical and meteorological data. All hardware components are included according to the prototype node described in Sections 2.2 and 2.3. Table 4 gives the costs corresponding to the utility grid monitoring node. Finally, the costs of the gateway node are depicted in Table 5. The global costs of the proposed system is less than 100 Euro. Nevertheless, this cost can be reduced depending on the number of nodes to be produced and/or purchased. This cost is lower than other commercial solutions that usually provide less information and a reduced number of parameters, such as Efergy Pro [80], Victron Energy [81] or Solar Monitor [82]. Moreover, these commercial solutions usually need some additional components to store and manage data for subsequent analysis.

Table 3. PV module and meteorological data: monitoring node cost.

Description	Number	Unit Price (Euro)	Total Price (Euro)
emonTx Arduino Shield SMT	1	3.14	3.14
RFM69HW 433 Mhz Wireless Transceiver	1	1.85	1.85
PV module (5 Wp, 22 V, 30 W)	1	8.75	8.75
Cement resistance 5 W 10 Ω 10R 5%	1	0.13	0.13
AC-AC Power Supply Adapter	1	4.95	4.95
Non-invasive AC Sensor	1	4.31	4.31
30 A DC Hall Current Sensor	1	1.58	1.58
5 V DC USB Power Adapter	1	2.40	2.40
Digital Temperature and Humidity Sensor	1	0.71	0.71
LM35 TO-220 temperature	1	1.13	1.13
2.54 mm PCB Screw Connector	6	0.17	1.02
Aluminum Electrolytic Capacitor 400 V	2	0.02	0.04
Metal film resistance 1 M 1.2 M 1.5 M 2 M 2.2 M Ω	6	0.05	0.30
Prototype PCB Universal Board	1	0.35	0.35
Outdoor enclosure and wiring	1	3.50	3.50
Total			**34.16**

Table 4. Utility grid monitoring node cost.

Description	Number	Unit Price (Euro)	Total Price (Euro)
emonTx Arduino Shield SMT	1	3.14	3.14
RFM69HW 433Mhz Wireless Transceiver	1	1.94	1.94
AC-AC Power Supply Adapter	1	4.95	4.95
Non-invasive AC Sensor	1	4.31	4.31
5 V DC USB Power Adapter	1	2.06	2.06
2.54 mm PCB Screw Connector	6	0.17	1.02
Aluminum Electrolytic Capacitor 400 V	2	0.02	0.04
Metal Film Resistors 1%	8	0.03	0.24
Prototype PCB Universal Board	1	0.35	0.35
Outdoor enclosure and wiring	1	3.50	3.50
Total			**21.55**

Table 5. Gategaway node cost.

Description	Number	Unit Price (Euro)	Total Price (Euro)
Raspberry Pi 3 Model B Board	1	32.33	32.33
Sd card 32 Gb	1	3.27	3.27
5 V DC USB Power Adapter	1	2.06	2.06
Raspberry ABS Case Black Transparent	1	2.05	2.05
RFM69HW 433 Mhz Wireless Transceiver	1	1.85	1.85
RFM69 Breakout Board	1	1.00	1.00
Total			**42.56**

3. Results and Solution Assessment

From the calibrated hardware low-cost solution (Section 2.3) and the web-application described in Section 2.4, the proposed system has been tested and assessed in a Spanish PV power plant under real conditions. With this aim, PV Soltec Solar-trakers 250 Wp modules connected to the grid were monitored in the CETENMA SOLAR installations for several months [83]. To assess the proposed solution, all variables were also measured with standard equipment. Both sets of data were then compared to evaluate the suitability of the proposed low-cost solution. Indeed, solar irradiance was monitored by the Kipp and Zonen CM21 standard pyranometer, also used for calibration purposes in the specific literature [84]. Meteorogical data, including temperature, relative humidity, and wind speed, were collected using data-acquisition system NI PCI 6221. This data-acquisition

card has recently been used for monitoring PV electrical-power generation [85] and for relative humidity measurement [86]. Finally, electrical parameters were collected through a HAMEG HM8115-2 wattmeter and Fluke 434 Power grid analyzer. All variables were monitored and managed under an application developed by the authors under a *LabView* environment. Figure 8 depicts the monitored PV installation and the equipment used to assess the proposed low-cost solution.

As was previously mentioned, the proposed low-cost system was assessed for several months to provide the suitability of this solution under real PV-installation conditions. From the monitored variables, the proposed low-cost system was also able to detect possible PV solar-panel abnormalities in line with other contributions [87]. Figure 9 compares temperature and solar-irradiance data collected by the proposed low-cost solution and standard equipment. In addition, Figure 10 shows the PV-generated power data from the low-cost solution and the commercial data-logger system, as well as the AC grid voltage. Differences between both collected results have been determined and compared under IEC-61724 requirements. Table 6 summarizes these differences, including limits of IEC-61724 permissible errors and providing the suitability of the present solution.

Table 6. Results.

Parameter	IEC61724 Required Accuracy	Results
Current	1%	0.81%
Voltage	1%	0.74%
Power	2%	0.55%

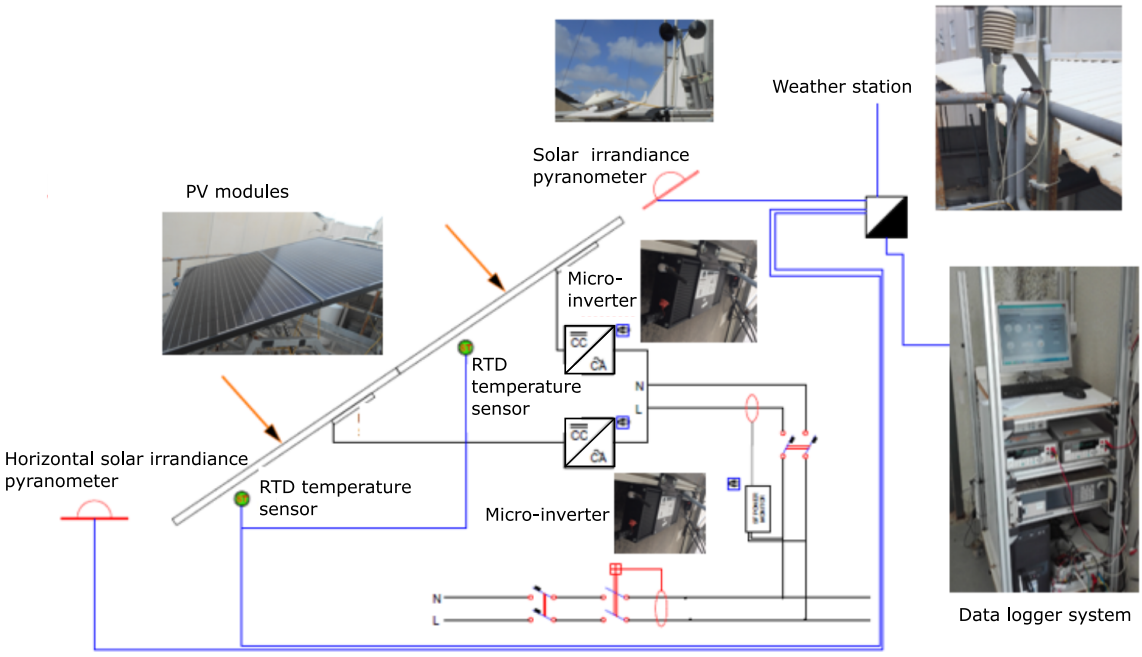

Figure 8. Photovoltaic (PV) module installation: monitoring and assessment.

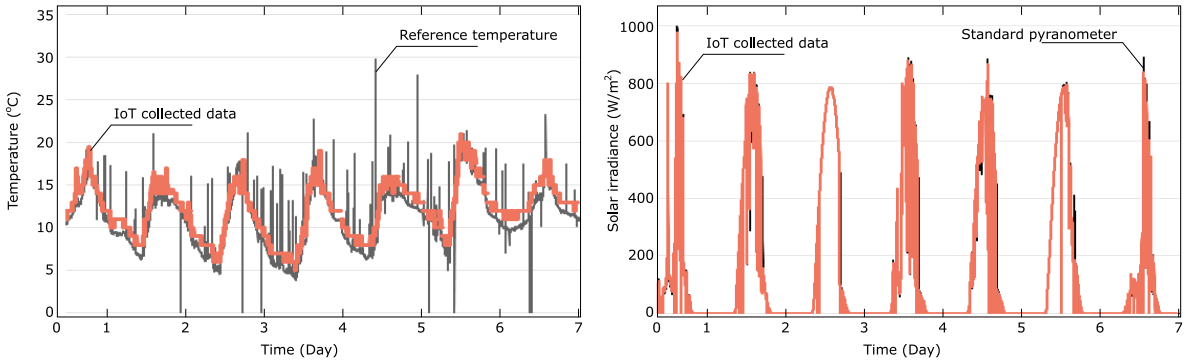

Figure 9. Temperature and solar-irradiance data comparison: low-cost proposed system vs. standard equipment.

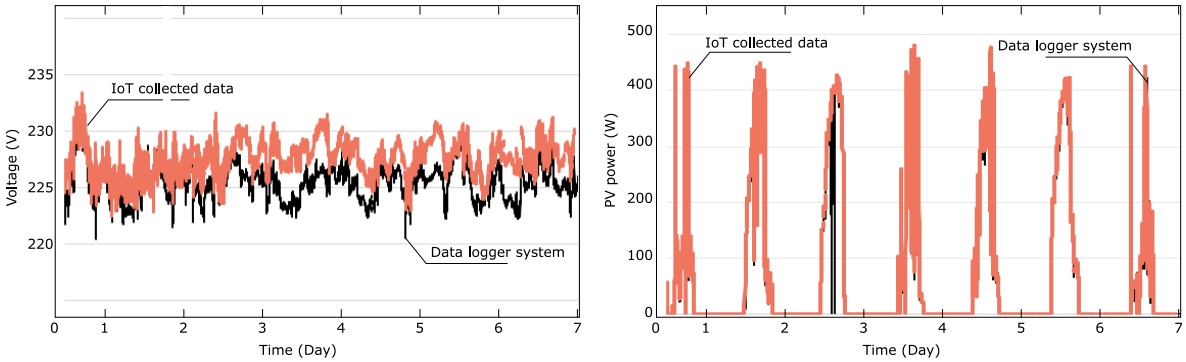

Figure 10. PV-generated power comparison: low-cost proposed system vs. data-logger comparison.

The proposed system was also implemented in a real PV solar installation (5 kWp) to monitor and collect electrical and meteorological data during different weeks. This PV power plant is an over-roof installation connected to the grid and located in the Universidad Politécnica de Cartagena, southeast Spain. It involves 18 PV modules Saclima AMS 310 Wp comprising two strings connected in parallel. The selected inverter was Ingeteam 4.6 TL 5 kW. The power demand of this building is always considerably higher than the maximum active power supplied by this PV power plant. Therefore, the generated active power is totally used to reduce the active power demanded by the building.

By considering meteorological and electrical collected data, Figure 11 summarizes some details of the proposed solution implementation in this real PV installation connected to the grid. Nodes for electric and meteorological monitored data are included in the figure according to the isolation levels required by the nodes under outdoor conditions. PV-module variables are also monitored. As an example of the PV module collected data, Figure 12 shows electrical data corresponding to both DC and AC variables. PV-module DC current and global DC current provided by the PV installation are also shown. Figure 13 compares irradiance levels and the active power generated by the PV installations, which are also monitored by the proposed solution. The collected PV-module and ambient-temperature data are also included in the figure. According to these results, the suitability and flexibility of this solution is shown to be able to be applied not only in new installations, but also in PV power plants currently in force.

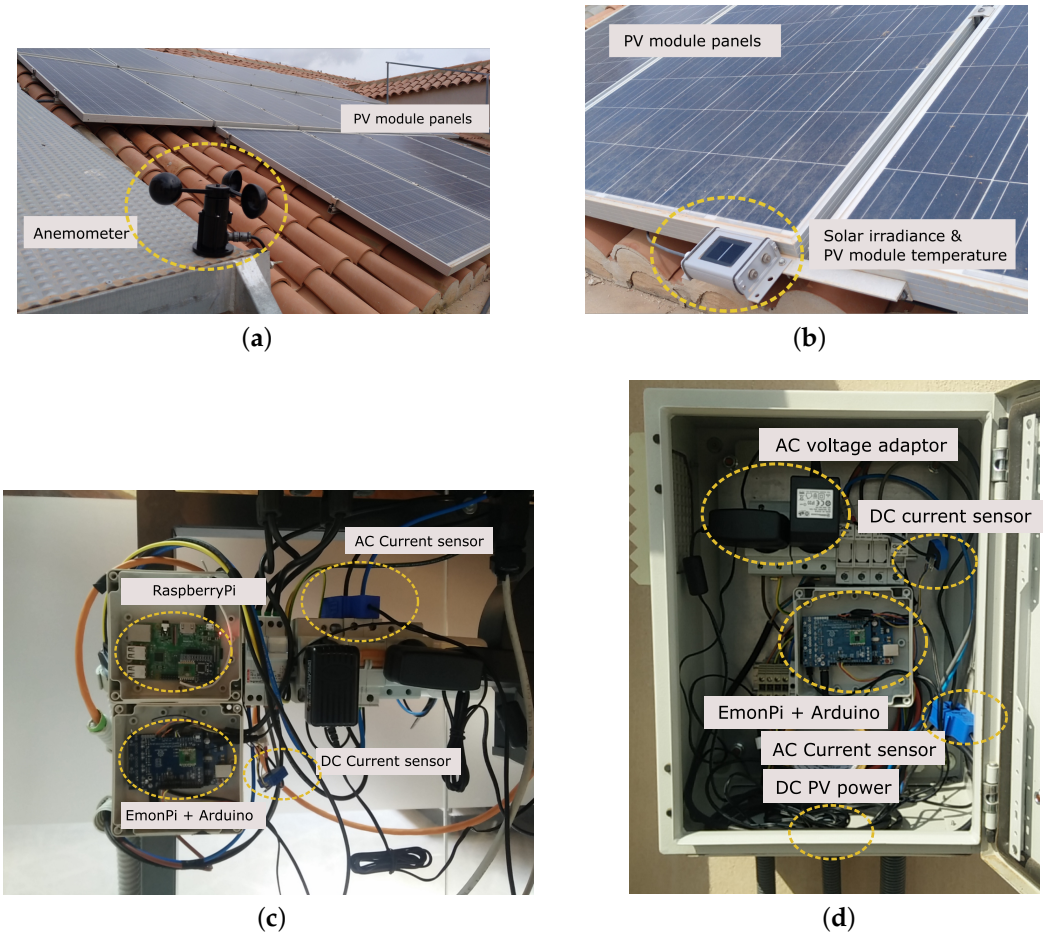

Figure 11. Low-cost proposed system: implementation and details: (**a**) meteorological data monitor; (**b**) DC electrical data (outdoor node); (**c**) AC electrical data (indoor node); and (**d**) DC electrical data (outdoor node).

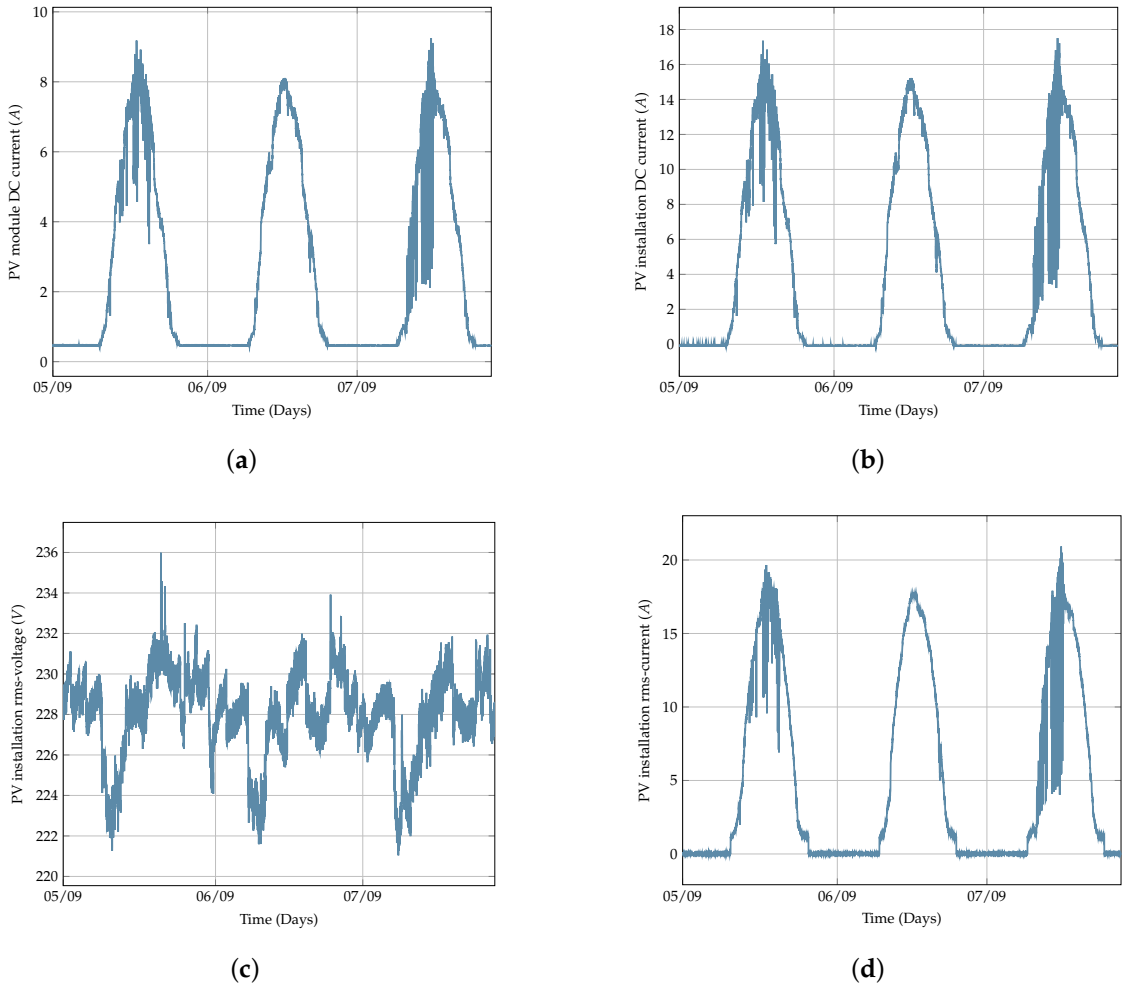

Figure 12. PV installation connected to the grid: AC and DC electrical variables: (**a**) PV module DC current; (**b**) PV installation DC current; (**c**) PV installation AC voltage (rms); and (**d**) PV installation AC current (rms).

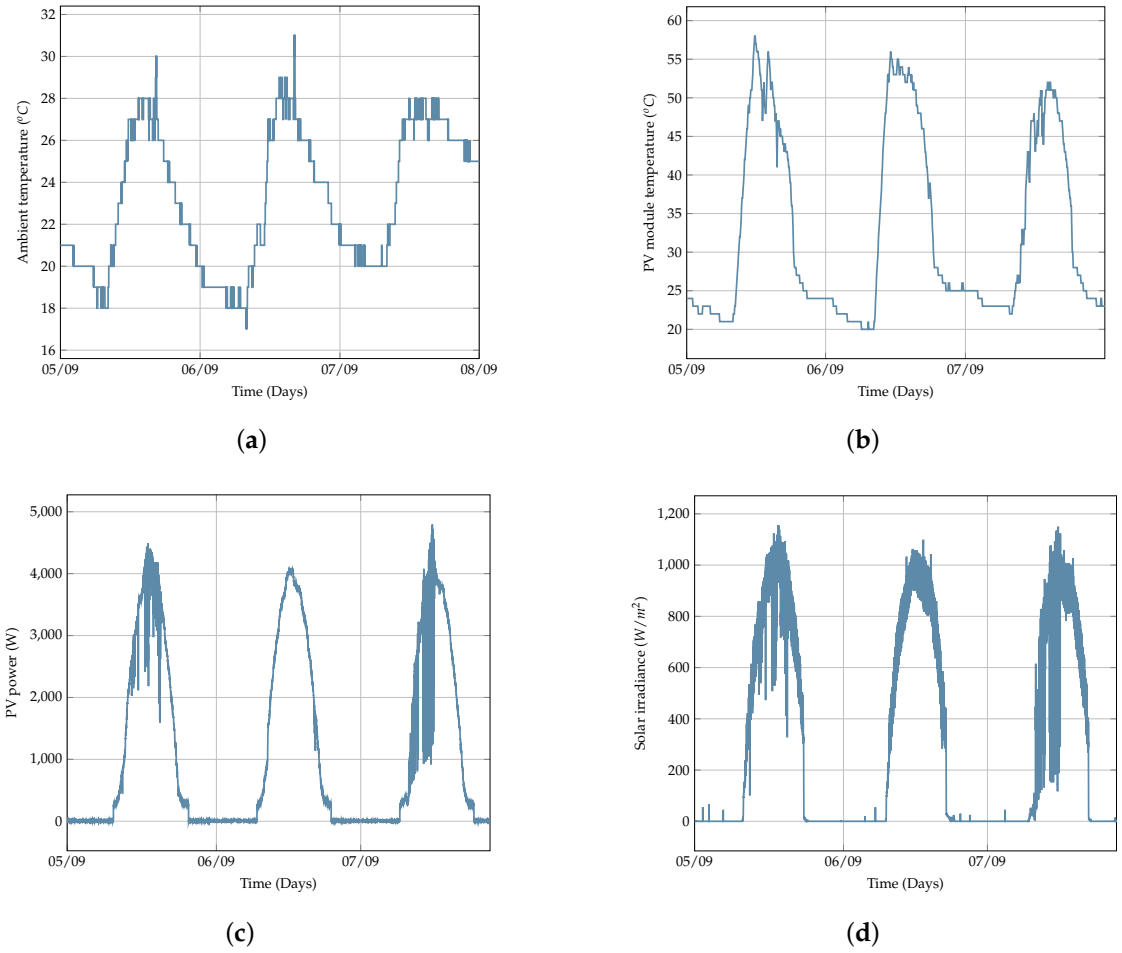

Figure 13. PV installation connected to the grid: monitored power and meteorological data: (**a**) ambient temperature; (**b**) PV module temperature; (**c**) PV installation: power; and (**d**) solar irradiance.

4. Conclusions

An alternative monitoring system for PV installations is described and assessed. The solution is based on a low-cost and open-source system according to IEC-61724 requirements. The proposed monitoring system collects both meteorological and electrical data at the PV-module level, providing a flexible and wireless architecture capable of being implemented in most PV installations. Sensors have been calibrated in a laboratory environment and the results fulfill the IEC-61724 minimum-accuracy values in terms of current, voltage, and power. PV-module temperature is also available from the proposed solution, with an average error lower than 4%. With regard to economic impact, the proposed monitoring solution cost is lower than current commercial solutions. Indeed, detailed cost information is given in the paper, including sensors and hardware requirements for the gateway and the corresponding nodes.

Different field-test campaigns have been carried out in Spanish PV installations connected to the grid. To assess the proposed solution, monitored data have been compared to data collected from commercial data-logger equipment, obtaining errors lower than 2% for meteorological and electrical variables. Extensive results are also included in the paper. Finally, a web-server interface has also been included to provide external client connection and monitoring. It is based on *emoncms*, an open-source web application for processing, logging, and visualizing energy and other environmental data.

Author Contributions: Data curation, J.M.P.-P., G.S.-N. and M.C.B.; Formal analysis, A.M.-A.; Funding acquisition, A.M.-A.; Investigation, G.S.-N.; Resources, J.M.P.-P.; Software, G.S.-N.; Supervision, A.M.-A.; Visualization, M.C.B; Writing–original draft, A.M.-A.; Writing–review and editing, A.M.-A.

Funding: This work was partially supported by the Spanish agreement (2017) between the Institute for Development of the Region of Murcia (INFO) and the Technological Center for Energy and Environment (CETENMA). The paper includes results of the activity conducted under the *"Research Program for Groups of Scientific Excellence at Region of Murcia (Spain)"*, the Seneca Foundation, and the Agency for Science and Technology of the Region of Murcia (Spain).

Acknowledgments: The authors thank the staff of the Universidad Politécnica de Cartagena (Spain) for services and facilities provided.

Conflicts of Interest: The authors declare no conflict of interest.

References

1. International Energy Agency. *Perspectives for the Energy Transition: Investment Needs for a Low-Carbon Energy System*; Technical Report, OECD/IEA and IRENA 2017; IEA Publications, Printed by German Federal Ministry for Economic Affairs and Energy, March 2017. Available online: http://www.irena.org/DocumentDownloads/Publications/Perspectives_for_the_Energy_Transition_2017.pdf (accessed on 27 October 2018).
2. Nieto, J.; Carpintero, O.; Miguel, L. Less than 2C? An Economic-Environmental Evaluation of the Paris Agreement. *Ecol. Econ.* **2018**, *146*, 69–84. [CrossRef]
3. IRENA. Solar PV Costs 2010–2015. Available online: http://www.irena.org/costs/ (accessed on 27 October 2018).
4. IRENA. *Renewable Capacity Statistics 2018*; International Renewable Energy Agency (IRENA): Abu Dhabi, UAE, 2018. Available online: http://irena.org/-/media/Files/IRENA/Agency/Publication/2018/Mar/IRENA_RE_Capacity_Statistics_2018.pdf (accessed on 27 October 2018). ISBN: 978-92-9260-057-0.
5. Best, R.; Burke, P.J. Adoption of solar and wind energy: The roles of carbon pricing and aggregate policy support. *Energy Policy* **2018**, *118*, 404–417. [CrossRef]
6. Kraan, O.; Kramer, G.; Nikolic, I. Investment in the future electricity system—An agent-based modelling approach. *Energy* **2018**, *151*, 569–580. [CrossRef]
7. Trujillo-Baute, E.; del Rio, P.; Mir-Artigues, P. Analysing the impact of renewable energy regulation on retail electricity prices. *Energy Policy* **2018**, *114*, 153–164. [CrossRef]
8. Ellabban, O.; Abu-Rub, H.; Blaabjerg, F. Renewable energy resources: Current status, future prospects and their enabling technology. *Renew. Sustain. Energy Rev.* **2014**, *39*, 748–764. [CrossRef]
9. Pietzcker, R.C.; Ueckerdt, F.; Carrara, S.; de Boer, H.S.; Després, J.; Fujimori, S.; Johnson, N.; Kitous, A.; Scholz, Y.; Sullivan, P.; et al. System integration of wind and solar power in integrated assessment models: A cross-model evaluation of new approaches. *Energy Econ.* **2017**, *64*, 583–599. [CrossRef]
10. Kamaruzzaman, Z. Effect of grid–connected photovoltaic systems on static and dynamic voltage stability with analysis techniques—A review. *Przegląd Elektrotech.* **2015**, *1*, 136–140. [CrossRef]
11. Hung, D.Q.; Shah, M.R.; Mithulananthan, N. Technical Challenges, Security and Risk in Grid Integration of Renewable Energy. In *Smart Power Systems and Renewable Energy System Integration*; Jayaweera, D., Ed.; Springer International Publishing: Cham, Switzerland, 2016; pp. 99–118. [CrossRef]
12. Chiandone, M.; Sulligoi, G.; Massucco, S.; Silvestro, F. Hierarchical Voltage Regulation of Transmission Systems with Renewable Power Plants: An overview of the Italian case. In Proceedings of the 3rd IET Renewable Power Generation Conference, Naples, Italy, 24–25 September 2014; pp. 261–265.
13. Bonfiglio, A.; Brignone, M.; Delfino, F.; Procopio, R. Optimal Control and Operation of Grid-Connected Photovoltaic Production Units for Voltage Support in Medium-Voltage Networks. *IEEE Trans. Sustain. Energy* **2014**, *5*, 254–263. [CrossRef]
14. Weckx, S.; D'hulst, R.; Driesen, J. Locational Pricing to Mitigate Voltage Problems Caused by High PV Penetration. *Energies* **2015**, *8*, 4607–4628. [CrossRef]
15. Smith, J.C.; Milligan, M.R.; DeMeo, E.A.; Parsons, B. Utility Wind Integration and Operating Impact State of the Art. *IEEE Trans. Power Syst.* **2007**, *22*, 900–908. [CrossRef]
16. Shi, J.; Lee, W.; Liu, Y.; Yang, Y.; Wang, P. Forecasting Power Output of Photovoltaic Systems Based on Weather Classification and Support Vector Machines. *IEEE Trans. Ind. Appl.* **2012**, *48*, 1064–1069. [CrossRef]

17. Bracale, A.; Caramia, P.; Carpinelli, G.; Di Fazio, A.R.; Ferruzzi, G. A Bayesian Method for Short-Term Probabilistic Forecasting of Photovoltaic Generation in Smart Grid Operation and Control. *Energies* **2013**, *6*, 733–747. [CrossRef]
18. Zamo, M.; Mestre, O.; Arbogast, P.; Pannekoucke, O. A benchmark of statistical regression methods for short-term forecasting of photovoltaic electricity production, part I: Deterministic forecast of hourly production. *Sol. Energy* **2014**, *105*, 792–803. [CrossRef]
19. Petrone, G.; Spagnuolo, G.; Teodorescu, R.; Veerachary, M.; Vitelli, M. Reliability Issues in Photovoltaic Power Processing Systems. *IEEE Trans. Ind. Electron.* **2008**, *55*, 2569–2580. [CrossRef]
20. Colak, I.; Sagiroglu, S.; Fulli, G.; Yesilbudak, M.; Covrig, C.F. A survey on the critical issues in smart grid technologies. *Renew. Sustain. Energy Rev.* **2016**, *54*, 396–405. [CrossRef]
21. Mahjoubi, A.; Mechlouch, R.; Brahim, A. A Low Cost Wireless Data Acquisition System for a Remote Photovoltaic (PV) Water Pumping System. *Energies* **2011**, *4*, 68–89. [CrossRef]
22. Han, J.; Choi, C.; Park, W.; Lee, I.; Kim, S. PLC-based photovoltaic system management for smart home energy management system. *IEEE Trans. Consum. Electron.* **2014**, *60*, 184–189. [CrossRef]
23. Han, J.; Jeong, J.D.; Lee, I.; Kim, S.H. Low-cost monitoring of photovoltaic systems at panel level in residential homes based on power line communication. *IEEE Trans. Consum. Electron.* **2017**, *63*, 435–441. [CrossRef]
24. Wang, Y.; Wen, H.; Hou, X.; Tang, H.; Sun, H.; Zheng, K.; Li, S. Comparison of Differential-Mode and Mixed-Mode Conducted Emission for Household Appliances in Power-Line Communication System. *IEEE Trans. Electromagn. Compat.* **2017**, *59*, 2023–2028. [CrossRef]
25. Pop-Calimanu, I.M.; Anna, T.; Popescu, V.; Muntean, G. A Low Cost System for Testing and Monitoring the Performance of Photovoltaic Module. *Adv. Electr. Comput. Eng.* **2013**, *13*, 93–98. [CrossRef]
26. Dhimish, M.; Holmes, V.; Mehrdadi, B. Grid-connected PV monitoring system (GCPV-MS). In Proceedings of the 2016 4th International Symposium on Environmental Friendly Energies and Applications (EFEA), Belgrade, Serbia, 14–16 September 2016; pp. 1–6. [CrossRef]
27. Papageorgas, P.; Piromalis, D.; Antonakoglou, K.; Vokas, G.; Tseles, D.; Arvanitis, K. Smart Solar Panels: In-situ Monitoring of Photovoltaic Panels based on Wired and Wireless Sensor Networks. *Energy Procedia* **2013**, *36*, 535–545. [CrossRef]
28. Shariff, F.; Rahim, N.A.; Hew, W.P. ZigBee-based data acquisition system for online monitoring of grid-connected photovoltaic system. *Expert Syst. Appl.* **2015**, *42*, 1730–1742. [CrossRef]
29. Batista, N.; Melicio, R.; Matias, J.; Catalao, J. Photovoltaic and wind energy systems monitoring and building/home energy management using ZigBee devices within a smart grid. *Energy* **2013**, *49*, 306–315. [CrossRef]
30. Fuentes, M.; Vivar, M.; Burgos, J.; Aguilera, J.; Vacas, J. Design of an accurate, low-cost autonomous data logger for PV system monitoring using Arduino^{TM} that complies with IEC standards. *Sol. Energy Mater. Sol. Cells* **2014**, *130*, 529–543. [CrossRef]
31. Madeti, S.R.; Singh, S. Monitoring system for photovoltaic plants: A review. *Renew. Sustain. Energy Rev.* **2017**, *67*, 1180–1207. [CrossRef]
32. Molina-García, A.; Campelo, J.; Blanc, S.; Serrano, J.; García-Sánchez, T.; Bueso, M. A Decentralized Wireless Solution to Monitor and Diagnose PV Solar Module Performance Based on Symmetrized-Shifted Gompertz Functions. *Sensors* **2015**, *15*, 18459–18479. [CrossRef] [PubMed]
33. Friansa, K.; Haq, I.N.; Santi, B.M.; Kurniadi, D.; Leksono, E.; Yuliarto, B. Development of Battery Monitoring System in Smart Microgrid Based on Internet of Things (IoT). *Procedia Eng.* **2017**, *170*, 482–487. [CrossRef]
34. Wang, Y. Design and Implementation of a Wireless Sensor Network Node Based on Arduino. *Int. J. Online Eng.* **2017**, *13*, 128. [CrossRef]
35. Sipani, J.P.; Patel, R.H.; Upadhyahya, T.; Desai, A. Wireless Sensor Network for Monitoring & Control of Environmental Factors using Arduino. *Int. J. Interact. Mob. Technol.* **2018**, *12*, 15. [CrossRef]
36. Raspberry Pi Foundation. Available online: https://www.raspberrypi.org/ (accessed on 27 October 2018).
37. Cleevely, D. *Annual Review*; Technical Report; Raspberry-Pi Foundation: Cambridge, UK, 2017.
38. Anire, R.B.; Cruz, F.R.G.; Agulto, I.C. Environmental wireless sensor network using raspberry Pi 3 for greenhouse monitoring system. In Proceedings of the 9th IEEE International Conference on Humanoid, Nanotechnology, Information Technology, Communication and Control, Environment and Management, Manila, Philippines, 1–3 December 2017. [CrossRef]

39. Othman, N.A.; Zainodin, M.R.; Anuar, N.; Damanhuri, N.S. Remote monitoring system development via Raspberry-Pi for small scale standalone PV plant. In Proceedings of the 2017 7th IEEE International Conference on Control System, Computing and Engineering, Penang, Malaysia, 24–26 November 2017. [CrossRef]
40. Pereira, R.I.; Dupont, I.M.; Carvalho, P.C.; Jucá, S.C. IoT embedded linux system based on Raspberry Pi applied to real-time cloud monitoring of a decentralized photovoltaic plant. *Measurement* **2018**, *114*, 286–297. [CrossRef]
41. Lobaccaro, G.; Carlucci, S.; Lofstrom, E. A Review of Systems and Technologies for Smart Homes and Smart Grids. *Energies* **2016**, *9*, 348. [CrossRef]
42. Lu, X.; Wang, S.; Li, W.; Jiang, P.; Zhang, C. Development of a WSN based real time energy monitoring platform for industrial applications. In Proceedings of the 19th International Conference on Computer Supported Cooperative Work in Design, Calabria, Italy, 6–8 May 2015; pp. 337–342. [CrossRef]
43. Openenergymonitor. Available online: https://openenergymonitor.org/ (accessed on 27 October 2018).
44. HOPE MicroElectronics Co., Ltd. *RFM69CW Datasheet*; Technical Report; Available online: http://www.hoperf.com/upload/rf/RFM69CW-V1.1.pdf (accessed on 27 October 2018).
45. Kumar, A.; Hancke, G.P. Energy Efficient Environment Monitoring System Based on the IEEE 802.15.4 Standard for Low Cost Requirements. *IEEE Sens. J.* **2014**, *14*, 2557–2566. [CrossRef]
46. Fuertes, W.; Carrera, D.; Villacís, C.; Toulkeridis, T.; Galárraga, F.; Torres, E.; Aules, H. Distributed System as Internet of Things for a New Low-Cost, Air Pollution Wireless Monitoring on Real Time. In Proceedings of the 2015 IEEE/ACM 19th International Symposium on Distributed Simulation and Real Time Applications (DS-RT), Chengdu, China, 14–16 October 2015; pp. 58–67. [CrossRef]
47. Ram, S.A.; Siddarth, N.; Manjula, N.; Rogan, K.; Srinivasan, K. Real-time automation system using Arduino. In Proceedings of the 2017 International Conference on Innovations in Information, Embedded and Communication Systems (ICIIECS), Coimbatore, India, 17–18 March 2017; pp. 1–5. [CrossRef]
48. Nisio, A.D.; Noia, T.D.; Carducci, C.G.C.; Spadavecchia, M. Design of a low cost multipurpose wireless sensor network. In Proceedings of the 2015 IEEE International Workshop on Measurements Networking (M&N), Coimbra, Portugal, 12–13 October 2015; pp. 1–6. [CrossRef]
49. Rahim, A.; Ali, Z.; Bharti, R.; Sabeel, S.; Ramya, B.K. Design and Implementation of a Low Cost Wireless Sensor Network using Arduino and nRF24L01(+). *Int. J. Sci. Res. Eng. Technol.* **2016**, *5*, 307–309.
50. IEC 61724-1. *Photovoltaic System Performance Monitoring—Guidelines for Measurement, Data Exchange, and Analysis (Part 1)*; Technical Report 1; International Electrotechnical Commission (IEC)': Switzerland, Geneva, 2017.
51. del Ama Gonzalo, F.; Hernandez, J.A.; Moreno, B. Wireless low cost temperature and humidity sensors with PV microcells. Determination of design parameters by means of experimental measurements. In Proceedings of the 2016 5th International Conference on Electronic Devices, Systems and Applications (ICEDSA), Ras Al Khaimah, UAE, 6–8 December 2016; pp. 1–4. [CrossRef]
52. Priya, C.G.; AbishekPandu, M.; Chandra, B. Automatic plant monitoring and controlling system over GSM using sensors. In Proceedings of the 2017 IEEE Technological Innovations in ICT for Agriculture and Rural Development (TIAR), Chennai, India, 7–8 April 2017; pp. 173–176. [CrossRef]
53. Hulea, M.; Mois, G.; Folea, S.; Miclea, L.; Biscu, V. Wi-sensors: A low power Wi-Fi solution for temperature and humidity measurement. In Proceedings of the IECON 2013 39th Annual Conference of the IEEE Industrial Electronics Society, Vienna, Austria, 10–13 November 2013; pp. 4011–4015. [CrossRef]
54. Saha, S.; Majumdar, A. Data centre temperature monitoring with ESP8266 based Wireless Sensor Network and cloud based dashboard with real time alert system. In Proceedings of the 2017 Devices for Integrated Circuit (DevIC), Kalyani, India, 23–24 March 2017; pp. 307–310. [CrossRef]
55. Vicente, E.M.; Moreno, R.L.; Ribeiro, E.R. MPPT Technique Based on Current and Temperature Measurements. *Int. J. Photoenergy* **2015**, 1–9. [CrossRef]
56. Muellejans, H.; Zaaiman, W.; Dunlop, E.; Ossenbrink, H.A. Calibration of photovoltaic reference cells by global sunlight method. *Metrologia* **2005**, *42*, 360–367. [CrossRef]
57. Stokler, S.; Schillings, C.; Kraas, B. Solar resource assessment study for Pakistan. *Renew. Sustain. Energy Rev.* **2016**, *58*, 1184–1188. [CrossRef]
58. Hussain, F.; Othman, M.; Yatim, B.; Ruslan, H.; Sopian, K.; Anuar, Z.; Khairuddin, S. An improved design of photovoltaic/thermal solar collector. *Sol. Energy* **2015**, *122*, 885–891. [CrossRef]

59. Skoplaki, E.; Palyvos, J. Operating temperature of photovoltaic modules: A survey of pertinent correlations. *Renew. Energy* **2009**, *34*, 23–29. [CrossRef]
60. Kaldellis, J.; Kapsali, M.; Kavadias, K. Temperature and wind speed impact on the efficiency of PV installations. Experience obtained from outdoor measurements in Greece. *Renew. Energy* **2014**, *66*, 612–624. [CrossRef]
61. Copper, J.; Bruce, A.; Spooner, T.; Calais, M.; Pryor, T.; Watt, M. *Australian Technical Guidelines for Monitoring and Analysing Photovoltaic Systems*; Technical Report; Australian PV Institute (APVI): Sydney, Australia, 2013. [CrossRef]
62. Schwingshackl, C.; Petitta, M.; Wagner, J.E.; Belluardo, G.; Moser, D.; Castelli, M.; Zebisch, M.; Tetzlaff, A. Wind effect on PV module temperature: Analysis of different techniques for an accurate estimation. *Energy Procedia* **2013**, *40*, 77–86. [CrossRef]
63. Skoplaki, E.; Palyvos, J. On the temperature dependence of photovoltaic module electrical performance: A review of efficiency/power correlations. *Sol. Energy* **2009**, *83*, 614–624. [CrossRef]
64. Dubey, S.; Sarvaiya, J.N.; Seshadri, B. Temperature Dependent Photovoltaic (PV) Efficiency and Its Effect on PV Production in the World—A Review. *Energy Procedia* **2013**, *33*, 311–321. [CrossRef]
65. Skoplaki, E.; Boudouvis, A.; Palyvos, J. A simple correlation for the operating temperature of photovoltaic modules of arbitrary mounting. *Sol. Energy Mater. Sol. Cells* **2008**, *92*, 1393–1402. [CrossRef]
66. Emery, K.; Smith, R. *Monitoring System Performance*; Technical Report; National Renewable Energy Laboratory (NREL): Golden, CO, USA, 2011.
67. Yaácob, M.E.; Hizam, H.; Radzi, M.A.M.; Kadir, M. Field Measurement of PV Array Temperature for Tracking and Concentrating 1 kWp Generators Installed in Malaysia. *Int. J. Photoenergy 2013*, 1–8. [CrossRef]
68. Arunachalam, B.; Devi, R.; Patvardhan, A.; Aiswarya, R.; Prasen, V. Embedded Temperature Monitoring and Control Unit. In Proceedings of the International Conference on Recent Trends in Information, Telecommunication and Computing, Kerala, India, 12–13 March 2010; pp. 293–297. [CrossRef]
69. Ozemoya, A.; Swart, A.; Pienaar, H.; Schoeman, R. Factors impacting on the surface temperature of a PV panel. In Proceedings of the Southern Africa Telecommunication Networks and Applications Conference (SATNAC), Hermanus, South Africa, 6–9 Setptember 2013; pp. 1–5.
70. Dechang Electric Co. *SCT013-000 Current Transformer Datasheet*; Technical Report; Dechang Electric Co., Ltd. (CN): Shenzhen, China, 2015.
71. Pocero, L.; Amaxilatis, D.; Mylonas, G.; Chatzigiannakis, I. Open source IoT meter devices for smart and energy-efficient school buildings. *HardwareX* **2017**, *1*, 54–67. [CrossRef]
72. Openenergymonitor. Measuring AC Voltage with an AC to AC Power Adapter. Available online: https://learn.openenergymonitor.org/electricity-monitoring/voltage-sensing/measuring-voltage-with-an-acac-power-adapter (accessed on 27 October 2018).
73. Gabriele, T.; Pantoli, L.; Stornelli, V.; Chiulli, D.; Muttillo, M. Smart power management system for home appliances and wellness based on wireless sensors network and mobile technology. In Proceedings of the XVIII AISEM Annual Conference, Trento, Italy, 3–5 February 2015; pp. 1–4. [CrossRef]
74. Gyrard, A.; Datta, S.K.; Bonnet, C.; Boudaoud, K. A Semantic Engine for Internet of Things: Cloud, Mobile Devices and Gateways. In Proceedings of the 9th International Conference on Innovative Mobile and Internet Services in Ubiquitous Computing, Santa Cantarina, Brazil, 8–10 July 2015; pp. 336–341. [CrossRef]
75. Sethi, P.; Sarangi, S. Internet of Things: Architectures, Protocols, and Applications. *J. Electr. Comput. Eng.* **2017**, 1–25. [CrossRef]
76. Lee, Y.; Nair, S. A Smart Gateway Framework for IOT Services. In Proceedings of the 2016 IEEE International Conference on Internet of Things (iThings) and IEEE Green Computing and Communications (GreenCom) and IEEE Cyber, Physical and Social Computing (CPSCom) and IEEE Smart Data (SmartData), Chengdu, China, 15–18 December 2016; pp. 107–114. [CrossRef]
77. Vaupel, S.; Segura, L.L.O.; Vaupel, H. SmartCalculator: The individual and general cost-saving potential of dynamic electricity rates. In Proceedings of the 2016 IEEE International Conference on Industrial Technology (ICIT), Taipei, Taiwan, 14–17 March 2016; pp. 558–563. [CrossRef]
78. Sacoto-Cabrera, E.; Rodriguez-Bustamante, J.; Gallegos-Segovia, P.; Arevalo-Quishpi, G.; León-Paredes, G. Internet of Things: Informatic system for metering with communications MQTT over GPRS for smart meters. In Proceedings of the CHILEAN Conference on Electrical, Electronics Engineering, Information and Communication Technologies, Pucon, Chile, 18–20 October 2017; pp. 1–6. [CrossRef]

79. Openenergymonitor. Emoncms. Available online: http://emoncms.org (accessed on 27 October 2018).
80. Efergy. Efergy Pro. Available online: https://efergy.com/efergypro/ (accessed on 27 October 2018).
81. Victron Energy. Available online: https://www.victronenergy.com/ (accessed on 27 October 2018).
82. Solar Monitor. Available online: https://shop.solarmonitor.cz/en/7-solar-monitor-2 (accessed on 27 October 2018).
83. Soltec. *Solar-Traker Soltec*. 2017. Available online: http://www.soltec.com (accessed on 27 October 2018).
84. Martinez, M.; Andujar, J.; Enrique, J. A New and Inexpensive Pyranometer for the Visible Spectral Range. *Sensors* **2009**, *9*, 4615–4634. [CrossRef] [PubMed]
85. Bayrak, G.; Cebeci, M. Monitoring a grid connected PV power generation system with labview. In Proceedings of the 2013 International Conference on Renewable Energy Research and Applications (ICRERA), Madrid, Spain, 20–23 October 2013; pp. 562–567. [CrossRef]
86. Ocoleanu, C. Solution for humidity measurement using NI PCI 6221 and LabVIEW. In Proceedings of the IEEE 2nd International Forum on Research and Technologies for Society and Industry Leveraging a better tomorrow (RTSI), Bologna, Italy, 7–9 September 2016; pp. 1–5. [CrossRef]
87. Daliento, S.; Chouder, A.; Guerriero, P.; Pavan, A.M.; Mellit, A.; Moeini, R.; Tricoli, P. Monitoring, Diagnosis, and Power Forecasting for Photovoltaic Fields: A Review. *Int. J. Photoenergy* **2017**, 1–13. [CrossRef]

4.2. An alternative internet-of-things solution based on LoRa for PV power plants: data monitoring and management

Información adicional:

- Revista: Energies 12, no. 5: 881
- DOI: 10.3390/en12050881
- Fecha de publicación: Marzo 2019
- Disponible en: `https://www.mdpi.com/1996-1073/12/5/881`
- Referencia: [42]
  Paredes-Parra, J.M.; García-Sánchez, A.J.; Mateo-Aroca, A.; Molina-García, Á. An Alternative Internet-of-Things Solution Based on LoRa for PV Power Plants: Data Monitoring and Management. Energies 2019, 12, 881.
  `https://doi.org/10.3390/en12050881`

energies

MDPI

Article

An Alternative Internet-of-Things Solution Based on LoRa for PV Power Plants: Data Monitoring and Management

José Miguel Paredes-Parra [1], Antonio Javier García-Sánchez [2] and Antonio Mateo-Aroca [3] and Ángel Molina-García [3,*]

1 Technological Center for Energy and Environment (CETENMA), 30353 Cartagena, Spain; jmparedes@cetenma.es
2 Department of Information and Communication Technologies, Universidad Politécnica de Cartagena, 30202 Cartagena, Spain; antoniojavier.garcia@upct.es
3 Department of Electronic Technology, Universidad Politécnica de Cartagena, 30202 Cartagena, Spain; antonio.mateo@upct.es
* Correspondence: angel.molina@upct.es; Tel.: +34-968-32-5462

Received: 12 January 2019; Accepted: 2 March 2019; Published: 6 March 2019

Abstract: This paper proposes a wireless low-cost solution based on long-range (LoRa) technology able to communicate with remote PV power plants, covering long distances with minimum power consumption and maintenance. This solution includes a low-cost open-source technology at the sensor layer and a low-power wireless area network (LPWAN) at the communication layer, combining the advantages of long-range coverage and low power demand. Moreover, it offers an extensive monitoring system to exchange data in an Internet-of-Things (IoT) environment. A detailed description of the proposed system at the PV module level of integration is also included in the paper, as well as detailed information regarding LPWAN application to the PV power plant monitoring problem. In order to assess the suitability of the proposed solution, results collected in real PV installations connected to the grid are also included and discussed.

Keywords: PV monitoring; low-cost solutions; LoRa technology

1. Introduction

In most countries, fossil fuel consumption has been drastically increasing along with enhancements in the quality of life and industrialization, and a growing world population [1]. This relevant fossil fuel consumption not only leads to an increase in the rate of diminishing fossil fuel reserves, but also has a significant adverse influence on the environment and the threat of global climate change. Actually, renewable integration issues have drawn attention in the scientific literature lately, and recent contributions have been focused on the institutional challenges [2]. Within the electricity sector, renewable and clean power generation alternatives will play a relevant role in future power supply (i) to attain global public awareness and sensibility of the need for environmental protection, and (ii) to achieve less dependence on fossil fuels for energy production [3]. Indeed, Mancarella et al. affirm that power systems are among the most critical infrastructures of modern societies, being crucially important to boost their resilience under severe weather conditions and any future challenges focused on climate change concerns [4]. As a result, most road maps and scenarios forecast a relevant resurgence of low-carbon generator units in the electricity supply side mix [5]. From the different renewable resources, wind and PV solar solutions are considered as relatively mature technologies, with a significant impact on current power systems [6]. However, certain technical problems have been discussed in the literature about high penetration of renewables,

mainly focused on reliability, power quality, and stability [7]. In this way, the intermittent nature of such sources may increase the stress of the grid, mainly due to undesirable oscillations on the supply side [8], which may negatively affect the transmission system regulation [9]. Regarding PV power plants, their power generation is highly dependent on solar irradiance, ambient temperature, and other atmospheric parameters [10]. Consequently, fluctuations from grid-connected PV installations might lead to decreased grid reliability, compromising the demand–supply balance control [11]. Indeed, PV systems extensively integrated into low-voltage (LV) distribution grids may cause significant changes in feeder voltage profiles [12]. Consequently, it is very important to determine and monitor such weather parameters that can provide a more precise prediction of the PV power generated [13]. Therefore, the PV power plant integration into power systems must imply monitoring solutions. Moreover, Beránek et al. affirms that monitoring of PV system plants is an urgent and imperative activity for practical implementation of new ecologically clean solar plants [14].

Different solutions can be found in the specific literature to monitor PV power plants. Ramakrishna et al. affirm that the PV monitoring systems can be broadly classified as ground-based or space-based monitoring systems [15]. More specifically, some of these contributions are focused on monitoring locally PV data. In this way, Fuentes et al. describes a portable data logger based on standalone instruments [16]. LabVIEW has shown relevant characteristics for monitoring and communicating several devices simultaneously [17]. Bayrak et al. use a Labview data acquisition (DAQ) card for monitoring electrical measurement of a PV system [18]. Chouder et al. also present a detailed characterization of the performance and dynamic behavior of PV installations through LabVIEW real-time interface system [19]. Recently, a novel power line communication (PLC) method for a DC–DC power optimizer solution is proposed by Zhu et al. [20]. The data are modulated and then transmitted through the series-connected DC-power line to other DC–DC power optimizers. The parallel resonant coupling unit is used in [21] to monitor PV data into a high-frequency form to carry out the carrier communication. Wireless solutions to monitor PV installations at panel level have been also proposed by other authors. As an example, Ando et al. describes a complete wireless solution at panel level to estimate efficiency losses and anomalous aging of PV installations [22]. Similar contributions for individual monitoring of panels based on wireless technology can be found in [23]. An in–situ monitoring solutions for PV panels is proposed and evaluated by Papageorgas et al. in [24]. Moreno-García et al. presents an architecture of acquisition devices, including distributed wireless sensors, to monitor and supervise all the distributed devices in the plant [25]. An extension of this solution by detecting any failures or deviations in PV production can be found in [26]. A low-cost acquisition system to record data in micro SD card is presented by Fanourakis et al. in [27]. Regarding remote PV monitoring proposals, different contributions can be found in the specific literature. In this way, Zigbee technology has been proposed by different authors during recent years [28–31]. Li et al. also propose an on-line monitoring system based on Zigbee technology for Internet of Things purposes [32]. However, and according to [33], Zigbee technology is proven inefficient in large scale since it is not able to face up huge distances. A low cost IOT-based embedded system is described in [34]. This solution uses a GPRS module and a low cost microcontroller to send the power generated by a PV power plant. GSM voice channel for the communication of data has been also proposed, since the GSM network is readily available in rural areas [35]. As drawbacks, Pereira et al. affirm that this solution requires a SIM card with data transfer charging and can be installed only in places under phone coverage [36]. At residential level, an IoT solution based on Arduino with 3G connectivity technology is described and assessed in [37]. A comparison of different technologies—Ethernet, WiFi and ZigBee—for smart-house applications including RES is proposed in [38]. A user-friendly PV monitoring system based on a low-cost PLC is proposed by Han et al in [39]. A review focused on solutions for PV performance monitoring is discussed in [40].

From the Transmission and Distribution Network Operator point of view, a mass energy production coming from PV systems without the corresponding energy storage units and/or sufficient innovative electricity network architectures—such as micro-grids, smart-grids and web of cells—can

cause severe disturbances [41]. In Europe, Mateo et al. contribute to overcome the barriers that hamper a large-scale integration of PV installations in the electricity distribution grids, being necessary the integration of advanced monitoring and operation systems [42]. As an additional example, in Germany, 90% of renewable system capacity is connected to distribution grids, and smart grid investments should be promoted by German DSOs [43]. Current power systems thus require modernization in terms of sensing, communication technologies, measurements, and automation technologies, and subsequently, smart power grids arise as a suitable solution [44,45].

Considering previous approaches, this work provides a step forward: a wireless low-cost open-source monitoring solution based on long-range (LoRa) technology able to communicate with remote PV power plants. The aim is thus to monitor in real time wide zones under study, covering long distances with minimum power consumption and maintenance. This study is in line with previous works of the authors focused on PV monitoring [46,47]; as well as in line with recent contributions where PLC and wireless are considered the best candidates for communication purposes [48], and wireless is poised to play a significant role in shaping the capabilities of future measurement systems [49]. Besides, the cost of open-source solutions is usually considerably lower than commercially available devices, with little loss of accuracy and precision [16]. Moreover, commercial solutions present some drawbacks, as can be found in recent PV monitoring system reviews [50]. The main contributions are summarized as follows:

- Wide areas, referred to remote PV installations, are controlled via and communicated through a low-cost open-source solution based on LoRa technology.
- Data are gathered from the PV installations in accordance with the current IEC-61724 standards and industrial, scientific, and medical (ISM) band use regulations.
- The proposed solution is flexible to exchange data in real time among PV power plants in terms of power generation and weather parameters.

The rest of the paper is structured as follows: Section 2 describes wireless sensor network technology and particularly the LoRa approach. Section 3 gives detailed information regarding our proposed solution. Section 4 offers extensive results, evaluating the performance of our solution. To this end, different testing processes are conducted by the authors. Finally, conclusions are discussed in Section 5.

2. Wireless Sensor Network: LoRa Solution

Wireless sensor network (WSN) is a mature field in technology to sense physical parameters and transmit them wirelessly out of the coverage range of the measurement in situ. This is a potential area of interest for the scientific community, reinforcing some beliefs about the necessity for further research initiatives in a new wireless-network paradigm. In this context, the low-power wide-area network (LPWAN) is a recent WSN-based technology that emerged as an alternative wireless monitoring solution [51]. Different applications and contributions can be found, mainly focused on the industrial environment. In particular, this technology is currently drawing much attention for managing assets over wide areas, such as the monitoring and control of PV power plants and the operation of distributed energy systems. The main characteristics are its excellent long-range, low-power consumption and reduced computation capacity (like a long-range WSN). In fact, the operation of a distributed energy system usually requires flexible and reliable communication systems. However, cable-based communications are, in many cases, an infeasible solution due to their complex installation and maintenance. In distributed energy systems with high penetration of renewables and small generation units connected at different voltage levels, this wireless technology can help to overcome the lack of information in the performance and generation of these installations [52].

LPWAN is a generic term that encompasses a group of technologies, allowing wide area communications at lower cost points and reduced power consumption. LPWAN technologies have arisen in both licensed and unlicensed markets, such as LTE-M, Sigfox, long range (LoRa), and narrow

band (NB)-IoT. Among them, LoRa and NB-IoT are the most prominent, though they clearly present technical differences [53]. Presently, LoRa is an LPWAN approach receiving relevant consideration in the literature, because it can operate efficiently in unlicensed bands. Unlike LoRa, an NB-IoT network must be set up within an existing cellular network. This makes LoRa a more flexible solution than NB-IoT to meet the requirements of outlying districts [54]. It is worth noting that LoRa is inarguably the main actor in the current LPWAN scene, used in an unlicensed spectrum below 1 GHz and supported by many worldwide technology leaders (Cisco, Microchip, IBM, HP, etc.) [55]. From a technological point of view, LoRa provides a proprietary chirp spread spectrum (CSS) modulation to achieve communication distances greater than 700 km [56]. What makes LoRa stand out from other modulation methods is its unique spread spectrum technique, which provides robustness against interference and a very low minimum signal-to-noise ratio (SNR) for the receiver to be able to demodulate the signal. LoRa is thus a suitable solution for applications that require a very long battery lifetime and reduced cost. Moreover, as it strengthens, LoRa allows tuning of several physical transmission properties: the bandwidth and central frequency of the communication, the coding rate (CR, the ratio between the length of the packet and the length of the error-correction code), the transmission power, and the spreading factor (SF, defined as the ratio between the symbol rate and chip rate). Higher SF values enhance the sensitivity and range of communication at the expense of increasing the over-the-air time of the packets, thus consuming more transmission duty cycles (TDCs).

In the past few years, the interest of monitoring smart industries has increasingly become LoRa [57] as one technology solution demanded by many researchers [58,59]. Most of the contributions have been focused on analyzing the advantages, disadvantages, capabilities, and limits of current developments/deployments in several scenarios: industrial environments [60], civil infrastructures such as bridges [61] and public transport [62], line-of-sight and obstructed communications [63], and surveillance tasks to combat poachers in wildlife reserves in Africa [64]. In addition, LoRa performance has been compared to other LPWAN solutions such as Sigfox [65] and Weightless [66], as well as licensed options such as NB-IoT [67]. Other studies have dealt with the real scalability of current LoRa networks [68,69], the performance of their different configurations [70] or the download traffic analysis of these types of networks [71]. LoRa defines the physical level and LoRaWAN encompasses the link layer of the protocol stack and the system architecture [72]. LoRaWAN uses long-range star architecture in which gateways are used to relay messages between the end nodes and a central core network (see Figure 1). In a LoRaWAN scenario, nodes are not associated with a specific gateway. Instead, data transmitted by a node are typically received by multiple gateways. Furthermore, LoRaWAN uses the adaptive data rate (ADR) algorithm to estimate the CR and SF parameters under specific channel conditions. Subsequently, each gateway forwards the received packet from the end node to the cloud-based network server via standard IP connections. Different disadvantages can be identified when LoRaWAN solutions are implemented, intrinsic to operating in any ISM band. In particular, current international laws require a stringent duty cycle of 1%. This means the radio channel cannot be occupied more than 36 s per hour. In fact, this value is denoted as the maximum TDC allowed by the nodes to operate in ISM channels. This is an important concern for nodes managing critical assets (such as those found in the proposed solution), where LoRa and LoRaWAN must be able to report critical events within seconds. Therefore, node duty cycles should be set with the goal of reporting critical events under the entire conditions. It is precisely this type of situation that drew our attention and a question arose: 'Is it possible to obtain communications using LoRa technology, considering its stringent duty cycle under critical conditions (i.e., given the criticality of the reported event)?' Moreover, the end-node configuration is a crucial aspect for packet transmission purposes, since LoRa networks allow us to adjust not only frequency and power values, but also other parameters such as SF and CR, promoting robustness in the communications at the expense of increasing the packet over-the-air time.

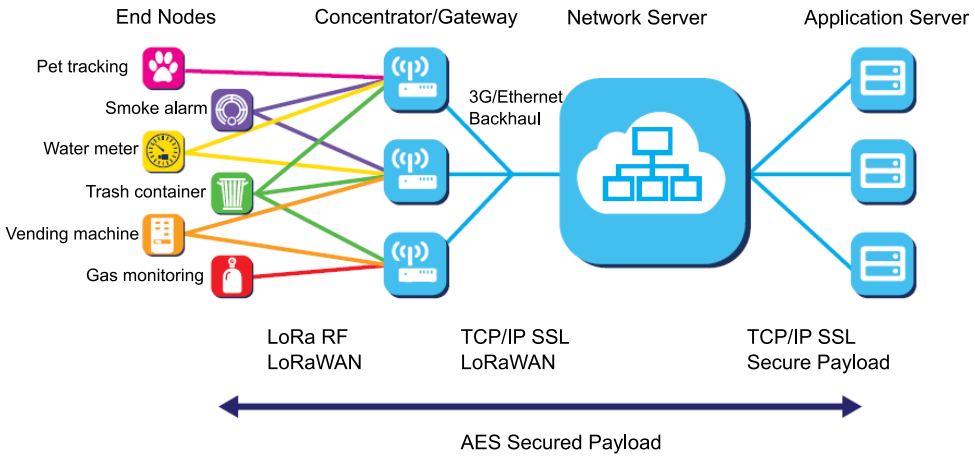

Figure 1. General overview of long-range (LoRa)/LoRa wireless area network (WAN) architecture.

To the best of the authors knowledge, contributions such as [73–75] use LoRa technology as the way of transmitting data collected by sensors in a PV Power Plant. In these contributions, authors installed a Lora communication module to dispatch packets to a Gateway including physical parameters such as current or temperature, without going into details about communication concerns. Unlike these works, we contribute with a solution which tackles these concerns more intensively than [73–75], ensuring the best performance for transmitting information from the PV installation to the Gateway and, consequently, increasing the system reliability. In this sense, and as will be discussed in Section 4, the transmission rate—bits per second—has been thoroughly tuned to achieve a suitable and acceptable RSSI (Received Signal Strength Indicator) and SNR figures in the proposed solution. For testing purposes, it has been considered the maximum SF allowed by the LoRa technology (SF12), with a CR value of 4/5 and below the maximum TDC.

3. Proposed Solution

3.1. General Overview: Topology

The proposed network architecture integrates LoRa–IoT infrastructure in a similar way to Figure 1. Therefore, by allowing for typical LoRa network topologies [76], a star topology including end devices, gateways, and a central network server is considered in the proposed solution. All selected sensors in charge of monitoring PV installations have to fulfill the IEC-61724 requirements. PV electrical data and weather parameters are gathered to estimate PV operating conditions and exchange meteorological and electrical data information. These data packets are sent to the LoRa gateway from the corresponding PV power plants. Subsequently, the received data are then forwarded to the network application via LAN connection. The design of the proposed system involves (i) end-node hardware selection, (ii) software-node configuration, and (iii) LoRa network server. These items are discussed in detail in the following.

3.2. End-Node Hardware: Sensors and Communication

The end node is in charge of gathering PV electrical data and weather conditions. Data packets are subsequently sent to the gateway. The main requirements accomplished by the end node are the following:

- Information from the PV module installed in the PV power plant is collected according to the current IEC-61724 standard requirements. These data provide relevant information for predictive maintenance purposes.
- Flexible, low-cost, and open-source solutions are required to carry out a suitable integration of the proposed system into real PV power plants.

- Nodes are able to run software, including a complete LoRa Class A. As mentioned, the end nodes operate under the license-exempt industrial, scientific, and medical (ISM) bands (EU 868 MHz/US 915 MHz) [77].

First, a hardware development platform was selected under the parameters of low cost and open-source software solutions. To this end, and taking into account previous experience, the Arduino platform [78], which offers a free development software environment to develop a prominent number of applications [79], was chosen. Other studies affirm the efficient reconfigurable security approach for WSN with Arduino-based systems [80]. Following these parameters, the Arduino One and Arduino Nano were considered as printed board platforms [81]. Both hardware solutions are based on ATmega328P with similar performance. As its main features, Arduino Uno comprises a 32 kB flash memory, 2 kB SRAM and 1 kB EEPROM, with 5 V operating voltage level and 14 digital I/O pins. The Arduino Nano is considered as a bridge between sensors and, for instance, a Raspberry Pi, which becomes it in a base station [82]. LoRa transceiver is also integrated in the device under the Arduino requirements [83].

Concerning the selected group of sensors, they have to be in line with the following requirements: they must (i) gather electrical PV parameters and weather conditions, and (ii) fulfill the IEC-61724 requirements. Moreover, the sensors are in accordance with previous works by the authors, where the same requirements were considered [16,84]. Local data collected by our proposed solution are thus able to estimate the PV module behavior and, in general, the PV installation performance. In terms of electrical data, AC and DC voltage and current variables are considered as parameters to be measured and collected for monitoring purposes. AC voltage measurement (V_{AC}) is implemented by an AC–AC power adaptor. An isolation transformer gives a physical separation and a quasi-sinusoidal waveform as an output signal. This signal is adapted by a voltage divider and sent to the Arduino board as an analog input. In a similar way, DC voltage (V_{DC}) is collected and adapted as an Arduino board analog input as well. For AC data (I_{AC}), a noninvasive Hall-effect sensor is provided for the proposed solution [85]. An accurate, low-offset, linear Hall sensor is selected and implemented by the authors to measure the DC current (I_{DC}) [86]. Both AC and DC sensors offer low-voltage output signals compatible with the Arduino input voltage range. With regard to weather parameters, the following variables are considered for monitoring purposes: solar irradiance, ambient temperature, and PV module temperature. To measure and gather solar irradiance, and assuming that the short-circuit current (ISC) is nearly proportional to the irradiance [87], it is measured in W/m^2 by a 5 Wp short-circuit encapsulated polycrystalline silicon module. A shunt resistance is chosen and implemented to adapt the voltage output within a suitable voltage range according to the Arduino analog input requirements. Calibration of this module was carried out by the authors through the CETENMA Solar TestBed, based on the global sunlight method available in [88]. Ambient temperature was measured near PV modules as an attempt to more accurately estimate the real environment of PV module conditions. A DHT22 temperature/humidity sensor with digital output was selected with this objective. The DHT22 sensor is directly supported by the Arduino IDE technology and, according to [89], it furnishes very accurate results with a fast refresh time. Other applications using the DHT22 sensor can be found in [90,91]. Most correlations in the scientific literature for PV electrical power as a function of the cell/module operating temperature and basic environmental variables are based on linear approaches [92]. Indeed, [93,94] affirm that PV module power output values depend linearly, but rather strongly, on the operating temperature. The authors note that the PV module temperature should be collected at the center of the back surface of the module and in the center of the array field location on the module, as pointed out by IEC-61829 method A [95]. In our proposed system, a low-cost solution employing the DS18S20 digital sensor is used with this goal. This digital thermometer achieves 9-bit Celsius temperature measurements, transferring them on a 1-wire bus [96]. A general diagram of the sensors and their connections with the Arduino board is depicted in Figure 2.

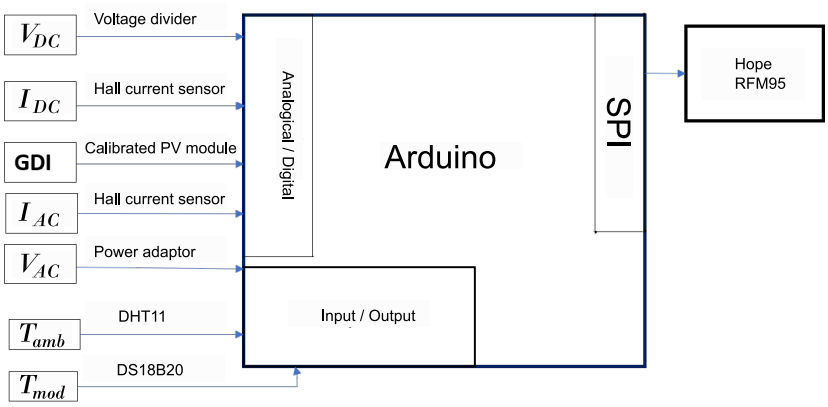

Figure 2. General diagram of sensors and Arduino connections.

The communication system is in charge of dispatching data packets thanks to a transceiver integrated into the Arduino board and operating in the EU-868 band [72]. The selected transceiver is the RFM95W module, fabricated by HOPE RF and configured as a LoRa TM modem [97]. In fact, the RFM95W configured for LoRa communication via 4-wire SPI bus was successfully tested in [98]. The main characteristics of this LoRa TM module are high efficiency and significant sensitivity (around −148 dBm). To achieve these advantages, this module is composed of a 6-GPIO interface configurable by software and with different interruptions usually linked to the operation of the RFM95W [99], and is able to support different modulations such as FSK/OOK, GFSK, MSK, or GMSK. Due to the small size of the RFM95W module, an adapter is required to provide breakout pins and the antenna plug-ins (Figure 3). Finally, the RFM95W works at 3.3 V and thus it cannot be directly connected to the Arduino Uno or Nano (both operating at 5 V). A voltage adapter is thus required to give the operating voltage range.

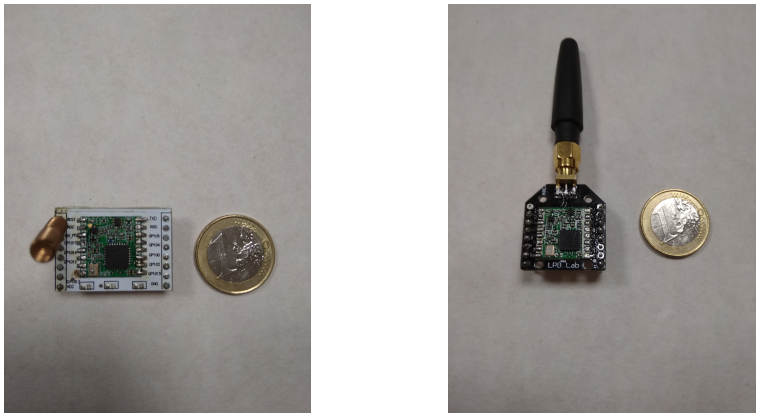

(**a**) (**b**)

Figure 3. Dispatching data packets: implemented transceivers. (**a**) RFM95 with an ESP8266 module adapter. (**b**) HOPE RFM95W transceiver with breakout board and 868 MHz antenna.

3.3. End-Node Software Configuration

The end-node software configuration was subsequently conducted after selecting the end-node hardware solution along with the sensors. First, Arduino firmware was implemented and tested in order to obtain the PV power plant parameters and values under the IEC-61724 standard [100] and the ISM band-use regulations. The selected firmware was the nano-lmic-v1.51-F.ino, which was downloaded from the LoRa LMIC library [101]. The Arduino code follows activation-by-personalization (ABP) rules, available in the LMIC library [83]. SScripts to read the data format were also developed and the payload adjusted to contain full information gathered by the

different sensors, following the format recommended by the IEC standard resolution. Please note that the payload has a length of 38 bytes, which has a relevant impact on the over-air time of the packets, as will be discussed in Section 4. The sampling period is another aspect to be considered in detail. In this sense, the IEC standard establishes that the sampling period of the different parameters under study varies proportionally to the solar irradiance. Under our operating conditions, parameters had to be sampled in intervals of 1 minute or less. On the other hand, in Europe, the duty cycle is regulated by the ETSI EN300.220 standard—Section 7.2.3—[102], which, as noted in Section 2, sets a duty cycle of 1%. Furthermore, from the spreadsheet developed and proposed by Matthijs Kooijman [103], the over-air time of the packets can be determined for different SFs. The over-air time corresponding to the worst case was then used to define our sampling rate. By considering our scenario, the duty cycle, and the over-air-time issue, data packets were sampled every 30 s. The parameters were then averaged and sent in time periods of 3 min. These values will be modified in a subsequent version to enforce the so-called *'Fair Access Policy'*, which limits the uplink airtime to 30 s per day and per node [104]. The downlink messages were set to 10 messages per day and per node.

3.4. LoRa Gateway/LoRa Network Server

A single-channel LoRa gateway was designed and implemented with a Raspberry Pi board. The LoRa radio communication module we selected is the Dragino Arduino shield from a Semtech SX1276 chip [105]. The Dragino shield can be directly connected to the Raspberry Pi. SPI connectors belonging to Dragino (MISO, MOSI, CLK, and NSSEL), VCC and GND are attached to the corresponding pins on the Raspberry Pi (CE0 on the RPI for SPI, *_nSSEL* and 3v3 for VCC). The operating system (OS) installed on the Raspberry Pi was Raspbian [106]. This single channel gateway software as well as its OS are supported by Thomas Telkamp at GitHub, and further information can be found in [107]. The single-channel LoRa gateway assembly and the coverage range are depicted in Figure 4. As described in Section 3.1, a LoRa network server is required to test the proposed application. With this aim, The Things Network (TTN) backend is used [108]. TTN is a community-driven project offering a free server to users; our proposed solution must connect the gateway to this free server. To this end, we created an account and registered the developed gateway. The gateway is located in Europe, selecting the European ISM band (868 MHz). After this setting process, the gateway is ready to be plugged in to the server. At this point, users can visualize the data packet transmission from the end nodes associated with this gateway, with a status of *'connected at web'*. In our case, two applications were developed: monitoring system testing and coverage range testing. Furthermore, the Arduino firmware implemented a different device address, `'DEVADDR'`, the network session key `'NWSKEY'`, and the application session key `'APPSKEY'`, which were developed and implemented before carrying out the corresponding validation tests discussed in detail in the following section.

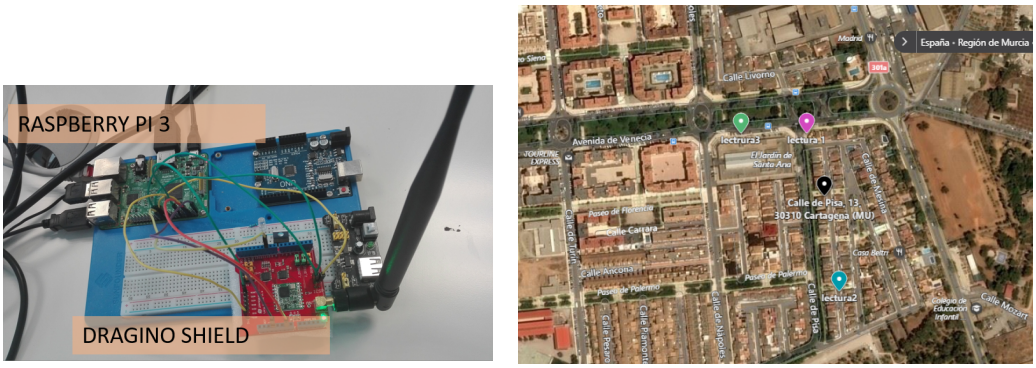

(**a**) (**b**)

Figure 4. Single-channel gateway. (**a**) Gateway assembly. (**b**) Gateway coverage range.

3.5. Economic Evaluation: Cost-Effectiveness

Finally, and in terms of cost-effectiveness, the proposed monitoring system is in line with other contributions discussed in Sections 1 and 2 based on non-commercial solutions. Our system is flexible to be configured in different locations and PV installations. With the aim of offering a low cost system, the different hardware components are based on open-source projects with a high cost effectiveness threshold. Table 1 gives the monitoring node cost, which is lower than other commercial solutions as was previously discussed. Moreover, these commercial solutions usually provide less information and a reduced number of parameters.

Table 1. PV monitoring node cost.

Description	Number	Unit Price (Euro)	Total Price (Euro)
PV module (5 Wp, 22 V, 30 W)	1	8.75	8.75
Cement resistance 5 W 10 Ω 10 R 5%	1	0.13	0.13
AC-AC power supply adapter	1	4.95	4.95
Non-invasive AC–sensor	1	4.31	4.31
5 V DC-USB power adapter	1	2.40	2.40
2.54 mm PCB screw connector	6	0.17	1.02
Aluminium electrolytic capacitor 400 V	2	0.02	0.04
Metal film resistance 1 M 1.2 M 1.5 M 2 M 2.2 M Ω	6	0.05	0.30
Prototype PCB universal board	1	0.35	0.35
Outdoor enclosure and wiring	1	3.50	3.50
RFM95 LoRa Breakout + SMA connector antenna	1	5.95	5.95
HOPE RFM95	1	4.05	4.05
DS12820 temperature sensor	1	0.99	0.99
DHT temperature and humidity sensor	1	2.52	2.52
Total cost			39.26

4. Results

This section summarizes the test bed conducted to evaluate the proposed system. System assembly, coverage range, and performance evaluation of the PV power plant are described with the goal of adding value to our proposal in terms of a sensing, monitoring, and data packet transmission solution in an IoT scenario.

4.1. System Assembly

First, the selected hardware components and sensors (end nodes) were tested in a laboratory environment to evaluate their performance under controlled conditions. After this initial testing, components and sensors were connected and assembled to provide a feasible solution able to operate under real conditions. To facilitate the integration of the proposed monitoring system into real PV power plants, components and sensors corresponding to the end nodes were divided into two subnodes, including most connectors commonly used in real PV installations connected to the grid: (i) a principal subnode involving a main controller, a transceiver with the corresponding voltage level converter, and a set of batteries for power supply requirements (see Figure 5); (ii) a secondary subnode in charge of measuring and collecting PV module variables. To test the appropriateness of the global solution, these nodes were first deployed in the solar laboratory of CETENMA, located in the Industrial Park of Cartagena (southeast Spain). This facility includes measurement equipment to check the performance of PV power plants and modules. For testing purposes, a single 250 Wp monocrystalline PV module connected to an SF 250 W Soltec SolarFighter microinverter was used (see Figure 6).

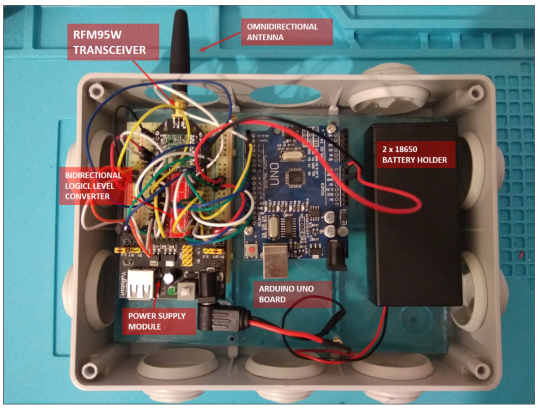

Figure 5. Detail of the system assembly. Principal subnode.

(**a**) (**b**)

Figure 6. Testing system located at the CETENMA SolarLab (Spain). (**a**) SolarLab outdoor test site details. (**b**) Secondary box details.

4.2. Coverage Range Characterization

A relevant objective of this work was to evaluate the suitability of the proposed solution to measure, collect, and send data from PV installations to a remote gateway. The coverage range of the initial gateway, discussed in Section 3.3, was not enough to achieve the objectives searched in the test bed. Indeed, the location and low performance of the antenna used for this gateway were likely the biggest drawbacks of the initial poor coverage range. To overcome this limitation, another gateway was implemented and installed at the Universidad Politecnica de Cartagena (Cartagena, Spain). This additional Gateway is called the TM RG186 Series LoRa-enabled gateway [109]. It is located on the roof of a researching building on the university campus (see Figure 7). The gateway was registered with TTN as well.

To ensure the communication of the proposed system, we conducted a test of the signal power and coverage range. To this end, a Global Positioning System (GPS) module was integrated into the end node to transmit the location coordinates. To visualize the position of each end node, the TTN Mapper software tool [110] was installed in the network server. This additional tool provides further information, such as RSSI and SNR. Furthermore, each end node was configured with a transmission power of 14 dBm and SF12 to carry out the set of tests. During these tests, a new gateway was identified 15 km from our installation in the solar laboratory of CETENMA. Figure 8 illustrates these results corresponding to the coverage testing process.

Figure 7. TM RG186 series LoRa-enabled gateway (Universidad Politecnica de Cartagena, Spain).

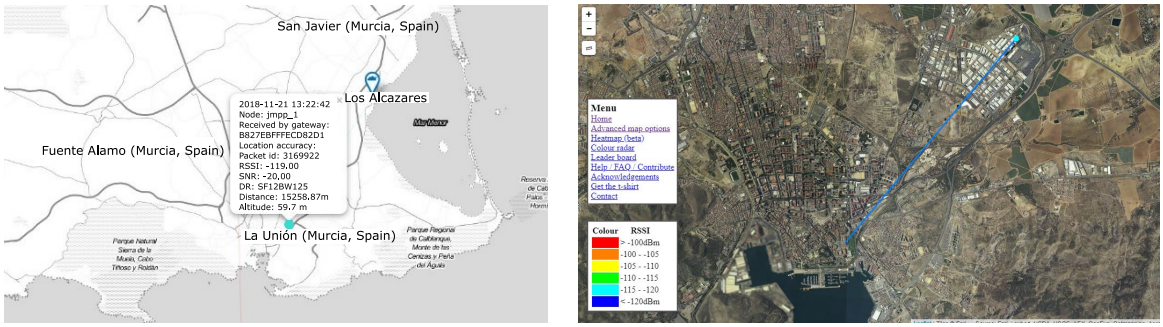

(**a**) (**b**)

Figure 8. Coverage testing analysis. (**a**) Gateway identification map. (**b**) Coverage testing results on The Things Network (TTN) Mapper website.

4.3. PV Power Plant Performance Evaluation

Considering the different coverage testing processes we previously carried out, discussed in Section 4.2, a 5 kW PV installation connected to the grid and located on the university campus was deployed to assess the PV monitoring properties of the proposed solution (see Figure 9). Electrical and environmental data were gathered from the PV power plant and sent to the gateway to be evaluated and discussed in subsequent analysis. Additional parameters such as encrypted payload, received signal strength indicator (RSSI), air time, signal-to-noise ratio (SNR), number of packets, and channel included in the LoRa packet are also available and can be downloaded from the TTN website.

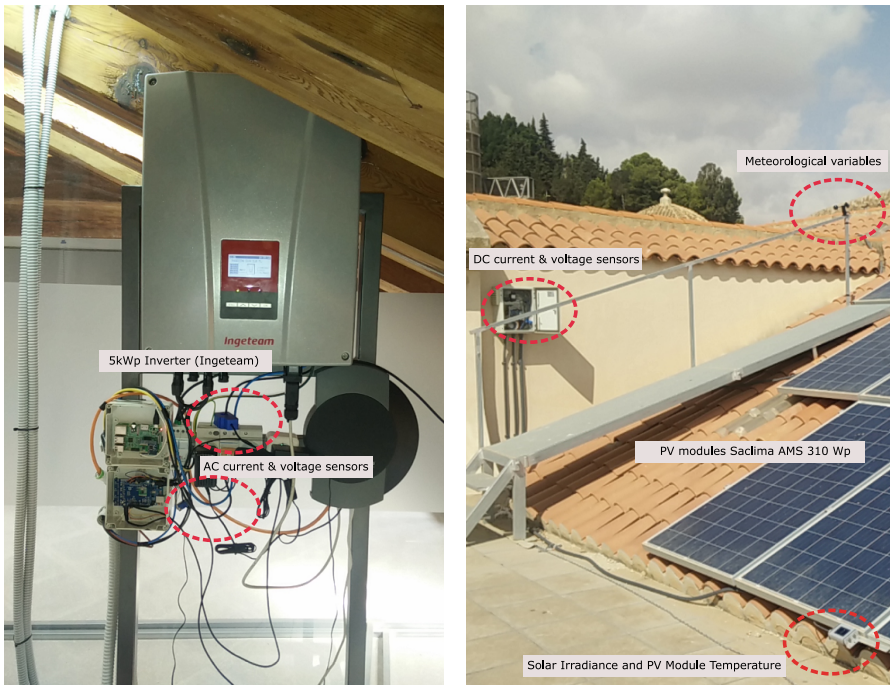

Figure 9. End nodes of 5 kWp PV installation monitoring.

A packet size of 38 bytes is considered enough to cover all the parameters for PV power plant monitoring purposes. The transmission power is 14 dBm and the SF metric is tuned from 10 to 12, which influences the data packet over-air time. Figure 10 shows the theoretical time on-air (ms) for each SF configuration depending on the payload length. These results allowed us to configure the sampling period for each SF: 60, 120, and 180 s for SF10, SF11, and SF12, respectively. Our test bed was conducted for 24 h. This time interval was enough to evaluate each SF configuration. It is relevant to point out that SF10 involves no reception of packets in the gateway, as a consequence of different concerns, such as (i) the limited over-air time due to the distance between the device and the gateway, around 4 km; (ii) the locations of end nodes; and (iii) the conditions of the signal propagation.

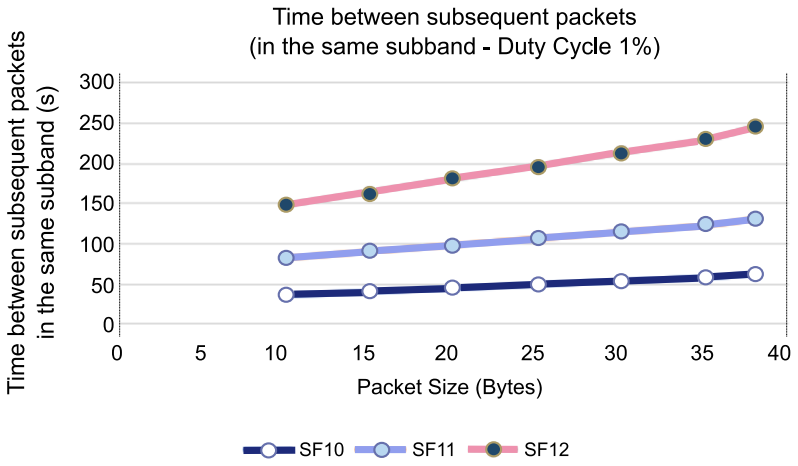

Figure 10. Theoretical time-on-air (ms) for different tested SF configurations.

Figure 11 illustrates the RSSI and SNR results obtained in November 2018 for SF11 and SF12. Table 2 shows additional metrics also discussed in this work: packet delivery ratio and time intervals between different data packets (inter-arrival time). The packet delivery ratio is defined as the ratio between the packets successfully received and the total data packets sent by the end nodes.

The inter-arrival time is determined by the time interval value corresponding to each packet received by the TTN web application. For SF11, our study reveals low RSSI and SNR values. As an example, the minimum signal strength in WiFi technology provides basic connectivity with reliable packet delivery around −80/−90 dBm. Concerning SF12, the RSSI and SNR metrics improved around 10%. However, the time interval between packets increased to 115 s, which is reasonable due to greater over-air time of the packets. In terms of the packet delivery ratio, SF11 showed poor performance, with most of the packets corrupted or completely lost. To overcome this drawback, it is necessary to increase the spreading factor (SF), which allows us to improve the metric sharply. It is remarkable that these outcomes are in line with recent contributions [111–113], which corroborates one of main advantages of using LoRa: its sensibility. In this respect, weak signals can stimulate the electronic communication of the LoRa device, resulting in successful packet delivery to the gateway. Finally, to verify that the payload is being decrypted correctly, data received by the TTN application are compared to the same data collected by a data logger of the test stand (see Figure 12). These results validate the feasibility and reliability of our proposal, as well as the accuracy of the implemented monitoring and communication solution.

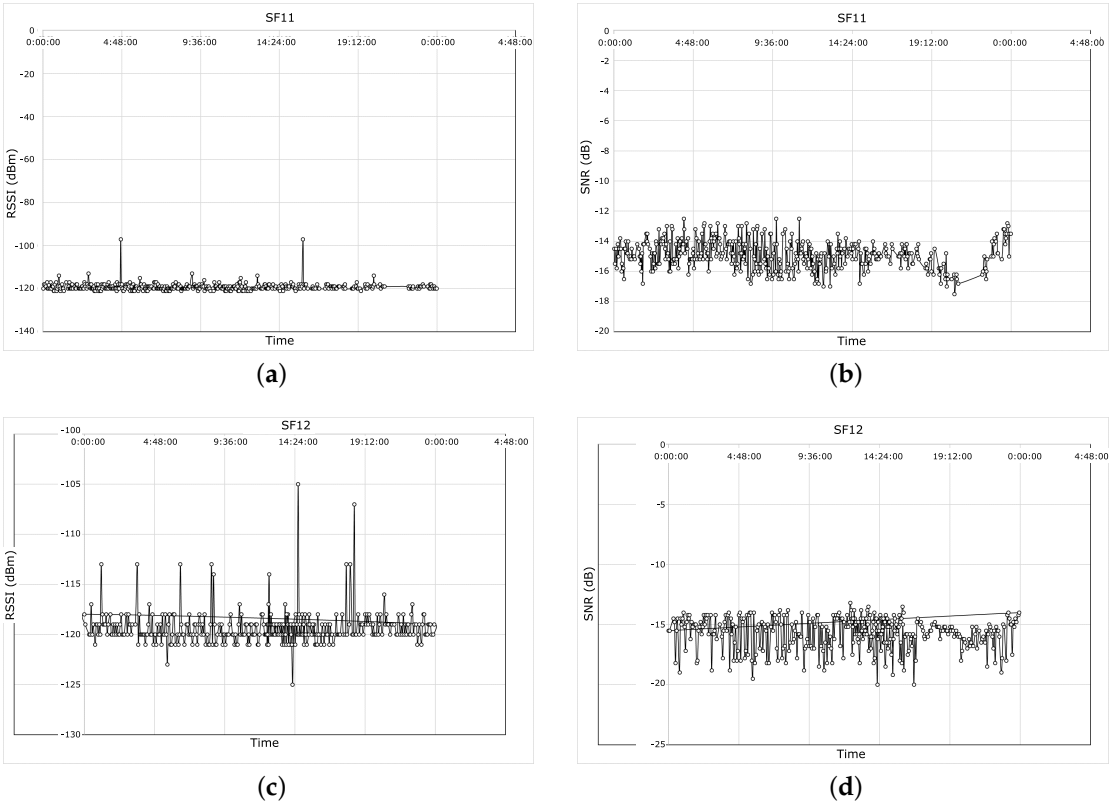

Figure 11. Coverage range tests. (**a**) Received signal strength indicator (RSSI) data (SF11). (**b**) Signal-to-noise ratio (SNR) results (SF11). (**c**) RSSI data (SF12). (**d**) SNR results (SF12).

Table 2. Packet delivery rate and inter-arrival time metrics. SF, spreading factor.

SF	Packet Data Sent	Packet Data Received	Packet Delivery Rate	Average Time between Packets (s)	Inter-Arrival Time (s)
11	559	307	55%	190.85	131.00
12	402	364	91%	273.13	246.00

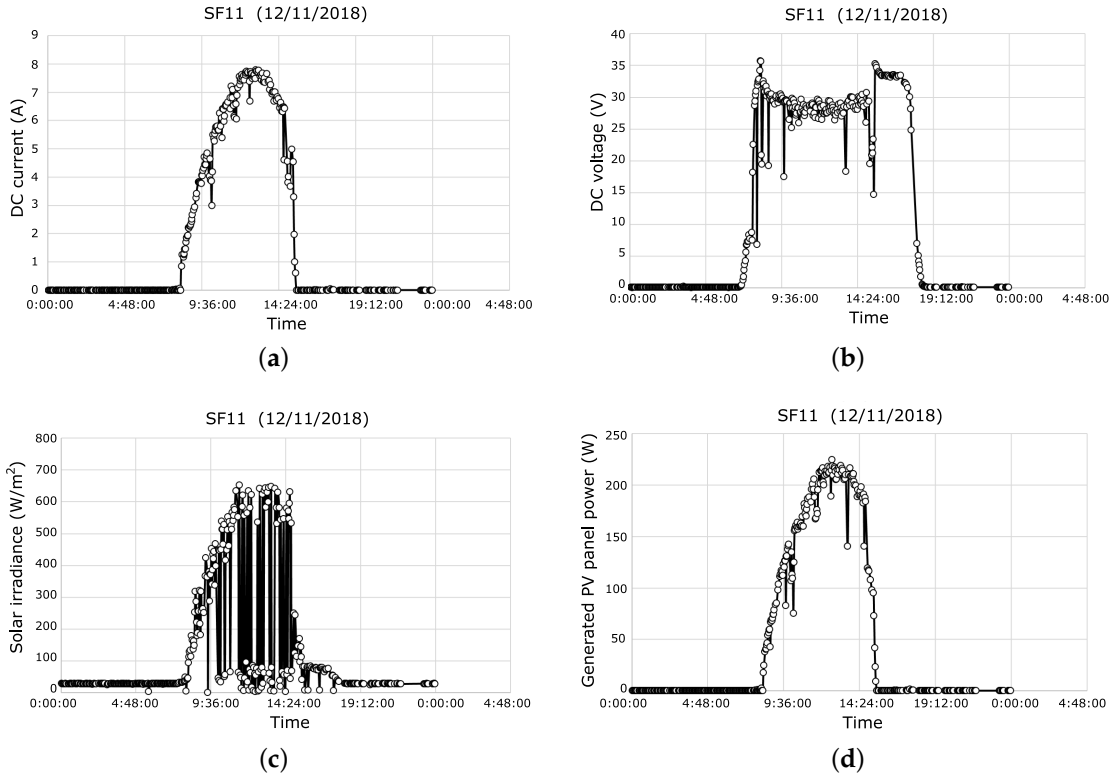

Figure 12. PV example of collected data (12 November 2018). (**a**) DC current data. (**b**) DC voltage data. (**c**) Solar irradiance data. (**d**) Generated active power.

5. Conclusions

A low-cost, open-source solution to monitor PV power plants was designed and evaluated. Our alternative system provides a powerful and straightforward solution, facilitating the integration of this renewable energy source into current power systems. As a novelty, long-range communication technology denoted as LoRa enables data transmission to a remote gateway, which allows us to evaluate the PV installation performance in real time. Extensive electrical and meteorological information is also available from the monitoring system. These data can be applied for predictive maintenance purposes. Moreover, these data have a remarkable impact on grid reliability and PV forecast accuracy.

A PV power plant connected to the grid (5 kW rate power) and located on the university campus (southeast Spain) was used to evaluate the monitoring system. Different field-test campaigns were conducted by the authors. From the results, it can be affirmed that aspects such as the distance between source and destination, the line-of-sight between source and destination, and propagation issues have a clear influence on the appropriate data reception process. Our study demonstrates that scenarios with a high spreading factor value (SF11 and SF12) satisfy an accurate reception of data packets. However, the corresponding over-air time considerably limits the number of transmissions. To overcome this drawback, the sampling time was adjusted in line with the packet air-time and according to the SF value. One of the main limitations of the LoRa solution is its restricted duty cycle (1%), which was taken into account for the testing process. Received data were also compared to data-logger equipment connected in situ in the PV installation. This comparison validates the electrical and meteorological variables gathered by different sensors, resulting in errors lower than 0.5%. Our proposed solution thus offers an alternative system to be implemented in remote PV power plants with the goal of monitoring and dispatching electrical and meteorological data.

Author Contributions: Data curation, J.M.P.-P.; Formal analysis, A.M.-G. and A.J.G.-S.; Funding acquisition, A.M.-A.; Investigation, A.J.G.-S.; Resources, J.M.P.-P.; Supervision, A.M.-G.; Visualization, A.M.-A.; Writing—original draft, A.M.-G.; Writing—review and editing, A.M.-G.

Funding: This work was partially supported by the Spanish agreement (2017) between the Institute for Development of the Region of Murcia (INFO) and the Technological Center for Energy and Environment (CETENMA). The paper includes results of activities conducted under the Research Program for Groups of Scientific Excellence at Region of Murcia (Spain), the Seneca Foundation, and the Agency for Science and Technology of the Region of Murcia (Spain). This work was also supported by project AIM, Ref. TEC2016-76465-C2-1-R (AEI/FEDER, UE).

Acknowledgments: The authors thank the staff of the Universidad Politécnica de Cartagena (Spain) for services and facilities provided.

Conflicts of Interest: The authors declare no conflict of interest.

Abbreviations

The following abbreviations are used in this manuscript:

ABP	Activation-by-personalisation
ADR	Adaptive data rate
CR	Coding rate
CSS	Chirp spread spectrum
ISC	Short-circuit current
LPWAN	Low-power wide-area networks
RSSI	Received signal strength indicator
SARIMA	Seasonal autoregressive integrated moving average
SF	Spreading factor
SNR	Signal-to-noise ratio
TDC	Transmission duty cycle
TTN	The Things Networ
WSN	Wireless sensor network

References

1. Panwar, N.; Kaushik, S.; Kothari, S. Role of renewable energy sources in environmental protection: A review. *Renew. Sustain. Energy Rev.* **2011**, *15*, 1513–1524. [CrossRef]
2. Verzijlbergh, R.; Vries, L.D.; Dijkema, G.; Herder, P. Institutional challenges caused by the integration of renewable energy sources in the European electricity sector. *Renew. Sustain. Energy Rev.* **2017**, *75*, 660–667. [CrossRef]
3. Nehrir, M.H.; Wang, C.; Strunz, K.; Aki, H.; Ramakumar, R.; Bing, J.; Miao, Z.; Salameh, Z. A Review of Hybrid Renewable/Alternative Energy Systems for Electric Power Generation: Configurations, Control, and Applications. *IEEE Trans. Sustain. Energy* **2011**, *2*, 392–403. [CrossRef]
4. Mancarella, P.; Panteli, M. Influence of Extreme Weather and Climate Change on the Resilience of Power Systems: Impacts and Possible Mitigation Strategies. *Electr. Power Syst. Res.* **2015**, *127*, 259–270.
5. Brouwer, A.S.; van den Broek, M.; Seebregts, A.; Faaij, A. Impacts of large-scale Intermittent Renewable Energy Sources on electricity systems, and how these can be modeled. *Renew. Sustain. Energy Rev.* **2014**, *33*, 443–466. [CrossRef]
6. Liang, X.; Mazin, H.E.; Reza, S.E. Probabilistic generation and transmission planning with renewable energy integration. In Proceedings of the 2017 IEEE/IAS 53rd Industrial and Commercial Power Systems Technical Conference (ICPS), Niagara Falls, ON, Canada, 6–11 May 2017; pp. 1–9. [CrossRef]
7. Kamaruzzaman, Z. Effect of grid-connected photovoltaic systems on static and dynamic voltage stability with analysis techniques—A review. *Przegląd Elektrotechniczny* **2015**, *1*, 136–140. [CrossRef]
8. Hung, D.Q.; Shah, M.R.; Mithulananthan, N. Technical Challenges, Security and Risk in Grid Integration of Renewable Energy. In *Smart Power Systems and Renewable Energy System Integration*; Jayaweera, D., Ed.; Springer International Publishing: Cham, Switzerland, 2016; pp. 99–118. [CrossRef]
9. Chiandone, M.; Sulligoi, G.; Massucco, S.; Silvestro, F. Hierarchical Voltage Regulation of Transmission Systems with Renewable Power Plants: An overview of the Italian case. In Proceedings of the 3rd Renewable Power Generation Conference, Naples, Italy, 24–25 September 2014. [CrossRef]
10. Behera, M.K.; Majumder, I.; Nayak, N. Solar photovoltaic power forecasting using optimized modified extreme learning machine technique. *Eng. Sci. Technol. Int. J.* **2018**, *21*, 428–438. [CrossRef]

11. Wang, F.; Zhen, Z.; Liu, C.; Mi, Z.; Hodge, B.M.; Shafie-khah, M.; Catalão, J.P. Image phase shift invariance based cloud motion displacement vector calculation method for ultra-short-term solar PV power forecasting. *Energy Convers. Manag.* **2018**, *157*, 123–135. [CrossRef]
12. Petinrin, J.; Shaaban, M. Impact of renewable generation on voltage control in distribution systems. *Renew. Sustain. Energy Rev.* **2016**, *65*, 770–783. [CrossRef]
13. Wolff, B.; Lorenz, E.; Kramer, O. Statistical Learning for Short-Term Photovoltaic Power Predictions. In *Studies in Computational Intelligence Computational Sustainability*; Springer: Berlin, Germany, 2016; Volume 645.
14. Beránek, V.; Olsan, T.; Libra, M.; Poulek, V.; Sedlacek, J.; Dang, M.Q.; Tyukhov, I. New Monitoring System for Photovoltaic Power Plants' Management. *Energies* **2018**, *11*, 2495. [CrossRef]
15. Madeti, S.R.; Singh, S. Monitoring system for photovoltaic plants: A review. *Renew. Sustain. Energy Rev.* **2017**, *67*, 1180–1207. [CrossRef]
16. Fuentes, M.; Vivar, M.; Burgos, J.; Aguilera, J.; Vacas, J. Design of an accurate, low-cost autonomous data logger for PV system monitoring using Arduino™ that complies with IEC standards. *Sol. Energy Mater. Sol. Cells* **2014**, *130*, 529–543. [CrossRef]
17. Belhadj Ahmed, C.; Kassas, M.; Essamuddin Ahmed, S. PV-standalone monitoring system performance using LabVIEW. *Int. J. Smart Grid Clean Energy* **2014**, *3*, 44–50. [CrossRef]
18. Bayarak, G.; Cebeci, M. Monitoring a grid connected PV power generation system with labview. In Proceedings of the 2013 International Conference on Renewable Energy Research and Applications (ICRERA), Madrid, Spain, 20–23 October 2013; pp. 562–567. [CrossRef]
19. Chouder, A.; Silvestre, S.; Taghezouit, B.; Karatepe, E. Monitoring, modelling and simulation of PV systems using LabVIEW. *Sol. Energy* **2013**, *91*, 337–349. [CrossRef]
20. Zhu, Y.; Wu, J.; Wang, R.; Lin, Z.; He, X. Embedding Power Line Communication in Photovoltaic Optimizer by Modulating Data in Power Control Loop. *IEEE Trans. Ind. Electron.* **2019**, *66*, 3948–3958. [CrossRef]
21. Mao, W.; Zhang, X.; Cao, R.; Wang, F.; Zhao, T.; Xu, L. A Research on Power Line Communication Based on Parallel Resonant Coupling Technology in PV Module Monitoring. *IEEE Trans. Ind. Electron.* **2018**, *65*, 2653–2662. [CrossRef]
22. Ando, B.; Baglio, S.; Pistorio, A.; Tina, G.; Ventura, C. Sentinella: Smart Monitoring of Photovoltaic Systems at Panel Level. *IEEE Trans. Instrum. Meas.* **2015**, *64*, 2188–2199. [CrossRef]
23. Prieto, M.; Pernía, A.; Nuno, F.; Diaz, J.; Villegas, P. Development of a Wireless Sensor Network for Individual Monitoring of Panels in a Photovoltaic Plant. *Sensors* **2014**, *14*, 2379–2396. [CrossRef] [PubMed]
24. Papageorgas, P.; Piromalis, D.; Antonakoglou, K.; Vokas, G.; Tseles, D.; Arvanitis, K. Smart Solar Panels: In-situ Monitoring of Photovoltaic Panels based on Wired and Wireless Sensor Networks. *Energy Procedia* **2013**, *36*, 535–545. [CrossRef]
25. Moreno-García, I.; Palacios-García, E.; Pallares-López, V.; Santiago, I.; González-Redondo, M.; Varo-Martínez, M.; Real-Calvo, R. Real–Time Monitoring System for a Utility–Scale Photovoltaic Power Plant. *Sensors* **2016**, *16*, 770. [CrossRef]
26. Moreno-García, I.M.; Palacios-García, E.J.; Santiago, I.; Pallares-López, V.; Moreno-Munoz, A. Performance monitoring of a solar photovoltaic power plant using an advanced real-time system. In Proceedings of the 2016 IEEE 16th International Conference on Environment and Electrical Engineering (EEEIC), Florence, Italy, 7–10 June 2016; pp. 1–6. [CrossRef]
27. Fanourakis, S.; Wang, K.; McCarthy, P.; Jiao, L. Low-cost data acquisition systems for photovoltaic system monitoring and usage statistics. *Earth Environ. Sci.* **2017**, *93*, 012048. [CrossRef]
28. Katsioulis, V.; Karapidakis, E.; Hadjinicolaou, M.; Tsikalakis, A. Wireless Monitoring and Remote Control of PV Systems Based on the ZigBee Protocol. In *Technological Innovation for Sustainability*; Camarinha-Matos, L.M., Ed.; Springer: Berlin/Heidelberg, Germany, 2011; pp. 297–304.
29. Ben Belghith, O.; Lassaad, S. Remote GSM module monitoring and Photovoltaic system control. In Proceedings of the 2014 First International Conference on Green Energy ICGE, Sfax, Tunisia, 25–27 March 2014; pp. 188–192. [CrossRef]
30. Zahurul, S.; Mariun, N.; Kah, L.; Hizam, H.; Othman, M.L.; Abidin, I.Z.; Norman, Y. A novel Zigbee-based data acquisition system for distributed photovoltaic generation in smart grid. In Proceedings of the 2015 IEEE Innovative Smart Grid Technologies—Asia (ISGT ASIA), Chengdu, China, 21–24 May 2015; pp. 1–6. [CrossRef]

31. Shariff, F.; Rahim, N.A.; Hew, W.P. Zigbee-based data acquisition system for online monitoring of grid-connected photovoltaic system. *Expert Syst. Appl.* **2015**, *42*, 1730–1742. [CrossRef]
32. Li, Y.F.; Lin, P.J.; Zhou, H.F.; Chen, Z.C.; Wu, L.J.; Cheng, S.Y.; Su, F.P. On-line monitoring system of PV array based on internet of things technology. *Earth Environ. Sci.* **2017**, *93*, 012078. [CrossRef]
33. Adhya, S.; Saha, D.; Das, A.; Jana, J.; Saha, H. An IoT based smart solar photovoltaic remote monitoring and control unit. In Proceedings of the 2016 2nd International Conference on Control, Instrumentation, Energy Communication (CIEC), Kolkata, India, 28–30 January 2016; pp. 432–436. [CrossRef]
34. Kekre, A.; Gawre, S.K. Solar photovoltaic remote monitoring system using IOT. In Proceedings of the 2017 International Conference on Recent Innovations in Signal processing and Embedded Systems (RISE), Bhopal, India, 27–29 October 2017; pp. 619–623. [CrossRef]
35. Tejwani, R.; Kumar, G.; Solanki, C. Remote Monitoring for Solar Photovoltaic Systems in Rural Application Using GSM Voice Channel. *Energy Procedia* **2014**, *57*, 1526–1535. [CrossRef]
36. Pereira, R.I.; Dupont, I.M.; Carvalho, P.C.; Jucá, S.C. IoT embedded linux system based on Raspberry Pi applied to real-time cloud monitoring of a decentralized photovoltaic plant. *Measurement* **2018**, *114*, 286–297. [CrossRef]
37. López-Vargas, A.; Fuentes, M.; Vivar, M. IoT Application for Real-Time Monitoring of Solar Home Systems Based on Arduino^{TM} With 3G Connectivity. *IEEE Sens. J.* **2019**, *19*, 679–691. [CrossRef]
38. Ahmed, M.A.; Kang, Y.C.; Kim, Y.C. Communication Network Architectures for Smart-House with Renewable Energy Resources. *Energies* **2015**, *8*, 8716–8735. [CrossRef]
39. Han, J.; Lee, I.; Kim, S. User-friendly monitoring system for residential PV system based on low-cost power line communication. *IEEE Trans. Consum. Electron.* **2015**, *61*, 175–180. [CrossRef]
40. Hadjipanayi, M.; Koumparou, I.; Philippou, N.; Paraskeva, V.; Phinikarides, A.; Makrides, G.; Efthymiou, V.; Georghiou, G. Prospects of photovoltaics in southern European, Mediterranean and Middle East regions. *Renew. Energy* **2016**, *92*, 58–74. [CrossRef]
41. Kyritsis, A.; Voglitsis, D.; Papanikolaou, N.; Tselepis, S.; Christodoulou, C.; Gonos, I.; Kalogirou, S. Evolution of PV systems in Greece and review of applicable solutions for higher penetration levels. *Renew. Energy* **2017**, *109*, 487–499. [CrossRef]
42. Mateo, C.; Frías, P.; Cossent, R.; Sonvilla, P.; Barth, B. Overcoming the barriers that hamper a large-scale integration of solar photovoltaic power generation in European distribution grids. *Sol. Energy* **2017**, *153*, 574–583. [CrossRef]
43. Matschoss, P.; Bayer, B.; Thomas, H.; Marian, A. The German incentive regulation and its practical impact on the grid integration of renewable energy systems. *Renew. Energy* **2019**, *134*, 727–738. [CrossRef]
44. Colak, I.; Sagiroglu, S.; Fulli, G.; Yesilbudak, M.; Covrig, C.F. A survey on the critical issues in smart grid technologies. *Renew. Sustain. Energy Rev.* **2016**, *54*, 396–405. [CrossRef]
45. Hancke, G.P.; Silva, B.; Hancke, G.P., Jr. The Role of Advanced Sensing in Smart Cities. *Sensors* **2013**, *13*, 393–425. [CrossRef] [PubMed]
46. Molina-Garcia, A.; Campelo, J.C.; Blanc, S.; Serrano, J.J.; Garcia-Sanchez, T.; Bueso, M.C. A Decentralized Wireless Solution to Monitor and Diagnose PV Solar Module Performance Based on Symmetrized-Shifted Gompertz Functions. *Sensors* **2015**, *15*, 18459–18479. [CrossRef] [PubMed]
47. Paredes-Parra, J.M.; Mateo-Aroca, A.; Silvente-Niñirola, G.; Bueso, M.C.; Molina-Garcia, A. PV Module Monitoring System Based on Low-Cost Solutions: Wireless Raspberry Application and Assessment. *Energies* **2018**, *11*. [CrossRef]
48. Madeti, S.; Singh, S. Comparative analysis of solar photovoltaic monitoring systems. *AIP Conf. Proc.* **2017**, *1859*, 1–6. [CrossRef]
49. Zahran, M.; Atia, Y.; Alhosseen, A.; El-Sayed, I. Wired and wireless remote control of PV system. *WSEAS Trans. Syst. Control* **2010**, *5*, 656–666.
50. Rahman, M.M.; Selvaraj, J.; Rahim, N.; Hasanuzzaman, M. Global modern monitoring systems for PV based power generation: A review. *Renew. Sustain. Energy Rev.* **2018**, *82*, 4142–4158. [CrossRef]
51. Usman, R.; Parag, K.; Mahesh, S. Low Power Wide Area Networks: An Overview. *IEEE Commun. Surv. Tutor.* **2017**, *19*, 855–873.
52. Song, Y.; Lin, J.; Tang, M.; Dong, S. An Internet of Energy Things Based on Wireless LPWAN. *Engineering* **2017**, *3*, 460–466. [CrossRef]

53. Sinha, R.S.; Wei, Y.; Hwang, S.H. A survey on LPWA technology: LoRa and NB-IoT. *ICT Express* **2017**, *3*, 14–21. [CrossRef]
54. Migabo, E.; Djouani, K.; Kurien, A.; Olwal, T. A Comparative Survey Study on LPWA Networks: LoRa and NB–IoT. In Proceedings of the Future Technologies Conference (FTC), Vancouver, BC, Canada, 29–30 November 2017; pp. 1045–1051.
55. LoRa-Alliance. The Internet of Things—An explosion of Connected Possibility. Available online: https://docs.wixstatic.com/ugd/eccc1ade5fda268ed945e885a43a39b38752 (accessed on 28 November 2018).
56. LoRa-Alliance. The Internet of Things—An Explosion of Connected Possibility. LoRa-Alliance. Available online: https://www.thethingsnetwork.org/article/ground-breaking-world-record-lorawan-packet-received-at-702-km-436-miles-distance (accessed on 28 November 2018).
57. LoRa. LoRa-Alliance. 2018. Available online: https://lora-alliance.org (accessed on 28 November 2018).
58. Magrin, D.; Centenaro, M.; Vangelista, L. Performance evaluation of LoRa networks in a smart city scenario. In Proceedings of the IEEE International Conference on Communications (ICC), Kansas , MO, USA, 20–24 May 2017; pp. 1–7.
59. Sorensen, R.; Kim, D.; Nielsen, J.; Popovski, P. Analysis of Latency and MAC–layer Performance for Class A LoRaWAN. *IEEE Wirel. Commun. Lett.* **2017**, *6*, 566–569. [CrossRef]
60. Haxhibeqiri, J.; Karaagac, A.; den Abeele, F.V.; Joseph, W.; Moerman, I.; Hoebeke, J. LoRa indoor coverage and performance in an industrial environment: Case study. In Proceedings of the 22nd IEEE International Conference on Emerging Technologies and Factory Automation (ETFA), Limassol, Cyprus, 12–15 September 2017; pp. 1–8.
61. Orfei, F.; Mezzetti, C.B.; Cottone, F. Vibrations powered LoRa sensor: An electromechanical energy harvester working on a real bridge. In Proceedings of the 2016 IEEE Sensors, Orlando, FL, USA, 30 October–3 November 2016; pp. 1–3.
62. James, J.G.; Nair, S. Efficient, real–time tracking of public transport, using LoRaWAN and RF transceivers. In Proceedings of the TENCON 2017 IEEE Region 10 Conference, Penang, Malaysia, 5–8 November 2017; pp. 2258–2261.
63. Rahman, A.; Suryanegara, M. The development of IoT LoRa: A performance evaluation on LoS and Non-LoS environment at 915 MHz ISM frequency. In Proceedings of the International Conference on Signals and Systems (ICSigSys), Bali, Indonesia, 16–18 May 2017; pp. 163–167.
64. Rwanda Parks. Available online: https://www.theverge.com/2017/7/20/16002752/smart-park-rwanda-akagera-poaching-lorawan (accessed on 28 November 2018).
65. Vejlgaard, B.; Lauridsen, M.; Nguyen, H.; Kovacs, I.; Mogensen, P.; Sorensen, M. Coverage and Capacity Analysis of Sigfox, LoRa, GPRS, and NB-IoT. In Proceedings of the IEEE 85th Vehicular Technology Conference (VTC Spring), Sydney, Australia, 4–7 June 2017; pp. 1–5.
66. Goursaud, C.; Gorce, J. Dedicated networks for IoT: PHY–MAC state of the art and challenges. *EAI Endorsed Transac. Int. Things* **2015**. . [CrossRef]
67. Persia, S.; Carciofi, C.; Faccioli, M. NB-IoT and LoRA connectivity analysis for M2M/IoT smart grids applications. In Proceedings of the AEIT International Annual Conference, Cagliari, Italy, 20–22 September 2017; pp. 1–6.
68. Martin, B.; Utz, R.; Thiemo, V.; Juan, M.A. Do LoRa Low-Power Wide-Area Networks Scale? In Proceedings of the 19th ACM International Conference on Modeling, Analysis and Simulation of Wireless and Mobile Systems, Malta, 13–17 November 2016; pp. 59–67. [CrossRef]
69. Georgiou, O.; Raza, U. Low Power Wide Area Network Analysis: Can LoRa Scale? *IEEE Wirel. Commun. Lett.* **2017**, *6*, 162–165. [CrossRef]
70. Bor, M.; Roedig, U. LoRa Transmission Parameter Selection. In Proceedings of the 2017 13th International Conference on Distributed Computing in Sensor Systems (DCOSS), Ottawa, ON, Canada, 5–7 June 2017. [CrossRef]
71. Alexandru-Ioan, P.; Usman, R.; Parag, K.; Mahesh, S. Does Bidirectional Traffic Do More Harm Than Good in LoRaWAN Based LPWA Networks? In Proceedings of the GLOBECOM 2017 IEEE Global Communications Conference, Singapore, 4–8 December 2017. [CrossRef]
72. Alliance, L. *What Is LoRaWAN*; A Technical Overview; LoRaWAN: London, UK, 2015.

73. Kraemer, F.; Ammar, D.; Bråten, A.; Tamkittikhun, N.; Palma, D. Solar Energy Prediction for Constrained IoT Nodes Based on Public Weather Forecasts. In Proceedings of the Seventh International Conference on the Internet of Things, Linz, Austria, 22–25 October 2017. [CrossRef]
74. Shuda, J.; Rix, A.; Booysen, M.T. Towards Module-Level Performance and Health Monitoring of Solar PV Plants Using LoRa Wireless Sensor Networks. In Proceedings of the 2018 IEEE PES/IAS Power Africa, Cape Town, South Africa, 28–29 June 2018. [CrossRef]
75. Choi, C.; Jeong, J.; Lee, I.; Park, W. LoRa based renewable energy monitoring system with open IoT platform. In Proceedings of the 2018 International Conference on Electronics, Information, and Communication (ICEIC), Honolulu, HI, USA, 24–27 January 2018; pp. 1–2. [CrossRef]
76. De Carvalho Silva, J.; Rodrigues, J.; Alberti, A.; Solic, P.; Aquino, A. LoRaWAN—A Low Power WAN Protocol for Internet of Things: A Review and Opportunities. In Proceedings of the 2017 2nd International Multidisciplinary Conference on Computer and Energy Science (SpliTech), Split, Croatia, 12–14 July 2017.
77. Nolan, K.E.; Guibene, W.; Kelly, M.Y. An evaluation of low power wide area network technologies for the Internet of Things. In Proceedings of the 2016 International Wireless Communications and Mobile Computing Conference (IWCMC), Paphos, Cyprus, 5–9 September 2016; pp. 439–444. [CrossRef]
78. Arduino. Arduino.org. Available online: http://arduino.cc/ (accessed on 28 November 2018).
79. Galadima, A.A. Arduino as a learning tool. In Proceedings of the 2014 11th International Conference on Electronics, Computer and Computation (ICECCO), Abuja, Nigeria, 29 September–1 October 2014; pp. 1–4. [CrossRef]
80. Kabir, A.F.M.S.; Shorif, M.A.; Li, H.; Yu, Q. A study of secured wireless sensor networks with XBee and Arduino. In Proceedings of the 2014 2nd International Conference on Systems and Informatics (ICSAI 2014), Shanghai, China, 15–17 November 2014; pp. 492–496. [CrossRef]
81. Arduino Manual. Arduino Microcontroller. Arduino.org. Available online: http://arduino.cc/en/Reference/HomePage (accessed on 28 November 2018).
82. Deshmukh, A.D.; Shinde, U.B. A low cost environment monitoring system using raspberry Pi and arduino with Zigbee. In Proceedings of the 2016 International Conference on Inventive Computation Technologies (ICICT), Coimbatore, India, 26–27 August 2016; Volume 3, pp. 1–6. [CrossRef]
83. Telkamp, T. IBM LMIC v1.5 (LoRaWAN in C) Adapted to Run under the Arduino Environment. Technical Report. 2016. Available online: https://github.com/things-nyc/testnode-arm-cortex-mbed-lmic-1.5 (accessed on 28 November 2018).
84. Han, J.; Jeong, J.D.; Lee, I.; Kim, S.H. Low-cost monitoring of photovoltaic systems at panel level in residential homes based on power line communication. *IEEE Trans. Consum. Electron.* **2017**, *63*, 435–441. [CrossRef]
85. YHDC. STC-013-000 Datasheet. Available online: https://datasheet4u.com/datasheet-pdf/YHDC/STC-013-000/pdf.php?id=1089416 (accessed on 28 November 2018).
86. MicroSystems, A. ACS712–Datasheet. Available online: http://www.alldatasheet.com/datasheet-pdf/pdf/168326/ALLEGRO/ACS712.html (accessed on 28 November 2018).
87. Vicente, E.M.; Moreno, R.L.; Ribeiro, E.R. MPPT Technique Based on Current and Temperature Measurements. *Int. J. Photoenergy* **2015**, 1–9. [CrossRef]
88. Harald, M.; Willem, Z.; Ewan, D.; Heinz, O. Calibration of photovoltaic reference cells by global sunlight method. *Metrologia* **2005**, *42*, 360. [CrossRef]
89. Priya, C.G.; AbishekPandu, M.; Chandra, B. Automatic plant monitoring and controlling system over GSM using sensors. In Proceedings of the 2017 IEEE Technological Innovations in ICT for Agriculture and Rural Development (TIAR), Chennai, India, 7–8 April 2017; pp. 173–176. [CrossRef]
90. Hulea, M.; Mois, G.; Folea, S.; Miclea, L.; Biscu, V. Wi-sensors: A low power Wi-Fi solution for temperature and humidity measurement. In Proceedings of the 39th Annual Conference of the IEEE Industrial Electronics Society, Vienna, Austria, 10–13 November 2013; pp. 4011–4015. [CrossRef]
91. Saha, S.; Majumdar, A. Data centre temperature monitoring with ESP8266 based Wireless Sensor Network and cloud based dashboard with real time alert system. In Proceedings of the 2017 Devices for Integrated Circuit (DevIC), Kalyani, India, 23–24 March 2017; pp. 307–310. [CrossRef]
92. Skoplaki, E.; Palyvos, J. On the temperature dependence of photovoltaic module electrical performance: A review of efficiency/power correlations. *Sol. Energy* **2009**, *83*, 614–624. [CrossRef]
93. Dubey, S.; Sarvaiya, J.N.; Seshadri, B. Temperature Dependent Photovoltaic (PV) Efficiency and Its Effect on PV Production in the World—A Review. *Energy Procedia* **2013**, *33*, 311–321. [CrossRef]

94. Skoplaki, E.; Boudouvis, A.; Palyvos, J. A simple correlation for the operating temperature of photovoltaic modules of arbitrary mounting. *Sol. Energy Mater. Sol. Cells* **2008**, *92*, 1393–1402. [CrossRef]
95. Emery, K.; Smith, R. *Monitoring System Performance*; Technical Report; National Renewable Energy Laboratory (NREL): Golden, CO, USA, 2011.
96. Maxim Integrated Products, Inc. DS18S20 DATASHEET. Available online: https://datasheets.maximintegrated.com/en/ds/DS18S20.pdf (accessed on 28 November 2018).
97. Electronic, H. RFM Datasheet. Available online: http://www.hoperf.com/upload/rf/RFM95969798W.pdf (accessed on 28 November 2018).
98. Van den Bossche, A.; Dalcé, R.; Val, T. OpenWiNo: An open hardware and software framework for fast-prototyping in the IoT. In Proceedings of the 2016 23rd International Conference on Telecommunications (ICT), Thessaloniki, Greece, 16–18 May 2016; pp. 1–6. [CrossRef]
99. Wendt, T.; Volk, F.; Mackensen, E. A benchmark survey of long range (LoRaTM) spread-spectrum-communication at 2.45 GHz for safety applications. In Proceedings of the 2015 IEEE 16th Annual Wireless and Microwave Technology Conference (WAMICON), Cocoa Beach, FL, USA, 13–15 April 2015; pp. 1–4. [CrossRef]
100. IEC 61724, Photovoltaic System Performance Monitoring-Guidelines for Measurement, Data Exchange, and Analysis. 2017. Available online: https://ci.nii.ac.jp/naid/10019072640/ (accessed on 28 November 2018).
101. IBM. IBM LMIC Framework. Arduino Port of the LMIC (LoraWAN-in-C, Formerly LoraMAC-in-C) Framework Provided by IBM. Available online: http://www.research.ibm.com/labs/zurich/ics/lrsc/lmic.html (accessed on 28 November 2018).
102. ETSI. EN300.220 Short Range Devices (SRD) Operating in the Frequency Range 25 MHz to 1000 MHz; Part 1 Technical Characteristics and Methods of Measurement. Available online: https://www.etsi.org/deliver/etsi_en/300200_300299/30022001/03.01.01_60/en_30022001v030101p.pdf (accessed on 28 November 2018).
103. Kooijman, M. LoRa(WAN) Airtime Calculator. Available online: https://docs.google.com/spreadsheets/d/1voGAtQAjC1qBmaVuP1ApNKs1ekgUjavHuVQIXyYSvNc/edit?usp=sharing (accessed on 28 November 2018).
104. Adelantado, F.; Vilajosana, X.; Tuset-Peiro, P.; Martinez, B.; Melià-Seguí, J.; Watteyne, T. Understanding the limits of LoRaWAN. *IEEE Commun. Mag.* **2017**, *55*, 48–54. [CrossRef]
105. Dragino. LoRa Wireless Products Family. Available online: http://wiki.dragino.com/index.php?title=Main_Page#LoRa_Wireless_Products_Family (accessed on 28 November 2018).
106. Foundation, R.P. Raspbian. Available online: https://www.raspberrypi.org/downloads/raspbian/ (accessed on 28 November 2018).
107. Telkamp, T. Single Channel LoRaWAN Gateway. Available online: https://github.com/tftelkamp/single_chan_pkt_fwd (accessed on 28 November 2018).
108. Network, T.T. Learn How to Grow the Network and Connect All Things. Available online: https://www.thethingsnetwork.org/docs/ (accessed on 28 November 2018).
109. Product Brief—Sentrius RG1xx Series Gateway. Available online: https://www.mouser.es/datasheet/2/223/Product%20Brief%20-%20Sentrius%20RG1xx%20Series%20Gateway-1113271.pdf (accessed on 28 November 2018).
110. Meijers, J. TTN Mapper. Available online: http://ttnmapper.org (accessed on 28 November 2018).
111. Sanchez-Iborra, R.; Sanchez-Gomez, J.; Ballesta-Vinas, J.; Skarmeta, A. Performance Evaluation of LoRa Considering Scenario Conditions. *Sensors* **2018**, *19*, 772. [CrossRef] [PubMed]
112. Augustin, A.; Yi, J.; Clausen, T.; Townsley, W. A Study of LoRa: Long Range & Low Power Networks for the Internet of Things. *Sensors* **2016**, *16*, 1466. [CrossRef]
113. SemTech. SemTech Manual Online. Available online: http://semtech.force.com/lora/LC_Answers_Questions?id=90644000000PmGvAAK (accessed on 28 November 2018).

4.3. A characterization of metrics for comparing satellite-based and ground-measured global horizontal irradiance data: a principal component analysis application

Información adicional:

- Revista: Sustainability 12: 2454
- DOI: 10.3390/su12062454
- Fecha de publicación: Marzo 2020
- Disponible en: `https://www.mdpi.com/2071-1050/12/6/2454`
- Referencia: [69]
  Bueso, M.C.; Paredes-Parra, J.M.; Mateo-Aroca, A.; Molina-García, A. A Characterization of Metrics for Comparing Satellite-Based and Ground-Measured Global Horizontal Irradiance Data: A Principal Component Analysis Application. Sustainability 2020, 12, 2454.
  `https://doi.org/10.3390/su12062454`

sustainability

MDPI

Article

A Characterization of Metrics for Comparing Satellite-Based and Ground-Measured Global Horizontal Irradiance Data: A Principal Component Analysis Application

Maria. C. Bueso [1,†], José Miguel Paredes-Parra [2,†] and Antonio Mateo-Aroca [3,†] and Angel Molina-García [3,*,†]

1 Department of Applied Mathematics and Statistics, Universidad Politécnica de Cartagena, 30202 Cartagena, Spain; mcarmen.bueso@upct.es
2 Technologic Center of Energy and Environment, 30202 Cartagena, Spain; jmparedes@cetenma.es
3 Department of Automatic, Electrical Engineering and Electronic Technology, Universidad Politécnica de Cartagena, 30202 Cartagena, Spain; antonio.mateo@upct.es
* Correspondence: angel.molina@upct.es; Tel.: +34-968-32-5462
† These authors contributed equally to this work.

Received: 21 February 2020; Accepted: 17 March 2020; Published: 20 March 2020

Abstract: The increasing integration of photovoltaic (PV) power plants into power systems demands a high accuracy of yield prediction and measurement. With this aim, different global horizontal irradiance (GHI) estimations based on new-generation geostationary satellites have been recently proposed, providing a growing number of solutions and databases, mostly available online, in addition to the many ground-based irradiance data installations currently available. According to the specific literature, there is a lack of agreement in validation strategies for a bankable, satellite-derived irradiance dataset. Moreover, different irradiance data sources are compared in recent contributions based on a diversity of arbitrary metrics. Under this framework, this paper describes a characterization of metrics based on a principal component analysis (PCA) application to classify such metrics, aiming to provide non-redundant and complementary information. Therefore, different groups of metrics are identified by applying the PCA process, allowing us to compare, in a more extensive way, different irradiance data sources and exploring and identifying their differences. The methodology has been evaluated using satellite-based and ground-measured GHI data collected for one year in seven different Spanish locations, with a one-hour sample time. Data characterization, results, and a discussion about the suitability of the proposed methodology are also included in the paper.

Keywords: correlation; global horizontal irradiance data; metrics; principal component analysis

1. Introduction

The integration of renewables into current power systems is attracting much attention. Indeed, sustainability of energy policies and their mid-term outlooks are currently a topic of interest for major agencies. Ellabban et al. affirm that the renewable energy resource potential is enormous, as such resources can, in principle, exponentially exceed the world's energy demand [1]. However, due to the intermittent nature of such renewable energy resources, it is necessary to address different challenging issues, as they are significantly different from the conventional resources [2]. Moreover, in terms of solar resources, the inherent variability of large-scale solar generation requires an accurate power/irradiance forecasting, which is critical to secure the economic operation of power systems and future smart grids [3].

A relevant number of methodologies have been proposed to measure and forecast global solar irradiation, being considered essential for the design, economic evaluation, and performance analysis of photovoltaic (PV) power plants and their integration into power systems [4,5]. A recent review of power forecasting models for renewables can be found in [6]. By considering the different methods and proposals, their validations were carried out through a variety of measures of errors based on the author's criteria and mainly focused on averaged statistical test results. Notton et al. proposed the application of artificial neural networks—assessed by relative root mean square error (rRMSE) and relative mean absolute error (rMAE)—to estimate solar irradiance on tilted planes [7]. In a similar way, relative mean bias error (rMBE), rRMSE, determination coefficient (R^2), and 'd' Willmott index were used to evaluate both artificial neural networks and support vector machine applications [8]. Bouchouicha et al. used root mean square error (RMSE) and rRMSE to validate a readjusted model over the Algerian Big South [9]. Noorian et al. evaluated 12 models to estimate hourly diffuse radiation on inclined surfaces by determining the rRMSE [10]. An extensive comparison—over 90 contributions—of estimated solar radiation models was performed by Teke et al., to suggest the most accurate models [11]. In this revision, and according to the most commonly used statistical test results, linear modeling, non-linear modeling, artificial intelligence modeling, and fuzzy approaches were compared accordingly.

According to the specific literature, it can be affirmed that most contributions are evaluated by applying the rRMSE and rMAE. During the last years, different applications have been proposed for global horizontal irradiance (GHI) based on new-generation geostationary satellites; highly appropriate to monitor remote areas and large-scale territories with minimum capital and operating costs. Subsequently, a growing number of solutions and databases are then available online to provide such potential, for instance PVWatts [12], PVGIS [13], Global Atlas [14] and SolarGIS [15]. Nevertheless, Piasecki et al. affirm in [16] that, to the best of the authors' knowledge, the satellite/reanalysis data have so far not been compared with the measurements provided by the National Institute of Meteorology and Water Management (Poland) from the renewable energy sources perspective. Other contributions are focused on analyzing these satellite data. For example, Bódis et al. combined satellite-based and statistical data sources with machine learning to provide a reliable assessment of the technical potential for rooftop PV electricity production with a spatial resolution of 100 m across the European Union (EU) [17]. Psiloglou et al. recently published a comparison between satellite-based data sets and reanalysis against ground measurements by considering only an isolated rural area [18]. Boca et al. evaluated a multiple–regression approach model for fast estimation of PV potentials over Europe and Africa based on the PVGIS database and through the mean absolute percent error (MAPE) [19].

Data based on moderate resolution imaging spectroradiometer (MODIS), along with conventional meteorological data, are used in [20] to estimate monthly-mean daily global solar radiation. Two statistics: general mean bias deviation (gMBD) and relative general mean bias deviation (rgMBD) are applied in [21] to validate the estimated GHI by using satellite-based spectral irradiance data. Pierro et al. provided RMSE scores to evaluate PV power estimation and forecasts through satellite and numerical weather prediction data [22]. In addition, Tang et al. used mean bias error (MBE), RMSE, and rRMSE to evaluate whether GHI estimations can be improved by increasing the frequency of satellite observations. Recently, the mean absolute difference (MAD) was determined in [23] to compare global irradiation from a satellite estimate model and on-ground measurements. Satellite-based solar radiation data were also used by Buffat et al. to estimate the rooftop solar irradiation potential over large regions. The correlation coefficient and a median monthly relative error were applied to estimate the accuracy of such estimations [24]. Other authors have proposed methods for estimating the direct normal irradiation from GOES geostationary satellite imagery for concentrating solar systems. In this case, MBE and RMSE averaged values are used to validate the methods [25]. Pfenninger et al. used RMSE results to validate long-term patterns of European PV output by means of 30 year hourly reanalysis and satellite data [26]. Ernst et al. compared ground-based and satellite-based irradiance data by using confidence interval results [27].

By considering the contributions previously discussed, and regarding the appropriate metrics, most of the authors propose and use the following strategies: RMSE, MBE, and the relative versions of each (rRMSE and rMBE), the mean absolute error (MAE), Pearson correlation coefficient (r), and the standard deviation of the residual (SD). Moreno et al. is a recent example of the metric application from Meteosat Second Generation (MSG) images [28]. Gueymard reviews validation methodologies and statistical performance indicators for modeled solar radiation data, dividing possible statistical indicators into four categories, directly proposed by the author [29]. In this framework, a review of the literature demonstrates that there is a lack of agreement in validation strategies for a bankable, satellite-derived solar irradiance dataset [30]. Therefore, and due to the lack of agreement in validation methodologies of solar irradiance datasets, the aim of this paper is focused on the following objectives:

- An extended estimations of metrics to compare GHI satellite data to on-ground data.
- A correlation analysis to identify similarities by considering homogeneous behaviors of such metrics.
- A principal component analysis (PCA) application to divide the metrics into different categories and propose independent indicator groups to be considered for comparison data purposes.

The rest of the paper is structured as follows. Section 2 describes the proposed methodology; Section 3 gives a description of the case study; Section 4 provides results and discusses the suitability of the proposed characterization; and finally, conclusions are given in Section 5.

2. Methodology

According to the literature review, different metrics have been defined and used to validate the GHI data from ground measures or satellite–derived data. Table 1 summarizes such definitions by including expressions and mathematical references, where GHI_i^{sat} and GHI_i^{grn} represent the i^{th} satellite-based GHI and the ground-measured GHI values, respectively. GHI_0 is the normalized value and n is the number of data samples. By considering previous contributions, a diversity of averaged GHI values have been suggested as the normalizing value in order to determine the relative magnitude of error metrics. For example, Paoli et al. compute the normalized error metrics from the mean global radiation obtained on the season [31]; Nik et al. calculate monthly mean hourly global solar radiation values [32]; and Lu et al. estimate daily global solar radiation [33]. A detailed review of accuracy tests used in the specific literature was reviewed by Teke et al. in [11]. Therefore, and taking into account the proposed characterization of metrics, the daily average GHI values are considered by the authors to normalize and determine the relative magnitude of error metrics. From the expressions and approaches proposed in previous contributions to characterize the metrics, it is desirable to determine the similarities among them and propose different groups of metrics in order to estimate the complementary information in a data comparison process. A characterization and classification methodology to identify similarities among metrics applied on the GHI data is thus proposed and described. This approach classifies the metric differences for a large amount of irradiance data determined through a variety of sources: satellite–derived, on-ground installations, and/or estimated irradiation values. Therefore, an autonomous and flexible solution to compare different irradiation data sources is proposed in this work; allowing us to select complementary metrics, which offer non-redundant information to evaluate differences among those irradiation data.

Table 1. Definition of the error metrics.

Definition	Abbreviation	Expression	References
Mean Square Error	MSE	$\mathrm{MSE} = \frac{1}{n}\sum_{i=1}^{n}\left(GHI_i^{sat} - GHI_i^{grn}\right)^2$	[3,11]
Root Mean Square Error	RMSE	$\mathrm{RMSE} = \sqrt{\mathrm{MSE}}$	[3,9–11,18,20,25,26,28–30,34]
Normalized RMSE	nRMSE	$\mathrm{nRMSE} = \frac{\mathrm{RMSE}}{GHI_0}$	[7–11,18,19,22,23,25,28,30,34]
Mean Bias Error	MBE	$\mathrm{MBE} = \frac{1}{n}\sum_{i=1}^{n}\left(GHI_i^{sat} - GHI_i^{grn}\right)$	[3,9–11,18,20,25,28–30,34]
Normalized MBE	nMBE	$\mathrm{nMBE} = \frac{\mathrm{MBE}}{GHI_0}$	[7,8,10,11,18,21,23,25,30,34]
Mean Absolute Error	MAE	$\mathrm{MAE} = \frac{1}{n}\sum_{i=1}^{n}\left\lvert GHI_i^{sat} - GHI_i^{grn}\right\rvert$	[3,11,21,28–30,34]
Normalized MAE	nMAE	$\mathrm{nMAE} = \frac{\mathrm{MAE}}{GHI_0}$	[7,21,23,28,34]
Mean Absolute Percentage Error	MAPE	$\mathrm{MAPE} = \frac{1}{n}\sum_{i=1}^{n}\frac{\left\lvert GHI_i^{sat} - GHI_i^{grn}\right\rvert}{GHI_i^{sat}}$	[11,19]
Shape Based Distance	SBD	$\mathrm{SBD} = 1 - \max_{w} NCC_w(GHI^{sat}, GHI^{grn})$, where NCC_w is a normalized cross correlation sequence between the series GHI^{sat} and GHI^{grd}.	[35,36]
Dynamic Time Warping	DTW	$\mathrm{DTW} = \min_{W}\sum_{k=1}^{K} d(w_k)$, where $W = \{w_1, w_2, \ldots, w_k, \ldots, w_K\}$ represent a warping path between the series GHI^{sat} and GHI^{grd} subjected to several constraints and $d(w_k) = dist(GHI_{i_k}^{sat}, GHI_{i_k}^{grn})$.	[36,37]

The proposed methodology is first based on an estimation of metrics for the different irradiation data sources. Subsequently, a matrix of differences for the different metrics is then determined for each station, according to the selected sample time—a one-hour sample time for the case study discussed in Section 4. After this initial metric estimation, a multiple correlation analysis is carried out on each station, to identify metrics with a relevant (or not) dependence. This correlation analysis is then used as the input for a clustering process, grouping by each location, those metrics with similar behaviors and thus, metrics that provide similar information. A graphical representation is proposed by the authors to visualize in a more convenient way these multiple correlation results as well as the clustering process.

From these results, we can then compare the clustering results for all locations, estimating the homogeneity of the different groups according to the specific locations. In a complementary way, a statistical analysis—the mean and standard deviation—is then applied to each metric correlation coefficient corresponding to all considered locations. This statistical analysis gives an additional estimation of the homogeneity of such correlations, as well as their independence (or not) from the specific locations. Subsequently, from the clustering process and the additional statistical analysis, we can then estimate the metric correlation dependence from the locations, as well as the similarity of the metric grouping according to a visual comparison of the clustering process.

Figure 1 schematically shows the proposed methodology by considering m different metrics determined from p-locations and corresponding to n-days hourly data. The correlation and metric clustering are then carried out by each specific location. Subsequently, a metric clustering estimation for all locations is proposed to determine the homogeneity of such metric clustering processes, including an additional statistical analysis for each group of metrics.

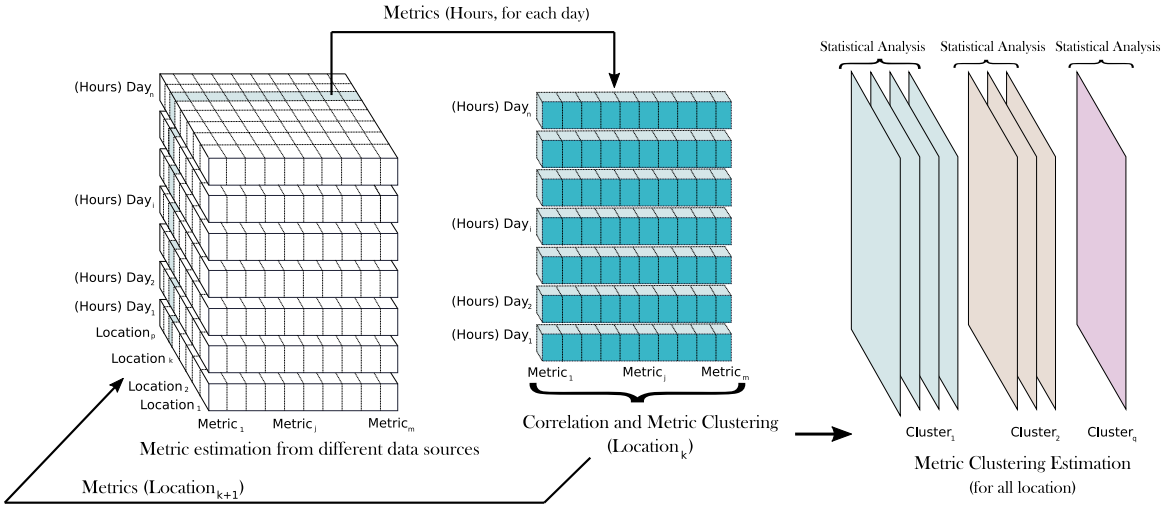

Figure 1. The correlation analysis and clustering process. General scheme.

From the previous clustering and statistical analysis, we then propose to apply PCA for all metrics and locations. In fact, PCA is helpful in this context, when the group of variables—the metrics depicted in Table 1—are highly correlated and a dimensionality reduction is convenient. Moreover, PCA is also an appropriate solution to identify the *'principal components'*, which account for most of the variance in the observed/measured variables [38]. In our case, an m–dimensional vector $[x_1, x_2, \ldots, x_m]$ is initially identified corresponding to the different metrics determined. A $(p \times n) \times m$ data matrix X corresponds to the x_{ij} observations of the j^{th} variable. We then estimate a linear combination of each m–dimensional vector $[x_1, x_2, \ldots, x_m]$ of matrix X with maximum variance. Such linear combinations are given by

$$\sum_{r=1}^{r=m} \lambda_r \cdot x_r = X_\lambda, \tag{1}$$

where λ is a m-dimensional vector of constants $[\lambda_1, \lambda_2, \ldots, \lambda_m]$, and the variance of any such linear combination is given by $\mathrm{var}(X_\lambda) = \lambda' \cdot S \cdot \lambda$, with S being the sample covariance–variance matrix associated with the data and $'$ denoting the transpose. Identifying the linear combination with maximum variance is equivalent to determining an m-dimensional vector maximizing $\lambda' \cdot S \cdot \lambda$ and requiring $\lambda' \cdot \lambda = 1$. A Lagrange multiplier approach with constraints can be then used to show that the full set of eigenvectors of S is the solution to the linear combination with a maximum variance problem, obtaining up to m new linear combinations,

$$X_{\lambda_y} = \sum_{r=1}^{r=m} \lambda_{r,y} \cdot x_r, \tag{2}$$

which successively maximize variance, uncorrelated with other linear combinations [39]. PCA is thus a statistical technique for reducing the dimension of the initial data, increasing their interpretability, but at the same time, minimizing any information loss. A recent PCA review and developments can be found in [40]. Therefore, and by determining these principal components and their corresponding metric relations, different groups of differences—errors—are then identified and graphically represented. Moreover, they can be selected independently to provide a complementary information about the irradiance data source discrepancies. Figure 2 shows graphically the PCA application on the irradiance data metrics. As can be seen, different principal components are then estimated according to the metric dependence, decreasing the initial m-dimension of the metrics, allowing for a low-dimensional graphical representation and providing a reduced number of components independent among them. It is relevant to point out that this metric characterization has not been discussed previously in the

specific literature; previous authors proposed a variety of different metrics without analyzing their dependence and subsequently neglecting the possible redundancies of such metrics.

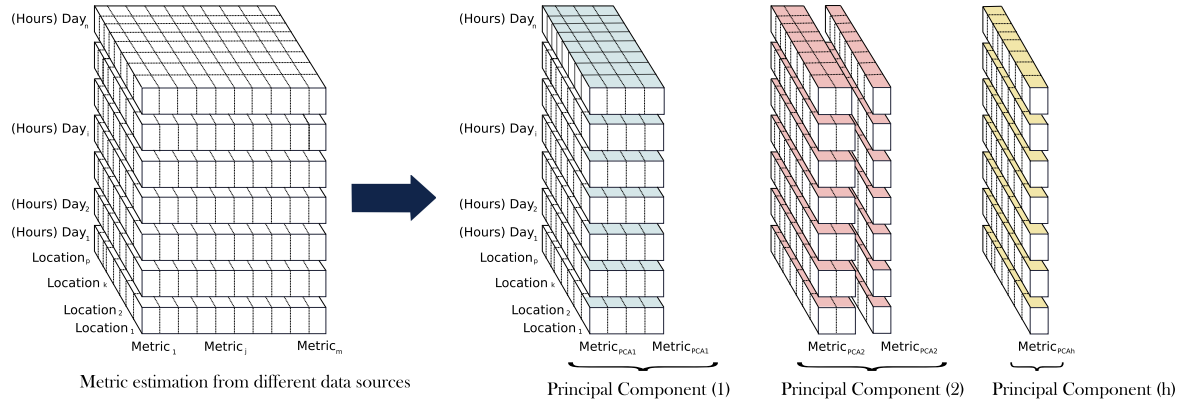

Figure 2. Principal component analysis (PCA). Graphical scheme.

The proposed methodology is implemented in the well-known `R` environment [41]. The following contribution packages are used for methodology implementation purposes: `ggplot2` to create graphics [42], `corrplot` to visualize correlation matrices [43], `FactoMineR` for the PCA application [44], and `dtw` and `dtwclust` for the dynamic time warping (DTW) and shape based distance (SBD) metrics estimation [45,46].

3. Case Study

Different ground-based meteorological stations were considered, comparing their GHI data to the satellite-based values for one year (2018). For the present analysis, the Network of the Agricultural Information System of Murcia (SIAM) was selected to provide ground-based irradiance data. SIAM consists of 49 automatic stations, ground-based installations that are geographically distributed along the Region of Murcia (11,300 km^2); 32 stations are from the Murcian Institute of Agricultural and Food Research and Development (IMIDA) Regional Government of Murcia, 15 are from the Spanish Ministry of Agriculture, Food and Environment, one is from the Universidad Politécnica de Cartagena (Murcia, Spain), and one is from the City Council of Mazarrón (Murcia, Spain). The IMIDA and Ministry stations were financially supported by European fund projects [47].

Figure 3 shows some examples of such meteorological stations and Figure 4 depicts some examples of data available online from these ground-based stations. As an attempt to cover a relevant area of study, seven ground-based stations geographically distributed along this south-east Spanish Region have been selected for the present analysis. In this way, Figure 5 shows the selected ground-based station locations in universal transverse Mercator (UTM) coordinates. The different colors in Figure 5 are related to the altitude of each ground-based meteorological station (depicted in UTM coordinates). Regarding satellite-based irradiance data, and among the different satellite-based irradiance data currently available online, the authors selected Copernicus, which is the European Union's Earth Observation Programme. This online platform provides a variety of information services based on satellite earth observation and in situ (non-space) data. The programme is currently coordinated and managed by the European Commission and it is implemented in partnership with the member states, the European Space Agency (ESA), the European Organisation for the Exploitation of Meteorological Satellites (EUMETSAT), the European Centre for Medium-Range Weather Forecasts (ECMWF), EU Agencies, and Mercator Océan. A relevant amount of global data is then available to provide information and help service providers, public authorities and other international organizations. The information services provided are freely and are openly accessible to its users [48].

Figure 3. Example of the ground-based meteorological stations (Source: SIAM-IMIDA [47]).

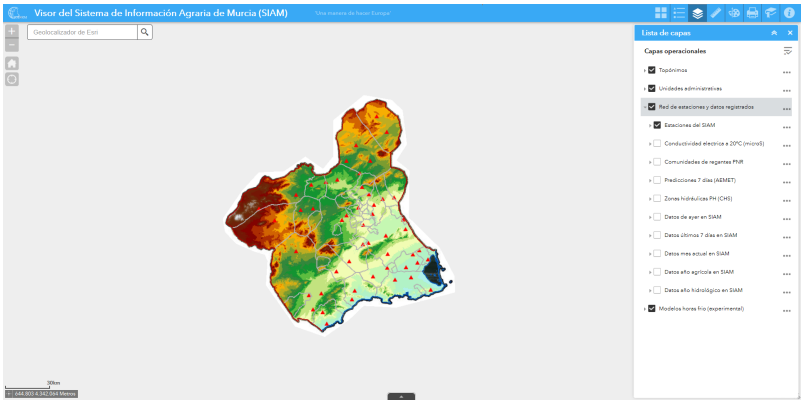

Figure 4. Ground-based data available online: graphical example of data (Source: SIAM-IMIDA [49]).

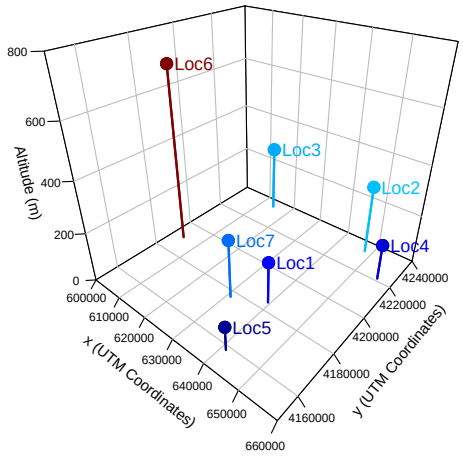

Figure 5. Ground-based meteorological station locations (universal transverse Mercator (UTM) coordinates).

According to the information available in the Network of the SIAM, irradiance values were collected by such ground-based meteorological stations, providing hourly average GHI data. Ten-minute sampling time is available for the Copernicus satellite-based data. Therefore, the corresponding hourly average satellite GHI values were then determined from the Copernicus satellite-based data to compare to the ground-based data. Nevertheless, and in line with the study presented by Kim et al. in [50], hourly average values can smooth the error metric bias. Moreover, if the instantaneous snapshot values are used in the error metric evaluation, the results would be worse. In this case, a total amount of 429,240 data points were initially analyzed, which correspond to the ground-based and satellite-based values accordingly. By considering this initial group of GHI values, a preliminary comparison of data was required to visualize some possible discrepancies among

the sources and data. With this aim, Figure 6 summarizes some consecutive days along 2018 and compares both the irradiance database values by considering hourly average values. The time series of bias, as satellite-based as ground-measured GHI values, are also included in such figure. These days correspond to weeks covering all seasons of the year, where the irradiance levels are considerably different and where several cloudy days and oscillating irradiance values can be also identified.

As a preliminary analysis, the irradiance data from both sources are significantly similar. Moreover, both irradiance curves are practically overlapping and, as was expected, a detailed metric analysis was required to compare the different sources in a more extended way. Subsequently, an estimation of metrics is then determined according to Table 1, where a variety of metrics used and proposed by previous contributions is summarized. With this aim, Figure 7 shows the daily evolution of such metrics, depending on each location and with a one hour sample time. Table 2 summarizes some descriptive statistics of the error metrics (including average values, minimum, maximum, and quartiles). These metrics were determined from both irradiation data sources and they provide a variety of alternatives to estimate the differences between the data. From these metrics, a characterization and classification by considering the proposed methodology, as described in Section 2, was carried out by the authors. The results are presented and discussed in Section 4. In addition, PCA was also applied to identify the main relationships among the metrics, reduce the number of variables and allow us a graphical representation of such metrics in a low-dimensional environment.

Table 2. Descriptive statistics of the error metrics.

	MSE	RMSE	nRMSE	MBE	nMBE	MAE	nMAE	MAPE	SBD	DTW
Minimum	29	5.37	0.0118	−128.35	−0.6236	4.62	0.0087	2.7	0.00001	98.2
1st Quartile	1036	32.19	0.0861	−23.94	−0.0698	25.02	0.0677	16.5	0.00092	479.3
Median	2700	51.96	0.1589	−6.96	−0.0186	38.80	0.1187	25.8	0.00510	702.8
Mean	4979	59.38	0.1894	−2.85	−0.0068	43.36	0.1388	57.1	0.01174	754.4
3rd Quartile	5821	76.29	0.2542	13.66	0.0383	55.73	0.1859	43.6	0.01546	975.4
Maximum	92,278	303.77	0.9690	178.53	0.5054	188.80	0.6904	2976.4	0.21422	2525.8

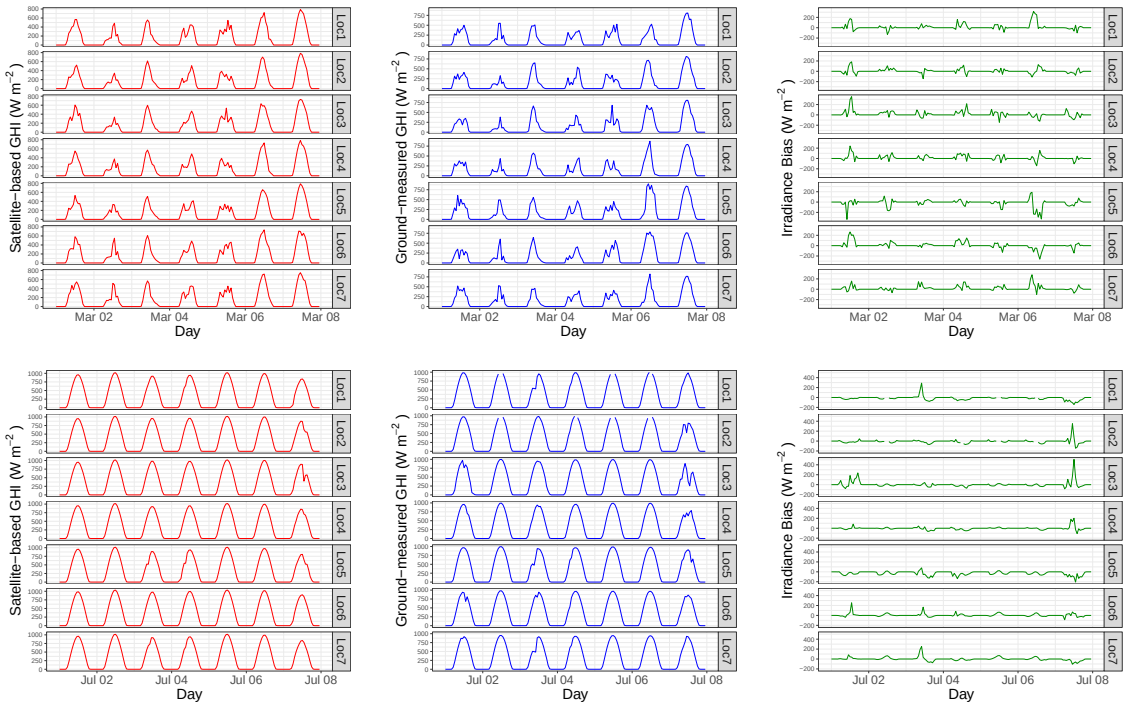

Figure 6. *Cont.*

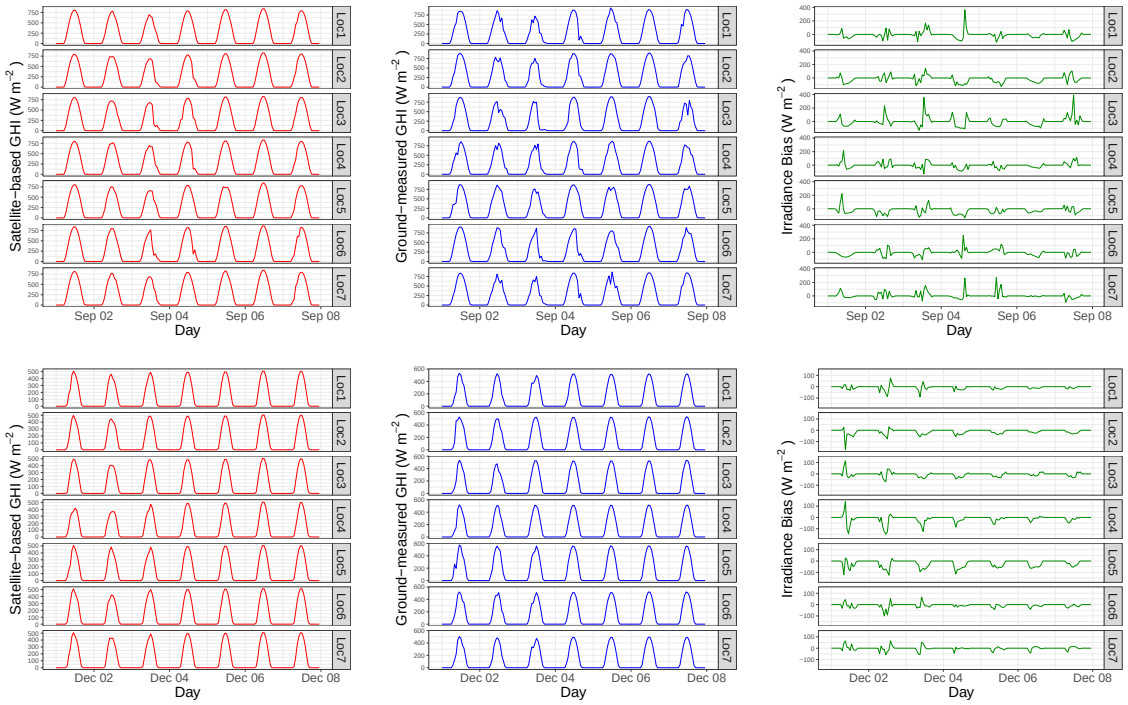

Figure 6. Examples of satellite-based hourly global horizontal irradiance (GHI), locally ground-measured GHI, and irradiance bias (One week of March, July, September, and December 2018).

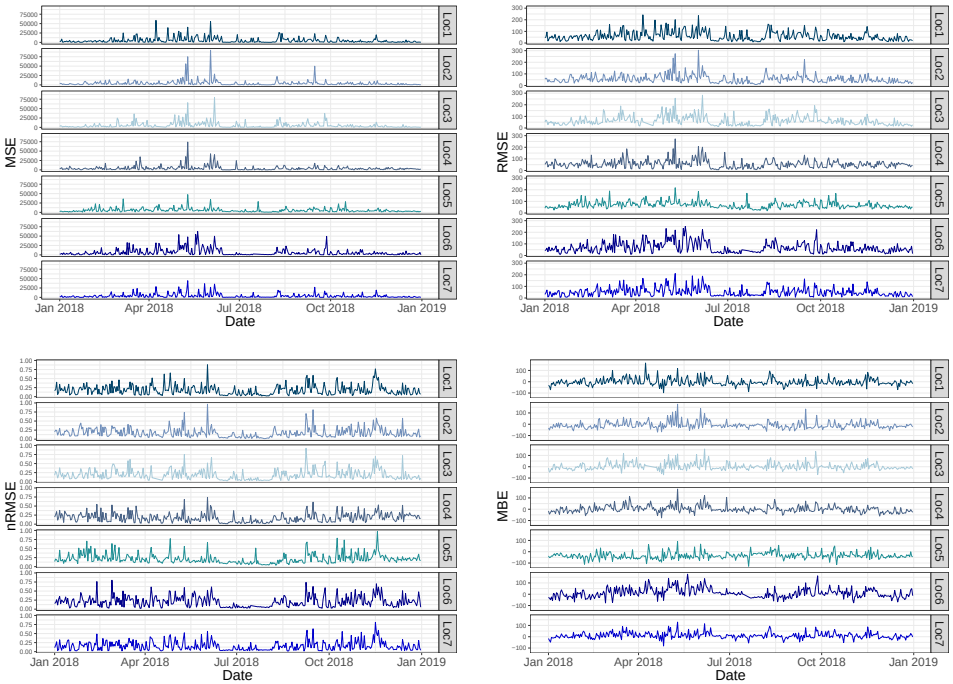

Figure 7. *Cont*.

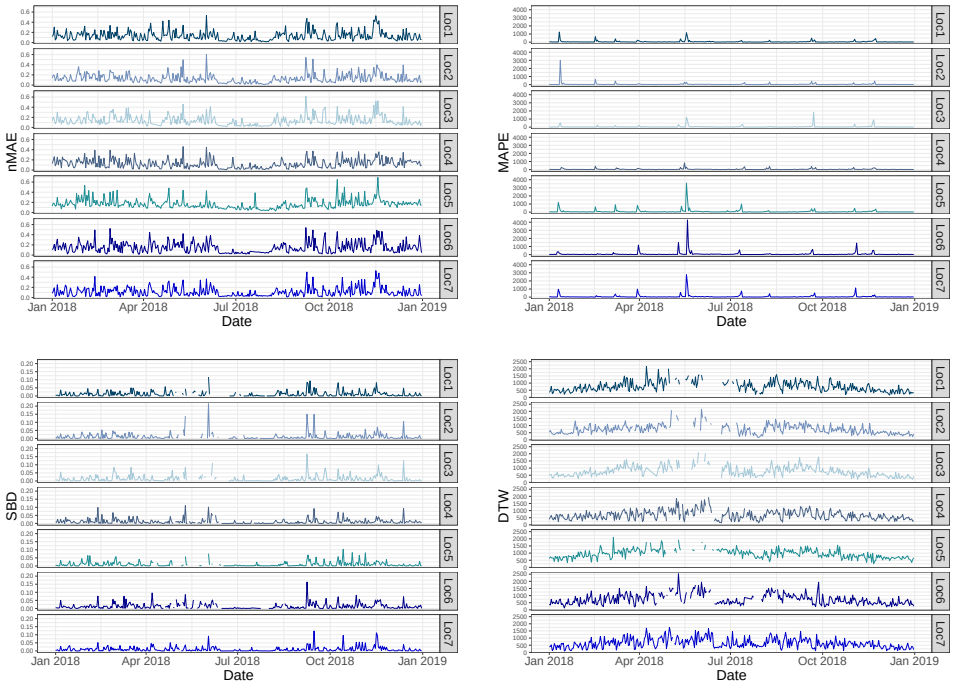

Figure 7. Daily evolution of the difference metrics at each location.

4. Results

As was previously discussed, by considering the different metrics summarized in Table 1 and according to the database described in Section 3, a total of ten metrics are determined by each location, with a one hour sample time and using the 2018 GHI data. Consequently, 17,520 values are then available by each location. An example of such different metrics can be found in Figure 7. From these preliminary results, an initial correlation analysis for the different locations is first carried out by the authors, in line with the proposed methodology depicted in Figure 1. These correlations are summarized in Figure 8, where all of the locations are individually analyzed and depicted. As can be seen, some groups of metrics can be identified, which correspond to a more relevant correlation. Therefore, these preliminary results provide an initial identification of groups of metrics that are highly correlated and, consequently, they offer a similar metric information. As an attempt to characterize the variability of these correlations in terms of the diversity introduced by the geographical dispersion, an additional statistical analysis was proposed and carried out as well. With this aim, Figure 8 also shows the mean and standard deviation values of the correlation coefficients by considering the metrics results of each location. As can be seen, and in this specific case study, the statistical results provide a low variability of metric correlations and, consequently, it is then proposed to analyze all of the metrics simultaneously and independently of the location. Therefore, the rest of the proposed methodology can be applied simultaneously to all metric estimations and without any dependence on the geographical location. Nevertheless, the proposed methodology can also be applied to other situations where the location dependence is more relevant and it cannot be neglected. In that case, the rest of methodology will be repeated by each location. As an additional result, and following with the present case study, Figure 9 shows the correlation matrices of the error metrics by considering all locations simultaneously. A similar group of relevant correlations is also identified in line with the previous correlation results depicted in Figure 8.

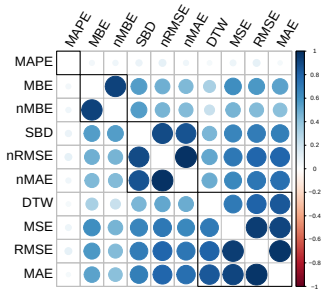

(**a**) Correlation matrix (Loc1).

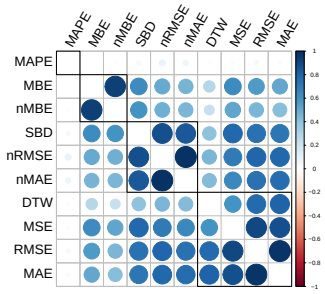

(**b**) Correlation matrix (Loc2).

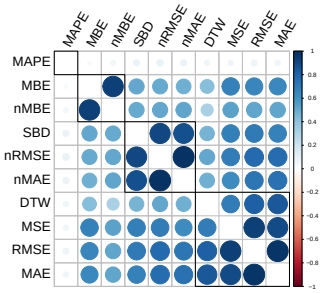

(**c**) Correlation matrix (Loc3).

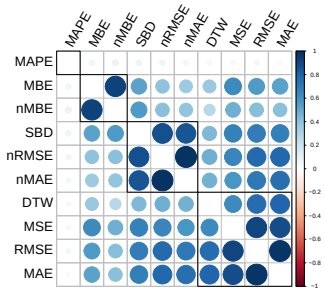

(**d**) Correlation matrix (Loc4).

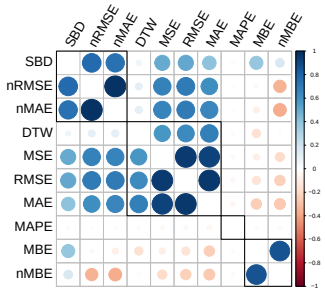

(**e**) Correlation matrix (Loc5).

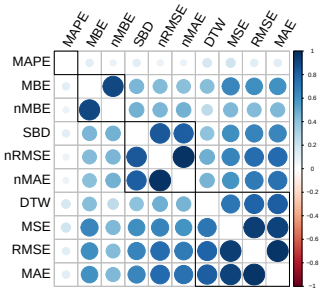

(**f**) Correlation matrix (Loc6).

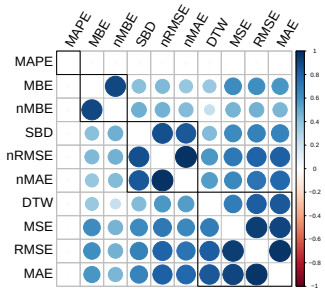

(**g**) Correlation matrix (Loc7).

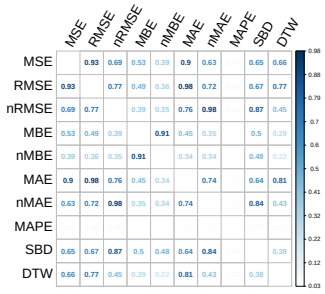

(**h**) Means.

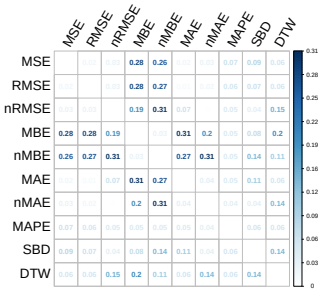

(**i**) Standard deviations.

Figure 8. (**a**–**g**) The correlation matrices of the error metrics for each separate location. (**h**,**i**) The means and standard deviations of the correlation coefficients of the error metrics, obtained at each location.

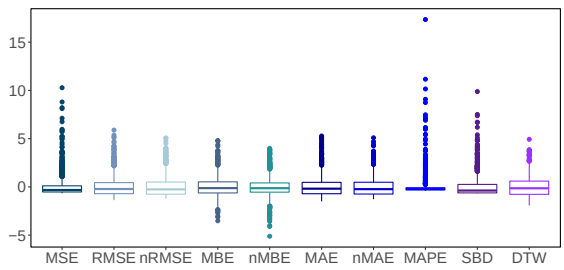

(**a**)

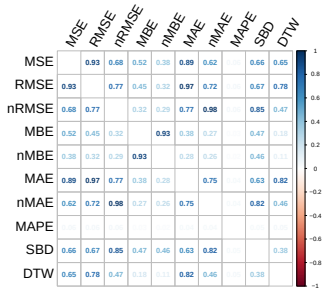

(**b**)

Figure 9. (**a**) Boxplots of the scaled error metrics for all locations. (**b**) Correlation matrix of error metrics for all locations.

In order to explore patterns of similarities and gain an understanding of the structure of variability between metrics, the PCA approach was then applied to the metrics. A reduction of dimension was also achieved by using such analysis. Moreover, by considering only the most relevant components, it should be informative enough to allow for pattern detection in similar metric studies. With this aim, and considering the proposed methodology by including the PCA approach from all metrics and locations as discussed in Section 2—and graphically given in Figure 2 for the current case study—the *'principal components'* are subsequently estimated for all metric results. By applying the PCA technique, Figure 10 shows the scree plot of the components (eigenvalues and percentage of variance accounted for by the principal components). As can be seen, when considering only the four most representative principal components, about 94% of the metric variability can be identified, which significantly reduces the metric dimension from 10-dimensions—see Table 1 and preliminary results in Figure 7—to four-dimensions. Therefore, and by considering these results, the first component explains 58.2% of the total variability, while the second component explains 16.1%, leaving the remaining third and fourth component with the explanation of around 10% of the variability for each one. As a consequence, an effective and convenient dimension reduction is achieved by considering the first four components of the PCA algorithm. For a more extensive analysis, the Appendix summarizes both eigenvalue and eigenvector results—see Tables A1 and A2, respectively.

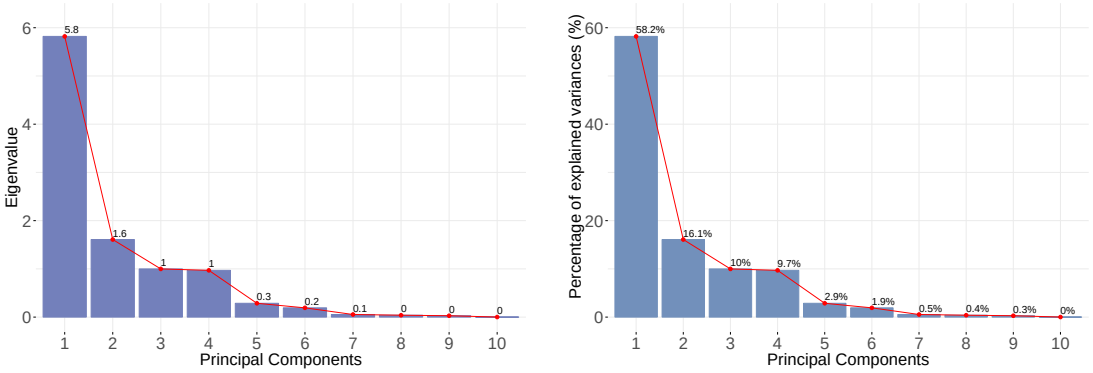

Figure 10. Scree plot of the components extracted by PCA.

With regard to the relevance of each metric on the selected *'principal components'*, Table 3 provides the relative weight of each metric for the corresponding relevant principal components. The bold marked values in Table 3 correspond to the most influent metrics for each principal component. In line with these results, Figure 11 gives the contributions, as a percentage, for each metric variable to the most relevant dimension corresponding to the PCA application. In addition, a dashed-line has been included to point out such relevant metrics corresponding to each dimension. Moreover, the dimensions clearly depend on different metrics, which enhances the preliminary correlations given in Figures 8 and 9. Consequently, and in line with a main objective of this work, it is then possible to identify different groups of metrics that provide complementary information and, thus, they can be combined to characterize convenient differences among different database sources.

Table 3. Relative weight of each metric for the most relevant principal components.

	MSE	RMSE	nRMSE	MBE	nMBE	MAE	nMAE	MAPE	SBD	DTW
PC1	**0.37**	**0.39**	**0.37**	0.24	0.20	**0.39**	**0.35**	0.03	**0.35**	0.29
PC2	−0.02	−0.13	−0.12	**0.62**	**0.66**	−0.18	−0.15	−0.01	0.08	−0.28
PC3	0.07	0.06	−0.14	0.05	0.02	0.04	−0.16	**0.95**	−0.14	0.16
PC4	−0.23	−0.21	**0.40**	−0.15	−0.05	−0.22	**0.42**	**0.31**	**0.40**	**−0.48**

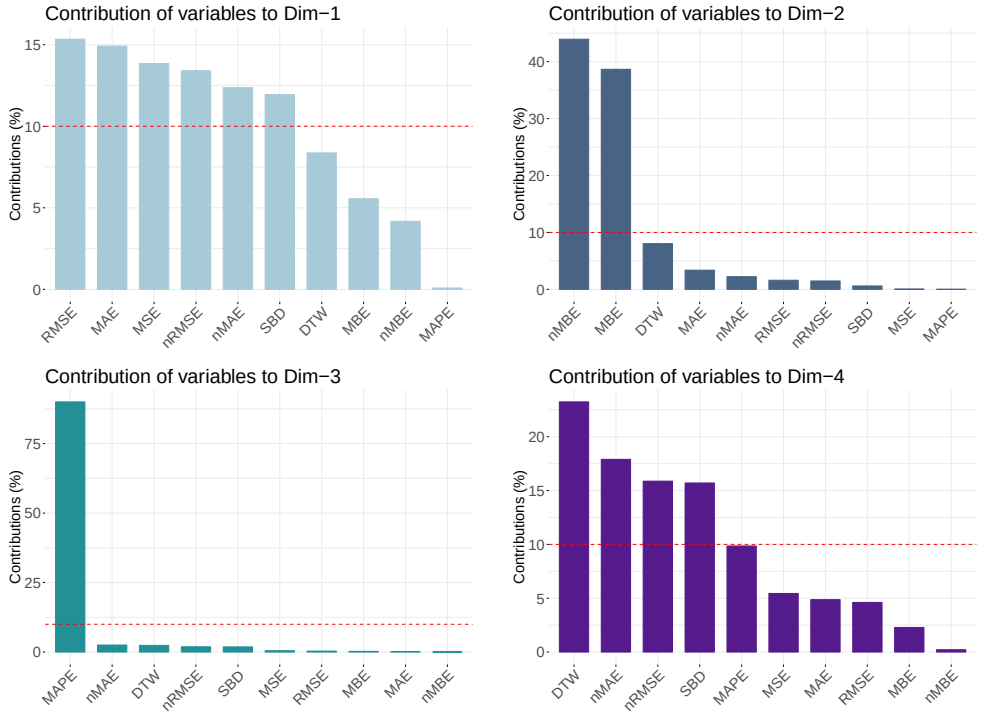

Figure 11. Contributions (%) of each variable to each dimension of the PCA.

Finally, Figure 12 summarizes the metric correlation with the four selected *'principal components'*, which represent about 94% of the global metric variability. In this graphical representation, circles correspond to $r^2 = 50\%$ and 100% variability explained by the components respectively. Therefore, the area within both circles contains the most representative metrics depending on each principal component. These results are thus a complementary characterization of the metrics, considering their correlation with the selected principal components.

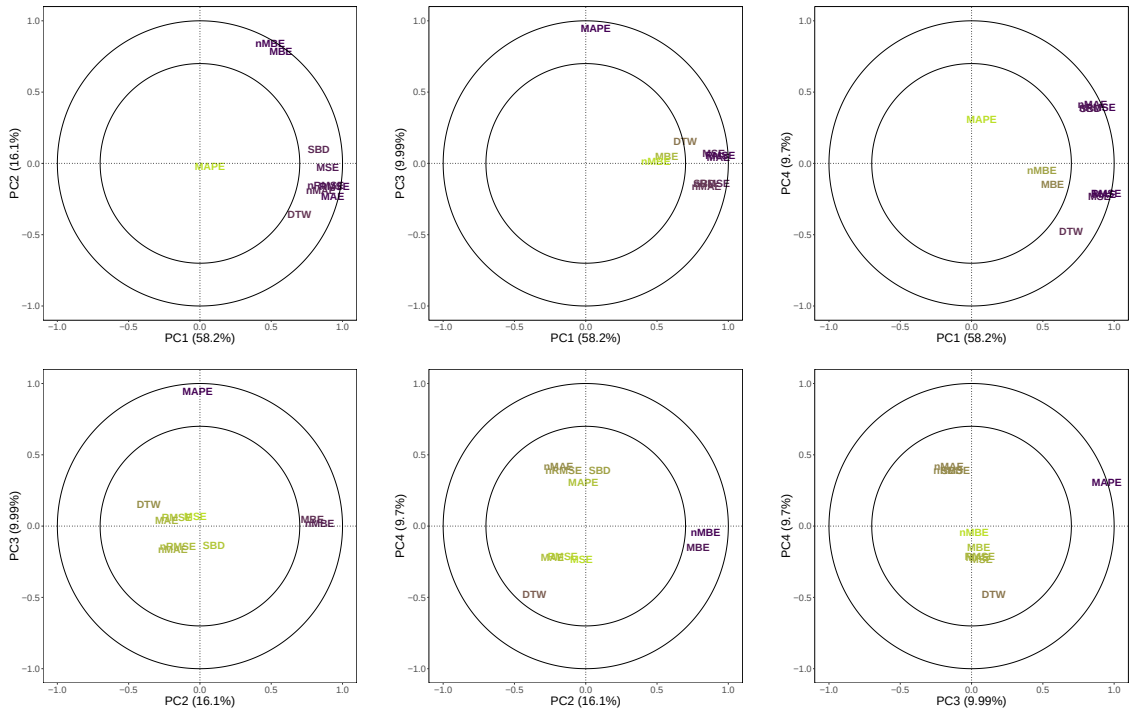

Figure 12. Correlation plots of the first four components of the PCA applied to the metrics.

5. Conclusions

A characterization of metrics based on GHI data from different sources is described and assessed in order to identify different groups of similar metrics. From the specific literature, a group of ten different metrics is initially selected, which have been proposed by other contributions to compare different irradiation data. A location dependence analysis and a PCA application process is proposed to characterize such metrics and identify the similarities and explore the differences among them. The proposed methodology has been evaluated from satellite-based and ground-measured GHI data collected for one year in seven different Spanish locations, using average hourly estimations. We analyzed an initial database of 429,240 data points, which corresponds to the satellite-based and ground-measured values accordingly. The selected metrics are determined by each pair of irradiance data and the correlation matrices for each location are estimated.

PCA application allows us to explore similarities among metrics and identify the most relevant *'principal components'*. Moreover, a reduction of dimension is also addressed by this technique. In this case, a group of four-*'principal components'* is selected, which accounts for 94% of the metric variability. Therefore, a dimension reduction and an identification of metric groups with similar information are provided, which outlines the suitability of the process. Moreover, the initial variety metrics are representative of different principal components and, thus, it is possible to identify and select such groups of metrics that offer complementary information. Non-redundant information metric groups are then available to determine the differences among irradiation database sources. This work provides a solution to compare metrics, despite the lack of agreement in validation strategies for irradiance databases that has been currently detected by the authors.

Author Contributions: Conceptualization, A.M.-G. and M.C.B.; methodology, M.C.B.; validation, J.M.P.-P., A.M.-A., and A.M.-G.; formal analysis, M.C.B.; resources, J.M.P.-P.; data curation, M.C.B.; writing—original draft preparation, A.M.-G.; writing—review and editing, A.M.-G. and A.M.-A. All authors have read and agreed to the published version of the manuscript.

Funding: The paper includes results of activities conducted under the Research Program for Groups of Scientific Excellence at Region of Murcia (Spain), the Seneca Foundation, and the Agency for Science and Technology of the Region of Murcia (Spain). This work was also supported by the Spanish Ministry of Economy and Competitiveness and the European Union–FEDER Funds, ENE2016-78214–C2-1-R.

Conflicts of Interest: The authors declare no conflict of interest.

Abbreviations

The following abbreviations are used in this manuscript:

ECMWF	The European Centre for Medium-Range Weather Forecasts
ESA	The European Space Agency
EU	The European Union
EUMETSAT	The European Organisation for the Exploitation of Meteorological Satellites
GHI	Global Horizontal Irradiance
GOES	Geostationary Operational Environmental Satellite
IMIDA	Murcian Institute of Agricultural and Food Research and Development
MODIS	Moderate Resolution Imaging Spectroradiometer
MSG	Meteosat Second Generation
PCA	Principal Component Analysis
PV	Photovoltaic
PVGIS	Photovoltaic Geographical Information System
SIAM	Agricultural Information System of Murcia
UTM	Universal Transverse Mercator

Symbols in metrics:

DTW	Dynamic Time Warping
GHI^{grd}	Ground-measured GHI
GHI^{sat}	Satellite-based GHI
gMBD	General Mean Bias Deviation
MAD	Mean Absolute Difference
MAE	Mean Absolute Error
MAPE	Mean Absolute Percentage Error
MBE	Mean Bias Error
MSE	Mean Square Error
NCC	Normalized Cross-Correlation
nMAE	Normalized Mean Absolute Error
nMBE	Normalized Mean Bias Error
nRMSE	Normalized Root Mean Square Error
r	Pearson Correlation Coefficient
rgMBD	Relative General Mean Bias Deviation
rMAE	Relative Mean Absolute Error
rMBE	Relative Mean Bias Error
RMSE	Root Mean Square Error
rRMSE	Relative Root Mean Square Error
R^2	Determination Coefficient
SBD	Shape Based Distance
SD	Standard Deviation

Appendix A

Table A1. Eigenvalues and percentage of variance explained associated with each component in the PCA.

Component	Eigenvalue	Percentage of Variance (%)	Cumulative Percentage of Variance (%)
1	5.8202	58.2016	58.2016
2	1.6084	16.0838	74.2854
3	0.9991	9.9911	84.2765
4	0.9697	9.6970	93.9735
5	0.2866	2.8663	96.8397
6	0.1923	1.9229	98.7627
7	0.0543	0.5432	99.3059
8	0.0394	0.3937	99.6996
9	0.0287	0.2871	99.9868
10	0.0013	0.0132	100.0000

Table A2. Principal components (eigenvectors) in the PCA.

	Dim 1	Dim 2	Dim 3	Dim 4	Dim 5	Dim 6	Dim 7	Dim 8	Dim 9	Dim 10
MSE	0.3721	−0.0239	0.0700	−0.2333	−0.6377	0.1253	0.2759	0.5481	0.0517	0.0002
RMSE	0.3917	−0.1266	0.0590	−0.2147	−0.2114	−0.1170	−0.1351	−0.4730	−0.5169	0.4620
nRMSE	0.3662	−0.1214	−0.1379	0.3984	0.0682	−0.2498	−0.1452	0.1887	−0.4829	−0.5626
MBE	0.2357	0.6217	0.0505	−0.1512	−0.0338	−0.1281	−0.6789	0.1086	0.2052	−0.0119
nMBE	0.2043	0.6629	0.0181	−0.0467	0.2937	−0.0698	0.6199	−0.0684	−0.1904	−0.0005
MAE	0.3862	−0.1836	0.0420	−0.2206	−0.0372	−0.2242	0.1497	−0.4859	0.5214	−0.4297
nMAE	0.3517	−0.1495	−0.1590	0.4231	0.2162	−0.3663	0.0723	0.2198	0.3608	0.5340
MAPE	0.0291	−0.0131	0.9487	0.3139	−0.0019	−0.0100	0.0033	−0.0107	0.0142	−0.0009
SBD	0.3456	0.0776	−0.1362	0.3963	−0.0097	0.7963	−0.0584	−0.2198	0.1132	0.0117
DTW	0.2893	−0.2835	0.1553	−0.4820	0.6390	0.2613	−0.0913	0.3016	−0.0595	0.0073

References

1. Ellabban, O.; Abu-Rub, H.; Blaabjerg, F. Renewable energy resources: Current status, future prospects and their enabling technology. *Renew. Sustain. Energy Rev.* **2014**, *39*, 748–764. [CrossRef]
2. Wang, L.; Singh, C.; Kusiak, A. Guest Editorial: Special Issue on Ontegration of Intermittent Renewable Energy Resources into Power Grid. *IEEE Syst. J.* **2012**, *6*, 2–3. [CrossRef]
3. Wan, C.; Zhao, J.; Song, Y.; Xu, Z.; Lin, J.; Hu, Z. Photovoltaic and solar power forecasting for smart grid energy management. *CSEE J. Power Energy Syst.* **2015**, *1*, 38–46. [CrossRef]
4. Shi, J.; Lee, W.; Liu, Y.; Yang, Y.; Wang, P. Forecasting power output of photovoltaic systems based on weather classification and support vector machines. *IEEE Trans. Ind. Appl.* **2012**, *48*, 1064–1069. [CrossRef]
5. Yang, C.; Thatte, A.A.; Xie, L. Multitime-scale data-driven spatio-temporal forecast of photovoltaic generation. *IEEE Trans. Sustain. Energy* **2015**, *6*, 104–112. [CrossRef]
6. Ahmed, A.; Khalid, M. A review on the selected applications of forecasting models in renewable power systems. *Renew. Sustain. Energy Rev.* **2019**, *100*, 9–21. [CrossRef]
7. Notton, G.; Paoli, C.; Vasileva, S.; Nivet, M.L.; Canaletti, J.L.; Cristofari, C. Estimation of hourly global solar irradiation on tilted planes from horizontal one using artificial neural networks. *Energy* **2012**, *39*, 166–179. [CrossRef]
8. dos Santos, C.M.; Escobedo, J.F.; Teramoto, E.T.; da Silva, S.H.M.G. Assessment of ANN and SVM models for estimating normal direct irradiation (Hb). *Energy Convers. Manag.* **2016**, *126*, 826–836. [CrossRef]
9. Bouchouicha, K.; Hassan, M.A.; Bailek, N.; Aoun, N. Estimating the global solar irradiation and optimizing the error estimates under Algerian desert climate. *Renew. Energy* **2019**, *139*, 844–858. [CrossRef]
10. Noorian, A.M.; Moradi, I.; Kamali, G.A. Evaluation of 12 models to estimate hourly diffuse irradiation on inclined surfaces. *Renew. Energy* **2008**, *33*, 1406–1412. [CrossRef]
11. Teke, A.; Yıldırım, H.B.; Celik, O. Evaluation and performance comparison of different models for the estimation of solar radiation. *Renew. Sustain. Energy Rev.* **2015**, *50*, 1097–1107. [CrossRef]
12. Dobos, A. *PVWatts Version 5 Manual*; National Renewable Energy Laboratory (NREL): Denver, CO, USA, 2014. Available online: http://www.nrel.gov/docs/ (accessed on 1 December 2019).
13. Uri, M.; Huld, T.; Dunlop, E. PV-GIS: A web-based solar radiation database for the calculation of PV potential in Europe. *Int. J. Sol. Energy* **2005**, *24*, 55–67. [CrossRef]
14. International Renewable Energy Agency (IRENA). Global Atlas for Renewable Energy: Overview of Solar and Wind Maps. Available online: https://irena.masdar.ac.ae/gallery/#gallery (accessed on 1 December 2019).
15. SOLARGIS. Weather Data and Software for Solar Power Investments. 2019. Bratislava Slovakia. Available online: https://solargis.com/ (accessed on 1 December 2019).
16. Piasecki, A.; Jurasz, J.; Kies, A. Measurements and reanalysis data on wind speed and solar irradiation from energy generation perspectives at several locations in Poland. *SN Appl. Sci.* **2019**, *1*, 865. [CrossRef]
17. Bódis, K.; Kougias, I.; Jager-Waldau, A.; Taylor, N.; Szabó, S. A high-resolution geospatial assessment of the rooftop solar photovoltaic potential in the European Union. *Renew. Sustain. Energy Rev.* **2019**, *114*, 109309. [CrossRef]
18. Psiloglou, B.; Kambezidis, H.; Kaskaoutis, D.; Karagiannis, D.; Polo, J. Comparison between MRM simulations, CAMS and PVGIS databases with measured solar radiation components at the Methoni station, Greece. *Renew. Energy* **2020**, *146*, 1372–1391. [CrossRef]
19. Bocca, A.; Bergamasco, L.; Fasano, M.; Bottaccioli, L.; Chiavazzo, E.; Macii, A.; Asinari, P. Multiple-regression method for fast estimation of solar irradiation and photovoltaic energy potentials over Europe and Africa. *Energies* **2018**, *11*. [CrossRef]
20. Feng, J.; Wang, W.; Li, J. An LM–BP neural network approach to estimate monthly-mean daily global solar radiation using MODIS atmospheric products. *Energies* **2018**, *11*, 3510. [CrossRef]
21. Amillo, A.M.G.; Huld, T.; Vourlioti, P.; Müller, R.; Norton, M. Application of satellite-based spectrally-resolved solar radiation data to PV performance studies. *Energies* **2015**, *8*, 3455–3488. [CrossRef]
22. Pierro, M.; Felice, M.D.; Maggioni, E.; Moser, D.; Perotto, A.; Spada, F.; Cornaro, C. Data-driven upscaling methods for regional photovoltaic power estimation and forecast using satellite and numerical weather prediction data. *Sol. Energy* **2017**, *158*, 1026–1038. [CrossRef]

23. Antonanzas-Torres, F.; Cañizares, F.; Perpiñán, O. Comparative assessment of global irradiation from a satellite estimate model (CM SAF) and on-ground measurements (SIAR): A Spanish case study. *Renew. Sustain. Energy Rev.* **2013**, *21*, 248–261. [CrossRef]
24. Buffat, R.; Grassi, S.; Raubal, M. A scalable method for estimating rooftop solar irradiation potential over large regions. *Appl. Energy* **2018**, *216*, 389–401. [CrossRef]
25. Porfirio, A.C.; Ceballos, J.C. A method for estimating direct normal irradiation from GOES geostationary satellite imagery: Validation and application over Northeast Brazil. *Sol. Energy* **2017**, *155*, 178–190. [CrossRef]
26. Pfenninger, S.; Staffell, I. Long–term patterns of European PV output using 30 years of validated hourly reanalysis and satellite data. *Energy* **2016**, *114*, 1251–1265. [CrossRef]
27. Ernst, M.; Thomson, A.; Haedrich, I.; Blakers, A. Comparison of ground-based and satellite-based irradiance data for photovoltaic yield estimation. *Energy Procedia* **2016**, *92*, 546–553. [CrossRef]
28. Moreno, A.; Gilabert, M.; Camacho, F.; Martínez, B. Validation of daily global solar irradiation images from MSG over Spain. *Renew. Energy* **2013**, *60*, 332–342. [CrossRef]
29. Gueymard, C.A. A review of validation methodologies and statistical performance indicators for modeled solar radiation data: Towards a better bankability of solar projects. *Renew. Sustain. Energy Rev.* **2014**, *39*, 1024–1034. [CrossRef]
30. Bright, J.M. Solcast: Validation of a satellite-derived solar irradiance dataset. *Sol. Energy* **2019**, *189*, 435–449. [CrossRef]
31. Paoli, C.; Voyant, C.; Muselli, M.; Nivet, M.L. Forecasting of preprocessed daily solar radiation time series using neural networks. *Sol. Energy* **2010**, *84*, 2146–2160. [CrossRef]
32. Nik, W.W.; Ibrahim, M.; Samo, K.; Muzathik, A. Monthly mean hourly global solar radiation estimation. *Sol. Energy* **2012**, *86*, 379–387. [CrossRef]
33. Lu, N.; Qin, J.; Yang, K.; Sun, J. A simple and efficient algorithm to estimate daily global solar radiation from geostationary satellite data. *Energy* **2011**, *36*, 3179–3188. [CrossRef]
34. Yang, L.; Gao, X.; Li, Z.; Jia, D.; Jiang, J. Nowcasting of surface solar irradiance using FengYun-4 satellite observations over China. *Remote Sens.* **2019**, *11*. [CrossRef]
35. Paparrizos, J.; Gravano, L. K-Shape: Efficient and accurate clustering of time series. In Proceedings of the 2015 ACM SIGMOD International Conference on Management of Data, Melbourne, Victoria, Australia, 31 May–4 June 2015; pp. 1855–1870. [CrossRef]
36. Molina-García, A.; Fernández-Guillamón, A.; Gómez-Lázaro, E.; Honrubia-Escribano, A.; Bueso, M.C. Vertical wind profile characterization and identification of patterns based on a shape clustering algorithm. *IEEE Access* **2019**, *7*, 30890–30904. [CrossRef]
37. Keogh, E.; Ratanamahatana, C.A. Exact indexing of dynamic time warping. *Knowl. Inf. Syst.* **2005**, *7*, 358–386. [CrossRef]
38. Combes, C.; Azema, J. Clustering using principal component analysis applied to autonomy—Disability of elderly people. *Decis. Support Syst.* **2013**, *55*, 578–586. [CrossRef]
39. Jolliffe, I. Principal Component Analysis. In *International Encyclopedia of Statistical Science*; Lovric, M., Ed.; Springer: Berlin/Heidelberg, Germany, 2011; pp. 1094–1096._455. [CrossRef]
40. Jolliffe, I.T.; Cadima, J. Principal component analysis: a review and recent developments. *Philos. Trans. R. Soc. A Math. Phys. Eng.* **2016**, *374*. [CrossRef]
41. R Core Team. *R: A Language and Environment for Statistical Computing*; R Foundation for Statistical Computing: Vienna, Austria, 2018.
42. Wickham, H. *ggplot2: Elegant Graphics for Data Analysis*; Springer: New York, NY, USA, 2016.
43. Wei, T.; Simko, V. R Package 'Corrplot': Visualization of a Correlation Matrix, version 0.84; October 2017. Available online: https://cran.r-project.org/web/packages/corrplot/corrplot.pdf (accessed on 1 December 2019).
44. Lê, S.; Josse, J.; Husson, F. FactoMineR: A Package for Multivariate Analysis. *J. Stat. Softw.* **2008**, *25*, 1–18. [CrossRef]
45. Giorgino, T. Computing and Visualizing Dynamic Time Warping Alignments in R: The dtw Package. *J. Stat. Softw.* **2009**, *31*, 1–24. [CrossRef]
46. Sarda-Espinosa, A. Dtwclust: Time Series Clustering Along with Optimizations for the Dynamic Time Warping Distance, R Package version 5.5.6; December 2019. Available online: https://cran.r-project.org/web/packages/dtwclust/dtwclust.pdf (accessed on 10 January 2020).

47. Network of the Agricultural Information System of Murcia (SIAM), 2019. Available online: https://siam.imida.es/ (accessed on 27 January 2020).
48. European Union's Earth Observation Programme, 2019. Available online: https://www.copernicus.eu/ (accessed on 27 January 2020).
49. Online Viewer of the Agricultural Information System of Murcia, 2019. Available online: https://geoportal.imida.es/siam/ (accessed on 27 January 2020).
50. Kim, C.K.; Kim, H.G.; Kang, Y.H.; Yun, C.Y. Toward Improved Solar Irradiance Forecasts: Comparison of the Global Horizontal Irradiances Derived from the COMS Satellite Imagery Over the Korean Peninsula. *Pure Appl. Geophys.* **2017**, *174*, 2773–2792. [CrossRef]

4.4. Sensitive parameter analysis for solar irradiance short-term forecasting: application to LoRa-based monitoring technology

Información adicional:

- Revista: Sensors 22, no. 4: 1499
- DOI: 10.3390/s22041499
- Fecha de publicación: Febrero 2022
- Disponible en: `https://www.mdpi.com/1424-8220/22/4/1499`
- Referencia: [99] Bueso, M.C.; Paredes-Parra, J.M.; Mateo-Aroca, A.; Molina-García, A. Sensitive Parameter Analysis for Solar Irradiance Short-Term Forecasting: Application to LoRa-Based Monitoring Technology. Sensors 2022, 22, 1499. `https://doi.org/10.3390/s22041499`

sensors

MDPI

Article

Sensitive Parameter Analysis for Solar Irradiance Short-Term Forecasting: Application to LoRa-Based Monitoring Technology

M.C. Bueso [1], J. M. Paredes-Parra [2], A. Mateo-Aroca [3] and A. Molina-García [3,*]

[1] Department of Applied Mathematics and Statistics, Universidad Politécnica de Cartagena, 30202 Cartagena, Spain; mcarmen.bueso@upct.es
[2] Technologic Center of Energy and Environment, 30202 Cartagena, Spain; jmparedes@cetenma.es
[3] Department of Automatic, Electrical Engineering and Electronic Technology, Universidad Politécnica de Cartagena, 30202 Cartagena, Spain; antonio.mateo@upct.es
* Correspondence: angel.molina@upct.es; Tel.: +34-968-32-5462

Abstract: Due to the relevant penetration of solar PV power plants, an accurate power generation forecasting of these installations is crucial to provide both reliability and stability of current grids. At the same time, PV monitoring requirements are more and more demanded by different agents to provide reliable information regarding performances, efficiencies, and possible predictive maintenance tasks. Under this framework, this paper proposes a methodology to evaluate different LoRa-based PV monitoring architectures and node layouts in terms of short-term solar power generation forecasting. A random forest model is proposed as forecasting method, simplifying the forecasting problem especially when the time series exhibits heteroscedasticity, nonstationarity, and multiple seasonal cycles. This approach provides a sensitive analysis of LoRa parameters in terms of node layout, loss of data, spreading factor and short time intervals to evaluate their influence on PV forecasting accuracy. A case example located in the southeast of Spain is included in the paper to evaluate the proposed analysis. This methodology is applicable to other locations, as well as different LoRa configurations, parameters, and networks structures; providing detailed analysis regarding PV monitoring performances and short-term PV generation forecasting discrepancies.

Keywords: LoRa technology; PV monitoring; sensitive parameter analysis

Citation: Bueso, M.C.; Paredes-Parra, J.M.; Mateo-Aroca, A.; Molina-García, A. Sensitive Parameter Analysis for Solar Irradiance Short-Term Forecasting: Application to LoRa-Based Monitoring Technology . *Sensors* **2022**, *1*, 0. https://doi.org/

Academic Editor: Fco Javier Rodríguez

Received: 25 December 2021
Accepted: 8 February 2022
Published:

1. Introduction

The high integration of variable renewable energy sources (vRES) into current power systems, mainly wind and solar photovoltaic (PV) power plants, can be a key component of the resulting low-carbon power systems. However, their intermittency requires more flexibility from the rest of the power system to maintain certain grid stability and reliability levels [1]. Consequently, the increase in demand variability created by such intermittent sources presents new challenges to provide relevant system flexibility [2]. In addition to these challenges, accurate forecasting of renewable generation is also required by both transmission and distribution system operators in order to mitigate the negative impact on the grids of such variable and noncontrollable resources. According to Daliento et al., similar models are usually adopted for power forecasting for PV fields, which is important for both monitoring purposes and the management of the utility grid [3]. With this aim, different solar PV power generation forecasting solutions can be found in the specific literature [4]. The forecasting timeframe, also called horizon, is firstly defined according to the grid operation and under both spatial and temporal resolutions. Different forecast horizons can be then defined, varying from seconds to days or weeks ahead. Regarding spatial horizons, they can also be spanned from single site to regional forecasts [5]. In [6], a new model based on hourly measurements is proposed and evaluated. In [7], the application of neural networks for photovoltaic power generation forecasting purposes is explored by Oudjana et al. Other forecasting neural network-based solutions

can be found in the specific literature [8–12]. Naveed Akhter et al. [13] present a critical and systematic review of photovoltaic (PV) power forecasting methods, mostly focused on machine learning and metaheuristic based-solutions. An extreme learning machine technique is used for PV power forecasting of a real time model [14]. A revision of solar irradiance and PV power forecasting, both topics combined as "solar forecasting", using text mining is discussed in [15]. Barbieri et al. [16] conclude that cell/module temperature and irradiance can be considered as the best approaches for an accurate PV power forecasting; mainly under cloudy conditions with hardly predictable power generation fluctuations. A probabilistic forecast review focused on inherently erroneous of different forecasting strategies is discussed and quantified in [17]. Short-term photovoltaic power generation forecasting is also an important task in renewable energy power system planning and operating. In fact, Kaur et al. [18] affirm that short-term electricity trading to balance demand and generation offers a remarkable economic opportunity to integrate larger shares of vRES into future power grids. A novel multi-timescale data-driven forecast model to improve the accuracy of short-term PV power production is proposed by Yang et al. [19]. Dambreville et al. [20] propose a new approach of global horizontal irradiance (GHI) forecasting for very short-term by using a spatio–temporal autoregressive model.

From the specific literature, observed weather data are commonly applied on the solar PV generation forecasting model [21]. Subsequently, the solar PV forecasting model performance is then evaluated by quantifying discrepancies between such forecasts and the weather measurements through the use of traditional statistical error metrics, such as the mean bias error or the root mean square error (RMSE) [22]. For example, the mean absolute percentage error (MAPE), and mean absolute error (MAE) indicators are used in [23] to evaluate the performance of day-ahead photovoltaic power forecasting models based on deep learning neural network. Normalized root mean square error (nRMSE) is used in [24] to evaluate the forecasting errors. In a similar way, Huang et al. describe a comparative study of solar PV power forecasting methods based on nRMSE [25]. An extensive comparison of simple forecasting methodologies with more sophisticated solutions over 32 photovoltaic (PV) plants of different sizes and technology over a whole year is carried out by Gigoni et al. [26]. However, there is a lack of contributions focused on evaluating possible forecasting errors and minor accurate results derived from the inherent communication network failures: packet losses, possible packet collisions, etc., as well as the short time period influence of such GHI forecasting accuracy. Indeed, possible communication failure can significantly affect both gathering data and forecasting results [27]. Subsequently, and by considering such missed contributions in the specific literature about this issue, the present paper analyzes the influence of the LoRa solution—identified by the literature as a promise and suitable technology—on the GHI short-term forecasting accuracy, by considering real communication architecture/layout and specific LoRa performance characteristics. In addition, current datasets available from satellite-based installations, ground-based installations, and solar PV power plants connected to the grid are also considered for evaluation. In this way, a case example located in the southeast of Spain is included in the paper to assess the suitability of the proposed methodology. The main contributions of this paper can be summarized as (i) a methodology to evaluate GHI short-term forecasting accuracy for different node layouts and LoRa parameters based on a random forest prediction model; (ii) a sensitive analysis of LoRa parameters and short-term intervals on the GHI forecasting values based on a variety of metrics; and (iii) a case study from 2019 GHI data (one-minute sample time), 400 km^2 area, 289 potential nodes under consideration, and a total of 13,140 simulations. This methodology thus provides a preliminary extensive analysis of potential LoRa network characteristics and node layout in terms of data accuracy, packets, and GHI forecasting possibilities before the installation was completed.

The rest of the paper is structured as follows. Section 2 discusses PV power plant monitoring and the use of LoRa technology as a solution to be implemented in such installations. Section 3 describes the proposed methodology. A case example is presented

in Section 4. Results and discussion are provided in Section 5. Finally, conclusions are given in Section 6.

2. Pv Monitoring: LoRa Communication Technology

2.1. General Overview

A variety of PV monitoring strategies based on the output PV power plants and their nature have been proposed in the literature; being performed remotely or locally on site. New advanced monitoring techniques are continuously under investigation; mainly due to the evolution and relevant integration of PV installations into power systems. A recent PV monitoring review is analyzed by Triki-Lahiani et al. [28]; discussing their differences, advantages, and limits. An impedance-based monitoring method for detection of distribution system current behavior is presented in [29]. This monitoring technique can be used for small variation of PV penetration level, and for some fast transient detection, such as the effect of cloud movement on a PV system.

2.2. Lora-Based Communication System

Although different wireless technologies—such as Bluetooth, Zigbee, Wi-Fi, GSM, Sigfox, or LoRa—have been evaluated for PV solar monitoring through wireless sensors networks, LoRa technology has been chosen as the wireless technology due to its long range and low power consumption [30]. Moreover, this technology has received significant attention in recent years from network operators and solution providers [31–34]. An impartial and fair overview regarding the capabilities and the limitations of LoRaWAN is discussed by Adelantado et al. [35] to clarify its comprehension and avoid inflated expectations. LoRa uses six spreading factors (SF07 to SF12) to adapt the data rate and range trade-off. It can be affirmed that a higher spreading factor (SF) allows longer range at the expense of lower data rate [36]. The LoRa data rate depends on the channel bandwidth and the SF, ranging from 0.3 kbps to 27 kbps [37]. According to Mikhaylov et al. [38], messages transmitted with different SFs can be received simultaneously by LoRa base stations, 243 bytes being the maximum payload length for each message.

A collision behavior model, $C(x, y)$, for LoRa network between node x and node y is proposed by Bor et al. [39]. A collision rate analysis with a single LoRa gateway was reported by Alenezi et al. [40]—depending on the number of nodes and the SF for one (20 byte) packet each hour for 24 h (125 kHz bandwidth). In [41], Zhang et al. propose an alternative low-power wide area network information monitoring approach based on LoRa and NB-IoT. In this case, the communication distance in a complex environment was up to 1.6 km, with a system communication packet loss rate of around 3%. Silva et al. [42] test LoRa (long range) technology and LoRaWAN protocol in a precision viticulture scenario using low-power data acquisition devices, distanced 400 m away from the nearest gateway. With regard to the communication area parameter, Liu et al. [43] present a low-power, real-time air quality monitoring system also based on the LoRa technology being able to reach to approximately 2 km. A range of 9.27 km was achieved with SF12 and a bandwidth of 125 kHz in [44], for module-level monitoring of solar PV plants. The LoRa communication usefulness for monitoring the climate information of PV power plants was tested by Jeong et al. [45]. From the test results, it can be affirmed that the communication range for the PV climate information transmission reaches 1.3 km. In general, it can be assumed that LoRa radio chipsets use a maximum of 100 mW when transmitting, with a range of 10 to 30 km in suburban areas. In [46], it is affirmed that LoRa performs much better in comparison to FSK in most scenarios. It also highlights the successful transmission ranges within suburban scenarios up to 10 km.

3. Methodology

3.1. Lora Parameter Modeling

In the specific literature, a review of LoRa simulation environments can be found in [47], where aspects such as the selection of LoRa parameters or the device energy

consumption were revised and compared. For example, LoRaSim was described as a well-known custom-built discrete-event simulator implemented with SimPy [39]. It allows us to place a group of N LoRa-nodes and M LoRa-stations in a bidimensional space. A directional antennae is also considered for simulation purposes and identification of LoRa parameters. In this way, a comparison between the use of directional antennae facing multiple base stations as methods of dealing with LoRa internetwork interference is carried out in [48]. However, these solutions do not analyze the influence and sensitive of LoRa nodes on the PV forecasting accuracy, under different communication errors/discrepancies and a diversity of LoRa node layouts.

The transmission parameters define the LoRa node communication characteristics. As discussed in Section 2.1, LoRa provides three bandwidth (BW) settings—125, 250, or 500 kHz, and six different spreading factor (SF) values. According to Croce et al. [49], a larger bandwidth translates to a data rate increase and a receiver sensitivity deterioration. Conversely, higher SFs can be used to improve the link robustness at the cost of lower data rates. LoRa modulation is derived from chirp spread spectrum (CSS). LoRa CSS modulations with BW of 125 kHz are assumed in this work, 1% duty cycle, and a default radiated transmit power of 14 dBm. Croce et al. [50] identified six different SFs: from SF07 to SF12. In Europe, both 868 MHz and 433 MHz bands are allowed to be used. Transmitted power is limited to 14 dBm effective isotropic radiated power (EIRP), with a 1% duty cycle limit of on-air time, and the transmitted power limited to 14 dBm effective isotropic radiated power (EIRP). Table 1 summarizes the LoRa/LoRaWAN main characteristics [51]. According to the specific literature, there is pseudo orthogonality among SFs, having the advantage that multiple signal reception is possible [52]. Table 2 shows the estimated range for different SFs (from SF07 to SF10) that can be used for uplink messages on a 125 kHz channel depending on the terrain: longer distances can be achieved in a rural environment than in an urban environment [53].

Table 1. LoRa/LoRaWAN main characteristics based on the EU 863–870 MHz data rates.

0	SF12/125 kHz	250
1	SF11/125 kHz	440
2	SF10/125 kHz	980
3	SF09/125 kHz	1760
4	SF08/125 kHz	3125
5	SF07/125 kHz	5470
6	SF06/250 kHz	11,000
7	FSK: 50 kbps 440	50,000

Table 2. LoRa spreading factor (SF).

Spreading Factor (SF)	Range (Depending on the Terrain)
SF10	8 km
SF09	6 km
SF08	4 km
SF07	4 km

For a specific SF, the narrower the bandwidth, the higher the receiver sensitivity [54]. Consequently, the data rate selection is then considered as a trade-off between message duration and communication range. Different tools allow us to estimate time on air and optimum bandwidth. For the present proposal, the time interval on air for a 51-byte payload for each specific SF is considered. The payload size is defined as the maximum payload length. For each transmission, the payload can range from 2 to 255 octets, reaching the data rate up to 50 kbps when channel aggregation is used [55] under the assumption that any packet arrivals follow a Poisson law—thus, considering a uniform distribution of the payloads, their lengths are between 1 and 51 bytes [56]. According to Centenaro et al. [57],

it can be assumed that the data transmission in a LoRaWAN presents a typical 1% duty-cycle constraint; from the nodes to their corresponding gateways in a single hop allocated on different sub-bands. Indeed, the European regulations currently ask for adherence to 1% duty cycle per sub-band or applying any mechanism based on "listen-before-talk and adaptive frequency agility" [58]. Table 3 summarizes the corresponding time intervals between subsequent starting packets (s) for a 1% duty-cycle.

Table 3. Time interval between subsequent packets (1% duty-cycle).

Spreading Factor (SF)						
SF12	SF11	SF10	SF09	SF08	SF07	SF06
Time Interval between Subsequent Packets (s)						
214	115	62	33	18.5	10	6

As previously described, LoRaWAN is built as a star-of-stars topology, where the devices located in the defined grid are able to send packets to a gateway which is then responsible for forwarding those packages to a network server [59]. It is assumed that each end-device selects a specific SF based on the data rate and the distance to the gateway. A radial equidistant distribution with homogeneous end-device density is thus considered, being the energy consumption of j-radial annulus proportional to the airtime. In order to give a more realistic simulation, the study of LPWAN modeling proposed by Georgiou and Raza [60] is used to analyze the capability of this technology to scale. This study also includes an outage probability model which occurs at the gateway, called outage condition [61]. Table 4 gives the outage of a desired signal in the uplink that can occur at the gateway, if the received signal to noise ratio (SNR) is below the SF specific threshold.

Table 4. Signal to noise ratio (SNR) limits.

Spreading Factor (SF)	**Signal to Noise Ratio (SNR) Limit $q(j)$**
SF07	−7.5 dB
SF08	−10.0 dB
SF09	−12.5 dB
SF10	−15.0 dB
SF 11	−17.5 dB
SF 12	−20.0 dB

It can be then determined the packet delivery ratio, defined as the ratio between the client of packages originated by the "application layer" and the number of packages received by the sink at the final destination [62]. From this parameter, we obtain the probability function that any packet should be lost. We consider a Rayleigh channel, in line with Duda and Heusse [63]. The received signal power is affected by a multiplicative random variable with an exponential distribution of unit mean (and standard deviation). Consequently, the signal power depends on the Rayleigh fading gain and the distance, keeping the noise power constant for a 125 kHz wide band ($N = -123$ dBm). A maximum transmission power of $P = 14$ dBm is considered for simulations; the successful transmission probability being with data rate DR_j and at distance l_j:

$$H(l_j) = exp\left(\frac{N \cdot q_j}{P \cdot g(l_j)}\right), \tag{1}$$

where $g(l_j)$ is the average channel gain at distance l_j, P is the transmission power (in dBm), q_j is the signal to noise ratio (SNR) threshold for DR_j, and N is the wide band (in dBm). The path loss attenuation is estimated by using the Radio Mobile software package [64]. It uses the terrain information and the mathematical model to calculate the coverage area from the fixed radiation point taken as mobile reference point [65]. The irregular terrain

model (ITM) is used as a propagation model. It estimates radio propagation losses over irregular terrain in the range 0.020 to 20 GHz frequencies as a function of space and distance and the variability of signal in time [66]. The Okumura–Hata model [67] has also been recently proposed and assessed for path loss attenuation, mostly focused on comparing the performance LoRaWAN analysis in urban scenarios.

In the simulations, it is assumed that all transmitters (i) send packets with the same payload length; (ii) do not switch the SF from one packet to another during the same simulation test—despite that the adaptive data rate is one of the main strengths of LoRa [68]; (iii) do not change the transmit power from one packet to another during the same simulation test; and (iv) all of the transmitters have the same number of packets to send. An example of maximum communication ranges on ground (15 km) and on water (30 km) can be found in [69], including packet loss ratio, depending on the distance and assuming maximum signal SF—868 MHz ISM band using 14 dBm transmit power.

3.2. Spatio–temporal PV Forecasting

As discussed in Section 1, different probabilistic models for spatio–temporal PV forecasting can be found in the specific literature. However, only a few spatio–temporal models for short-term probabilistic forecasting can be identified [70], which are based on regression trees [71], the vectorial autoregressive model and gradient boosting combination [72], the kNN method [73], multivariate predictive distributions [74], and Gaussian random fields [75]. A least absolute shrinkage and selection operator (LASSO) regression method was also presented by Yang et al. [76] for sub–5–min solar irradiance forecasting. A flexible spatio–temporal model to estimate PV production forecasts was recently proposed by Agoua et al. [77] for horizons up to 6 h ahead, evaluating the effect of different spatial and temporal data sources on the accuracy of the forecasts. According to Muhammad et al. [78], the ARX model is the simplest black box linear model, based on a structure that is known as the most common input–output model. In this work, the author selected the random forest (RF) approach, mainly due to its simplicity to deploy, low computational cost, and ease in interpreting the input interactions. The RF algorithm is then used to find an adequate predictor function f. The RF algorithm is an ensemble learner, proposing a set of decision trees that vote on a final result. Dudek [79] affirmed that this model operates on patterns of the time series seasonal cycles, considerably simplifying the forecasting problem—mainly when a time series exhibits heteroscedasticity, trend, non–stationarity, and multiple seasonal cycles. To train and test the RF algorithm, different partitions of the data are used accordingly. Firstly, the parameter-tuning process of the RF learning is carried out through the training set. Subsequently, the test set is used to estimated the final metrics. An R package `ranger` to be used as a fast RF implementation for high-dimensional data is used in this work [80].

By considering the aim of this paper, a smart persistence and RF model is proposed for spatio–temporal PV forecasting, from the general expression given for time series [81],

$$\hat{Y}_k(t+h) = f(Y_k(t), Y_k(t-1), Y_k(t-2), \ldots, Y_k(t-d)), \tag{2}$$

where $\hat{Y}_k(t+h)$ is the k^{th} sensor forecasting and time step $t+h$, h is the horizon (in minutes) for which the prediction is being made, $Y_k(t-l)$ is the data past collected at the l^{th} lag, $l = 0, \ldots, d$. This general expression can be generalized and further extended to include other relevant information about radiation, weather, statistical measures, etc.

$$\begin{aligned} \hat{Y}_k(t+h) = f(&Y_1(t), Y_1(t-1), Y_1(t-2), \ldots, Y_1(t-d), \\ &Y_2(t), Y_2(t-1), Y_2(t-2), \ldots, Y_2(t-d), \\ &\ldots, \\ &Y_m(t), Y_m(t-1), Y_m(t-2), \ldots, Y_m(t-d)), \end{aligned} \tag{3}$$

being Y_j, for $j = 1, \ldots, m$, the predictors to be used and $Y_j(t-l)$ a single predictor (see Figure 1), and h the prediction horizon. This extended expression allows us to use additional information aside from the PV production data. Different measurement scenarios are then proposed and evaluated for GHI forecasting comparison purposes, as described in Section 3.3. GHI estimated data are thus forecast on short time horizons from 15 to 45 min. The time steps are set as 1 min, and d = 15 min. It means that, to forecast $\hat{Y}_k(t+h)$, as can be seen in Figure 1, the time interval data from t to $t-15$ is considered as input for prediction. The d parameter can be modified depending on the time step and the number of nodes (from 1 to m) included in each case study. The parameters are estimated according to the prediction training strategy depicted in Figure 2. The clear sky index $K_t(t)$ is used in the forecasting model. Assuming to be stationary enough, it is defined as follows:

$$K_t(t) = \frac{GHI(t)}{GHI_{sc}(t)}, \tag{4}$$

being, thus, the ratio of the measured GHI to GHI under clear sky conditions (GHI_{sc}). The training and forecasting processes are summarized in Figure 3, in line with recent studies also focused on machine learning forecast model analysis applied to solar power forecasting [82].

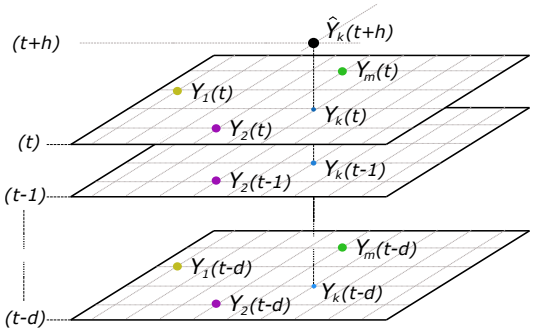

Figure 1. Smart persistence and RF model proposed for spatio–temporal forecasting.

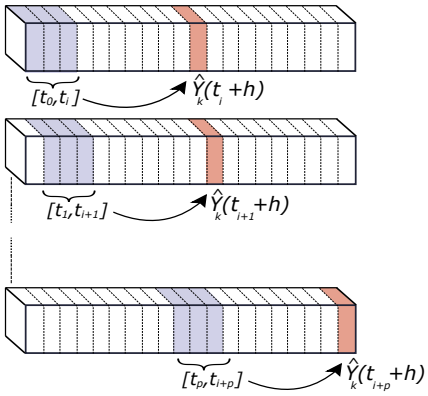

Figure 2. Forecast training strategy for a prediction horizon (h).

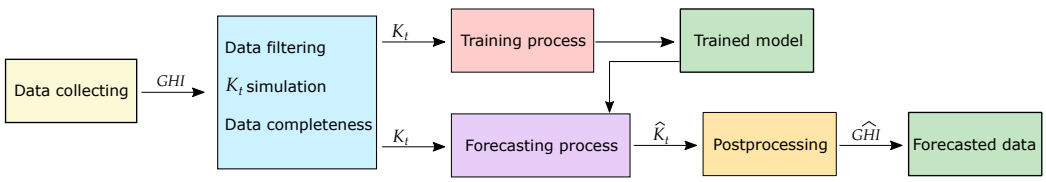

Figure 3. Training and forecast processes from collected data by using the clear sky index (K_t).

3.3. Proposed Global Methodology

This work aims to evaluate the influence of LoRa performance characteristics and its architecture/layout on the short-term PV forecasting, by considering the RF model described in Section 3.2. Firstly, a node selection and distribution based on LoRaWAN technology is carried out according to a predefined forecasting point of interest and a possible group of potential on-ground sites or satellite based-installations. From these specifications, a one-minute sample time database is defined on each node, as well as the forecasting point of interest. The RF algorithm is used to find a suitable predictor function f and, then, to forecast short-term solar values on such location by considering different forecasting time intervals—from 15 to 45 min. These predictions are estimated under a variety of scenarios: (i) assuming SF = SF09 for all nodes and 0% loss of data; (ii) assuming SF from SF09 to SF12 on each node and 0% loss of data; and (iii) assuming SF from SF09 to SF12 on each node and loss of data from 0% to 50%. Subsequently, the solar forecasting values corresponding to the different scenarios are then compared. Discrepancies and similarities are calculated, discussing the influence of the different realistic LoRa parameters on the solar forecasting process. As previously analyzed by the authors in [83], different metrics can be found in the specific literature to determine discrepancies. From this classification, normalized root mean square error (nRMSE), mean absolute percentage error (MAPE), and dynamic time warping (DTW) are determined to provide complementary information and characterize convenient discrepancies among the PV short-term forecasting data by considering SF09 and 0% loss of data and the rest of scenarios. Figure 4 summarizes the proposed methodology. In addition, a sensitive analysis based on SF parameter and loss of data variability is also included, determining the differences among discrepancies with respect to the forecasting PV values with SF09 and 0% loss of data. The methodology and simulations were implemented in the `R`–environment [84]. Different contribution software packages were used for methodology implementation purposes. In this case, `data.table` for fast and memory efficient data manipulation [85], `ranger` for a fast RF implementation [80], and `dtw` and `dtwclust` for the DTW metric estimation [86].

4. Case Example: Datasets Used

Nonnenmacher et al. [87] affirm that satellite images based on prediction methods are mostly used for intraday forecasts lower than four hours. Based on this assumption, a total area of 400 km^2 located in the Region of Murcia (11,300 km^2, southeast of Spain) is selected as a case example. This region is a promising area to integrate solar PV power plants, with 5.2 kWh/m^2· day as averaged annual global irradiation [88]. Figure 5 shows a general overview of this area, covering a 17 × 17 grid portion with a total of 289 points under consideration and a forecasting point identified in the center of this grid that is selected for GHI estimated data—corresponding to $\hat{Y}_k(t+h)$ according to expression (2). The considered spacing between all pairs of grid points is assumed as 2.5 km. Day-ahead GHI estimated data are downloaded from the Copernicus European Project servers [89]—from January to December 2019. In addition, ground data are also available based on the Network of the Agricultural Information System of the Region of Murcia (SIAM), giving additional ground-based GHI data. The SIAM network consists of 49 ground-based automatic stations geographically distributed; 32 stations are from the Regional Murcia Institute of Agricultural and Food Research and Development (IMIDA), 15 stations are from the Spanish Ministry of Agriculture, Food and Environment, one station is from the Universidad Politécnica de Cartagena (Murcia, Spain), and one more is from the City Council of Mazarrón (Murcia, Spain). These ground-based stations are financially supported by several European fund projects [90], see Figure 6. A ground-based station located in the center of the grid corresponds to the forecasting point considered for this GHI forecasting analysis.

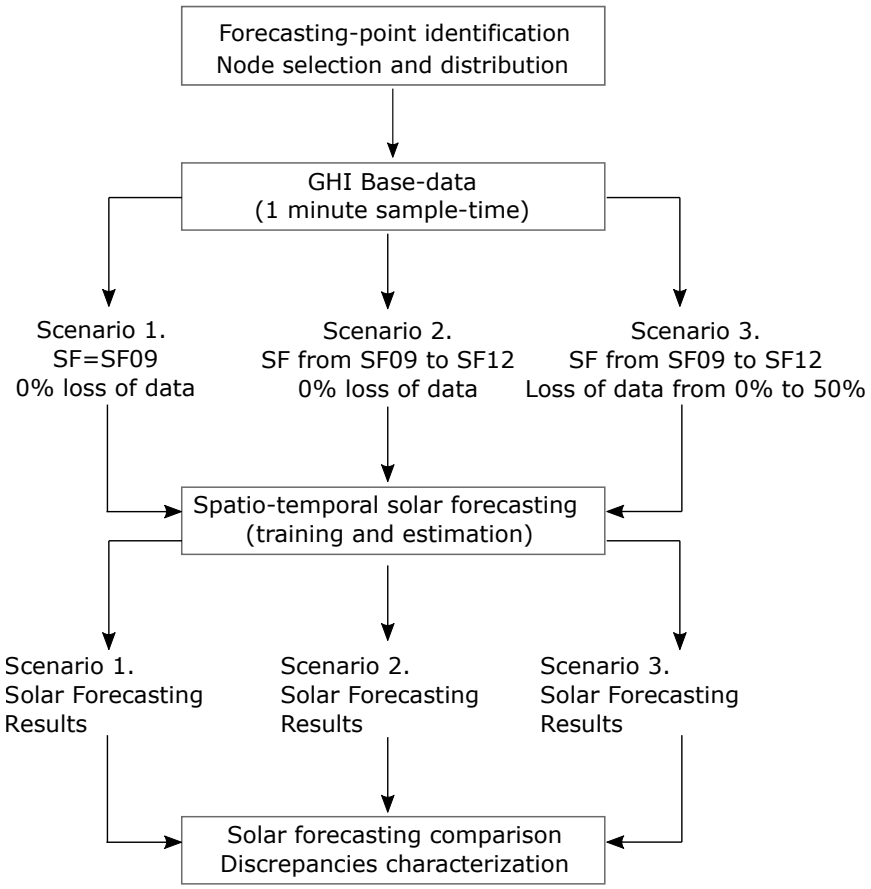

Figure 4. Proposed methodology: general scheme.

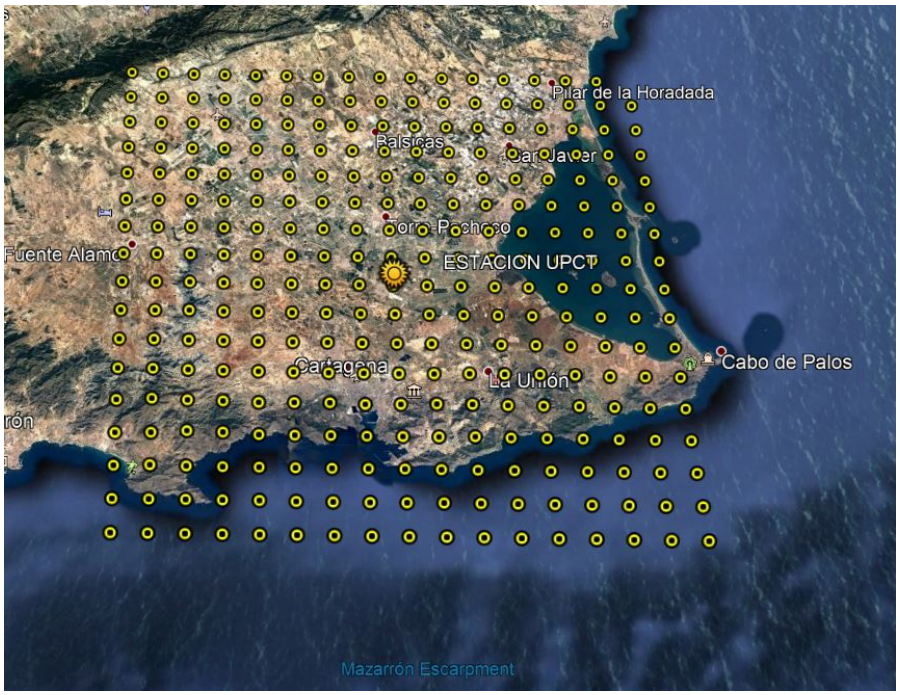

Figure 5. Case example: general overview and datasets (Region of Murcia, Spain).

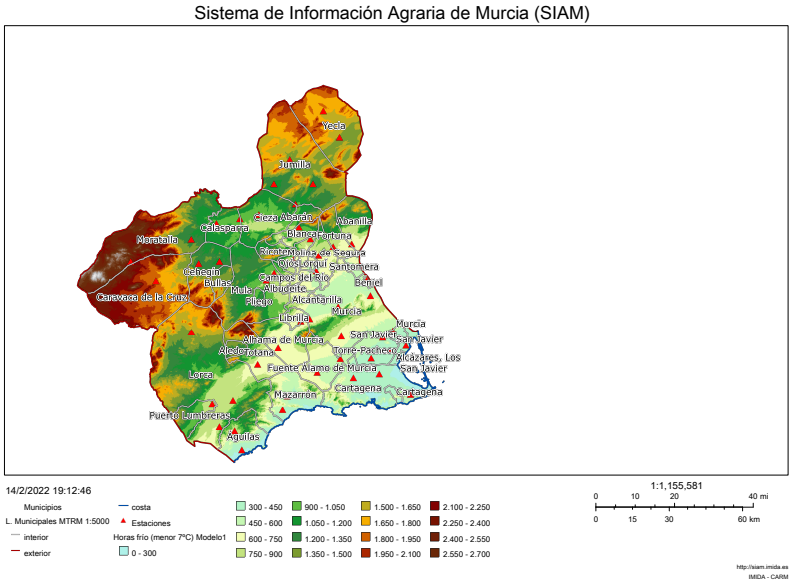

Figure 6. Case example: ground-based data available online (Region of Murcia, Spain) [90].

According to the proposed methodology described in Section 3.3, the LoRa node distribution is then selected by considering the initial grid depicted in Figure 5. With this aim, Figure 7 gives a general overview of the distribution of potential nodes, including UTM coordinates. Duda and Heusse [63] affirm that a more realistic assumption is to consider that the node density decreases with the inverse square of the gateway distance: a specific intensity of physical quantity is inversely proportional to the distance square from the source. Nevertheless, one node by each circular crown is considered and, thus, a homogeneous and minimum density distribution is considered to be evaluated and compared for short-term PV forecasting purposes. With regard to the LoRa parameters, and as can be found in the specific literature, the lowest transfer rate ensures the highest level of collisions [91]. Indeed, this configuration is the most used one, as it ensures the largest communication range by using a high SF (e.g., SF = 12). Therefore, a trade-off is then determined between increasing the communication range and reducing the transfer rate. As described in Section 3.1, different SF values are also considered in the different conditions. Therefore, different scenarios are considered for each day from the initial grid depicted in Figure 7, with forecast horizons ranging from 15 to 45 min with one-minute time resolution, and under a variety of SF LoRa parameters and loss of data values (see Figure 4). A general comparison of GHI prediction results for the case study is following discussed in Section 5.

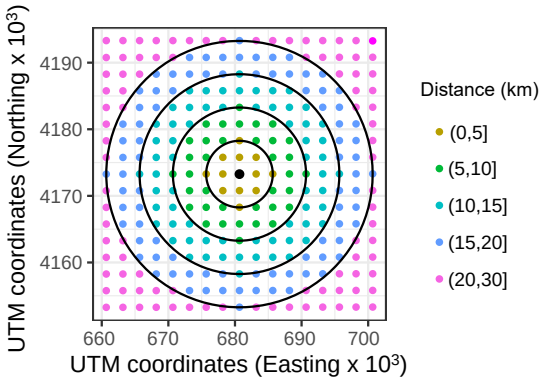

Figure 7. Case example: distribution of datasets (UTM coordinates).

5. Results

From the data corresponding to 2019, with one-minute time resolution, and as described in Section 4, different short-term PV solar forecasting periods were considered for simulations. More specifically, three different time horizons were defined: 15, 30, and 45 min. Each day was then simulated by considering such different time horizons for forecasting purposes. In addition, and with the aim to compare the impact of both loss of data and the selected SF, simulations were carried out under such conditions: 0%, 25%, and 50% loss of data; as well as from SF12 to SF09. Indeed, and according to the discussion given in Section 3.1—see Tables 2 and 3, the selected SF considerably affects the robustness at the cost of lower data rates. These results allow us to evaluate the impact of each parameter and give a preliminary analysis of the influence of these conditions and situations before implementing a real communication and sensoring network. Therefore, each day is simulated through a $3 \times 4 \times 3$ matrix of possible loss of data, foresting time intervals and selected SF, as schematically depicted in Figure 8. Subsequently, 36 different conditions are considered for each day, including three different losses of data percentages, four different SF parameters, and three different forecasting time intervals. In line with the case example shown in Figure 5 and the initial node layout based on UTM coordinates and depicted in Figure 7, an arbitrary node site location is selected and given in Figure 9, including the distribution of selected points for the analysis and the distance to the forecasting point. Subsequently, and as previously discussed, one node is selected on each circular crown with the aim of forecasting GHI data in the center of the grid, corresponding to the $\hat{Y}(t+h)$—see expression (3). The selected nodes are labeled as 119, 170, 115, 60, and 254, respectively.

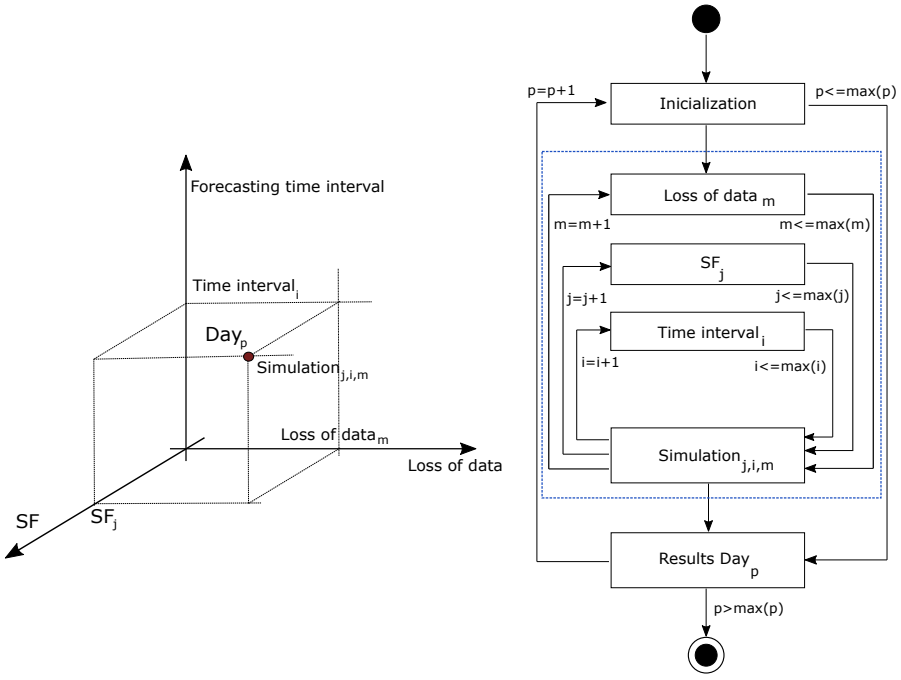

Figure 8. Case example: simulation general scheme.

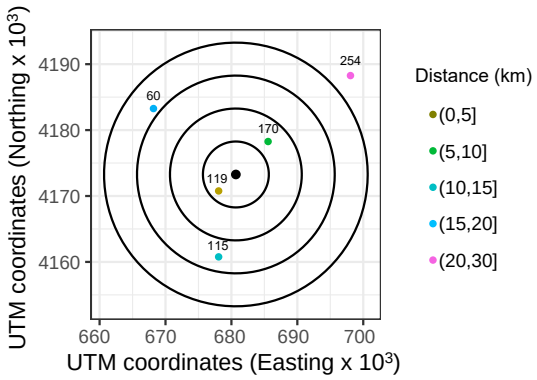

Figure 9. Case example: distribution of points selected and the forecasting point marked in black color (UTM coordinates).

By considering the 2019 data for the methodology evaluation, the corresponding daily GHI curves are then forecast according to the preliminary selection of possible nodes and the different conditions. In summary, a global of 13,140 simulations were carried out by the authors. These estimated data allow us to analyze in detail the influence of each variable on the short-term forecasting accuracy and the different possibilities to implement a real sensoring network in terms of data gathering accuracy and reliability for forecasting purposes. As an example of the forecast curves for each day, Figure 10 shows the irradiance data corresponding to two arbitrary days—labeled as day 108 and 144, respectively, including clear sky GHI data—see dashed line. As can be seen, data corresponding to the selected nodes given in Figure 9 are plotted, as well as the forecasting point marked in black color being the GHI observed data—corresponding to $Y_k(t+h)$. From these initial data, Figure 11 compares the measured and forecast irradiance values for the two previous days—labeled as day 108 and 144—and considers the selected different conditions for each day: loss of data percentages, different SF parameters, and different forecasting time intervals. Subsequently, 36 different forecasting GHI results are determined for each day. In addition, as a complementary result, Figure 12 compares these curves, including the expected clear sky GHI values. These forecasting data are thus determined for 15, 30, and 45 min time horizons, varying the SF parameter from 09 to 12 and considering 0%, 25%, and 50% loss of data scenarios.

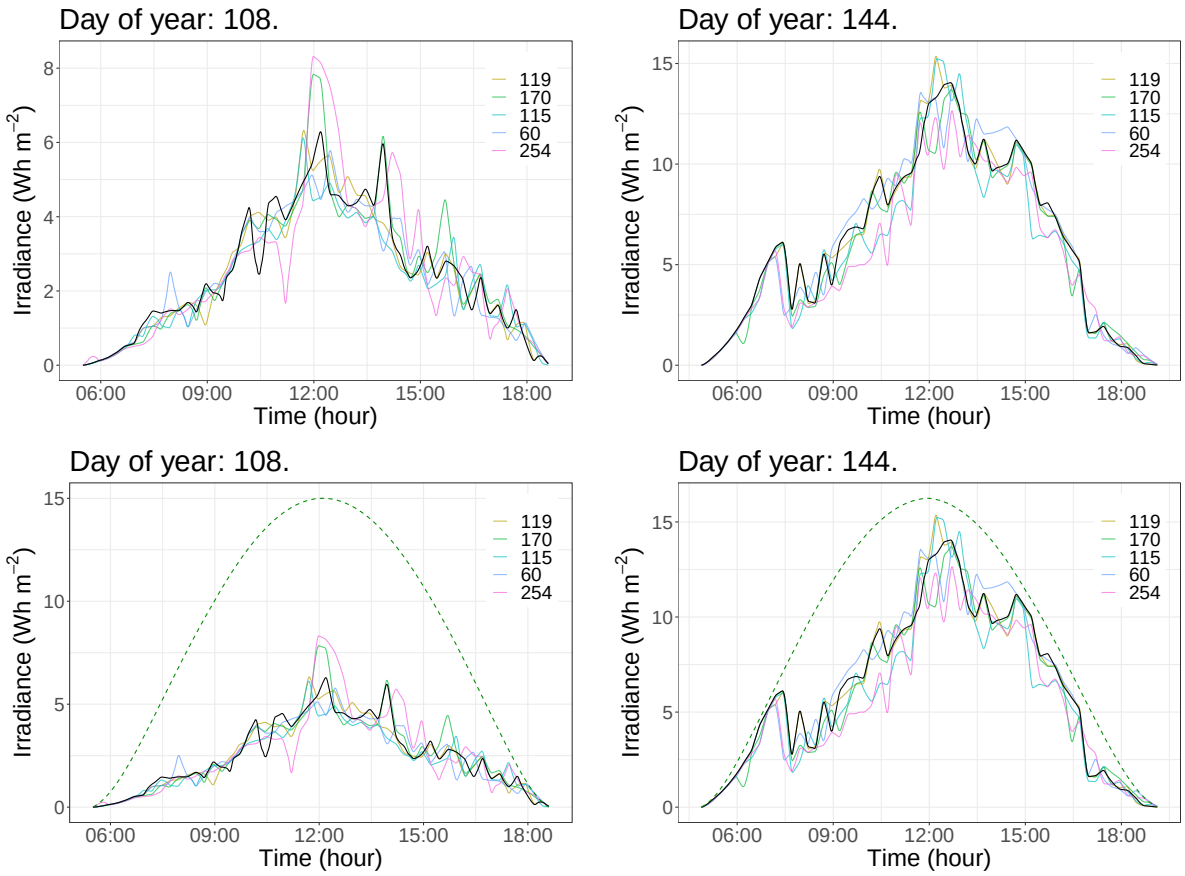

Figure 10. Example of irradiance data for two days: curves used for short-term forecasting purposes—clear sky GHI data included in dashed line. Curve in the forecasting point is marked in black color.

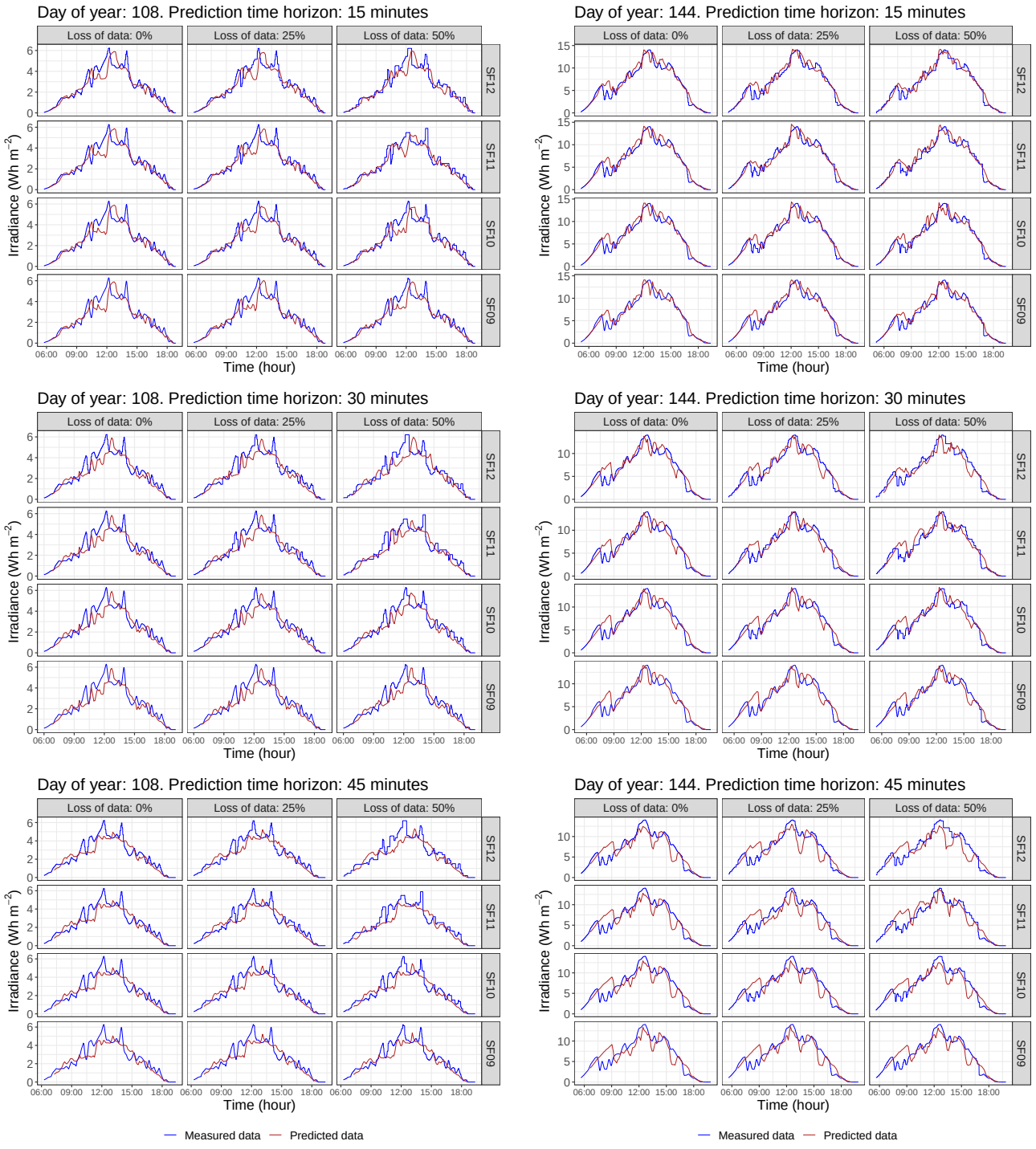

Figure 11. Comparison of estimated and monitored GHI data for different time horizon, SF, and loss of data scenarios.

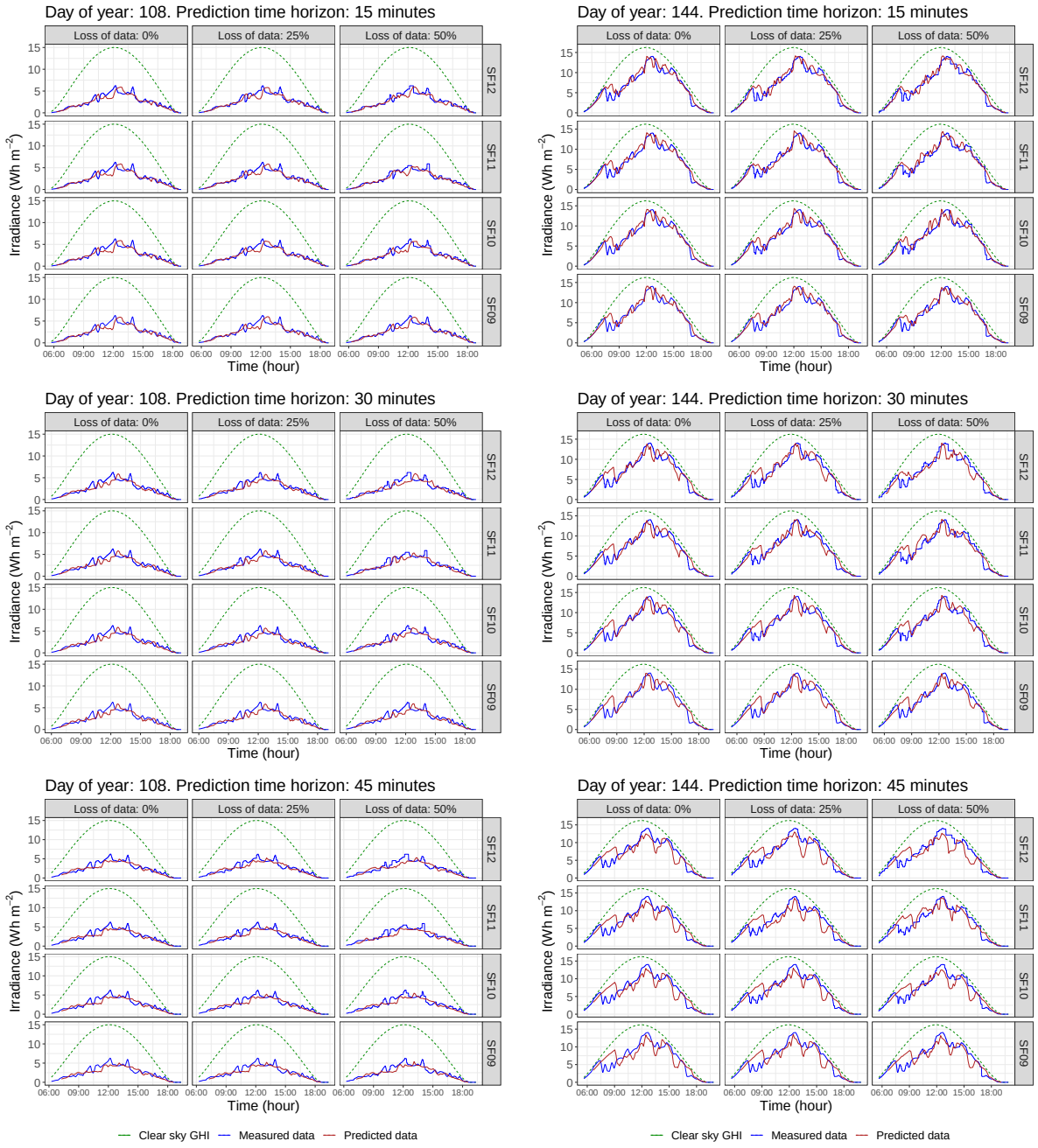

Figure 12. Comparison of estimated, monitored, and clear sky GHI data for different time horizon, SF, and loss of data scenarios.

With the aim of estimating the influence of each parameters by considering all simulations along the 2019 data, a sensitive analysis was carried out determining discrepancies between the estimated daily GHI values for the selected node and the corresponding daily measured GHI values. Firstly, Figure 13 shows the global histograms and the truncated histograms of such discrepancies based on normalized root mean square error (nRMSE) among the measured GHI data and the forecasting GHI values for the selected node and by considering the different time horizon, SF, and loss of data scenarios. Therefore, 36 global and truncated histograms were determined from the 13,140 simulations. As can be seen, the truncated histograms retain more than 90% of such discrepancies and are considered suitable enough for this sensitive analysis. Secondly, and according to the variety of errors and differences available in the specific literature, as well as the comparison conducted by the authors in [83], the mean absolute percentage error (MAPE) and dynamic time

warping (DTW) were also selected as metric estimations—see Section 3.3. Indeed, and as can be found in [92], DTW is considered as an appropriate technique to estimate and find an optimal alignment between two time-dependent sequences under a set of restrictions. DTW was initially used to compare different speech patterns, and also successfully applied in other fields, such as information retrieval and data mining. Additionally, DTW can be applied to detect and cope with different speeds and time deformations associated with time-dependent data. Recently, the `R` package `IncDTW` based on the DTW improved the possibilities to classify time series or clusters [93]. To analyze in detail the influence of each variable, Figure 14 shows the truncated histogram for these simulations using discrepancies based on MAPE and DTW metrics. As can be seen from these discrepancies, a higher loss of data range involves more relevant discrepancies, and these values present a secondary peak from 20% to 30% values. In terms of SF parameter, the vast values of discrepancies slightly shift from the [0, 10] interval (for SF09) to [10, 20] interval (for SF12). Therefore, a longer time interval between subsequent packets—see Table 3—implies higher discrepancy errors. These results are similar for the other analyzed forecasting short time intervals—30 and 45 min, respectively, as summarized in Figure 14.

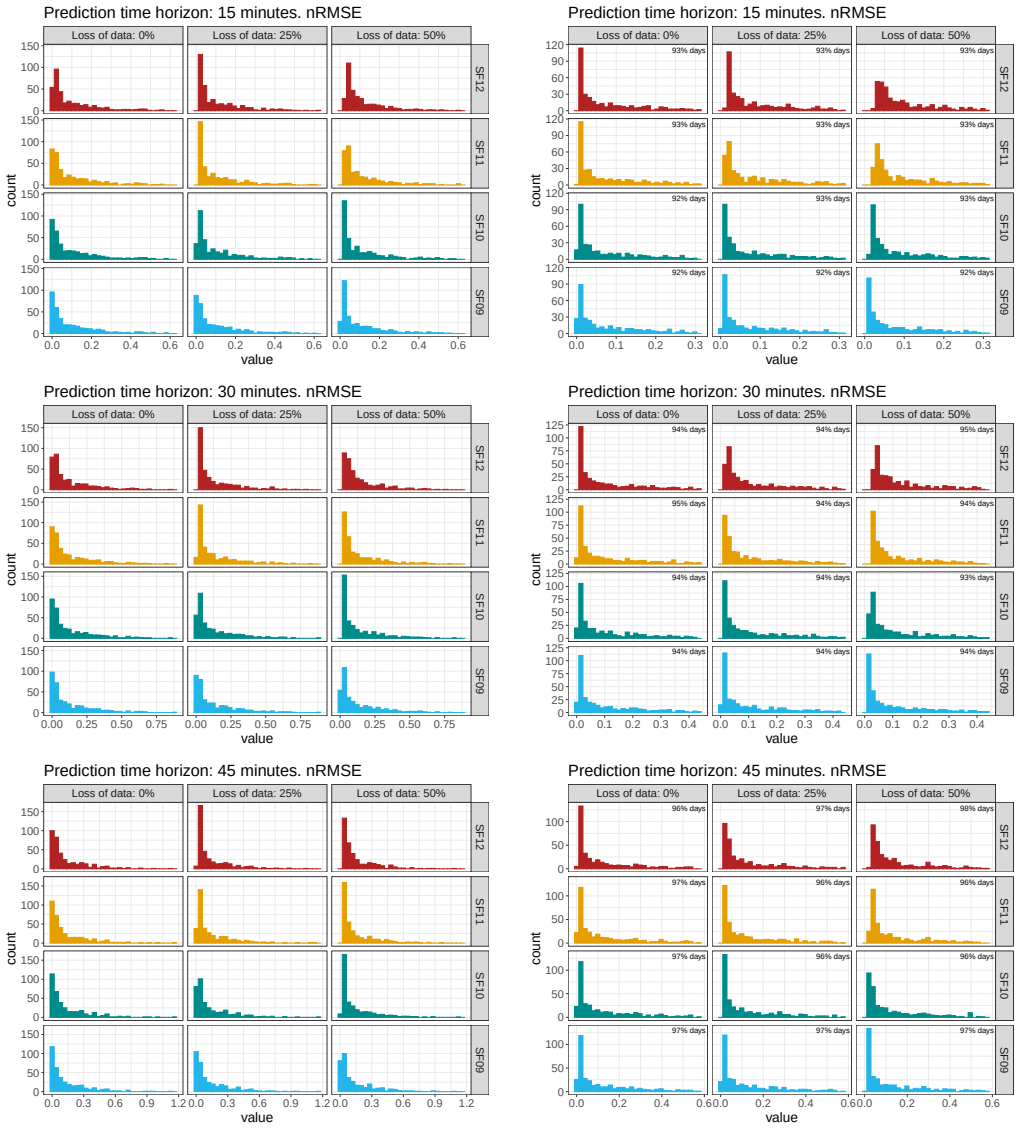

Figure 13. Summary of discrepancies for forecasting and monitoring data based on nRMSE. Histogram (**left**) and truncated histogram (**right**).

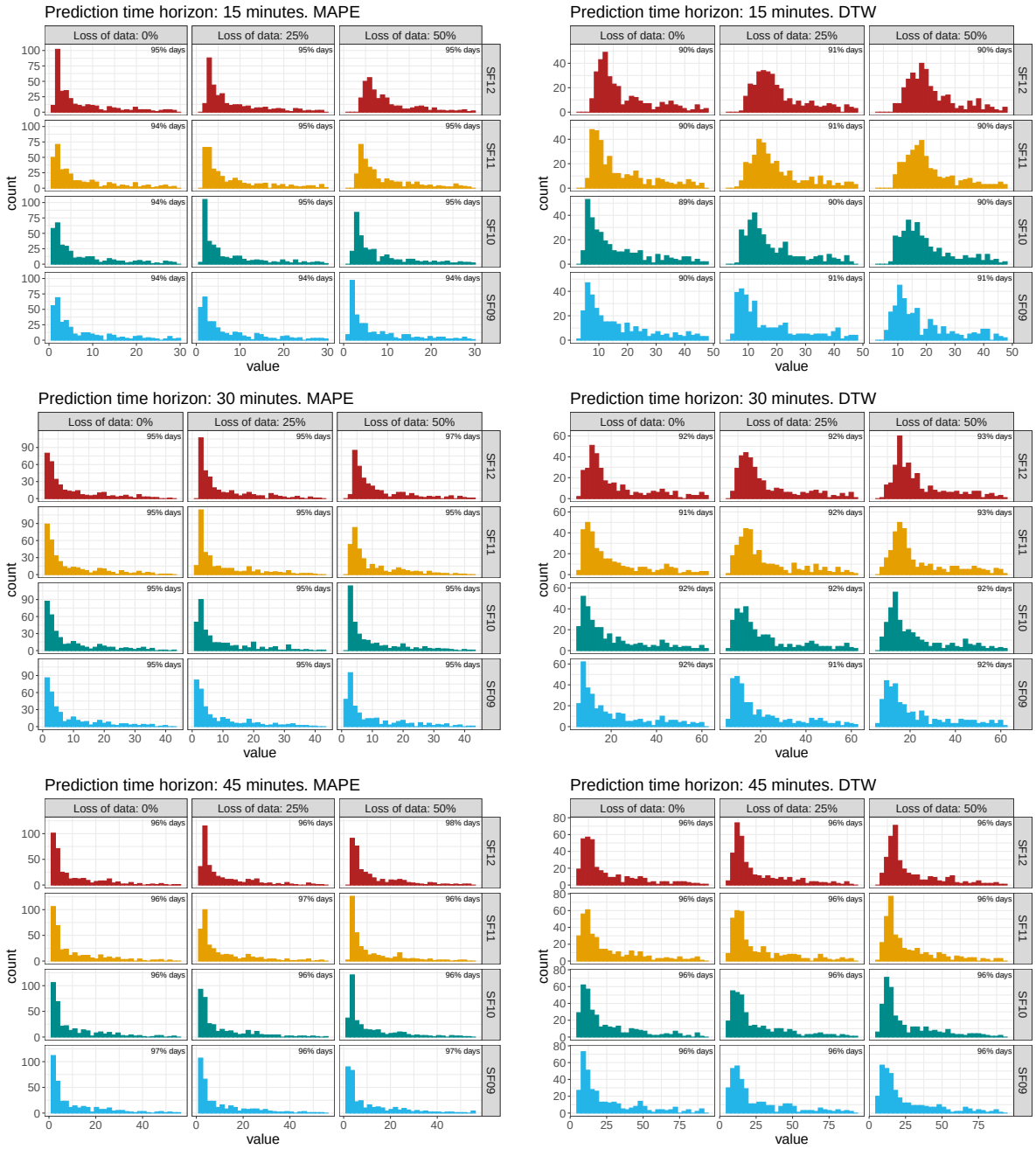

Figure 14. Summary of discrepancies for forecasting and monitoring data based on MAPE and DTW. Truncated histograms.

As an alternative sensitive analysis, Figure 15 shows a boxplot diagram of the discrepancies based on nRMSE, MAPE, and DTW metrics classified according to different clear sky GHI ratio $\overline{K}_t$: [0, 0.65], (0.65, 0.85], and (0.85, 1], respectively. All simulations corresponding to 2019 data are considered to determine these global metrics; thus, 36 different conditions are assumed for each day depending on the defined $3 \times 4 \times 3$ matrix of possible loss of data, SF parameter, and short time period values selected for this case study. From the results, larger time horizons address less-accurate GHI estimations, and higher clear sky GHI ratio values imply more accurate GHI estimations. Moreover, high $\overline{K}_t$ GHI ratio days should be not considered for LoRa network performance evaluation, as they are not sensitive to loss of data nor SF parameter values. Subsequently, low $\overline{K}_t$ GHI ratio days should be considered for estimating discrepancies and GHI forecasting accuracy,

as well as potential errors allowed for short-term forecasting purposes depending on the corresponding loss of data, short time periods, and SF parameters.

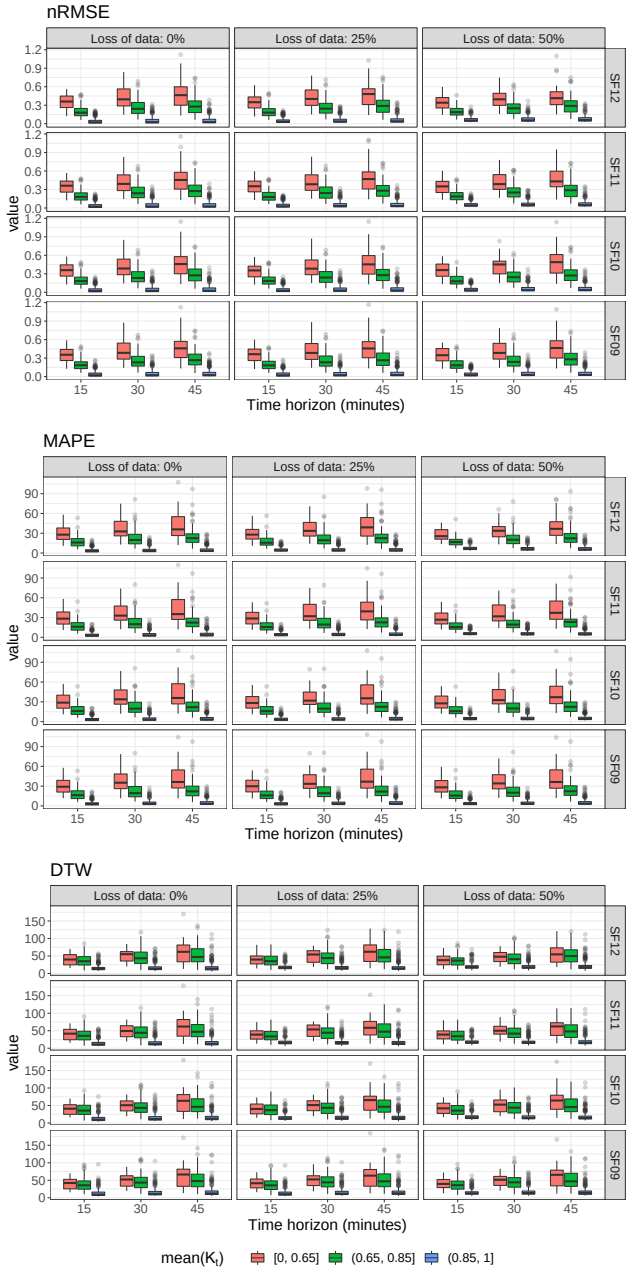

Figure 15. Boxplot of the discrepancies based on nRMSE, MAPE, and DTW.

Finally, an additional metric analysis is also provided to compare the difference evolution of SF09, 0% loss of data (corresponding to 'Scenario 1' in Figure 4), and for each short time interval to the rest of the other daily possible conditions and under nRMSE, MAPE, and DTW metric estimations. With this aim, Figure 16 summarizes the boxplot results of differences among 'Scenario 1' (for each short-term time interval) and the other daily conditions (SF values and loss of data). As can be seen, differences are higher with larger loss of data for any metric—see boxplots for the same row and short time interval. In addition, discrepancies are increasing from SF09 to SF12, when loss of data and short time interval variables are kept constant. The results under different daily conditions are divided by considering clear sky GHI ratio intervals $\overline{K}_t$—[0, 0.65], (0.65, 0.85], and (0.85, 1]. The corresponding boxplot differences for SF09 and 0% loss of data, for each short time interval

in comparison to the rest of daily conditions and for all metrics are determined and depicted in Figure 17. In general, differences are higher for lower $\overline{K}_t$ values and, as previously affirmed, low $\overline{K}_t$ GHI ratio days should be considered for evaluating GHI forecasting accuracy approaches and suitable node layouts. Consequently, and depending on the discrepancies range allowed in each case by the specific application, this methodology gives a preliminary analysis for the LoRa-based PV monitoring architectures and potential node layouts. Additionally, it gives an estimation of forecasting GHI estimations and the influence of SF and loss of data variables on the GHI value accuracy. Therefore, both reliability and robustness of the collected data to be used for forecasting purposes are able to be analyzed and evaluated.

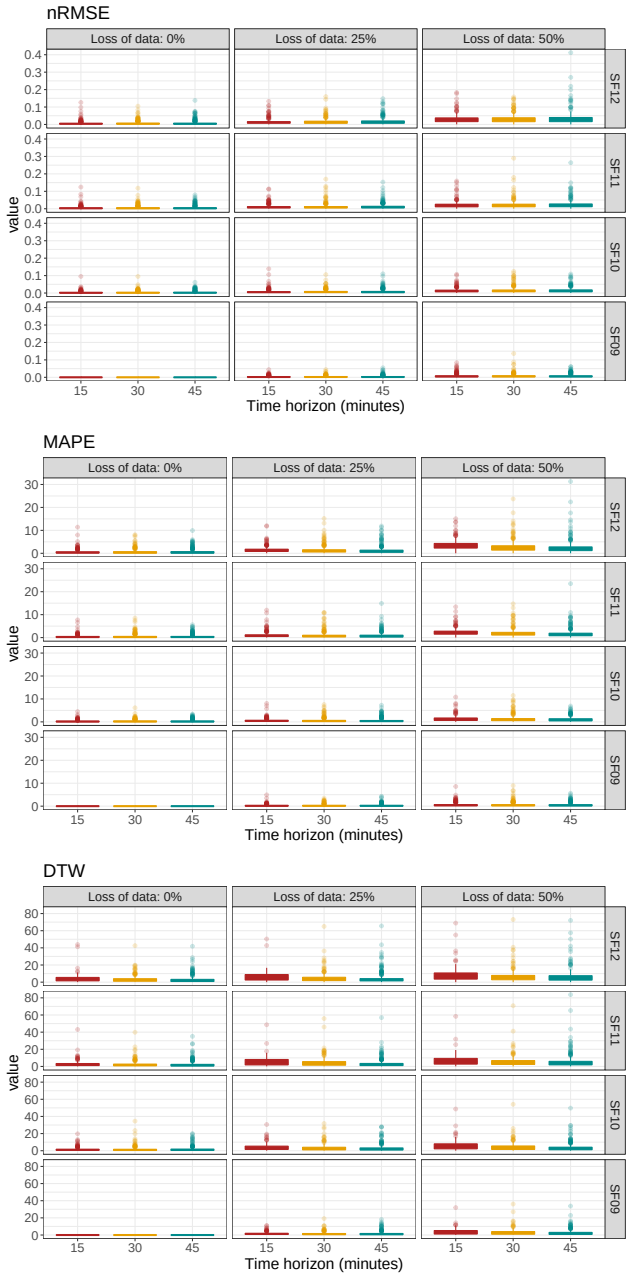

Figure 16. Boxplot of differences based on SF09 and 0% loss of data: nRMSE, MAPE, and DTW metrics.

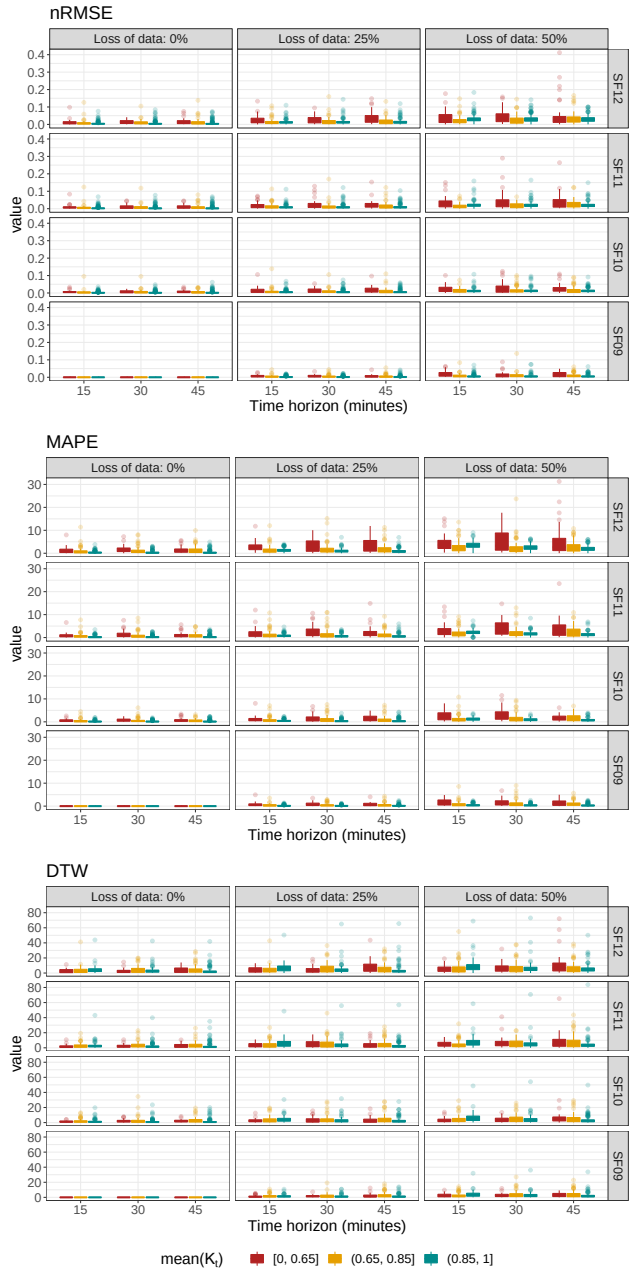

Figure 17. Boxplot of differences based on SF09 and 0% loss of data: nRMSE, MAPE, and DTW metrics for different K_t clear sky GHI ratios.

6. Conclusions

A methodology to evaluate different LoRa-based PV monitoring configurations in terms of short-term GHI forecasting characterization of metrics is described and assessed. A location analysis of nodes based on potential loss of data, short-term time intervals, and SF ranges are considered to analyze their influence on such short-term GHI forecasting purposes. The methodology also allows us to evaluate different node layouts and forecasting approaches. A random forest model is proposed in this work as suitable forecasting method under nonstationary and multiple seasonal cycle data. A case study located in the southeast of Spain is included to evaluate the methodology. Satellite-based GHI data collected for 2019 covering a 17 $\times$ 17 grid portion with a total of 289 points under consideration are considered, with one-minute sample time data. The short-term GHI forecasting simulations for each day included different loss of data ranges, forecasting time intervals (15, 30, and 45 min), and SF values (from SF09 to SF12). A total of 36 different conditions for each were

considered, running 13,140 simulations for the corresponding global 2019 GHI data. The results allow us to explore the influence of loss of data, SF values, and short-term time intervals on the corresponding GHI forecasting accuracy. In addition, different LoRa node layouts can be also evaluated in terms of data accuracy and GHI forecasting estimations. In general, higher clear sky GHI ratio values imply more accurate GHI estimations, being less sensitive to loss of data or SF parameter values. Subsequently, low $\overline{K}_t$ GHI ratio days should be considered for estimating potential errors allowed for short-term forecasting purposes depending on the corresponding loss of data, short time periods, and SF parameters. A sensitive analysis is included in the work from complementary metrics: nRMSE, MAPE, and DTW. These results give additional information to characterize discrepancies among collected and forecast GHI data as a consequence of LoRa parameters and/or node layout. This methodology thus provides a preliminary analysis of potential LoRa network characteristics and sensoring in terms of data accuracy, packets, and GHI forecasting possibilities.

Author Contributions: Conceptualization, A.M.-G. and J.M.P.-P.; methodology, M.C.B.; software, M.C.B.; validation, A.M.-A. and J.M.P.-P.; formal analysis, M.C.B.; resources, A.M.-A.; data curation, M.C.B.; writing—original draft preparation, A.M.-G.; writing—review and editing, A.M.-G. All authors have read and agreed to the published version of the manuscript.

Funding: This research was funded by the Fondo Europeo de Desarrollo Regional/Ministerio de Ciencia e Innovación–Agencia Estatal de Investigación (FEDER/MICINN-AEI), project RTI2018–099139–B–C21.

Institutional Review Board Statement: Not applicable.

Informed Consent Statement: Not applicable.

Data Availability Statement: The datasets generated and/or analyzed during this study are available from the corresponding author on reasonable request.

Conflicts of Interest: The authors declare no conflict, of interest.

Abbreviations

The following abbreviations are used in this manuscript:

BW	Bandwidth
CSS	Chirp spread spectrum
DTW	Dynamic time warping
GHI	Global horizontal irradiance
ITM	Irregular terrain model
LASSO	Least absolute shrinkage and selection operator
LoRa	Long range
MAE	Mean absolute error
MAPE	Mean absolute percentage error
nRMSE	Normalized root mean square error
PV	Photovoltaic
RF	Random forest
RMSE	Root mean square error
SF	Spreading factor
SNR	Signal to noise ratio
vRES	Variable renewable energy sources

References

1. Brouwer, A.S.; van den Broek, M.; Zappa, W.; Turkenburg, W.C.; Faaij, A. Least–cost options for integrating intermittent renewables in low-carbon power systems. *Appl. Energy* **2016**, *161*, 48–74, doi:10.1016/j.apenergy.2015.09.090.
2. Eltawil, M.A.; Zhao, Z. Grid-connected photovoltaic power systems: Technical and potential problems—A review. *Renew. Sustain. Energy Rev.* **2010**, *14*, 112–129, doi:10.1016/j.rser.2009.07.015.

3. Daliento, S.; Chouder, A.; Guerriero, P.; Pavan, A.M.; Mellit, A.; Moeini, R.; Tricoli, P. Monitoring, Diagnosis, and Power Forecasting for Photovoltaic Fields: A Review. *Int. J. Photoenergy* **2017**, *2017*, 1–13, doi:10.1155/2017/1356851.
4. Das, U.K.; Tey, K.S.; Seyedmahmoudian, M.; Mekhilef, S.; Idris, M.Y.I.; Deventer, W.V.; Horan, B.; Stojcevski, A. Forecasting of photovoltaic power generation and model optimization: A review. *Renew. Sustain. Energy Rev.* **2018**, *81*, 912–928, doi:10.1016/j.rser.2017.08.017.
5. Antonanzas, J.; Osorio, N.; Escobar, R.; Urraca, R.; de Pison, F.M.; Antonanzas-Torres, F. Review of photovoltaic power forecasting. *Sol. Energy* **2016**, *136*, 78–111, doi:10.1016/j.solener.2016.06.069.
6. Gandoman, F.H.; Raeisi, F.; Ahmadi, A. A literature review on estimating of PV–array hourly power under cloudy weather conditions. *Renew. Sustain. Energy Rev.* **2016**, *63*, 579–592, doi:10.1016/j.rser.2016.05.027.
7. Hamid Oudjana, S.; Hellal, A.; Hadj Mahamed, I. Short term photovoltaic power generation forecasting using neural network. In Proceedings of the 2012 11th International Conference on Environment and Electrical Engineering, Venice, Italy, 18–25 May 2012; pp. 706–711.
8. Chen, C.; Duan, S.; Cai, T.; Liu, B. Online 24-h solar power forecasting based on weather type classification using artificial neural network. *Sol. Energy* **2011**, *85*, 2856–2870, doi:10.1016/j.solener.2011.08.027.
9. Rana, M.; Koprinska, I.; Agelidis, V.G. Forecasting solar power generated by grid connected PV systems using ensembles of neural networks. In Proceedings of the 2015 International Joint Conference on Neural Networks (IJCNN), Killarney, Ireland, 12–17 July 2015; pp. 1–8.
10. Chu, Y.; Urquhart, B.; Gohari, S.M.; Pedro, H.T.; Kleissl, J.; Coimbra, C.F. Short-term reforecasting of power output from a 48 MWe solar PV plant. *Sol. Energy* **2015**, *112*, 68–77, doi:10.1016/j.solener.2014.11.017.
11. Liu, L.; Liu, D.; Sun, Q.; Li, H.; Wennersten, R. Forecasting Power Output of Photovoltaic System Using a BP Network Method. *Energy Procedia* **2017**, *142*, 780–786, doi:10.1016/j.egypro.2017.12.126.
12. de Paiva, G.M.; Pimentel, S.P.; Marra, E.G.; de Alvarenga, B.P.; Mussetta, M.; Leva, S. Intra-day forecasting of building-integrated PV systems for power systems operation using ANN ensemble. In Proceedings of the 2019 IEEE Milan PowerTech, Milan, Italy, 23–27 June 2019; pp. 1–5.
13. Akhter, M.N.; Mekhilef, S.; Mokhlis, H.; Shah, N.M. Review on forecasting of photovoltaic power generation based on machine learning and metaheuristic techniques. *IET Renew. Power Gener.* **2019**, *13*, 1009–1023.
14. Behera, M.K.; Majumder, I.; Nayak, N. Solar photovoltaic power forecasting using optimized modified extreme learning machine technique. *Eng. Sci. Technol. Int. J.* **2018**, *21*, 428–438, doi:10.1016/j.jestch.2018.04.013.
15. Yang, D.; Kleissl, J.; Gueymard, C.A.; Pedro, H.T.; Coimbra, C.F. History and trends in solar irradiance and PV power forecasting: A preliminary assessment and review using text mining. *Sol. Energy* **2018**, *168*, 60–101, doi:10.1016/j.solener.2017.11.023.
16. Barbieri, F.; Rajakaruna, S.; Ghosh, A. Very short-term photovoltaic power forecasting with cloud modeling: A review. *Renew. Sustain. Energy Rev.* **2017**, *75*, 242–263, doi:10.1016/j.rser.2016.10.068.
17. van der Meer, D.; Widén, J.; Munkhammar, J. Review on probabilistic forecasting of photovoltaic power production and electricity consumption. *Renew. Sustain. Energy Rev.* **2018**, *81*, 1484–1512, doi:10.1016/j.rser.2017.05.212.
18. Kaur, A.; Nonnenmacher, L.; Pedro, H.T.; Coimbra, C.F. Benefits of solar forecasting for energy imbalance markets. *Renew. Energy* **2016**, *86*, 819–830, doi:10.1016/j.renene.2015.09.011.
19. Yang, C.; Thatte, A.A.; Xie, L. Multitime–Scale Data–Driven Spatio–Temporal Forecast of Photovoltaic Generation. *IEEE Trans. Sustain. Energy* **2015**, *6*, 104–112.
20. Dambreville, R.; Blanc, P.; Chanussot, J.; Boldo, D. Very short term forecasting of the Global Horizontal Irradiance using a spatio–temporal autoregressive model. *Renew. Energy* **2014**, *72*, 291–300, doi:https://doi.org/10.1016/j.renene.2014.07.012.
21. Sangrody, H.; Sarailoo, M.; Zhou, N.; Tran, N.; Motalleb, M.; Foruzan, E. *IET Renew. Power Gener.* **2017**, *11*, 1274–1280.
22. Gueymard, C.A. A review of validation methodologies and statistical performance indicators for modeled solar radiation data: Towards a better bankability of solar projects. *Renew. Sustain. Energy Rev.* **2014**, *39*, 1024–1034, doi:10.1016/j.rser.2014.07.117.
23. Wang, K.; Qi, X.; Liu, H. A comparison of day-ahead photovoltaic power forecasting models based on deep learning neural network. *Appl. Energy* **2019**, *251*, 113315, doi:10.1016/j.apenergy.2019.113315.
24. Kardakos, E.G.; Alexiadis, M.C.; Vagropoulos, S.I.; Simoglou, C.K.; Biskas, P.N.; Bakirtzis, A.G. Application of time series and artificial neural network models in short-term forecasting of PV power generation. In Proceedings of the 2013 48th International Universities' Power Engineering Conference (UPEC), Dublin, Ireland, 2–5 September 2013; pp. 1–6.
25. Huang, Y.; Lu, J.; Liu, C.; Xu, X.; Wang, W.; Zhou, X. Comparative study of power forecasting methods for PV stations. In Proceedings of the 2010 International Conference on Power System Technology, Zhejiang, China, 24-28 October 2010; pp. 1–6.
26. Gigoni, L.; Betti, A.; Crisostomi, E.; Franco, A.; Tucci, M.; Bizzarri, F.; Mucci, D. Day-Ahead Hourly Forecasting of Power Generation From Photovoltaic Plants. *IEEE Trans. Sustain. Energy* **2018**, *9*, 831–842.
27. Chaojun, G.; Yang, D.; Jirutitijaroen, P.; Walsh, W.M.; Reindl, T. Spatial Load Forecasting With Communication Failure Using Time-Forward Kriging. *IEEE Trans. Power Syst.* **2014**, *29*, 2875–2882.
28. Triki-Lahiani, A.; Abdelghani, A.B.B.; Slama-Belkhodja, I. Fault detection and monitoring systems for photovoltaic installations: A review. *Renew. Sustain. Energy Rev.* **2018**, *82*, 2680–2692, doi:10.1016/j.rser.2017.09.101.
29. Mortazavi, H.; Mehrjerdi, H.; Saad, M.; Lefebvre, S.; Asber, D.; Lenoir, L. A Monitoring Technique for Reversed Power Flow Detection With High PV Penetration Level. *IEEE Trans. Smart Grid* **2015**, *6*, 2221–2232.

30. Shuda, J.E.; Rix, A.J.; Booysen, M.J. Towards Module-Level Performance and Health Monitoring of Solar PV Plants Using LoRa Wireless Sensor Networks. In Proceedings of the 2018 IEEE PES/IAS PowerAfrica, Cape Town, South Africa, 28–29 June 2018; pp. 172–177.
31. Haxhibeqiri, J.; De Poorter, E.; Moerman, I.; Hoebeke, J. A Survey of LoRaWAN for IoT: From Technology to Application. *Sensors* **2018**, *18*, 3995, doi:10.3390/s18113995.
32. Sherazi, H.H.R.; Piro, G.; Grieco, L.A.; Boggia, G. When Renewable Energy Meets LoRa: A Feasibility Analysis on Cable-Less Deployments. *IEEE Internet Things J.* **2018**, *5*, 5097–5108, doi:10.1109/JIOT.2018.2839359.
33. Behjati, M.; Mohd Noh, A.B.; Alobaidy, H.A.H.; Zulkifley, M.A.; Nordin, R.; Abdullah, N.F. LoRa Communications as an Enabler for Internet of Drones towards Large-Scale Livestock Monitoring in Rural Farms. *Sensors* **2021**, *21*, 5044, doi:10.3390/s21155044.
34. Zhou, Q.; Zheng, K.; Hou, L.; Xing, J.; Xu, R. Design and Implementation of Open LoRa for IoT. *IEEE Access* **2019**, *7*, 100649–100657, doi:10.1109/ACCESS.2019.2930243.
35. Adelantado, F.; Vilajosana, X.; Tuset-Peiro, P.; Martinez, B.; Melia-Segui, J.; Watteyne, T. Understanding the Limits of LoRaWAN. *IEEE Commun. Mag.* **2017**, *55*, 34–40.
36. Mekki, K.; Bajic, E.; Chaxel, F.; Meyer, F. A comparative study of LPWAN technologies for large-scale IoT deployment. *ICT Express* **2019**, *5*, 1–7, doi:10.1016/j.icte.2017.12.005.
37. Sornin, N.; Luis, M.; Eirich, T.; Kramp, T.; Hersent, O. *Lorawan Specification*; LoRa alliance, January, 2015. Available online: https://lora-alliance.org/wp-content/uploads/2020/11/2015_-_lorawan_specification_1r0_611_1.pdf (accessed on 30 November 2021).
38. Mikhaylov, K.; Juha Petaejaejaervi.; Haenninen, T. Analysis of Capacity and Scalability of the LoRa Low Power Wide Area Network Technology. In Proceedings of the European Wireless 2016, 22th European Wireless Conference, Oulu, Finland, 18–20 May 2016; pp. 1–6.
39. Bor, M.C.; Roedig, U.; Voigt, T.; Alonso, J.M. Do LoRa Low–Power Wide–Area Networks Scale? In Proceedings of the 19th ACM International Conference on Modeling, Analysis and Simulation of Wireless and Mobile Systems, Malta, Malta, 13–17 November 2016; pp. 59–67, doi:10.1145/2988287.2989163.
40. Alenezi, M.; Chai, K.K.; Chen, Y.; Jimaa, S. Ultra–dense LoRaWAN: Reviews and challenges. *IET Commun.* **2020**, *14*, 1361–1371.
41. Zhang, X.; Zhang, M.; Meng, F.; Qiao, Y.; Xu, S.; Hour, S. A Low-Power Wide-Area Network Information Monitoring System by Combining NB-IoT and LoRa. *IEEE Internet Things J.* **2019**, *6*, 590–598.
42. Silva, N.; Mendes, J.; Silva, R.; dos Santos, F.N.; Mestre, P.; Serôdio, C.; Morais, R. Low-Cost IoT LoRa Solutions for Precision Agriculture Monitoring Practices. In *Progress in Artificial Intelligence*; Moura Oliveira, P., Novais, P., Reis, L.P., Eds.; Springer International Publishing: Cham, Switzerland, 2019; pp. 224–235.
43. Sujuan Liu.; Chuyu Xia.; Zhenzhen Zhao. A low-power real-time air quality monitoring system using LPWAN based on LoRa. In Proceedings of the 2016 13th IEEE International Conference on Solid-State and Integrated Circuit Technology (ICSICT), Hangzhou, China, 25–28 October 2016; pp. 379–381.
44. Shuda, J.; Rix, A.; Booysen, M.T. Module-Level Monitoring Of Solar PV Plants Using Wireless Sensor Networks. In Proceedings of the 26th Southern African Universities Power and Engineering Conference (SAUPEC 2018), Johannesburg, South Africa, 24–26 January 2018; pp. 1–6.
45. Jeong, J.; Shin, Y.; Lee, I. Long-Range Transmission of Photovoltaic Climate Information through the LoRa Radio. In Proceedings of the 2018 International Conference on Information and Communication Technology Convergence (ICTC), Jeju, Korea, 17–19 October 2018; pp. 956–959.
46. Erturk, M.A.; Aydın, M.A.; Buyukakkaşlar, M.T.; Evirgen, H. A Survey on LoRaWAN Architecture, Protocol and Technologies. *Future Internet* **2019**, *11*, 216, doi:10.3390/fi11100216.
47. Bouras, C.; Gkamas, A.; Katsampiris Salgado, S.A.; Kokkinos, V. Comparison of LoRa Simulation Environments. In *Advances on Broad-Band Wireless Computing, Communication and Applications*; Barolli, L., Hellinckx, P., Enokido, T., Eds.; Springer International Publishing: Cham, Switzerland, 2020; pp. 374–385.
48. Voigt, T.; Bor, M.; Roedig, U.; Alonso, J. Mitigating Inter-network Interference in LoRa Networks. In Proceedings of the International Conference on Embedded Wireless Systems and Networks, Uppsala, Sweden, 20–22 February 2017; pp. 323 – 328.
49. Croce, D.; Gucciardo, M.; Mangione, S.; Santaromita, G.; Tinnirello, I. Impact of LoRa Imperfect Orthogonality: Analysis of Link-Level Performance. *IEEE Commun. Lett.* **2018**, *22*, 796–799, doi:10.1109/LCOMM.2018.2797057.
50. Croce, D.; Gucciardo, M.; Tinnirello, I.; Garlisi, D.; Mangione, S. Impact of Spreading Factor Imperfect Orthogonality in LoRa Communications. In *Digital Communication. Towards a Smart and Secure Future Internet*; Piva, A., Tinnirello, I., Morosi, S., Eds.; Springer International Publishing: Cham, Switzerland, 2017; pp. 165–179.
51. Froiz-Míguez, I.; Lopez-Iturri, P.; Fraga-Lamas, P.; Celaya-Echarri, M.; Blanco-Novoa, Ó.; Azpilicueta, L.; Falcone, F.; Fernández-Caramés, T.M. Design, Implementation, and Empirical Validation of an IoT Smart Irrigation System for Fog Computing Applications Based on LoRa and LoRaWAN Sensor Nodes. *Sensors* **2020**, *20*, 6865, doi:10.3390/s20236865.
52. Oh, J.; Lim, D.W.; Kang, K.M. The Impact of Imperfect Orthogonality of LoRa Communication in Multiple Drone Identification. In Proceedings of the 2021 International Conference on Information and Communication Technology Convergence (ICTC), Jeju, Korea, 20–22 October 2021; pp. 906–908, doi:10.1109/ICTC52510.2021.9621180.
53. Seller, O. *Predicting LoRaWAN Capacity*; Technical Report; Semtech: Camarillo, CA, USA, 2020.

54. Cuomo, F.; Campo, M.; Caponi, A.; Bianchi, G.; Rossini, G.; Pisani, P. EXPLoRa: Extending the performance of LoRa by suitable spreading factor allocations. In Proceedings of the 2017 IEEE 13th International Conference on Wireless and Mobile Computing, Networking and Communications (WiMob), Rome, Italy, 9–11 October 2017; pp. 1–8, doi:10.1109/WiMOB.2017.8115779.
55. Sagala, A.; Siahaan, D.; Nadeak, T.; Sitorus, E. Low Power—Low Rate Vessel Tracking System (VTS) in Territorial Waters. In Proceedings of the 2019 International Conference of Computer Science and Information Technology (ICoSNIKOM), Medan, Indonesia, 28–29 November 2019; pp. 1–5, doi:10.1109/ICoSNIKOM48755.2019.9111615.
56. Augustin, A.; Yi, J.; Clausen, T.; Townsley, W.M. A Study of LoRa: Long Range & Low Power Networks for the Internet of Things. *Sensors* **2016**, *16*, 1466, doi:10.3390/s16091466.
57. Centenaro, M.; Vangelista, L.; Kohno, R. On the impact of downlink feedback on LoRa performance. In Proceedings of the 2017 IEEE 28th Annual International Symposium on Personal, Indoor, and Mobile Radio Communications (PIMRC), Montreal, QC, Canada, 8–13 October 2017; pp. 1–6.
58. Haxhibeqiri, J.; Karaagac, A.; Van den Abeele, F.; Joseph, W.; Moerman, I.; Hoebeke, J. LoRa indoor coverage and performance in an industrial environment: Case study. In Proceedings of the 2017 22nd IEEE International Conference on Emerging Technologies and Factory Automation (ETFA), Limassol, Cyprus, 12–15 September 2017; pp. 1–8, doi:10.1109/ETFA.2017.8247601.
59. Bankov, D.; Khorov, E.; Lyakhov, A. *On the Limits of LoRaWAN Channel Access*; International Conference on Engineering and Telecommunication (EnT), Moscow, Russia, 29-30 November 2016, pp. 10–14, doi:10.1109/EnT.2016.011.
60. Georgiou, O.; Raza, U. Low Power Wide Area Network Analysis: Can LoRa Scale? *IEEE Wirel. Commun. Lett.* **2017**, *6*, 162–165, doi:10.1109/LWC.2016.2647247.
61. Abdul Latiff, N.A.; Ismail, I.S.; H., M. Scalability Performance for Low Power Wide Area Network Technology using Multiple Gateways. *Int. J. Adv. Comput. Sci. Appl.* **2020**, *11*, pp: 212–218, doi:10.14569/IJACSA.2020.0110128.
62. Fazeldehkordi, E.; Amiri, I.S.; Akanbi, O.A. Chapter 2—Literature Review. In *A Study of Black Hole Attack Solutions*; Fazeldehkordi, E., Amiri, I.S., Akanbi, O.A., Eds.; Syngress, Massachusetts, United States, 2016; pp. 7–57, doi:10.1016/B978-0-12-805367-6.00002-8.
63. Duda, A.; Heusse, M. *Spatial Issues in Modeling LoRaWAN Capacity*; 2019; pp. 191–198, Miami Beach, United States. doi:10.1145/3345768.3355932.
64. RF Propagation Simulation Software. 2020. Available online: http://radiomobile.pe1mew.nl/ (accessed on 30 November 2021).
65. Fujdiak, R.; Mlynek, P.; Misurec, J.; Strajt, M. Simulated Coverage Estimation of Single Gateway LoRaWAN Network. In Proceedings of the 2018 25th International Conference on Systems, Signals and Image Processing (IWSSIP), Maribor, Slovenia, 20–22 June 2018; pp. 1–4, doi:10.1109/IWSSIP.2018.8439232.
66. Abdelraheem, A.M.; Abdalla, M.A. Prediction of WiMAX radio wave propagation over outdoor irregular terrains and spacing. In Proceedings of the 2014 31st National Radio Science Conference (NRSC), Cairo, Egypt, 28–30 April 2014; pp. 167–174, doi:10.1109/NRSC.2014.6835073.
67. Harinda, E.; Hosseinzadeh, S.; Larijani, H.; Gibson, R.M. Comparative Performance Analysis of Empirical Propagation Models for LoRaWAN 868MHz in an Urban Scenario. In Proceedings of the 2019 IEEE 5th World Forum on Internet of Things (WF-IoT), Limerick, Ireland, 15–18 April 2019; pp. 154–159, doi:10.1109/WF-IoT.2019.8767245.
68. Kufakunesu, R.; Hancke, G.P.; Abu-Mahfouz, A.M. A Survey on Adaptive Data Rate Optimization in LoRaWAN: Recent Solutions and Major Challenges. *Sensors* **2020**, *20*, 5044, doi:10.3390/s20185044.
69. Petajajarvi, J.; Mikhaylov, K.; Roivainen, A.; Hanninen, T.; Pettissalo, M. On the coverage of LPWANs: Range evaluation and channel attenuation model for LoRa technology. In Proceedings of the 2015 14th International Conference on ITS Telecommunications (ITST), Copenhagen, Denmark, 2–4 December 2015; pp. 55–59, doi:10.1109/ITST.2015.7377400.
70. Agoua, X.G.; Girard, R.; Kariniotakis, G. Probabilistic Models for Spatio—Temporal Photovoltaic Power Forecasting. *IEEE Trans. Sustain. Energy* **2019**, *10*, 780–789, doi:10.1109/TSTE.2018.2847558.
71. Nagy, G.I.; Barta, G.; Kazi, S.; Borbély, G.; Simon, G. GEFCom2014: Probabilistic solar and wind power forecasting using a generalized additive tree ensemble approach. *Int. J. Forecast.* **2016**, *32*, 1087–1093.
72. Bessa, R.J.; Trindade, A.; Silva, C.S.; Miranda, V. Probabilistic solar power forecasting in smart grids using distributed information. *Int. J. Electr. Power Energy Syst.* **2015**, *72*, 16–23.
73. Huang, J.; Perry, M. A semi-empirical approach using gradient boosting and k–nearest neighbors regression for GEFCom2014 probabilistic solar power forecasting. *Int. J. Forecast.* **2016**, *32*, 1081–1086.
74. Golestaneh, F.; Gooi, H.B.; Pinson, P. Generation and evaluation of space–time trajectories of photovoltaic power. *Appl. Energy* **2016**, *176*, 80–91.
75. Zhang, B.; Dehghanian, P.; Kezunovic, M. Spatial-temporal solar power forecast through use of Gaussian conditional random fields. In Proceedings of the 2016 IEEE Power and Energy Society General Meeting (PESGM), Boston, MA, USA, 17–21 July 2016; pp. 1–5.
76. Yang, D.; Ye, Z.; Lim, L.H.I.; Dong, Z. Very short term irradiance forecasting using the lasso. *Sol. Energy* **2015**, *114*, 314–326.
77. Agoua, X.G.; Girard, R.; Kariniotakis, G. Photovoltaic Power Forecasting: Assessment of the Impact of Multiple Sources of Spatio-Temporal Data on Forecast Accuracy. *Energies* **2021**, *14*, 1432, doi:10.3390/en14051432.
78. Muhammad, B.; Azmi, K.Z.M.; Ibrahim, Z.; bin Mohd Faudzi, A.A.; Pebrianti, D. Simultaneous computation of model order and parameter estimation for system identification based on opposition-based simulated Kalman filter. In Proceedings of the 2018 SICE International Symposium on Control Systems (SICE ISCS), Tokyo, Japan, 9–11 March 2018; pp. 105–112, doi:10.23919/SICEISCS.2018.8330163.

79. Dudek, G. Short-Term Load Forecasting Using Random Forests. In *Intelligent Systems'2014*; Filev, D., Jabłkowski, J., Kacprzyk, J., Krawczak, M., Popchev, I., Rutkowski, L., Sgurev, V., Sotirova, E., Szynkarczyk, P., Zadrozny, S., Eds.; Springer International Publishing: Cham, Switzerland, 2015; pp. 821–828.
80. Wright, M.N.; Ziegler, A. ranger: A Fast Implementation of Random Forests for High Dimensional Data in C++ and R. *J. Stat. Softw.* **2017**, *77*, 1–17, doi:10.18637/jss.v077.i01.
81. Huertas Tato, J.; Centeno Brito, M. Using Smart Persistence and Random Forests to Predict Photovoltaic Energy Production. *Energies* **2019**, *12*, 100, doi:10.3390/en12010100.
82. Duchaud, J.L.; Voyant, C.; Fouilloy, A.; Notton, G.; Nivet, M.L. Trade-Off between Precision and Resolution of a Solar Power Forecasting Algorithm for Micro-Grid Optimal Control. *Energies* **2020**, *13*, 3565, doi:10.3390/en13143565.
83. Bueso, M.C.; Paredes-Parra, J.M.; Mateo-Aroca, A.; Molina-García, A. A Characterization of Metrics for Comparing Satellite-Based and Ground-Measured Global Horizontal Irradiance Data: A Principal Component Analysis Application. *Sustainability* **2020**, *12*, 2454, doi:10.3390/su12062454.
84. R–Core–Team; *R: A Language and Environment for Statistical Computing*; R Foundation for Statistical Computing, Vienna, Austria, 2021. Available online: https://www.R-project.org/ (accessed on 30 November 2021).
85. Dowle, M.; Srinivasan, A. *Data.table: Extension of 'Data.frame'*; R package version 1.14.2; September, 2019. Available online: https://cran.r-project.org/web/packages/data.table/data.table.pdf (accessed on 30 November 2021).
86. Sardá-Espinosa, A. Comparing time-series clustering algorithms in r using the dtwclust package. *R Package Vignette* **2017**, *12*, 41.
87. Nonnenmacher, L.; Coimbra, C.F. Streamline-based method for intra-day solar forecasting through remote sensing. *Sol. Energy* **2014**, *108*, 447–459, doi:10.1016/j.solener.2014.07.026.
88. Solar Irradiation Data, CETA-CIEMAT. 2020. Available online: http://www.adrase.com/en/ (accessed on 30 November 2021).
89. Copernicus European Union's Earth Observation Programme. 2020. Available online: http://copernicus.eu (accessed on 30 November 2021).
90. Network of the Agricultural Information System of Murcia (SIAM). 2019. Available online: https://www.imida.es/siam/ (accessed on 30 November 2021).
91. Lavric, A.; Popa, V. Performance Evaluation of LoRaWAN Communication Scalability in Large-Scale Wireless Sensor Networks. *Wirel. Commun. Mob. Comput.* **2018**, pp. 1–9, doi:10.1155/2018/6730719.
92. Dynamic Time Warping. In *Information Retrieval for Music and Motion*; Springer: Berlin/Heidelberg, Germany, 2007; pp. 69–84, doi:10.1007/978-3-540-74048-3_4.
93. Leodolter, M.; Plant, C.; Brändle, N. IncDTW: An R Package for Incremental Calculation of Dynamic Time Warping. *J. Stat. Softw.* **2021**, *99*, 1–23, doi:10.18637/jss.v099.i09.

4.5. Democratization of PV micro-generation system monitoring based on narrowband-IoT

Información adicional:

- Revista: Sensors 22, no. 13: 4966
- DOI: 10.3390/s22134966
- Fecha de publicación: Junio 2022
- Disponible en: https://www.mdpi.com/1424-8220/22/13/4966
- Referencia: [43]
  Paredes-Parra, J.M.; Jiménez-Segura, R.; Campos-Peñalver, D.; Mateo-Aroca, A.; Ramallo-González, A.P.; Molina-García, A. Democratization of PV Micro-Generation System Monitoring Based on Narrowband-IoT. Sensors 2022, 22, 4966. https://doi.org/10.3390/s22134966

sensors

MDPI

Article

Democratization of PV Micro-Generation System Monitoring Based on Narrowband-IoT

José Miguel Paredes-Parra [1], Raquel Jiménez-Segura [2], David Campos-Peñalver [1], Antonio Mateo-Aroca [2], Alfonso P. Ramallo-González [3] and Angel Molina-García [2,*]

[1] Technological Center of Energy and Environment (CETENMA), 30353 Cartagena, Spain; jmparedes@cetenma.es (J.M.P.-P.); david.campos@cetenma.es (D.C.-P.)
[2] Departament of Automatics, Electrical Engineering and Electronic Technology, Universidad Politécnica de Cartagena, 30202 Cartagena, Spain; raquel.jimenez@edu.upct.es (R.J.-S.); antonio.mateo@upct.es (A.M.-A.)
[3] Department of Information and Communications Engineering, Computer Science Faculty, University of Murcia, 30100 Murcia, Spain; alfonsop.ramallo@um.es
* Correspondence: angel.molina@upct.es; Tel.: +34-968-32-5462

Abstract: Power system configuration and performance are changing very quickly. Under the new paradigm of prosumers and energy communities, grids are increasingly influenced by microgeneration systems connected in both low and medium voltage. In addition, these facilities provide little or no information to distribution and/or transmission system operators, increasing power system management problems. Actually, information is a great asset to manage this new situation. The arrival of affordable and open Internet of Things (IoT) technologies is a remarkable opportunity to overcome these inconveniences allowing for the exchange of information about these plants. In this paper, we propose a monitoring solution applicable to photovoltaic self-consumption or any other microgeneration installation, covering the installations of the so-called 'prosumers' and aiming to provide a tool for local self-consumption monitoring. A detailed description of the proposed system at the hardware level is provided, and extended information on the communication characteristics and data packets is also included. Results of different field test campaigns carried out in real PV self-consumption installations connected to the grid are described and analyzed. It can be affirmed that the proposed solution provides outstanding results in reliability and accuracy, being a popular solution for those who cannot afford professional monitoring platforms.

Keywords: photovoltaic microgeneration; NB-IoT technology; monitoring network; Internet of Things

Citation: Paredes-Parra, J.M.; Jiménez-Segura, R.; Campos-Peñalver, D.; Mateo-Aroca A.; Ramallo-González, A.P.; Molina-García, A. Democratization of PV Micro-Generation System Monitoring Based on Narrowband-IoT. *Sensors* **2022**, *22*, 4966. https://doi.org/10.3390/s22134966

Academic Editor: Grzegorz Fusiek

Received: 19 May 2022
Accepted: 25 June 2022
Published: 30 June 2022

1. Introduction

In recent years, most countries have established ambitious renewable energy targets for their electricity generation to foster sustainable and low-emission initiatives. In line with the European and COP21 decarbonization environmental objectives [1], Spain has promoted new legislation providing support and an optimized framework for the Renewable Energy Sources (RES) integration, mainly wind power plants and solar photovoltaic (PV) installations [2]. These new regulations, together with a significant reduction in the cost of PV technology as a result of their own technological maturity, have addressed the enormous growth in the integration of such solutions. Subsequently, a relevant number of PV installations can be found at different voltage levels; mainly under the alternative cooperatively-owned organizations giving a substantially different model of energy distribution and provision [3]. In Europe, and more specifically in Spain, PV installations have been widely integrated by prosumers as feasible strategies to decrease power demand, fulfill emission agreements and accelerate self-consumption growth rates [4]. These policies can have relevant consequences on the design and operation of distribution networks to which most prosumers are connected [5]. Under this scenario, guaranteeing a safe and

reliable RES integration is a remarkable challenge to be solved by power systems in the coming years [6]. Actually, high RES integration is included in the Strategic Energy Technology Plan (SET Plan) of the European Union—see Activity 4: Operation and diagnosis of Photovoltaic Plants, highlights the digitization of the energy sector as a fundamental and crucial element for the EU [7]. In parallel to the current developments of technology, digitization offers new opportunities for system operators and facility managers and maintainers by optimizing the operation of their assets, reducing their operating costs and allowing greater renewable integration. In this context, real-time medium- and low-voltage grid monitoring and control under the new technologies will lead to significant improvement of grid efficiency and hosting capacity [8]. Moreover, local and timely management of distributed resources and self-consumption installations will be the key to ensure efficiency and stability at the distribution and the operation level [9]. Among the different solutions, PV self-consumption systems constitute a remarkable challenge for distributed generation contributing to future smart grids [10].

With regard to solar PV monitoring technologies, various review contributions can be found in the specific literature from different points of view [11–13]. Nevertheless, both environmental and technical factors can significantly affect the PV power generation—partial shading due to moving clouds, module temperature, humidity, the mounting angle, etc. Further explorations are then required to design an effective solar PV monitoring technology [14]. In addition, the use of monitoring systems in large-scale PV systems can be justified despite their high costs [15]. However, monitoring systems in medium and small PV installations may address additional and high costs unacceptable to most users. For this reason, data acquisition and monitoring solutions using low-cost platforms have been widely proposed in recent years [16]. The advance of technologies such as IoT and Industry 4.0 have allowed the implementation of new monitoring solutions as an alternative to traditional centralized systems. These solutions mainly aim to detect anomalies of PV solar plants and for maintenance purposes. Different approaches can be found in recent literature. Madeti et al. [11] provided a comprehensive review of PV monitoring systems, comparing most of PV monitoring evaluation techniques in terms of their relative performances. This contribution also examined sensors, controllers in data acquisition systems, data transmission methods and data storage and analysis. In [17], Sunarso et al. proposed a low-cost PV monitoring system based on an open-source Arduino platform and demonstrated its use for the assessment of PV monitoring and supervision potential. The system developed by Sunarso et al. can monitor solar irradiance, electric outputs and temperature of multiple solar panels. A similar approach can be found in [18], where the authors described a prototype for a portable data logger that integrates standalone instruments with open-source hardware technologies for monitoring PV systems. The proposed datalogger accomplished the accuracy requirements of the IEC standards for PV systems. In 2019, López-Vargas et al. [19] improved the design with a new version of this low-cost datalogger to overcome the shortcomings related to power consumption, the limited voltage range and the user interface for stand-alone PV systems located in remote areas deprived of telecommunications networks. Data were stored on an SD card to work autonomously. This work continued with a new design that included allowing 3G technology to monitor the PV systems remotely via web or via mobile application [20]. Regarding communications, Ansari et al. [14] reviewed various monitoring technologies for PV power plants focused on data processing modules and data transmission protocols. They showed key issues and limitations of this technology. In terms of transmission protocol, this work selected LoRa as a relevant data transmission solution, but it was not suitable for large payloads. Moreover, a continuous data packet sending process should be avoided due to some rules and constraints regarding the frequency band, which is in line with other recent contributions [21].

From the limitations of the techniques found in the specific literature, and considering the requirements of the application at hand, the authors previously proposed a solution using a Raspberry Pi that served as a comprehensive solar PV monitoring following the

IEC-61724 requirements. The solution was used at the module level [22]. It was tested and assessed at real PV solar installations with remarkable results. The tests took some months in CETENMA SOLAR installations facilities. A 250 Wp module connected to the grid with a Soltec Solarfighter microinverter was monitored, as well as a 5 kWp ver-roof installation connected to the grid and located in the Universidad PolitÃl'cnica de Cartagena (Spain) during some weeks. All variables were collected with standard equipment at both facilities. The results showed that the estimated error rate was lower than 2%. From this preliminary design, a low-cost LoRa-based solar PV monitoring system to communicate solar PV power plants located in remote locations was subsequently proposed in [23]. This topology used an Arduino Board with an RFM95W transceiver fabricated by HOPE RF configured as a LoRa TM modem available for the EU-868 MHz band [24]. The solution stored data in a packet size of 38 bytes with a transmission power of 14 dBm and spreading factor (SF) metric ranging from 10 to 12. An alternative system to be implemented in remote PV power plants for monitoring and dispatching electrical and meteorological data was then proposed and evaluated. This study demonstrated that the line of sight between source and destination and propagation issues had a clear influence on the suitable data reception process. As a main drawback, this solution only allowed a limited number of transmissions, due to the over-air time of works with high spreading factor value (SF11 and SF12) to ensure an accurate reception of data packets with a restricted duty cycle (1%). In addition, a LoRa sensitive analysis was conducted by the authors in [25] for PV short-time forecasting accuracy estimation.

By considering this preliminary background, as well as the lack of contributions focused on monitoring self-consumption PV solar installations and providing information to prosumers in terms of consumption/production profiles [26], the main contributions of this paper are described below:

- A novel monitoring solution for the operation and maintenance of self-consumption PV systems is proposed and assessed.
- The solution is based on Internet of Things (IoT) applications by using Narrowband IoT (NB-IoT).
- The new design uses the Pycom IoT platform with NB-IoT as data transmission technology.

The Pycom development board FiPy and sensor shield Pysense have recently been proposed to monitor environmental variables such as humidity, temperature, altitude, pressure, or light [27].

The rest of the paper is structured as follows: Section 2 introduces NB-IoT technology; Section 3 discusses materials and methods; Section 4 describes the use case; Section 5 discusses both collected data and results; finally, conclusions are given in Section 6.

2. Communications: NB-IoT

Low-power, wide-area (LPWA) technologies are targeting most emerging markets and applications. LPWA is a recent generic term involving different technologies focused on enabling wide area communications, minimizing power consumption and cost [28]. LPWA has become a relevant growing space in IoT since in general LPWA solutions are perfectly suitable for such IoT applications that only need to transmit low amounts of data over a long range. Other researchers proposed a ZigBee network tested with WiFi for smart grid applications. However, these tools have limited capability for analyzing real scenarios and, according to Sultania et al. [29] ZigBee uses the same frequency band as WiFi, which can lead to potential radio interference. Consequently, most of the developed LPWA technologies have arisen in both unlicensed and licensed markets, such as SigFox, LTE-M, NB-IoT and long range (LoRa). Among them, Shina et al. [30] affirmed that NB-IoT and LoRa solutions are the two leading emergent technologies,despite the important technical differences in terms of network architecture, physical features and MAC protocol between them. Table 1 compares different network schemes and communication technologies.

Table 1. Network schemes and communication technologies properties.

Network Schemes	Technologies	Data Transfer Rate	Typical Coverage Range	Latency
HAN	Ethernet, PLC, Zigbee, WLAN, Z-Wave	10–100 kbps	up to 500 m	10 ms–1 s
BAN/IAN	Ethernet, PLC, Wimax, WLAN	100 kbps–1 Mbps	up to 1 km	10 ms–2 s
NAN	Ethernet, PLC, DSL, Fiber–Optics, WiMax, NB–IoT, LoRa	100 kbps–10 Mbps	0.1–10 km	10–50 ms
WAN	PLC, Ethernet, Fiber–Optics, LoRa, WiMax	10 Mbps–1 Gbps	10–100 km	10 µs–20 ms

Recently, different comparative studies are available in the specific literature evaluating LoRa and NB-IoT technologies [31]. Examples of new network architectures combining both technologies can be found in [32,33]. In terms of vulnerabilities, LoRaWAN and NB-IoT give sufficient security guarantees, but according to Coman et al. [34] both technologies need to be properly enforced. The NB-IoT technology was standardized in 2016 by the Third Generation Partnership Project (3GPP), considerably increasing the NB-IoT applications for wireless data communication purposes [35]. In addition, the presence of NB-IoT modules in the IoT device market share by 2030 will considerably increase too [36]. NB-IoT is compatible with LTE-M, with transmission speed of 150 kbps and a coverage range of 15 km. It is a licensed technology deployed in 79 countries, with an investment of $598 billion [37]. In this case, NB-IoT is selected by the authors for PV power plant monitoring and communication network evaluation. This proposal is in line with other recent network applications, such as Smart Water Grid (SWG) [38], water quality monitoring [39] or sustainable farming irrigation [40]. In all cases, NB-IoT was selected as a suitable candidate due to high scalability in comparison to other technologies, such as LoRaWAN and SigFox. Li et al. [41] demonstrated that NB-IoT satisfied both qualitative and quantitative requirements in terms of security, reliability and scalability. The relevant presence of IoT–infrastructure devices, the remarkable variety of applications and the use of various data processing solutions have recently led to the fact that traditional data center architectures do not allow the software configuration nor the physical scaling for tasks to be solved. Moreover, they are no longer able to provide the current required indicators focused on stability, controllability or productivity [42]. On the other hand, and regarding industrial applications, Ballerini et al. [43] concluded that NB-IoT offered the highest quality of service (QoS) while also ensuring data delivery, being a potential replacement to LoRaWAN when communication reliability was a required factor. In addition, NB-IoT was also proposed as an alternative solution for real-time demand response, able to monitor, control and connect electrical appliances [44].

In this paper, we propose an NB-IoT solution for PV power plant monitoring and communication purposes focused on self-consumption installations. Our approach is in line with recent contributions focused on PV installations [45–47]. We extend the use of IoT technology toward prosumers, providing an alternative solution for future distribution system scenarios in which a high renewable penetration would lead to higher peaks of generation as a consequence of potential reverse power flows at the medium voltage/low voltage (MV/LV) distribution transformers [48].

3. IoT Monitoring Solution

3.1. General Architecture

The proposed system uses a FiPy development board as the main hardware. FiPy is a low-cost ESP-32 development board produced by Pycom manufacturer, which includes WiFi, Bluetooth, LoRa, Sigfox and dual LTE-M (CAT M1 and NBIoT) technologies. This platform allows us to test different communication technologies excluding any hardware modification. Table 2 summarizes the most relevant technical features of these boards [49].

Table 2. FiPy specifications.

CPU - Xtensa© dual–core 32–bit LX6 microprocessor(s), up to 600 DMIPS - Hardware floating point acceleration - Python multi–threading - An extra ULP–coprocessor that can monitor GPIOs, the ADC channels and control most of the internal peripherals during deep–sleep mode while only consuming 25 μA.
Networks - WiFi (1 km range) - BLE - Cellular LTE-CAT M1/NB1 (Total world–wide support) - LoRa - Sigfox
Memory - RAM: 520 kB + 4 MB - External flash: 8 MB - GPIO: Up to 22 - Hardware floating point acceleration - Python multi–threading
Interfaces - 2 ×UART, 2 × SPI, I2C, micro SD card - Analog channels: 8 (12–bit ADC), 2 (8–bit DAC) - Timers: 2 of 64 bit with PWM with up to 16 channels - DMA on all peripherals - GPIO: up to 22
Hash/Encryption - SHA, MD5, DES, AES
RTC - Running at 32 kHz
Range - Node range: up to 50 km
Power - Voltage Input: 3.3 V–5.5 V - 3v3 output capable of sourcing up to 400 mA
Size - 55 mm × 20 mm × 3.5 mm (excluding headers)

Pycom is programmed in MicroPython language [50]. For this purpose, it is necessary to use Pymakr, which is an Integrated Development Environment (IDE) plugin for popular code editors, such as Atom and Visual Studio Code. Pymakr thus makes the development of IoT edge devices running microPython easier [51]. Although it is possible to program FiPy via Pybytes, Visual Studio Code is an IDE widely used for this purpose. With regard to the code developed by the authors, Figure 1 shows the structure and main blocks of such code schematically. Firstly, the sensors are configured and set, the FiPy microcontroller being able to collect data from such sensors. Secondly, a reading process of data from the sensors is carried out, and subsequently, the corresponding message is sent via LTE

including the gathered data. It is then necessary to verify if the device is connected to the Pybytes platform. Indeed, eventual disconnections were detected during the testing, and a reconnection process was included in the following terms: Once the connection is verified, the message can be sent to the platform via LTE. This process is repeated with one-minute sample time during the total of sunlight daily hours. FiPy is set on deep-sleep under low sunlight conditions, in line with other contributions [52].

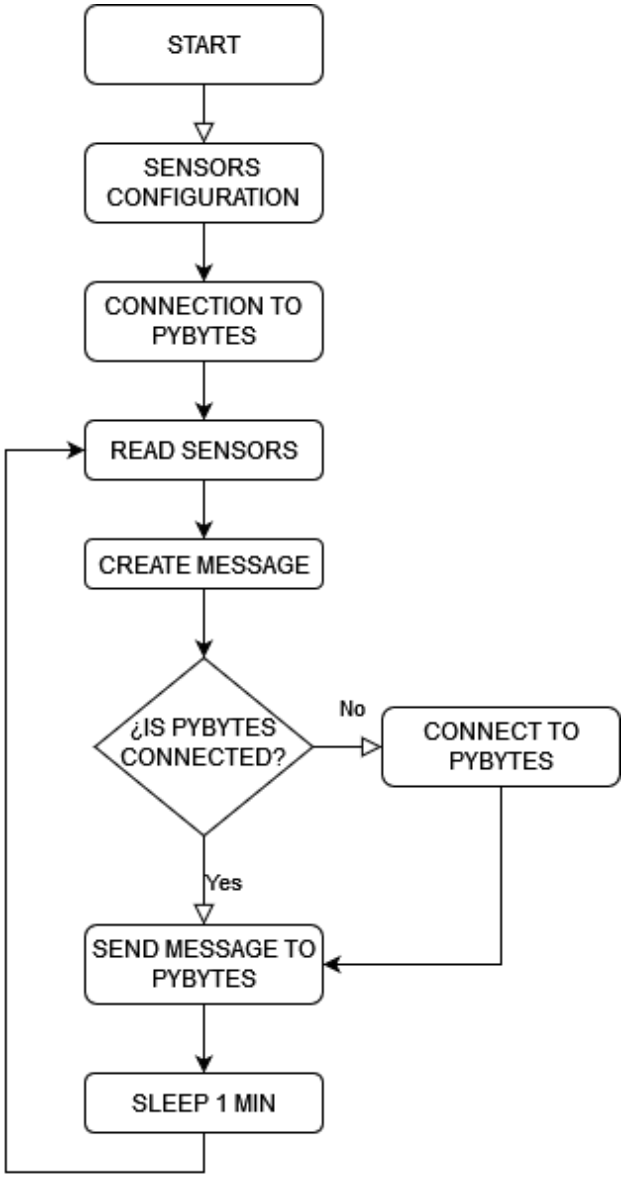

Figure 1. Flow diagram for the microcontroller.

Pybytes is a free cloud-based device management platform for all Pycom development boards and modules. It provides a mobile app, allowing us to manage devices directly from a smartphone. It is possible to change the priority of the used networks: WiFi, Bluetooth and LPWAN networks. Pybytes also provides an easy to use dashboard to quickly create an application that sends data to the platform and allows us to choose among different types of data visualization. That dashboard updates automatically, and subsequently, the user can visualize current status of the devices and received data in real time. It is also possible to integrate Pybytes with a Cloud provider: AWS, Microsoft Azure, Webhooks and Google Cloud. A recent infrastructure based on Pycom development board FiPy and sensor shield Pysense to collect and send data to the remote cloud over Wi-Fi and Long Range (LoRa)

protocols is also described in [27] for remote monitoring conditions. In this case, to provide greater reliability and synchronicity to the data, a DS1302 RTC was incorporated. Thanks to this module, the sending of packets to Pybytes was controlled every minute as were the deep-sleep mode periods for suitable energy saving. This module provided us with a temporary time stamp, helping us when drawing conclusions from the measured data. In addition, and due to the constant disconnections of the Pycom LTE network, different solutions were tested by the authors. The connection to the network was configured by following the official documentation. The script was set to send packets every minute over NB-IoT. In parallel, the firmware of the FiPy microcontroller used was developed to perform a ping to the Pybytes platform and thus verify correct communication. If that ping was not answered due to any connection drop, then it would wait 10 min for the next ping. If this second ping was not answered either, then the watchdog timer was triggered, and the system rebooted to re-establish communication. Consequently, under a communication failure event, 10 min of information would be lost as the microcontroller remains on hold. This operation cannot be modified in the program, but it is a matter of firmware configuration.

3.2. Hardware

With regard to hardware components, the selected sensors as well as the calibration process and the prototype encapsulation are now described. In fact, the selected sensors provide an analog output necessary to calibrate them, in our case by using the Transmille 3000A Series calibrator. The sensors are in charge of monitoring PV installations under the IEC-61724 requirements. The IEC-61724 standards were previously proposed to analyze PV system performance under a variety of climates [53]. In our solution, PV electrical data and weather parameters are gathered to estimate PV operating conditions and exchange meteorological and electrical data. More specifically, the ACS758 current sensor [54] and the YHDC HV25 voltage sensor were selected.

3.2.1. DC-Output Current: Acs758 Hall-Based Effect Sensor

A breakout board for the ACS758 Hall effect linear current sensor was selected for measuring the DC current of the PV module string. The thickness of the copper conductor of this sensor allows the device to survive under high current conditions. The ACS758 provides an analog voltage output signal that varies linearly with the current value. The output voltage of the sensor varies significantly depending on the input current value. Therefore, different currents were applied within the available measurement interval, ranging from −50 A to 50 A DC. In this case, we used a calibration current range from 0 A to 20 A, in steps of 1 A. Subsequently, the sensor output voltage was measured through the FiPy microcontroller, see Figure 2. With this aim, a script was defined to convert the measured value into an estimated current value. The sensor sensitivity provided by the manufacturer was 40 mV/A, for a channel up to 5 V. In our case, the microcontroller channel input was 3.3 V, and subsequently the sensitivity to be used was 26.4 mV/A. The offset voltage was 1.65 V for 0 A, corresponding to 50% of the FiPy microcontroller analogical offset range. The relative error was estimated by comparing the real input current to the measured current values, with a maximum error of 4%. Different current sensors were calibrated and compared to evaluate their performance and accuracy within the expected current range. Figure 3 compares two current sensor calibration processes. An additional source of potential errors in the current sensor output is the sensitivity of the FiPy analog input channel, which is 20 mV/A.

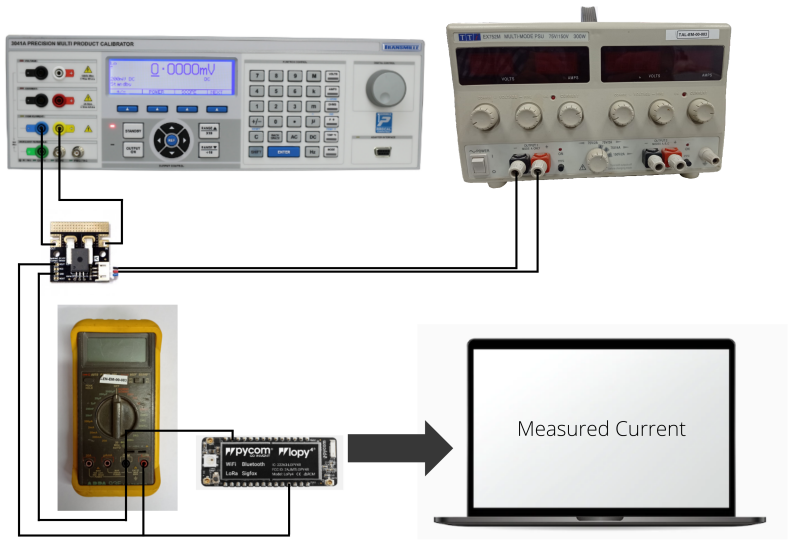

Figure 2. Current sensor calibration assembly: Transmille 3000A Series calibrator, ammeter, regulated power supply and current sensor.

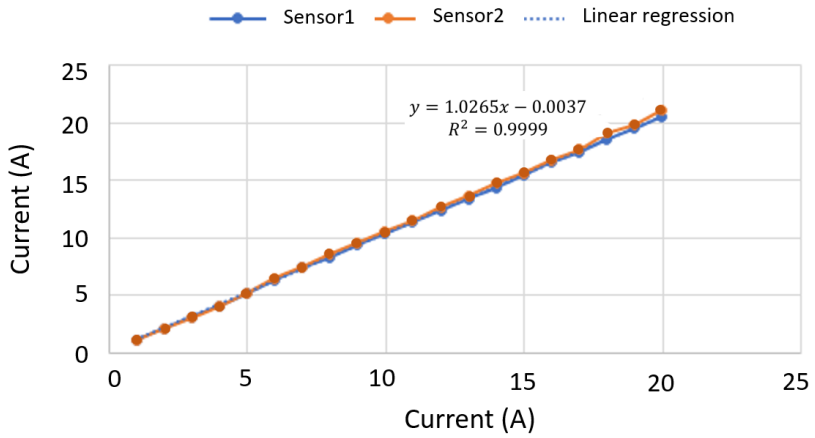

Figure 3. Current sensor calibration process: comparison of input current vs measured current.

3.2.2. DC-Output Voltage: Yhdc Hv25 Sensor

Regarding the DC voltage measurement, the low-cost YHDC HV25 sensor was selected. It allows us to measure voltages up to 1000 V, scaling them to 5 V. Since the analog inputs were used according to the Pycom FiPy microcontroller—working at 3.3 V, it was necessary to include a voltage divider circuit between the sensor output and the analog–pin input. This voltage divider consists of a 56 kΩ resistor and two 56 kΩ resistors in series. In this way, an output of 3.3 V is obtained for an input of 1000 V, with a sensitivity of 3.3 mV/V. With the aim of calibrating the sensor, a set of measurements were carried out from from 0 V to 1000 V, in steps of 50 V. For this purpose, a symmetrical voltage supply of ±12 V and a variable voltage output signal were used together with the 3041A precision multi-product calibrator, see Figure 4. A set of input voltage measurements were compared to the real DC voltage to obtain a calibration curve for this voltage sensor. In a similar way to Section 3.2.1, an additional set of measurements were also collected to estimate the relative error under different boards. By considering that each solar panel had an open-circuit voltage (V_{oc}) of 50 V, the determined relative error was lower than 3%.

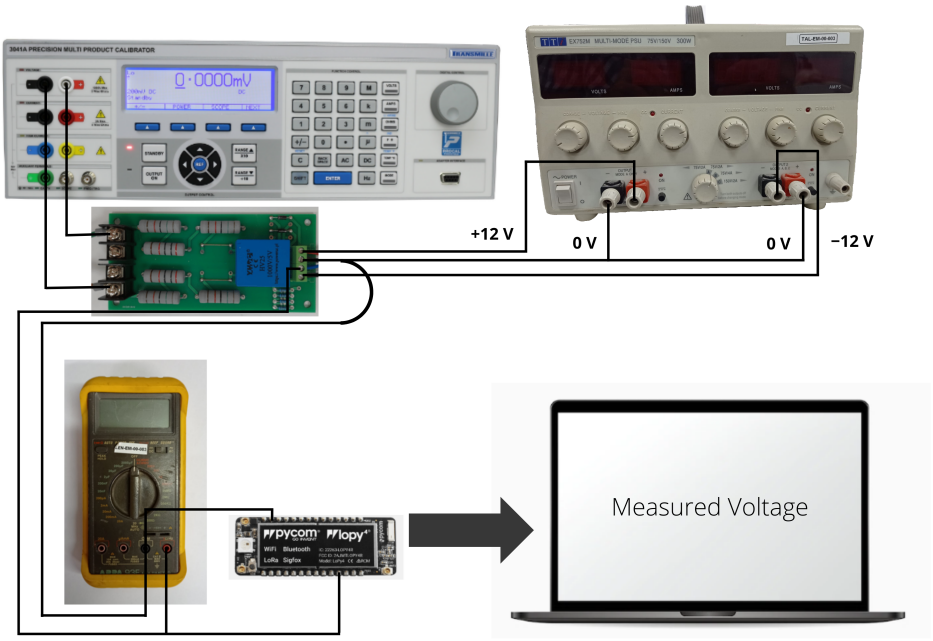

Figure 4. Voltage sensor calibration assembly. Transmille 3000A Series calibrator and voltage sensor.

Due to the high error obtained in the low range of measurement—lower than 50 V—the option of recalculating the voltage divider was then proposed by the authors. The target was to equate the maximum input of 3.3 V to 800 V to test if the sensor precision could be improved below 50 V. After a series of testing measurements, the option was finally discarded since they did not significantly improve the results, and there was a risk of obtaining a voltage higher than 800 V that could damage the equipment. It was observed that the selected sensor did not provide a suitable voltage output for inputs lower than 50 V. Therefore, a voltage divider was included in the laboratory tests to allow collecting voltage data below such a threshold instead of using the YHDC HV25 sensor. This voltage divider was formed by two resistances: 10 kΩ and 1 kΩ, respectively. The output signal was then collected from the 1 kΩ voltage value. Given the high variability of the error for each YHDC HV25 plate, the option of calibrating each board individually, with its own calibration line, was selected. With this aim, Figure 5 compares the calibration process for three different voltage sensor boards. In addition, Table 3 shows the estimated relative errors for these three different voltage sensor boards. As shown in these results, the proposed board has minor accuracy at low voltage levels but high accuracy over the expected operating voltage ranges in medium and small PV installations. Therefore, it is accepted for our proposals.

Table 3. Relative Error YHDC HV25.

Range (V)	Board 1	Board 2	Board 3
50–950	2.93%	2.66%	2.83%
150–1000	2.51%	2.57%	1.49%

3.2.3. Solar PV Module Temperature: Ds18b20 Digital

The DS18B20 is a digital thermometer providing from 9-bit to 12-bit Celsius temperature measurements up to 125 °C [55]. There is also a watertight package that protects the sensor and allows it to be submerged in a liquid without damage available. Since it is a digital sensor, the read signal does not degrade due to wiring distance. It can work in

one-wire mode with an accuracy of ±0.5 °C and 12-bit resolution. Various sensors can also be used on the same pin, as they can be internally programmed with a unique 64-bit ID to identify and differentiate them. The operating range is 3 to 5 V, being able to be used in virtually any system by the use of microcontrollers. Further information of temperature sensor analysis for PV solar module temperature measurement can be found in [56]. The DS18X20 class from the onewire.py library [57] was also included to properly use this sensor with the FiPy. The code can be found in the Appendix A.

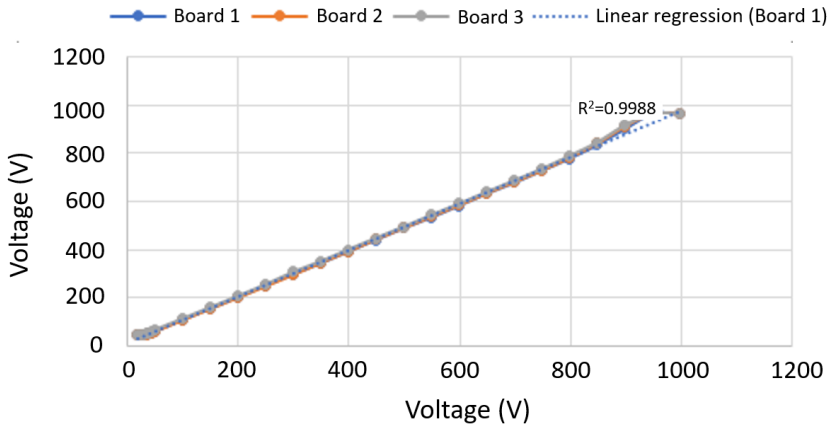

Figure 5. Voltage sensor calibration process: comparison of input voltage vs measured voltage.

3.2.4. Environmental Variables: Sht3x Sensor

The SHT31 is a combined humidity and temperature sensor specially designed for outdoor applications. Recent uses can be found in the building of monitoring applications [58,59]. Its performance characteristics allow the sensor for outdoor applications. It can work on 3.3 V and 5 V systems with very low power demand, offering fast and accurate measurement via I2C bus. The I2C class found in the micropython machine library was included to use this sensor, in addition to the `SHT3X.py` library available in [60]. The developed script can be found in the Appendix B. The irradiance is measured by a reference solar panel (W/m^2). This small PV module of 300 mW is directly connected with a shunt resistor for sampling the voltage generated by the sunlight—68 × 37 mm, mono-crystalline cells; 19% efficiency, 5 V, 60 mA. The analog signal is directly dependent on the irradiance. Further information can be found in [61]. It is calibrated using a pyranometer located close to the plate and in the same position, being then possible to relate the current generated by the reference plate and the available solar irradiance, see Figure 6.

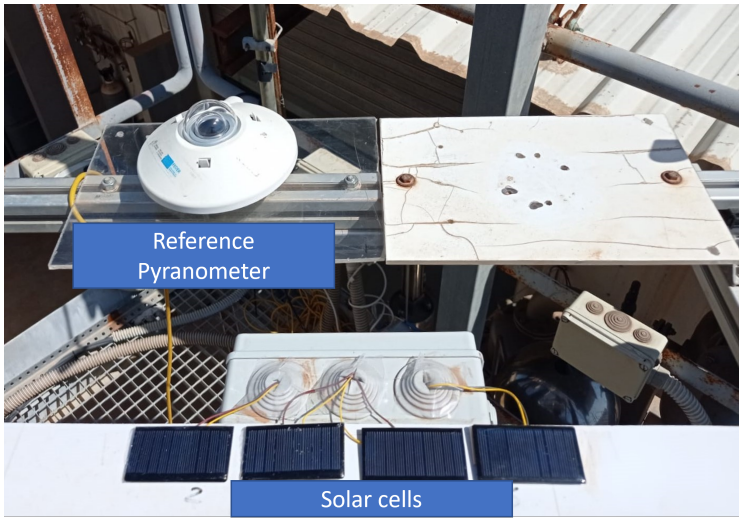

Figure 6. Solar panel calibration:lLaboratory environment.

3.3. Economic Evaluation: Cost-Effectiveness

Finally, and in terms of cost-effectiveness, the proposed monitoring system is in line with other contributions discussed in Sections 1 and 2. The proposed system is flexible to be configured in different locations and PV installations. With the aim of offering a low-cost system, the different hardware components are selected from open-source projects with a high cost effectiveness threshold. Table 4 gives the monitoring node cost, which is lower than other commercial solutions but higher that previous developments carried out by the authors [22,23]. Nevertheless, the global cost could be reduced by using other open-source platforms—such as Arduino—and depending on the number of nodes to be produced and/or purchased.

Table 4. PV monitoring node cost.

Description	Unit Price (Euro)
Mainboard: FiPy	59.4
Sensor: Irradiance	2.45
Sensor: PV DS1820 temperature sensor	1.5
Sensor: DHT temperature and humidity sensor	0.18
Sensor: Voltage sensors (DC)	18.4
Sensor: Current (DC)	17.5
Supply: PV module	9.95
Supply: Battery	6.9
Supply: DC/DC converter	7.9
Supply: DC Booster (24 V)	0.18
Outdoor enclosure and wiring	12
Total cost	136.36

4. Use Case Description

With the aim of evaluating the capability of the proposed solution in terms of measuring, collecting and transmitting data, a preliminary prototype with na FiPy was developed by using a protoboard. Some additional modifications and requirements were detected during this evaluation process. As an example, the inclusion of a potential divider to measure the voltage sensor output, as well as the necessity of increasing an additional input voltage for this sensor were considered, see Figure 7. After the preliminary assembly was tested, a first printed circuit board prototype was designed and milled to minimize the number of wires required by the system by using a computer numerical control (CNC) milling machine. In this case, the printed circuit board (PCB) design was carried out by using Fritzing [62]. It is an electronic design software including libraries for different elements. Flatcam was also used to create the GCode, finally used on the CNC machine that milled the PCB. Different versions were proposed and tested to improve different aspects of the design, mainly reducing sizes and elements required for the solution. Figure 8 shows the connection diagram schematically.

Electronic components need to be protected from moisture, direct sun radiation, dust and other external effects that could affect their normal operation. Moreover, to avoid any interference in control signals and to isolate those components under high voltage or intensity values, two different external boxes were designed using Onshape. It is a free-to-use CAD platform in which assemblies can be created by using different items to make a more complex design. Different recent applications can be found in the specific literature [63].

With the aim of providing power to the node, a PV solar module (6.5 W rate power) with a 2000 mAh Li-Ion Polymer battery was also included. The battery was selected to ensure system operation at night or during periods when solar radiation is not enough to provide the required energy under operating conditions. To ensure a relevant autonomy of the system, the micro-controller goes into deep sleep at night and under low radiation conditions. Figure 9 shows the prototype battery and power supply scheme.

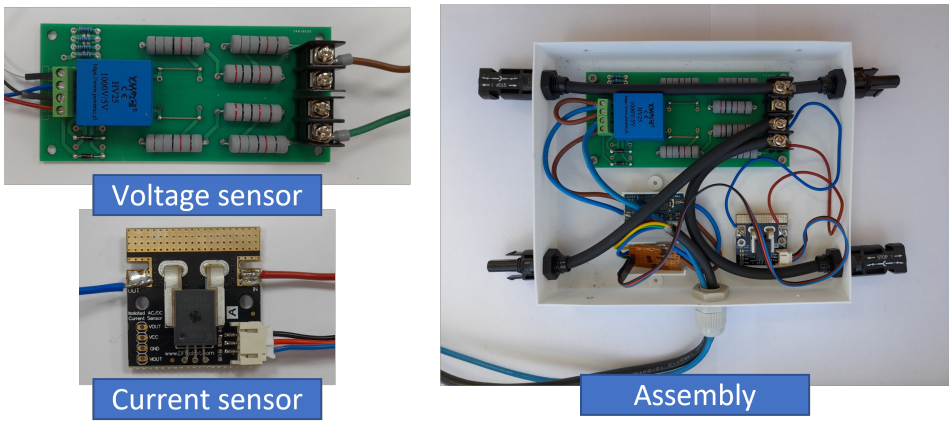

Figure 7. Prototype voltage and current sensors.

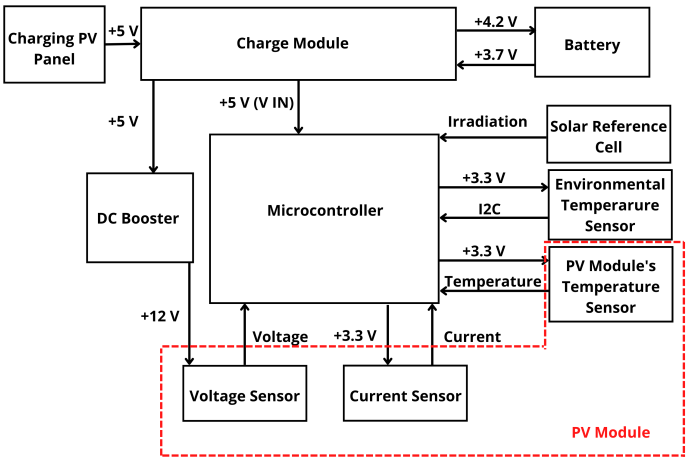

Figure 8. General scheme of the system electronics.

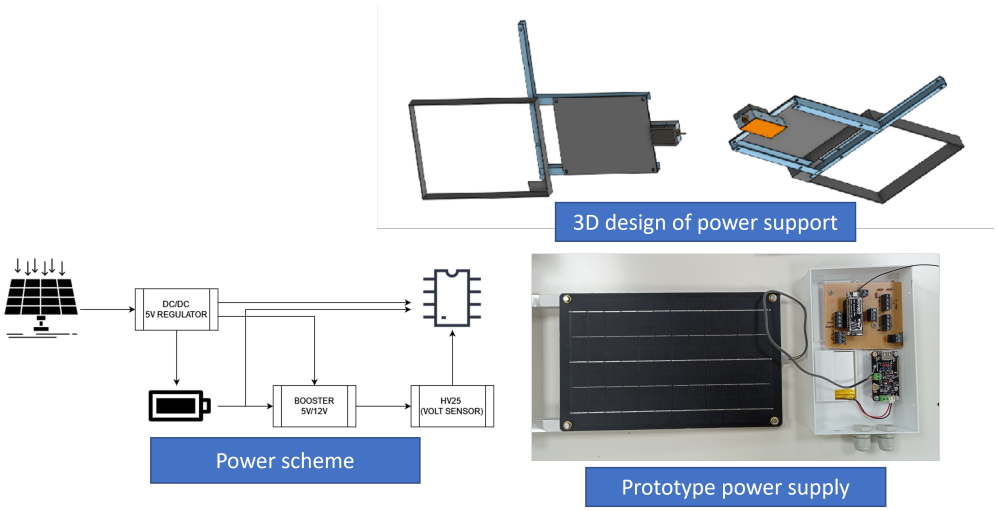

Figure 9. Power supply scheme of the system and prototype example.

5. Results

The proposed solution—both including hardware components and sensors—was tested in a laboratory environment, aiming to assess its performance under different

conditions. The solution was connected and assembled under outdoor conditions in a PV self-consumption installation to evaluate the solution feasibility to be implemented in a variety of real situations and conditions. The proposed system was initially tested at the solar laboratory of CETENMA, located in the Industrial Park of Cartagena (Spain). Such a facility includes measurement equipment to check the performance of PV power plants and modules. For testing purposes, a single 250 Wp monocrystalline PV module connected to an SF 250 W Soltec SolarFighter microinverter was used—V_{MPP} = 28.5 V, I_{MPP} = 8.8 A, V_{oc} = 34.6 V, I_{sc} = 9.4 A. Figure 10 shows some examples of field test campaigns and Figure 11 shows results corresponding to this calibration process.

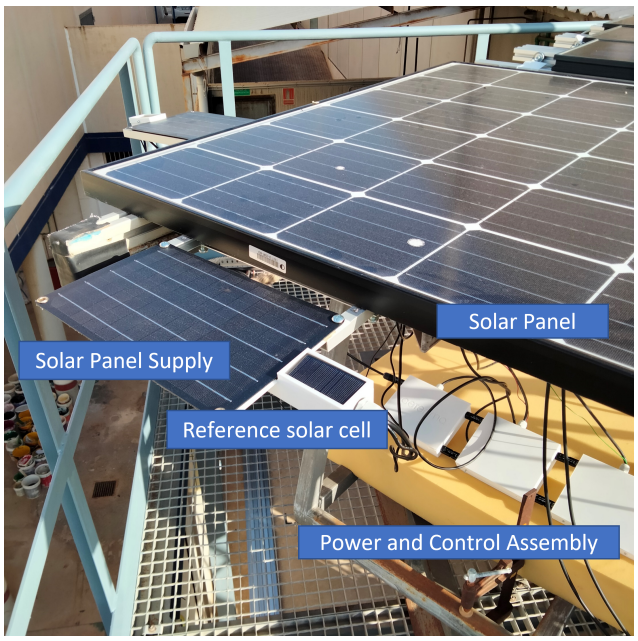

Figure 10. Case study. Example of field test campaign. Charging solar panel and reference cell assembled to the monitored PV module panel.

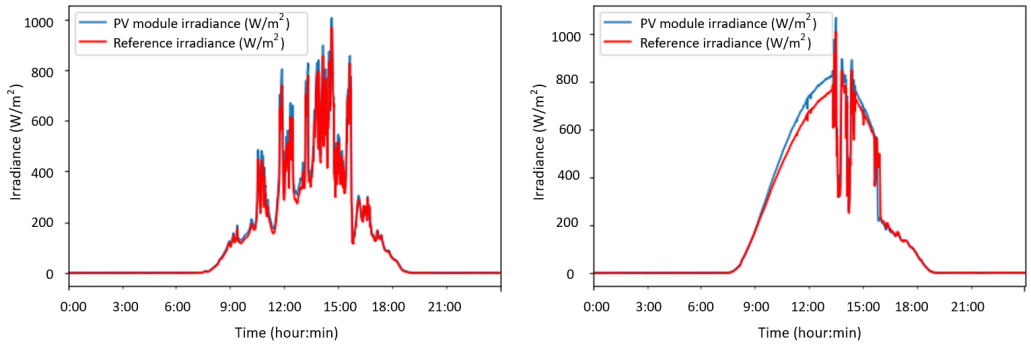

Figure 11. Calibration of the reference cell: comparison of data for two days.

From the power supply scheme shown in Figure 9, Figure 12 depicts voltage evolution and current demanded (positive) or supplied (negative) by the battery. The Pycom module consumption is around 200 mA over WiFi and 250 mA when the LTE communication protocol is selected. During the information sending process, up to 350 mA can be achieved. Figure 13 shows a detail of Pycom and battery power demand comparison. Regarding the received data through NB-Iot communications versus inverter data, voltage and current have enough precision, 2.45% and 3.9%, respectively, to evaluate the operation of the plant with security. A total of six packages were sent with one-minute sample time: 8 bytes/package for five packages and 10 bytes/package for the additional package. In

terms of electrical collected data, Figures 14 and 15 show both voltage and current data respectively. Even though the selected reference cells achieved suitable results during the calibration process, the received data show divergences during some periods of the day. These divergences are due to both material and design of the enclosure of the reference cell that, after some time, does not ensure that it remains in the plane of installation with modules of the plant, reducing the received radiation with low values of solar angles, see Figure 16. A new design for this enclosure is currently in progress. In terms of temperature gradients, Figure 17 compares PV module temperature to ambient temperature These data give additional information regarding PV operating temperature, which can be useful to estimate other parameters, such as the performance ratio. In addition, it is also possible to analyze the effect of irradiation and ambient temperature on PV system performance, as was suggested by other authors [64,65].

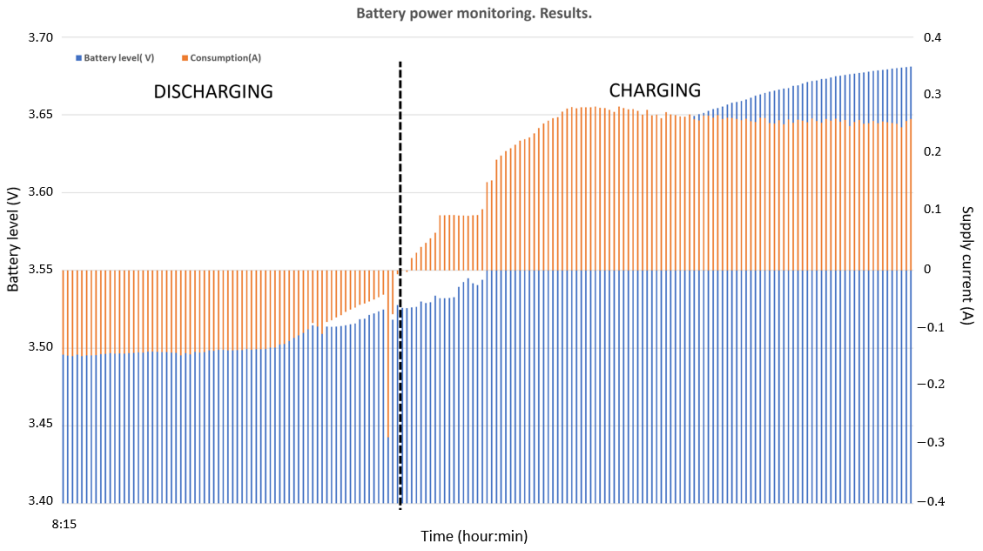

Figure 12. Example of battery charge and discharge time periods.

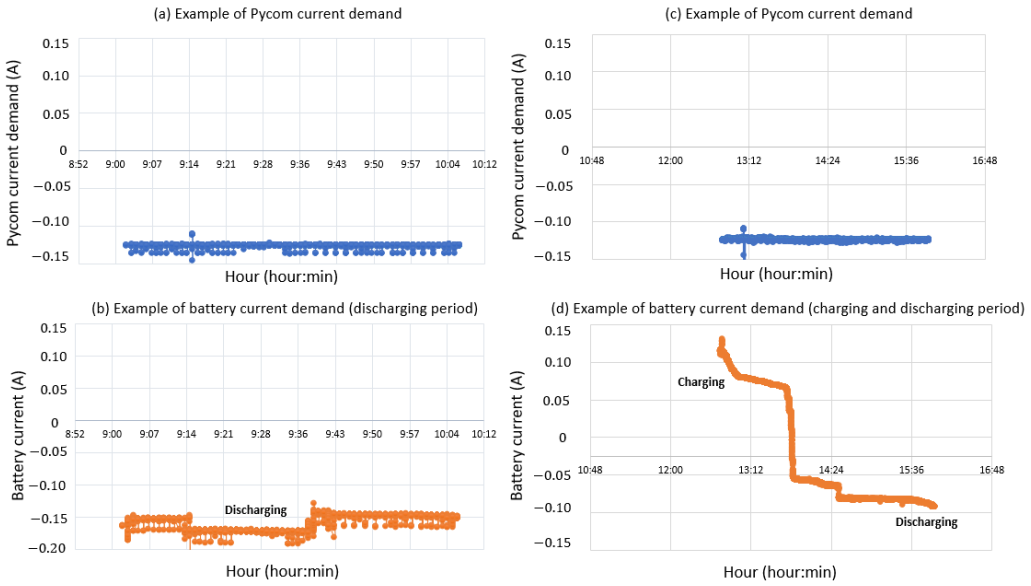

Figure 13. Examples of Pycom demand consumption and battery power monitoring: (**a**,**b**) discharging battery period; (**c**,**d**) charging and discharging battery period.

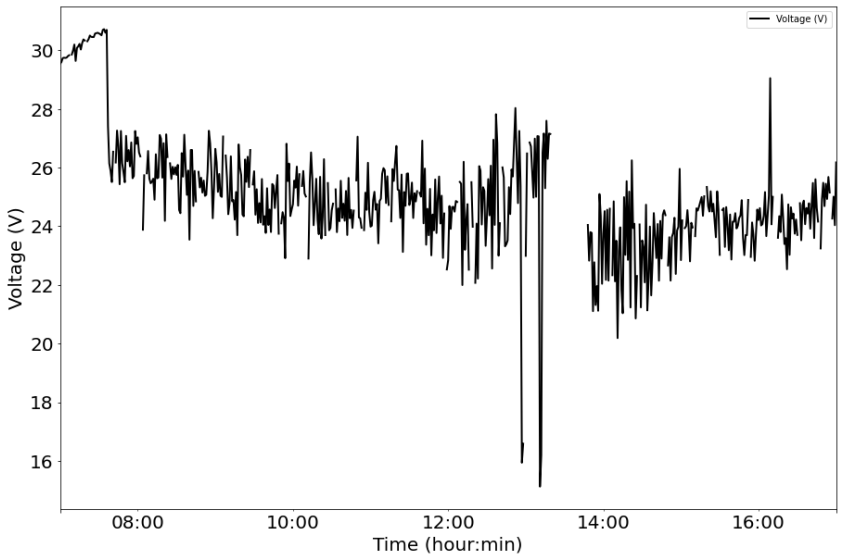

Figure 14. Example of collected voltage data: PV module monitored.

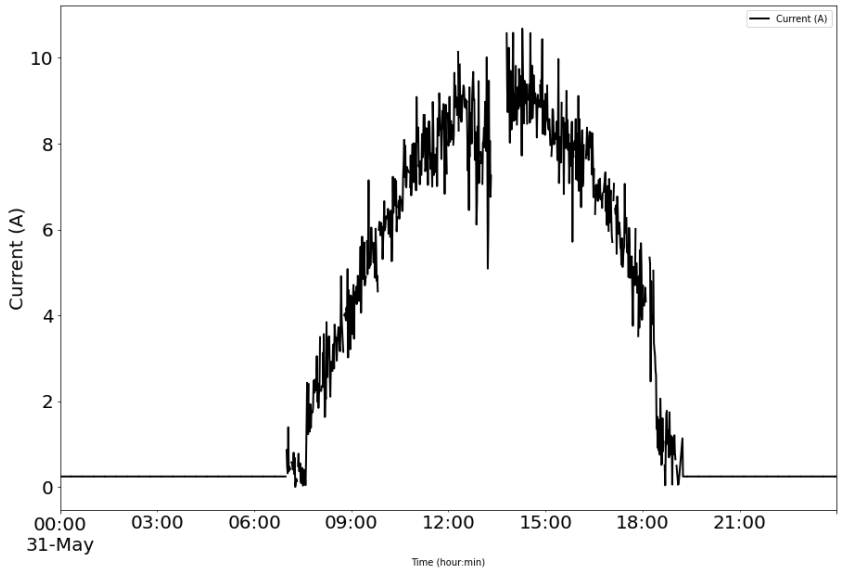

Figure 15. Example of collected current data: PV module monitored.

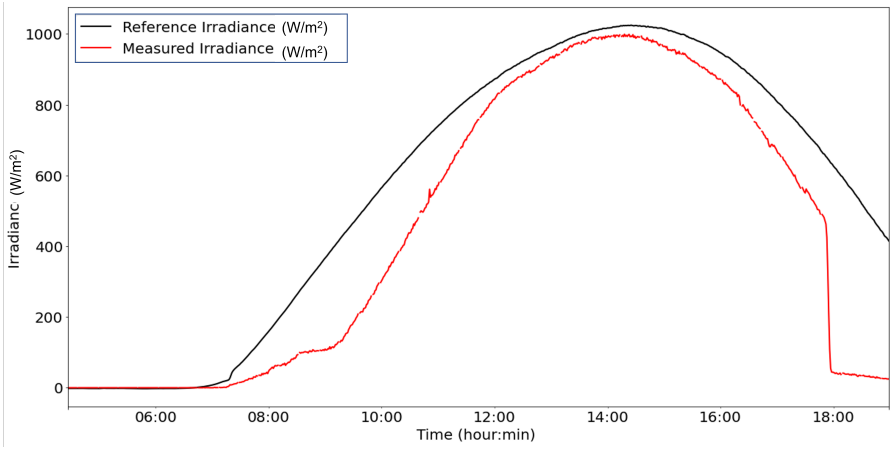

Figure 16. Example of collected data received in-plane irradiance.

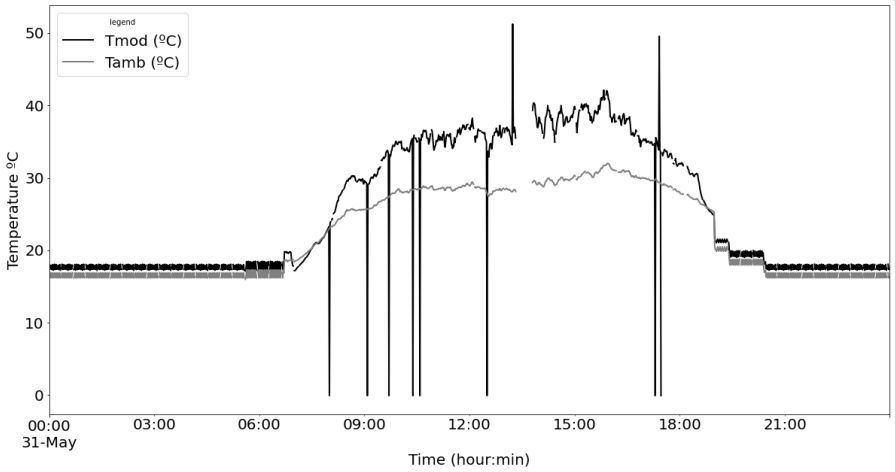

Figure 17. Comparison of PV module temperature vs. ambient temperature.

Regarding communication quality of the proposed solution, additional metrics used in previous works of the authors [22] are also discussed because no data of works with similar systems have been found to compare the results. These metrics are Packet delivery ratio, defined as the ratio between the packets successfully received and the total data packets sent by the end nodes and time intervals between different data packets (inter-arrival time) that is determined by the time interval value corresponding to each packet received. In the previous work that used Lorawan communications [22], the payload had a length of 38 bytes, almost equal size of this work, where the size of the sent string was 37 bytes, 4×5 floating bytes (measurements of each sensor) and 17 bytes of temporary fingerprint. With these similar conditions, our study reveals that the proposed system provides a reliable connectivity with a packet delivery error around 4.6% and stable time interval between packets of 60 s. These results validate the feasibility and reliability of our proposal improving the results obtained in previous works and overcoming limitations related to missing data packets and frequency of received data. Figure 18 shows these results.

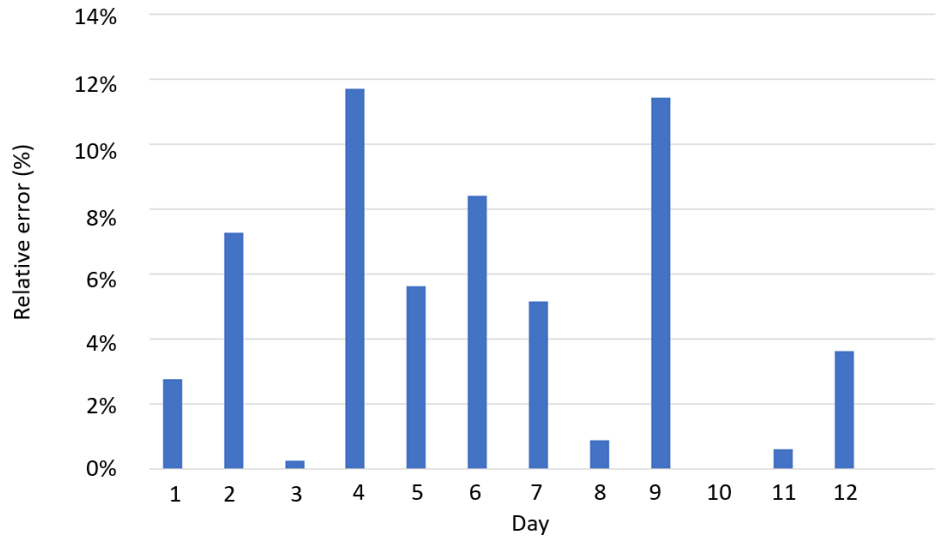

Figure 18. Communication relative errors: Average daily values.

6. Conclusions

The proliferation of PV installations either for self-consumption or with the aim of alleviating dependency on the grid is moving the energy system to more decentralized power generation. This new scenario allows users (who now are prosumers) to generate and/or consume their own energy. The lack of information about these PV systems emerge

as a relevant challenge for the management of micro- and medium-size grids, as the generation is more distributed. This paper describes a monitoring solution suitable to be applied for self-consumption or any other micro-generation installation, covering the installations of the so-called 'prosumers' and aiming to providing them with a tool that informs them about their local self-consumption. The proposed system allows us to monitor both electrical and environmental variables. A prototype was calibrated and successfully evaluated in a real PV self-consumption installation. Both current and voltage sensors were calibrated, determining 3% and 4% relative error, respectively, under laboratory conditions. The system includes a 6.5 W PV solar panel and a battery for energy requirements. Charge and discharge battery cycles were also monitored and included in the paper. Regarding the received data through NB-IoT communications versus inverter data, voltage and current have enough precision, 2.45% and 3.9%, respectively, to evaluate the operation of the plant with security. In addition, the proposed system provides a reliable connectivity with a packet delivery error around 4.6% and stable time interval between packets of 60 s. The size of the string was 37 bytes: 17 bytes of temporary fingerprint, 4×5 floating bytes. This solution is also able to be implemented in large PV power plants, as well as other alternative renewable installations.

Author Contributions: Conceptualization, J.M.P.-P. and A.M.-G.; methodology, A.P.R.-G. and A.M.-A.; software, R.J.-S. and D.C.-P.; formal analysis, R.J.-S. and J.M.P.-P.; resources, A.P.R.-G. and A.M.-A.; data curation, R.J.-S. and D.C.-P.; writing—original draft preparation, J.M.P.-P. and A.M.-G.; writing—review and editing, A.P.R.-G. and A.M.-G.; supervision, J.M.P.-P. and A.M.-G. All authors have read and agreed to the published version of the manuscript.

Funding: This work was partially supported by the Spanish agreement (2021) between the Institute for Development of the Region of Murcia (INFO) and the Technological Center for Energy and Environment (CETENMA). The paper includes results of the activity conducted under the 'Research Program for Groups of Scientific Excellence at Region of Murcia (Spain)' Project PVBRAIN (grant 2021.08.CT01.0035). A.P.R-G would like to thank European Commission Horizon Project PHOENIX (Project number: 893079).

Institutional Review Board Statement: Not applicable.

Informed Consent Statement: Not applicable.

Data Availability Statement: The data that support the findings of this study are available from the corresponding author, A.M.-G., upon reasonable request.

Conflicts of Interest: The authors declare no conflict of interest.

Abbreviations

The following abbreviations are used in this manuscript:

CNC	Computer numerical control
DSO	Distribution System Operator
IEC	International Electrotechnical Commission
IoT	Internet-of-Things
NB	Narrow band
LPWAN	Low-power wireless area network
LTE	Long-Term Evolution
MAC	Media Access Control
PCB	Printed circuit board
PV	Photovoltaic
Quality of service	QoS
RES	Renewable Energy Sources
SET Plan	Strategic Energy Technology Plan
TSO	Transmission System Operator

Appendix A. Sensor DS18X20: Python Code

```
from onewire import DS18X20, OneWire
    # Inicialization
    ow = OneWire(Pin('P11'))
    temp = DS18X20(ow)
    # Reading
    Tmod =  temp.read_temp_async()
    temp.start_conversion()
```

Appendix B. Sensor SHT3X: Python Code

```
from machine import I2C
import SHT3X
    # FiPy – I2C – Pin assignment
    i2c = I2C(0, pins=('P9','P10'))
    i2c.init(I2C.MASTER, baudrate=20000)
    # SHT3X
    sht3x = SHT3X.SHT3X(bus_obj=i2c, address=0x44)
    # Temp and Hum reading
    measurements = sht3x.get_measurement()
```

References

1. Di Silvestre, M.L.; Favuzza, S.; Sanseverino, E.R.; Zizzo, G. How Decarbonization, Digitalization and Decentralization are changing key power infrastructures. *Renew. Sustain. Energy Rev.* **2018**, *93*, 483–498. [CrossRef]
2. Cabrera, P.; Carta, J.A.; Lund, H.; Thellufsen, J.Z. Large-scale optimal integration of wind and solar photovoltaic power in water-energy systems on islands. *Energy Convers. Manag.* **2021**, *235*, 113982. [CrossRef]
3. Heras-Saizarbitoria, I.; SÃąez, L.; Allur, E.; Morandeira, J. The emergence of renewable energy cooperatives in Spain: A review. *Renew. Sustain. Energy Rev.* **2018**, *94*, 1036–1043. [CrossRef]
4. Rosales-Asensio, E.; de Simón-Martín, M.; Borge-Diez, D.; Pérez-Hoyos, A.; Comenar Santos, A. An expert judgement approach to determine measures to remove institutional barriers and economic non-market failures that restrict photovoltaic self-consumption deployment in Spain. *Sol. Energy* **2019**, *180*, 307–323. [CrossRef]
5. Mateo, C.; Cossent, R.; Gómez, T.; Prettico, G.; Frías, P.; Fulli, G.; Meletiou, A.; Postigo, F. Impact of solar PV self-consumption policies on distribution networks and regulatory implications. *Sol. Energy* **2018**, *176*, 62–72. [CrossRef]
6. Infield, D.; Freris, L. *Renewable Energy in Power Systems*; John Wiley & Sons: Hoboken, NJ, USA, 2020.
7. Eikeland, P.O.; Skjærseth, J.B. *The Politics of Low-Carbon Innovation*; Springer International Publishing: Cham, Switzerland, 2020. [CrossRef]
8. Repo, S.; Ponci, F.; Dede, A.; Della Giustina, D.; Cruz-Zambrano, M.; Al-Jassim, Z.; Amaris, H. Real-time distributed monitoring and control system of MV and LV distribution network with large-scale distributed energy resources. In Proceedings of the 2016 IEEE PES Innovative Smart Grid Technologies Conference Europe (ISGT-Europe), Ljubljana, Slovenia, 9–12 October 2016; pp. 1–6. [CrossRef]
9. Paiho, S.; Kiljander, J.; Sarala, R.; Siikavirta, H.; Kilkki, O.; Bajpai, A.; Duchon, M.; Pahl, M.O.; Wüstrich, L.; Lübben, C.; et al. Towards cross-commodity energy-sharing communities—A review of the market, regulatory, and technical situation. *Renew. Sustain. Energy Rev.* **2021**, *151*, 111568. [CrossRef]
10. Haegermark, M.; Kovacs, P.; Dalenbäck, J.O. Economic feasibility of solar photovoltaic rooftop systems in a complex setting: A Swedish case study. *Energy* **2017**, *127*, 18–29. [CrossRef]
11. Madeti, S.R.; Singh, S. Monitoring system for photovoltaic plants: A review. *Renew. Sustain. Energy Rev.* **2017**, *67*, 1180–1207. [CrossRef]
12. Rahman, M.; Selvaraj, J.; Rahim, N.; Hasanuzzaman, M. Global modern monitoring systems for PV based power generation: A review. *Renew. Sustain. Energy Rev.* **2018**, *82*, 4142–4158. [CrossRef]
13. Triki-Lahiani, A.; Bennani-Ben Abdelghani, A.; Slama-Belkhodja, I. Fault detection and monitoring systems for photovoltaic installations: A review. *Renew. Sustain. Energy Rev.* **2018**, *82*, 2680–2692. [CrossRef]
14. Ansari, S.; Ayob, A.; Lipu, M.S.H.; Saad, M.H.M.; Hussain, A. A Review of Monitoring Technologies for Solar PV Systems Using Data Processing Modules and Transmission Protocols: Progress, Challenges and Prospects. *Sustainability* **2021**, *13*, 8120. [CrossRef]
15. Mellit, A.; Kalogirou, S. Artificial intelligence and internet of things to improve efficacy of diagnosis and remote sensing of solar photovoltaic systems: Challenges, recommendations and future directions. *Renew. Sustain. Energy Rev.* **2021**, *143*, 110889. [CrossRef]

16. Rus-Casas, C.; Jiménez-Castillo, G.; Aguilar-Peña, J.D.; Fernández-Carrasco, J.I.; Muñoz-Rodríguez, F.J. Development of a Prototype for Monitoring Photovoltaic Self-Consumption Systems. *Electronics* **2020**, *9*, 67. [CrossRef]
17. Sunarso, A.; Andriani, D.; Iswanda, D.; Nurhaidah, N.; Pratomo, T.; Sihombing, H.; Muharram, Y.; Yuniarto, W.; Rusman, R. Assessment of Pv Potential Using a Low-Cost Monitoring System. *SSRN Electron. J.* **2022**. [CrossRef]
18. Fuentes, M.; Vivar, M.; Burgos, J.; Aguilera, J.; Vacas, J. Design of an accurate, low-cost autonomous data logger for PV system monitoring using Arduino™ that complies with IEC standards. *Sol. Energy Mater. Sol. Cells* **2014**, *130*, 529–543. [CrossRef]
19. López-Vargas, A.; Fuentes, M.; García, M.V.; Muñoz-Rodríguez, F.J. Low-Cost Datalogger Intended for Remote Monitoring of Solar Photovoltaic Standalone Systems Based on Arduino. *IEEE Sens. J.* **2019**, *19*, 4308–4320. [CrossRef]
20. López-Vargas, A.; Fuentes, M.; Vivar, M. IoT Application for Real-Time Monitoring of Solar Home Systems Based on Arduino With 3G Connectivity. *IEEE Sens. J.* **2019**, *19*, 679–691. [CrossRef]
21. Zorbas, D.; Caillouet, C.; Abdelfadeel Hassan, K.; Pesch, D. Optimal Data Collection Time in LoRa Networks—A Time-Slotted Approach. *Sensors* **2021**, *21*, 1193. [CrossRef]
22. Paredes-Parra, J.; Mateo-Aroca, A.; Silvente-Niñirola, G.; Bueso, M.; Molina-García, A. PV module monitoring system based on low-cost solutions: Wireless raspberry application and assessment. *Energies* **2018**, *11*, 3051. [CrossRef]
23. Paredes-Parra, J.; García-Sánchez, A.; Mateo-Aroca, A.; Molina-García, Á. An alternative internet-of-things solution based on LOra for PV power plants: Data monitoring and management. *Energies* **2019**, *12*, 881. [CrossRef]
24. Fuentes, A.F.; Tamura, E. LoRa-Based IoT Data Monitoring and Collecting Platform. In *Smart Cities*; Nesmachnow, S., Hernández Callejo, L., Eds.; Springer International Publishing: Cham, Switzerland, 2020; pp. 80–92.
25. Bueso, M.C.; Paredes-Parra, J.M.; Mateo-Aroca, A.; Molina-García, A. Sensitive Parameter Analysis for Solar Irradiance Short-Term Forecasting: Application to LoRa-Based Monitoring Technology. *Sensors* **2022**, *22*, 1499. [CrossRef] [PubMed]
26. Gautier, A.; Hoet, B.; Jacqmin, J.; Van Driessche, S. Self-consumption choice of residential PV owners under net-metering. *Energy Policy* **2019**, *128*, 648–653. [CrossRef]
27. Voisin-Grall, A.; Malaolu, O.O.; Zhu, Y.; Ahmed, T.; Al-Ahmed, S.A.; Shakir, M.Z. Remote Condition Monitoring: A Prototype Based on Pycom Development Board FiPy and Pysense. In Proceedings of the 2019 UK/China Emerging Technologies (UCET), Glasgow, UK, 21–22 August 2019; pp. 1–6. [CrossRef]
28. Sornin, N.; Luis, M.; Eirich, T.; Kramp, T.; Hersent, O. LoRa Alliance, LPWA Technologies Unlock New IoT Market Potential. LoRa Alliance. 2015. Available online: https://docplayer.net/23382599-Lpwa-technologies-unlock-new-iot-market-potential-a-white-paper-prepared-for-the-lora-alliance.html (accessed on 18 May 2022).
29. Sultania, A.K.; Mahfoudhi, F.; Famaey, J. Real-Time Demand Response Using NB-IoT. *IEEE Internet Things J.* **2020**, *7*, 11863–11872. [CrossRef]
30. Sinha, R.S.; Wei, Y.; Hwang, S.H. A survey on LPWA technology: LoRa and NB-IoT. *ICT Express* **2017**, *3*, 14–21. [CrossRef]
31. Lombardo, A.; Parrino, S.; Peruzzi, G.; Pozzebon, A. LoRaWAN Versus NB-IoT: Transmission Performance Analysis within Critical Environments. *IEEE Internet Things J.* **2022**, *9*, 1068–1081. [CrossRef]
32. Leenders, G.; Callebaut, G.; Ottoy, G.; Van der Perre, L.; De Strycker, L. Multi-RAT for IoT: The Potential in Combining LoRaWAN and NB-IoT. *IEEE Commun. Mag.* **2021**, *59*, 98–104. [CrossRef]
33. Peruzzi, G.; Pozzebon, A. Combining LoRaWAN and NB-IoT for Edge-to-Cloud Low Power Connectivity Leveraging on Fog Computing. *Appl. Sci.* **2022**, *12*, 1497. [CrossRef]
34. Coman, F.L.; Malarski, K.M.; Petersen, M.N.; Ruepp, S. Security Issues in Internet of Things: Vulnerability Analysis of LoRaWAN, Sigfox and NB-IoT. In Proceedings of the 2019 Global IoT Summit (GIoTS), Aarhus, Denmark, 17–21 June 2019; pp. 1–6. [CrossRef]
35. Dangana, M.; Ansari, S.; Abbasi, Q.H.; Hussain, S.; Imran, M.A. Suitability of NB-IoT for Indoor Industrial Environment: A Survey and Insights. *Sensors* **2021**, *21*, 5284. [CrossRef]
36. Al-Sarawi, S.; Anbar, M.; Abdullah, R.; Al Hawari, A.B. Internet of Things Market Analysis Forecasts, 2020–2030. In Proceedings of the 2020 Fourth World Conference on Smart Trends in Systems, Security and Sustainability (WorldS4), London, UK, 27–28 July 2020; pp. 449–453. [CrossRef]
37. Andrade, R.O.; Yoo, S.G. A Comprehensive Study of the Use of LoRa in the Development of Smart Cities. *Appl. Sci.* **2019**, *9*, 4753. [CrossRef]
38. Lalle, Y.; Fourati, L.C.; Fourati, M.; Barraca, J.P. A Comparative Study of LoRaWAN, SigFox, and NB-IoT for Smart Water Grid. In Proceedings of the 2019 Global Information Infrastructure and Networking Symposium (GIIS), Paris, France, 18–20 December 2019; pp. 1–6. [CrossRef]
39. Huan, J.; Li, H.; Wu, F.; Cao, W. Design of water quality monitoring system for aquaculture ponds based on NB-IoT. *Aquac. Eng.* **2020**, *90*, 102088. [CrossRef]
40. Cardoso, J.; Gloria, A.; Sebastiao, P. A Methodology for Sustainable Farming Irrigation using WSN, NB-IoT and Machine Learning. In Proceedings of the 2020 5th South-East Europe Design Automation, Computer Engineering, Computer Networks and Social Media Conference (SEEDA-CECNSM), Corfu, Greece, 25–27 September 2020; pp. 1–6. [CrossRef]
41. Li, Y.; Cheng, X.; Cao, Y.; Wang, D.; Yang, L. Smart Choice for the Smart Grid: Narrowband Internet of Things (NB-IoT). *IEEE Internet Things J.* **2018**, *5*, 1505–1515. [CrossRef]
42. Petrenko, A.S.; Petrenko, S.A.; Makoveichuk, K.A.; Chetyrbok, P.V. The IIoT/IoT device control model based on narrow-band IoT (NB-IoT). In Proceedings of the 2018 IEEE Conference of Russian Young Researchers in Electrical and Electronic Engineering (EIConRus), Moscow and St. Petersburg, Russia, 29 January–1 February 2018; pp. 950–953. [CrossRef]

43. Ballerini, M.; Polonelli, T.; Brunelli, D.; Magno, M.; Benini, L. NB-IoT Versus LoRaWAN: An Experimental Evaluation for Industrial Applications. *IEEE Trans. Ind. Inform.* **2020**, *16*, 7802–7811. [CrossRef]
44. Tiwari, A.; Pindoriya, N.M. Automated Demand Response in Smart Distribution Grid: A Review on Metering Infrastructure, Communication Technology and Optimization Models. *Electr. Power Syst. Res.* **2022**, *206*, 107835. [CrossRef]
45. Pereira, R.I.; Jucá, S.C.; Carvalho, P.C. IoT embedded systems network and sensors signal conditioning applied to decentralized photovoltaic plants. *Measurement* **2019**, *142*, 195–212. [CrossRef]
46. Ma, D.; Xie, X.; Chang, Y. Low Voltage Distributed Photovoltaic Power Station Connected Estimation Model Based on Dispatch Automation System. *IOP Conf. Ser. Earth Environ. Sci.* **2020**, *440*, 032028. [CrossRef]
47. Emamian, M.; Eskandari, A.; Aghaei, M.; Nedaei, A.; Sizkouhi, A.M.; Milimonfared, J. Cloud Computing and IoT Based Intelligent Monitoring System for Photovoltaic Plants Using Machine Learning Techniques. *Energies* **2022**, *15*, 3014. [CrossRef]
48. Ciocia, A.; Amato, A.; Di Leo, P.; Fichera, S.; Malgaroli, G.; Spertino, F.; Tzanova, S. Self-Consumption and Self-Sufficiency in Photovoltaic Systems: Effect of Grid Limitation and Storage Installation. *Energies* **2021**, *14*, 1591. [CrossRef]
49. Pycom Ltd. *FiPy 1.0 Datasheet*; Guildford: Surrey, UK, 2017; pp. 1–3. Available online: https://pycom.io/wp-content/uploads/2018/08/fipySpecsheetAugust2017n2-1.pdf (accessed on 18 May 2022).
50. Bell, C. *MicroPython for the Internet of Things*; Springer: Berlin/Heidelberg, Germany, 2017.
51. Dias, J.P.; Restivo, A.; Ferreira, H.S. Designing and constructing internet-of-Things systems: An overview of the ecosystem. *Internet Things* **2022**, *19*, 100529. [CrossRef]
52. Pietrosemoli, E.; Rainone, M.; Zennaro, M. On extending the wireless communications range of weather stations using LoRaWAN. In Proceedings of the 5th EAI International Conference on Smart Objects and Technologies for Social Good, Valencia, Spain, 25–27 September 2019; pp. 78–83.
53. Klise, K.A.; Stein, J.S.; Cunningham, J. Application of IEC 61724 Standards to Analyze PV System Performance in Different Climates. In Proceedings of the 2017 IEEE 44th Photovoltaic Specialist Conference (PVSC), Washington, DC, USA, 25–30 June 2017; pp. 3161–3166. [CrossRef]
54. Karsenty, A. A Comprehensive Review of Integrated Hall Effects in Macro–, Micro–, Nanoscales, and Quantum Devices. *Sensors* **2020**, *15*, 4163. [CrossRef]
55. Nurazizah, E.; Ramdhani, M.; Rizal, A. Rancang Bangun Termometer Digital Berbasis Sensor DS18B20 Untuk Penyandang Tunanetra. *eProc. Eng.* **2017**, *4*, 3294–3301.
56. Jovanovic, U.; Jovanovic, I.; Mancic, D. Overview of Temperature Sensors for Temperature Measurement of PV Modules. In Proceedings of the 2018 26th Telecommunications Forum (TELFOR), Belgrade, Serbia, 20–21 November 2018; pp. 1–8. [CrossRef]
57. pycom-Open Source Libraries. Available online: https://github.com/pycom/pycom-libraries/blob/master/examples/DS18X20/onewire.py (accessed on 27 April 2022).
58. Frei, M.; Deb, C.; Stadler, R.; Nagy, Z.; Schlueter, A. Wireless sensor network for estimating building performance. *Autom. Constr.* **2020**, *111*, 103043. [CrossRef]
59. Kuzmenkov, A.; Kuvshinov, D.; Buryachenko, S.Y.; Kaychenov, A.; Karachentseva, I.; Voronin, Z. Monitoring system for temperature and relative humidity of the experimental building. *J. Phys. Conf. Ser.* **2021**, *2131*, 052070. [CrossRef]
60. SHT3X.py-Open Source Libraries. Available online: https://github.com/dvsu/Sensirion-SHT3X-MicroPython/blob/main/sht3x.py (accessed on 27 April 2022).
61. Orsetti, C.; Muttillo, M.; Parente, F.; Pantoli, L.; Stornelli, V.; Ferri, G. Reliable and Inexpensive Solar Irradiance Measurement System Design. *Procedia Eng.* **2016**, *168*, 1767–1770. [CrossRef]
62. Knörig, A.; Wettach, R.; Cohen, J. Fritzing—A tool for advancing electronic prototyping for designers. In Proceedings of the 3rd International Conference on Tangible and Embedded Interaction 2009, Cambridge, UK, 16–18 February 2019.
63. Cunis, T.; Bronz, M. EDURA: An Evolvable Demonstrator for Upset Recovery Approaches with a 3D-printed Launcher. In Proceedings of the 9th International Micro Air Vehicle Conference and Competition, Toulouse, France, 18–21 September 2017.
64. Dubey, S.; Sarvaiya, J.N.; Seshadri, B. Temperature Dependent Photovoltaic (PV) Efficiency and Its Effect on PV Production in the World—A Review. *Energy Procedia* **2013**, *33*, 311–321. [CrossRef]
65. Eke, R.; Kavasoglu, A.S.; Kavasoglu, N. Design and implementation of a low-cost multi-channel temperature measurement system for photovoltaic modules. *Measurement* **2012**, *45*, 1499–1509. [CrossRef]

CAPÍTULO 5

RESUMEN DE LOS ARTÍCULOS

A continuación se presenta un breve resumen de los artículos publicados como parte de esta tesis doctoral.

5.1. Artículo 1. PV module monitoring system based on low-cost solutions: a wireless Raspberry application and assessment

5.1.1. Introducción

Este artículo propone un sistema de monitorización para plantas de energía fotovoltaica flexible, de bajo costo basado en hardware y software de acuerdo con los requisitos de la norma IEC-61724 'Photovoltaic system performance monitoring – Guidelines for measurement data exchange and analysis' [92].

Este sistema presenta una arquitectura en varios nodos comunicados de forma inalámbrica de cara a cumplir con la flexibilidad y la escalabilidad requerida para diferentes tipos de instalaciones fotovoltaicas. De hecho, se puede implementar en módulos fotovoltaicos independientemente de su configuración. La figura 5.1 muestra un esquema de la arquitectura propuesta.

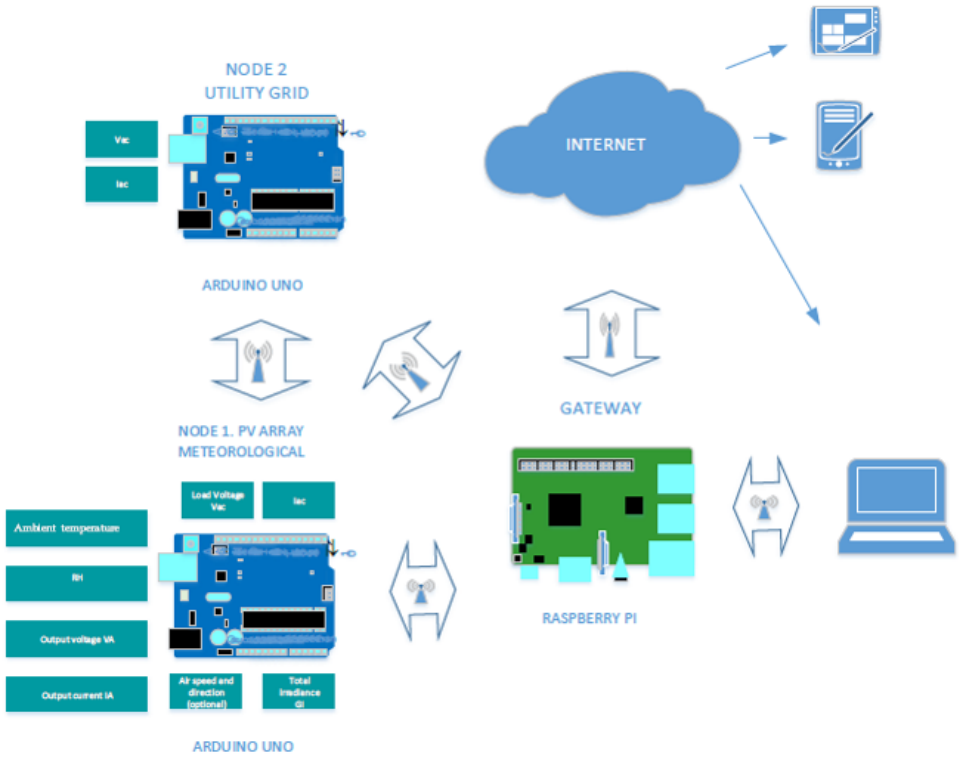

Figura 5.1: Arquitectura del sistema propuesto

5.1.2. Metodología

En una fase inicial se realizó una búsqueda de información bibliográfica y de mercado de sistemas de monitorización de instalaciones fotovoltaicas centrándonos en sistemas de bajo coste.

Partiendo del análisis de esta información se definió la plataforma de desarrollo, en concreto Arduino y se seleccionaron un conjunto de sensores para medir y registrar datos meteorológicos y eléctricos.

Estos sensores fueron testados y calibrados en laboratorio para posteriormente ser integrados en los diferentes nodos propuestos de cara a su validación en entorno real. En la figura 5.2 se muestra el detalle de la calibración del sensor de irradiancia.

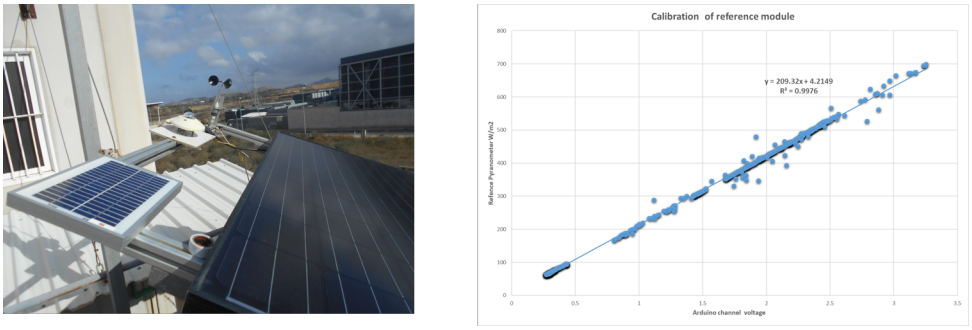

Figura 5.2: Calibración del sensor de irradiancia

Los nodos se programaron de forma que se recopilaran los datos eléctricos y ambientales con un intervalo de tiempo de muestreo de 30 segundos para, posteriormente, ser enviados a la nube a través de una puerta de enlace y ser registrados en una base de datos.

A continuación se llevó a cabo una demostración del funcionamiento del sistema completo en las instalaciones de CETENMA durante varios meses registrando también todas las variables con equipos estándar. Ambos datos han sido luego comparados para evaluar la idoneidad de la solución propuesta de bajo costo. Posteriormente el sistema propuesto también se ha implementado en una instalación solar fotovoltaica real (5 kWp) para monitorizar y recoger datos eléctricos y meteorológicos durante diferentes semanas.

Figura 5.3: Banco de ensayos en CETENMA

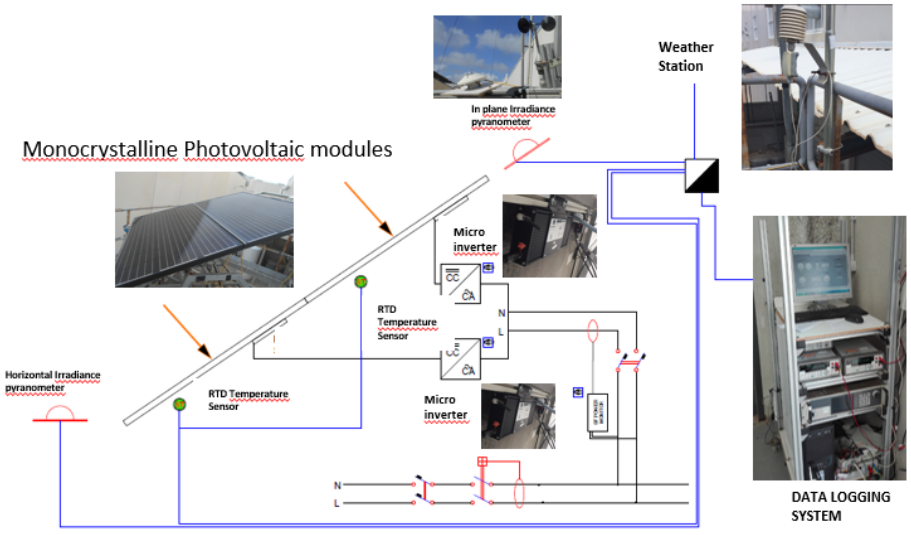

5.1.3. Resultados

Como se ha comentado anteriormente los sensores se testaron a nivel laboratorio. Los resultados obtenidos cumplen con los valores mínimos de precisión de la norma IEC-61724 en términos de corriente, voltaje y potencia y la temperatura del módulo fotovoltaico presenta un error promedio inferior al 4 %.

Tabla 5.1: Resultados

Parameter	IEC61724 Required Accuracy	Results
Current	1 %	0,81 %
Voltage	1 %	0,74 %
Power	2 %	0,55 %

Por otra parte, en los ensayos de campo donde se evaluaron los resultados en condiciones reales de una instalación fotovoltaica comparando las medidas del sistema con equipos de medida de referencia, se obtuvieron errores inferiores al 2 % para variables meteorológicas y eléctricas.

5.1.4. Conclusiones y contribución

Este artículo propone un sistema de monitorización para plantas de energía fotovoltaica flexible, de bajo costo basado en hardware y software de acuerdo con los requisitos de la norma IEC-61724 . Los sensores han sido calibrados en un entorno de laboratorio y el sistema completo en condiciones reales validando las viabilidad de la solución propuesta.

Las principales contribuciones de este trabajo se resumen a continuación:

- Las instalaciones fotovoltaicas se monitorizan a nivel de módulo fotovoltaico de acuerdo con el estándar IEC-61724 actual, estimando el rendimiento del módulo fotovoltaico y brindando mantenimiento predictivo.
- Se utilizan soluciones inalámbricas de código abierto y de bajo costo para facilitar la integración del sistema propuesto en plantas de energía fotovoltaica.
- La solución inalámbrica es flexible y se puede adaptar según el diseño y la configuración de los módulos fotovoltaicos.

5.2. Artículo 2. An alternative internet-of-things solution based on LoRa for PV power plants: data monitoring and management

5.2.1. Breve introducción

Este artículo publicado en 2019 dentro del número especial *Nanogrids, Microgrids, and the Internet of Things (IoT): towards the Digital Energy Network* de la revista *Energies* supone una continuación del trabajo 1 para evaluar una alternativa para comunicarse con plantas fotovoltaicas remotas.

Para ello, sobre la base de la monitorización descrita en [98] se incluye una tecnología de comunicaciones LPWAN en la capa de comunicación, que combina las ventajas de la cobertura de largo alcance y la baja demanda de energía, lo que permite intercambiar datos en un entorno de Internet de las Cosas (IoT).

En el documento también se incluyen y discuten los resultados obtenidos en instalaciones fotovoltaicas reales conectadas a la red.

5.2.2. Metodología

La metodología seguida para el desarrollo de la solución es similar a la del trabajo anterior comenzando con el diseño y montaje del nodo de medida de parámetros eléctricos y meteorológicos con hardware de bajo coste y código abierto. En la figura 5.4 se muestra una imagen del nodo desarrollado.

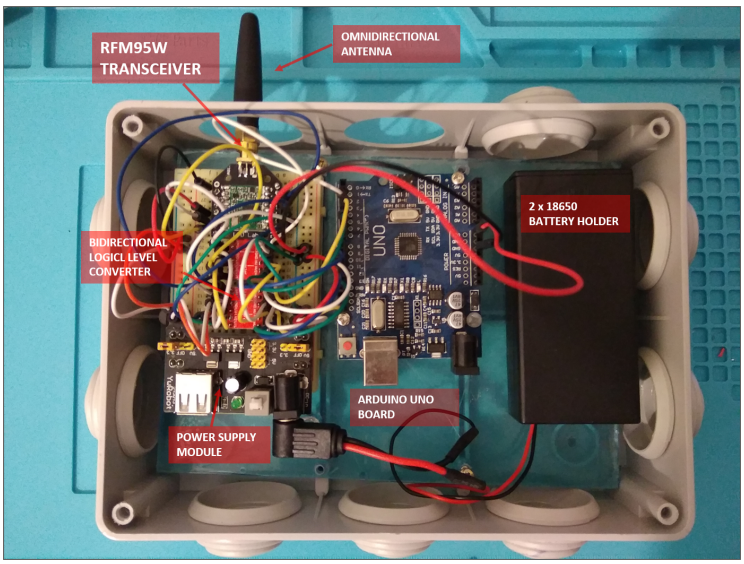

Figura 5.4: Nodo final desarrollado

Una vez desarrollado el nodo, se integra el nuevo sistema de comunicaciones siendo necesario como paso previo el desarrollo de una puerta de enlace LoRA (*gateway*)

debido a la ausencia de esta red de comunicaciones en la zona. Una vez finalizados estos elementos, se procede al desarrollo del software de los nodos y del servidor de red LoRA, evaluando en un primer momento su funcionamiento en un entorno de laboratorio para evaluar su rendimiento en condiciones controladas.

Después de esta prueba inicial, los componentes y sensores se conectaron y ensamblaron para proporcionar una solución factible capaz de operar en condiciones reales siendo necesario el dividir el sistema en dos subnodos que se instalaron para su ensayo en el laboratorio solar de CETENMA (ubicado en el Polígono Industrial de Cartagena) empleando para esta prueba un solo módulo fotovoltaico monocristalino de 250 Wp conectado a un microinversor Soltec SolarFighter de 250 W.

Un objetivo relevante de este trabajo fue evaluar la idoneidad de la solución propuesta para medir, recopilar y enviar datos desde instalaciones fotovoltaicas remotas por lo que hubo que implementar otro *gateway* debido al bajo rendimiento de la antena utilizada para la puerta de enlace desarrollada inicialmente.Este segundo *gateway* fue instalado en la Universidad Politécnica de Cartagena.

Para asegurar la comunicación del sistema propuesto, se realizó una prueba de la potencia de la señal y el rango de cobertura integrando en un modulo GPS en el nodo de medida para transmitir las coordenadas de ubicación.

Una vez finalizadas estas pruebas, se comenzó a monitorizar los datos de la planta fotovoltaica y a ser enviados al *gateway* para ser evaluados y discutidos en el análisis posterior.

5.2.3. Resultados

Para las pruebas se considera suficiente para cubrir todos los parámetros un tamaño de paquete de 38 bytes. Con una potencia de transmisión de 14 dBm se va ajustando el SF de 10 a 12 evaluándose los resultados durante ensayos de 24 horas en términos de RSSI, SNR y métricas adicionales como tasa de entrega de paquetes e intervalos de tiempo entre diferentes paquetes de datos (tiempo entre llegadas).

Tabla 5.2: Resultados obtenidos.

SF	Packet Data Sent	Packet Data Received	Packet Delivery Rate	Average Time between Packets (s)	Inter-Arrival Time (s)
11	559	307	55 %	190.85	131.00
12	402	364	91 %	273.13	246.00

El estudio revela valores bajos de RSSI y SNR para SF11. Con respecto a SF12, las métricas de RSSI y SNR mejoraron alrededor de un 10 % alcanzando una tasa de éxito de entrega cercana al 91 % con el inconveniente del alto tiempo entre envíos.

Finalmente, para verificar que los datos llegan correctos se comparan los datos recibidos por la aplicación con los mismos datos recopilados por un registrador de datos

del banco de pruebas validándose la viabilidad de la solución de monitorización y comunicación implementada.

5.2.4. Conclusiones y contribución

En este trabajo se diseñó y evaluó una solución de código abierto y de bajo costo para monitorizar plantas fotovoltaicas con la novedad de implementar como tecnología de comunicación LoRA, que es una tecnología de comunicaciones de largo alcance que permite la transmisión de datos a una puerta de enlace remota. Otras de las contribuciones importantes de este trabajo es analizar en mayor profundidad que otras contribuciones [94, 95, 96] la configuración del sistema de comunicaciones asegurando el mejor rendimiento para transmitir información desde la instalación fotovoltaica al *gateway* y, en consecuencia, aumentando la fiabilidad del sistema.

5.3. Artículo 3. A characterization of metrics for comparing satellite-based and ground-measured global horizontal irradiance data: a principal component analysis application

5.3.1. Breve introducción

En este artículo publicado en la revista *Sustainabilty* en 2020, comenzamos con los trabajos centrados en aspectos relativos a la predicción de generación de plantas fotovoltaicas. Para ello se analizaron diferentes enfoques para la predicción siendo uno de ellos la estimación de la irradiancia horizontal global (GHI) a partir de datos disponibles de satélites geoestacionarios de nueva generación, así como de otras estaciones de medida terrestres de irradiancia.

De acuerdo con la literatura específica, existe una falta de acuerdo en las estrategias de validación para un conjunto de datos de irradiancia derivados de satélites por lo que el objetivo de este trabajo se centra en los siguientes objetivos:

- Una estimación ampliada de métricas para comparar datos de GHI de satélite con datos terrestres.
- Un análisis de correlación para identificar similitudes considerando comportamientos homogéneos de dichas métricas.
- Una aplicación del análisis de componentes principales (PCA) para clasificar las métricas en diferentes categorías y proponer grupos de indicadores independientes para ser considerados con fines de comparación de datos.

5.3.2. Metodología

Como punto de partida se realiza un estudio bibliográfico para identificar las métricas empleadas para validar los datos de GHI a partir de medidas terrestres o datos derivados de satélite. Se seleccionan inicialmente un grupo de diez métricas diferentes.

Tabla 5.3: Métricas de error definidas.

Definition	Abbreviation	Expression	References
Mean Square Error	MSE	$\text{MSE} = \frac{1}{n}\sum_{i=1}^{n}\left(GHI_i^{sat} - GHI_i^{grn}\right)^2$	[100, 51]
Root Mean Square Error	RMSE	$\text{RMSE} = \sqrt{\text{MSE}}$	[100, 49, 50, 51, 58, 60, 65, 66, 101, 86, 68, 102]
Normalized RMSE	nRMSE	$\text{nRMSE} = \frac{\text{RMSE}}{GHI_0}$	[47, 48, 49, 50, 51, 58, 59, 62, 63, 65, 101, 68, 102]
Mean Bias Error	MBE	$\text{MBE} = \frac{1}{n}\sum_{i=1}^{n}\left(GHI_i^{sat} - GHI_i^{grn}\right)$	[100, 49, 50, 51, 58, 60, 65, 101, 86, 68, 102]
Normalized MBE	nMBE	$\text{nMBE} = \frac{\text{MBE}}{GHI_0}$	[47, 48, 50, 51, 58, 61, 63, 65, 68, 102]
Mean Absolute Error	MAE	$\text{MAE} = \frac{1}{n}\sum_{i=1}^{n}\left\lvert GHI_i^{sat} - GHI_i^{grn}\right\rvert$	[100, 51, 61, 101, 86, 68, 102]
Normalized MAE	nMAE	$\text{nMAE} = \frac{\text{MAE}}{GHI_0}$	[47, 61, 63, 101, 102]
Mean Absolute Percentage Error	MAPE	$\text{MAPE} = \frac{1}{n}\sum_{i=1}^{n}\frac{\left\lvert GHI_i^{sat} - GHI_i^{grn}\right\rvert}{GHI_i^{sat}}$	[51, 59]
Shape Based Distance	SBD	$\text{SBD} = 1 - \max_w NCC_w(GHI^{sat}, GHI^{grn})$, where NCC_w is a normalized cross correlation sequence between the series GHI^{sat} and GHI^{grd}.	[103, 104]
Dynamic Time Warping	DTW	$\text{DTW} = \min_W \sum_{k=1}^{K} d(w_k)$, where $W = \{w_1, w_2, \ldots, w_k, \ldots, w_K\}$ represent a warping path between the series GHI^{sat} and GHI^{grd} subjected to several constraints and $d(w_k) = dist(GHI_{i_k}^{sat}, GHI_{i_k}^{grn})$.	[105, 104]

Como fuente de datos se recopila información de GHI medidos en tierra y por satélite durante un año en siete ubicaciones diferentes de España, con un tiempo de muestreo de una hora.

La metodología propuesta se basa primero en una estimación de métricas para las diferentes fuentes de datos de irradiación para, posteriormente, determinar una matriz de diferencias para las diferentes métricas para cada estación, de acuerdo con el tiempo de muestro seleccionado: un tiempo de muestro de una hora.

Después de esta estimación inicial de métricas, se realiza un análisis de correlación múltiple para los datos recopilados en cada estación, para identificar métricas con una dependencia relevante (o no). Con este análisis de correlación se detectan aquellas métricas con comportamientos similares y, por lo tanto, métricas que brindan información similar.

Para visualizar de una manera más conveniente estos resultados de correlación múltiple, así como el proceso de agrupamiento se representan gráficamente las matrices de correlaciones. A partir de estos resultados, podemos comparar los resultados de agrupamiento para todas las ubicaciones, detectando la homogeneidad de los diferentes grupos según las ubicaciones específicas.

De manera complementaria, se obtienen los estadísticos media y desviación estándar para cada coeficiente de correlación de cada par de métricas correspondientes a todas las ubicaciones consideradas. De esta forma dispondremos de una estimación adicional de la homogeneidad de tales correlaciones, así como su independencia (o no) de las ubicaciones específicas. Posteriormente, podemos estimar la dependencia de la correlación entre métricas de las ubicaciones, así como la similitud de la agrupación de métricas según una comparación visual del proceso de agrupamiento.

La figura 5.5 muestra esquemáticamente la metodología propuesta al considerar m métricas diferentes correspondientes a datos observados cada hora durante n días en p ubicaciones. El análisis de correlación y el agrupamiento de métricas se llevan a cabo para cada ubicación específica.

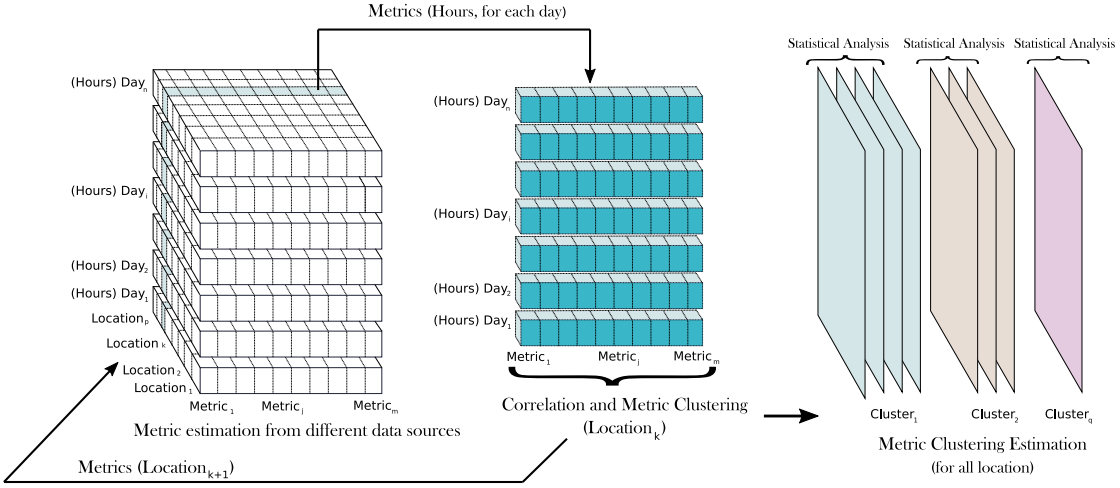

Figura 5.5: Análisis de las correlaciones y proceso de clustering Esquema general

Posteriormente, se propone la aplicación de PCA para caracterizar dichas métricas e identificar las similitudes y explorar las diferencias entre ellas. La metodología propuesta, mostrada de forma gráfica en la figura 5.6 ha sido evaluada a partir de datos de GHI medidos en tierra y por satélite recopilados durante un año en siete ubicaciones diferentes de España, utilizando estimaciones horarias medias.

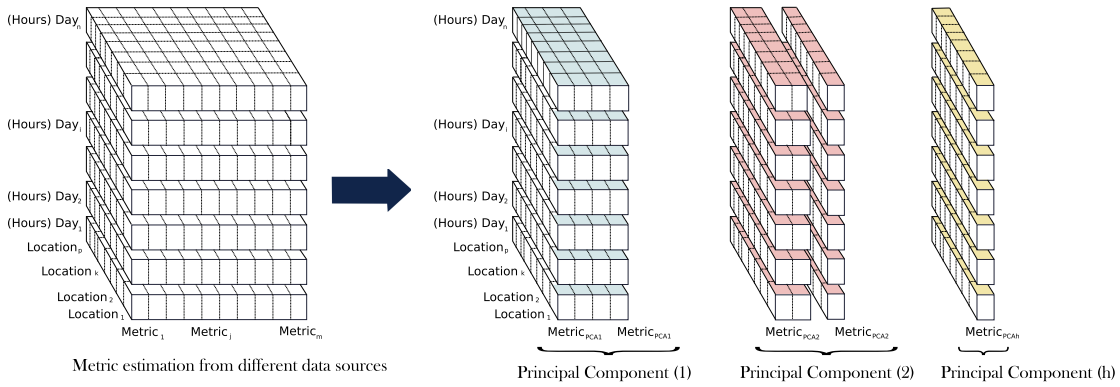

Figura 5.6: Análisis de Componentes Principales. Esquema general

5.3.3. Resultados

Para evaluar la metodología propuesta se consideraron diferentes estaciones meteorológicas terrestres, comparando sus datos GHI con los valores provenientes de satélite para un año (2018).

Para el presente análisis, se seleccionó la Red del Sistema de Información Agraria de Murcia (SIAM) para proporcionar datos de irradiancia terrestre [106]. Con respecto a los datos de irradiancia basados en satélite, se usaron datos de la red Copernicus, que es el Programa de Observación de la Tierra de la Unión Europea [107].

De acuerdo con la información disponible en la Red del SIAM, los valores de irradiancia fueron recogidos por dichas estaciones meteorológicas terrestres, proporcionando datos de GHI promedio por hora. Se dispone de un tiempo de muestreo de diez minutos para los datos basados en satélites de Copernicus que, para compararlos con los datos terrestres, se consideraron los valores promedio por hora. En la figura 5.7 se muestran algunos días consecutivos del año 2018 comparando los datos de ambas fuentes y las diferencias entre ellos.

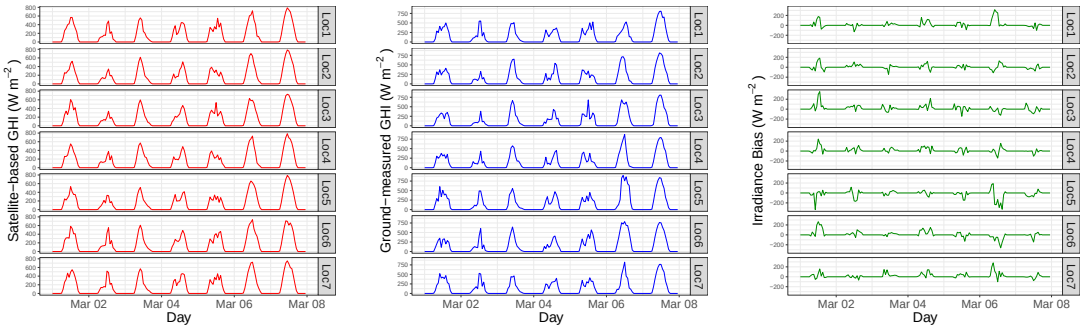

Figura 5.7: *Ejemplo de datos horarios de irradiancia global horizontal a partir de datos de satélite, medidos en tierra y sus diferencias*

Las métricas seleccionadas se calculan para las dos fuentes de datos de irradiancia y se estiman las matrices de correlación para cada ubicación. En la figura 5.8 se muestran los resultados para una de las localizaciones consideradas en el estudio.

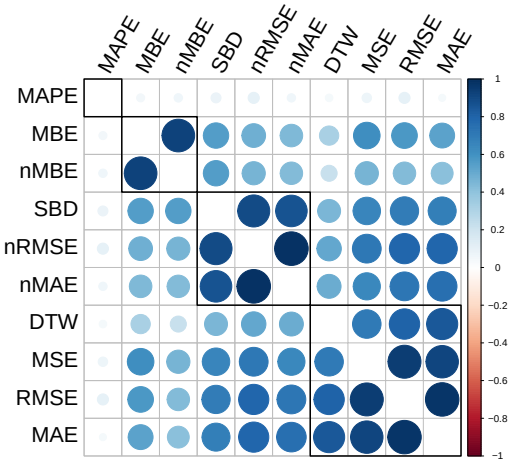

Figura 5.8: Matriz de correlaciones para una localización concreta

A partir de estas métricas, los autores llevaron a cabo una caracterización y clasificación considerando la metodología propuesta, como se describe en la sección 5.3.2, aplicando también el análisis de componentes principales (PCA) para identificar las principales relaciones entre las métricas, reducir el número de variables y permitirnos una representación gráfica de dichas métricas en un entorno de baja dimensión. La figura 5.9 muestra el gráfico de sedimentación de las componentes (valores propios y porcentaje de varianza explicada por las componentes principales).

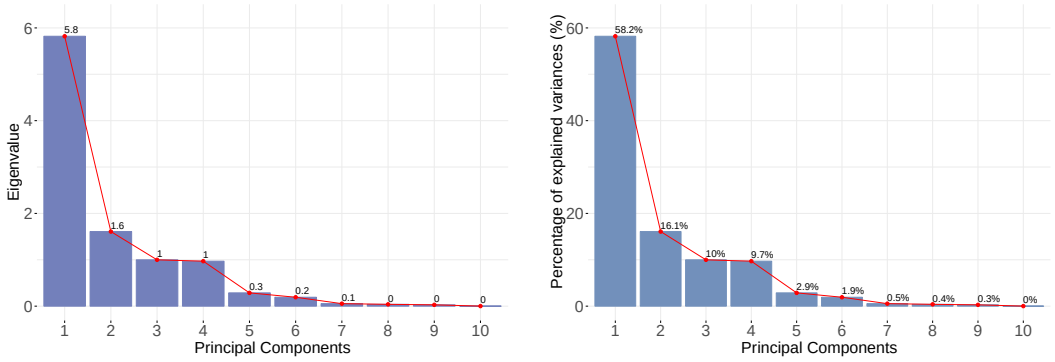

Figura 5.9: Gráfico de sedimentación

Como se puede observar, las cuatro primeras componentes principales representan alrededor del 94 % de la variabilidad total de las métricas, lo que reduce significativamente la dimensión de las métricas de 10 a dimensión cuatro.

5.3.4. Conclusiones y contribución

Por lo tanto, se identifican diferentes grupos de métricas aplicando el proceso PCA, lo que nos permite comparar, de una manera más extensa, diferentes fuentes de datos de irradiancia y explorar e identificar sus diferencias.

Se describe y evalúa una caracterización de métricas basada en datos de GHI de diferentes fuentes para identificar diferentes grupos de métricas similares. De la literatura específica, se selecciona inicialmente un grupo de diez métricas diferentes, que han sido propuestas por otras contribuciones para comparar diferentes fuentes de datos de irradiación. Se propone un análisis de correlación para detectar dependencia (o no) de la ubicación y un proceso de aplicación de PCA para caracterizar dichas métricas e identificar las similitudes y explorar las diferencias entre ellas.

La aplicación de PCA nos permite explorar similitudes entre métricas e identificar los componentes principales más relevantes. Además, esta técnica también aborda una reducción de la dimensión. En este caso, se selecciona un grupo de cuatro “componentes principales“, que representa el 94 % de la variabilidad total de las métricas. Por tanto, se proporciona una reducción de dimensiones y una identificación de grupos de métricas con información similar, que perfila la idoneidad del proceso.

5.4. Artículo 4. Sensitive parameter analysis for solar irradiance short-term forecasting: application to LoRa-based monitoring technology

5.4.1. Breve introducción

En este artículo publicado en la revista *Sensors* en 2022 continuamos avanzando en el objetivo de analizar ciertos aspectos relativos a la obtención de una predicción precisa de generación de energía en las instalaciones fotovoltaicas. Concretamente, en este trabajo se propone una metodología para evaluar el efecto de diferentes arquitecturas de monitorización de instalaciones fotovoltaicas basadas en LoRa para la extracción de datos sobre la predicción de generación de energía solar a corto plazo.

5.4.2. Metodología

La metodología propuesta se basa en un análisis de sensibilidad de los parámetros de una red de comunicaciones LoRa en términos de diseño de nodos, pérdida de datos, factor de dispersión e intervalos de tiempo cortos para evaluar su influencia en la precisión de la previsión de la generación fotovoltaica a corto plazo.

En primer lugar, se lleva a cabo una selección y distribución de nodos basada en la tecnología LoRaWAN de acuerdo con un punto de interés de predicción predefinido y un posible grupo de localizaciones potenciales en tierra o instalaciones basadas en satélite. A partir de estas especificaciones, se define una base de datos de tiempo de muestreo de un minuto en cada nodo, así como el punto de interés de predicción.

Para ello se parte de los datos de GHI de una malla de 17×17 con un total de 289 puntos en consideración, con datos de tiempo de muestreo de un minuto construida a partir de datos descargados del satélite Copernicus correspondientes al año 2019 [107]. Esta malla se muestra en la figura 5.10.

Se propone un modelo de predicción de tipo *Random Forest* lo que simplifica el problema de predicción, especialmente cuando la serie de tiempo presenta heterocedasticidad, no estacionariedad y múltiples ciclos estacionales. Este algoritmo se utiliza para pronosticar valores de radiación solares en la ubicación de interés considerando diferentes horizontes de predicción, de 15 a 45 min.

Las simulaciones de predicción de GHI a corto plazo para cada día incluyeron diferentes rangos de pérdida de datos (0 %, 25 % y 50 %), intervalos de tiempo de predicción (15, 30 y 45 min) y valores de SF (de SF09 a SF12). Se consideraron un total de 36 condiciones diferentes para cada día, ejecutando 13,140 simulaciones para los correspondientes valores de GHI de 2019.

El algoritmo de *Random Forest* se utiliza para pronosticar valores solares a corto

Figura 5.10: Caso de ejemplo: distribución espacial de la rejilla (Región de Murcia, Spain)

plazo en la ubicación de interés considerando diferentes horizontes de predicción de 15 a 45 min. Estas predicciones se estiman bajo una variedad de escenarios:

- asumiendo SF = SF09 para todos los nodos y 0 % de pérdida de datos;
- asumiendo SF de SF09 a SF12 en cada nodo y 0 % de pérdida de datos;
- asumiendo SF de SF09 a SF12 en cada nodo y pérdida de datos de 0 % a 50 %.

Posteriormente, se comparan los valores de previsión solar correspondientes a los diferentes escenarios. Se calculan las discrepancias y similitudes, discutiendo la influencia de los diferentes parámetros de configuración de la red LoRa en el proceso de predicción solar.

Como analizaron previamente los autores, se pueden encontrar diferentes métricas en la literatura específica para determinar las discrepancias. A partir de esta clasificación, se determinan el error cuadrático medio normalizado (nRMSE), el error porcentual absoluto medio (MAPE) y la deformación temporal dinámica (DTW) para proporcionar información complementaria y caracterizar discrepancias convenientes entre los datos de predicción de generación fotovoltaica a corto plazo al considerar SF09 y 0 % de pérdida de datos y resto de escenarios.

En la figura 5.11 se resume la metodología propuesta. Además, también se incluye un análisis de sensibilidad basado en el parámetro SF y pérdida de datos, determinando las diferencias respecto a los valores de predicción con SF09 y 0 % de pérdida de datos.

La metodología y las simulaciones se implementaron en el entorno `R` [108] utilizando diferentes paquetes de software como `data.table` para una manipulación de datos rápida y eficiente en memoria [109], `ranger` para una implementación rápida de Random Forest [110], `dtw` y `dtwclust` para la estimación de la métrica DTW [111].

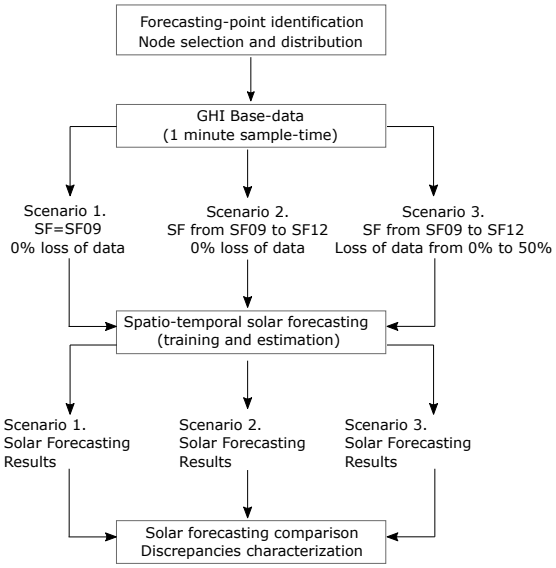

Figura 5.11: Metodología propuesta: Esquema general

5.4.3. Resultados

Los resultados nos permiten explorar la influencia de la pérdida de datos, los valores de SF y los intervalos de tiempo a corto plazo en la precisión de la predicción de la GHI correspondiente. A partir de los datos correspondientes a 2019, con resolución temporal de un minuto, se consideraron para las simulaciones diferentes periodos de predicción solar fotovoltaica a corto plazo. Más concretamente, se definieron tres horizontes temporales diferentes: 15, 30 y 45 minutos. Posteriormente, se simuló cada día considerando los diferentes horizontes de tiempo. Además, y con el fin de comparar el impacto tanto de la pérdida de datos como del Spreading Factor seleccionado, se realizaron las simulaciones en tales condiciones: 0 %, 25 % y 50 % de pérdida de datos; así como de SF12 a SF09 y que el SF seleccionado afecta considerablemente la robustez a costa de tasas de datos más bajas.

Estos resultados permiten evaluar el impacto de cada parámetro y dar un análisis preliminar de la influencia de estas condiciones y situaciones antes de implementar una red real de comunicación y detección.

En relación con el ejemplo de caso (presentado en la figura 5.10), el diseño inicial de los nodos (en coordenadas UTM) está representado en la figura 5.12.

Posteriormente, se seleccionó un nodo en cada corona circular con el objetivo de pronosticar los datos de GHI en el centro de la malla (punto de interés). La distribución de las localizaciones seleccionadas para el análisis junto con la distancia al punto de predicción de interés está incluida en la figura 5.13; los nodos seleccionados están etiquetados como 119, 170, 115, 60 y 254.

A continuación se comparan los valores de irradiancia medidos y pronosticados para los todos los días del año 2019 considerando las diferentes condiciones seleccionadas para cada día: porcentajes de pérdida de datos, diferentes parámetros SF y diferentes horizontes de predicción. En la figura 5.14 se muestra un ejemplo de resultados para el

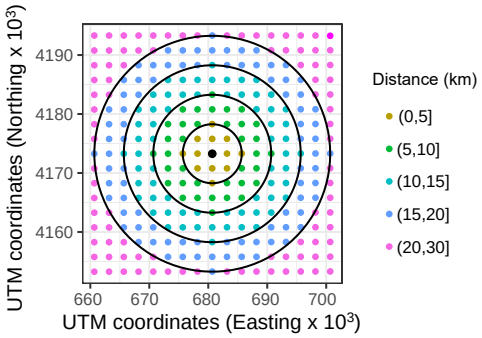

Figura 5.12: Caso de ejemplo: distribución de los nodos (Coordenadas UTM)

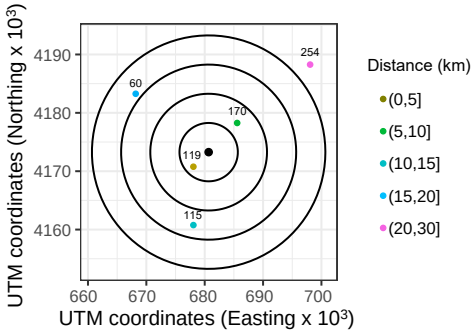

Figura 5.13: Caso de ejemplo: distribución de las localizaciones seleccionadas y el punto de interés para la predicción en color negro (Coordenadas UTM)

día 108 del año.

Posteriormente, con el objetivo de conocer la influencia de cada parámetro considerando todas las simulaciones realizadas, en total 13140 simulaciones, se llevó a cabo un análisis de sensibilidad para determinar las discrepancias entre los valores de GHI diarios estimados para el nodo seleccionado y los correspondientes valores de GHI diarios medidos.

En primer lugar, la figura 5.15 muestra un ejemplo que incluye los histogramas globales y los histogramas truncados realizados (en total se realizan 36 histogramas globales y truncados) de las discrepancias en función del error cuadrático medio normalizado (nRMSE) entre los datos de GHI medidos y los valores de GHI de predicción. Como se puede observar, los histogramas truncados retienen más del 90 % de tales discrepancias y se considera lo suficientemente adecuado para este análisis.

En segundo lugar, y de acuerdo a la variedad de errores y diferencias disponibles en la literatura específica, así como la comparación realizada por los autores [69], el error porcentual absoluto medio (MAPE) y el warping temporal dinámico (DTW) también fueron seleccionados como estimaciones métricas.

Para analizar en detalle la influencia de cada variable, la figura 5.16 muestra el histograma truncado para estas simulaciones usando discrepancias basadas en las métricas MAPE y DTW.

Como puede apreciarse en estas discrepancias, un mayor rango de pérdida de da-

tos implica discrepancias más relevantes y estos valores presentan un pico secundario de valores del 20 % al 30 %. En términos del parámetro SF, los valores mayores de las discrepancias se desplazan ligeramente del intervalo [0,10] (para SF09) al intervalo [10,20] (para SF12). Por lo tanto, un intervalo de tiempo más largo entre paquetes subsiguiente, implica errores de discrepancia más altos. Estos resultados son similares para los otros intervalos de tiempo analizados.

5.4.4. Conclusiones y contribución

En el artículo se incluye un ejemplo de caso situado en el sureste de España para evaluar el análisis propuesto. Esta metodología es aplicable a otras ubicaciones, así como a diferentes configuraciones, parámetros y estructuras de redes de LoRa; proporciona un análisis detallado sobre el rendimiento de la monitorización fotovoltaica y las discrepancias en la previsión de la generación fotovoltaica a corto plazo. Las principales contribuciones de este documento se pueden resumir como

- una metodología para evaluar la precisión de la predicción a corto plazo de GHI para diferentes diseños de nodos y parámetros LoRa basados en un modelo de predicción de *Random Forest*,
- un análisis de sensibilidad de los parámetros LoRa y los valores de predicción a corto plazo del GHI basados en una variedad de métricas,
- un estudio de caso a partir de datos de GHI de 2019 (tiempo de muestro de un minuto), área de 400 km^2, 289 nodos potenciales en consideración y un total de 13,140 simulaciones.

Por lo tanto, esta metodología proporciona un análisis preliminar extenso de las posibles características de la red LoRa y el diseño de nodos en términos de precisión de datos, paquetes y posibilidades de predicción de GHI antes de que se complete la instalación.

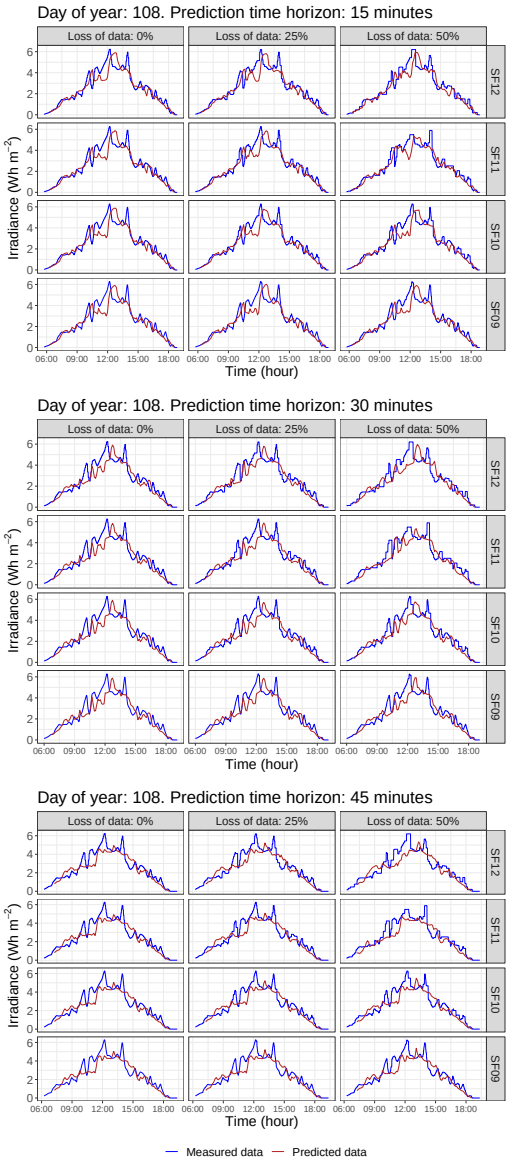

Figura 5.14: Comparación de la predicción de irradiancia global horizontal(GHI) y la medida para diferentes escenarios de horizontes de tiempo, spreading factor y pérdida de datos

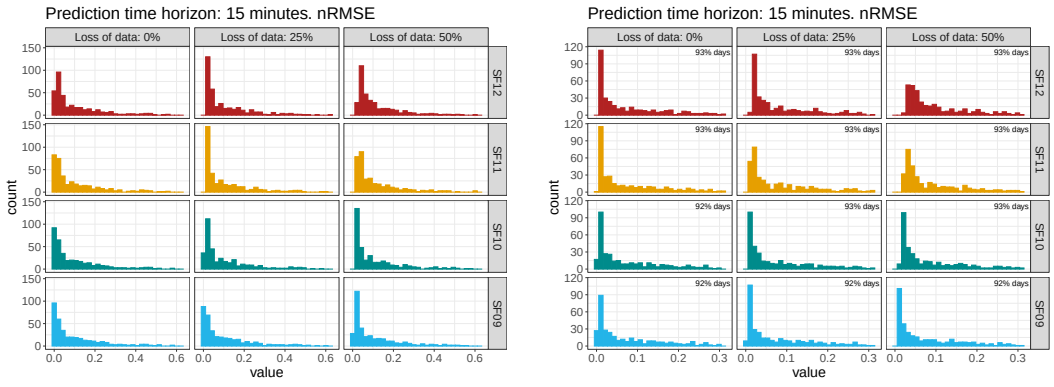

Figura 5.15: Resumen de las diferencias entre la predicción y los datos medidos basados en nRMSE. Histogramas (izqda.) e histogramas truncados (dcha)

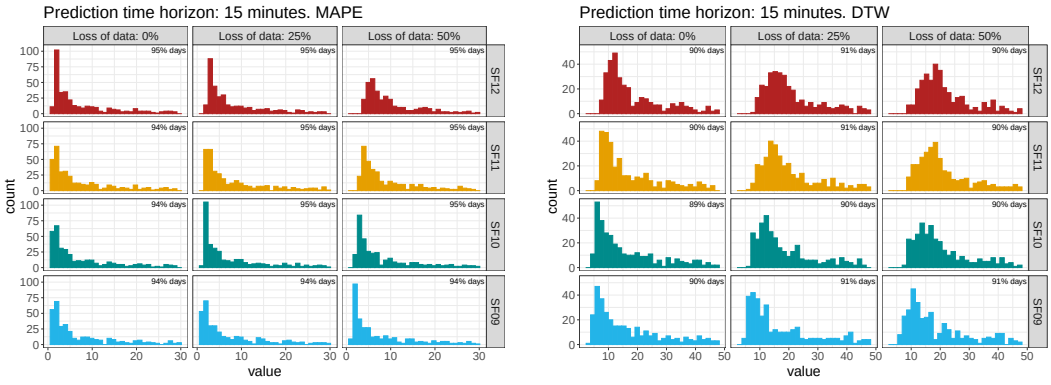

Figura 5.16: Resumen de las diferencias entre la predicción y los datos medidos basados en las métricas MAPE y DTW. Histogramas truncados

5.5. Artículo 5. Democratization of PV micro–generation system monitoring based on Narrowband–IoT

5.5.1. Breve introducción

En este trabajo [43], publicado recientemente en la revista *Sensors*, se realiza un rediseño y evaluación del sistema de monitorización propuesto para instalaciones fotovoltaicas.

Este nuevo diseño se realizó con el fin de ampliar su uso a otras instalaciones de microgeneración y para solventar algunas de las limitaciones en la capa de comunicaciones que presentaba el diseño anterior en cuanto a frecuencia de envío y tamaño del paquete. Se realiza una descripción detallada del hardware y software propuesto y se presentan los resultados de las campañas realizadas para su validación.

5.5.2. Metodología

La metodología seguida en este trabajo es la misma que la realizada en los trabajos anteriores [98, 42] tomando en este caso como punto de partida una nueva plataforma de Hardware FIpY de PYCOM a la que se le integrarán los sensores necesarios para la medida de parámetros eléctricos y meteorológicos conforme a la norma IEC61724 [92]. Los sensores necesarios son seleccionados, adquiridos y calibrados de forma previa a la integración. Una vez verificados en laboratorio, se desarrollan los circuitos necesarios para adaptar las señales y se realiza el diseño y prototipo de las cajas de montaje que al igual que en ocasiones anteriores se dividieron en varios nodos. En uno de estos nodos se incluye un panel solar y una batería junto con el sistema de adecuación de tensiones para dar total autonomía al sistema. Una vez desarrollados todos los elementos, estos son evaluados en las instalaciones del laboratorio solar de CETENMA como en los trabajos anteriores.

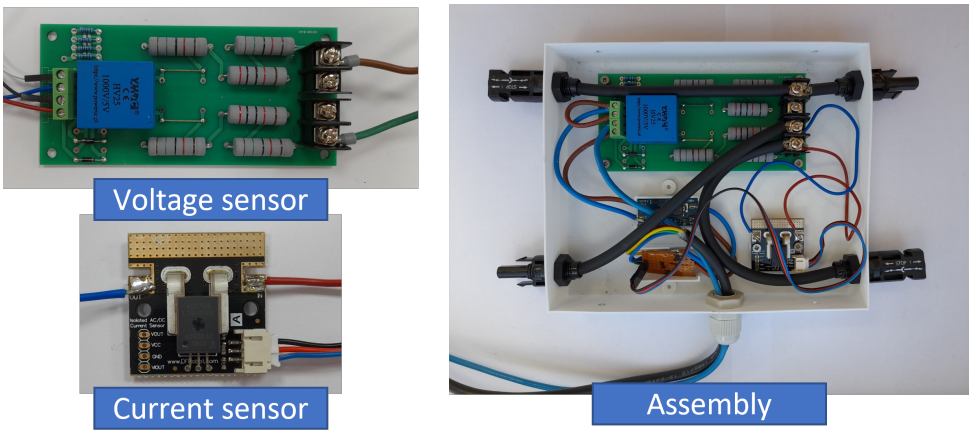

Figura 5.17: Prototipo del nodo de medida de voltaje e intensidad

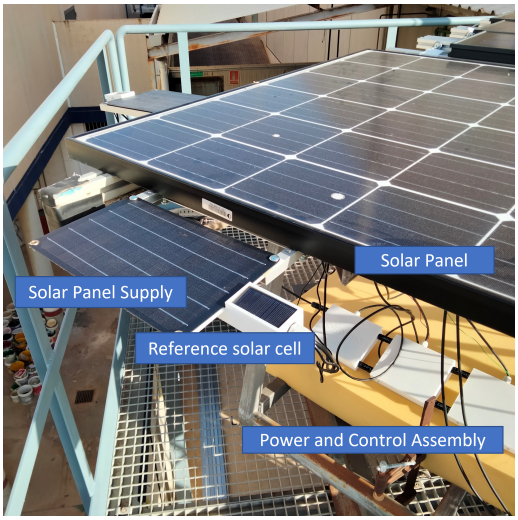

Figura 5.18: Caso de estudio. Panel solar de carga y celda de referencia ensamblados al módulo fotovoltaico monitorizado

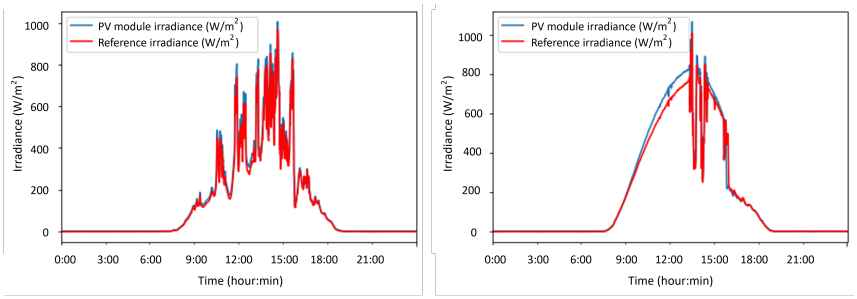

Figura 5.19: Caso de estudio. Comparativa de datos de irradiancia registrados

5.5.3. Resultados

La solución propuesta se probó en un entorno relevante con el objetivo de evaluar su desempeño en diferentes condiciones. La solución se conectó y montó en condiciones exteriores en una instalación de autoconsumo fotovoltaico para evaluar la viabilidad de la solución para ser implementada en una variedad de situaciones y condiciones reales. El sistema propuesto se probó en el laboratorio solar de CETENMA, ubicado en el Polígono Industrial de Cartagena (España). Esta instalación incluye equipos de medición para comprobar el rendimiento de las plantas y módulos de energía fotovoltaica. Para fines de prueba, se utilizó un solo módulo fotovoltaico monocristalino de 250 Wp conectado a un microinversor Soltec SolarFighter de SF de 250 W.

La figura 5.18 muestra algunos ejemplos de campañas de pruebas de campo y la Figura 5.19 incluye la comparación de los datos registrados por el sistema propuestos frente a un piranómetro de referencia.

En cuanto a los datos recibidos a través de las comunicaciones NB-Iot versus los datos registrados en laboratorio, la tensión y la corriente tienen una precisión suficiente, 2,45 % y 3,9 %, respectivamente, para evaluar el funcionamiento de la planta con seguridad. Se envían un total de seis paquetes con un tiempo de muestro de un minuto: 8 bytes/paquete para cinco paquetes y 10 bytes/paquete para el paquete adicional. En

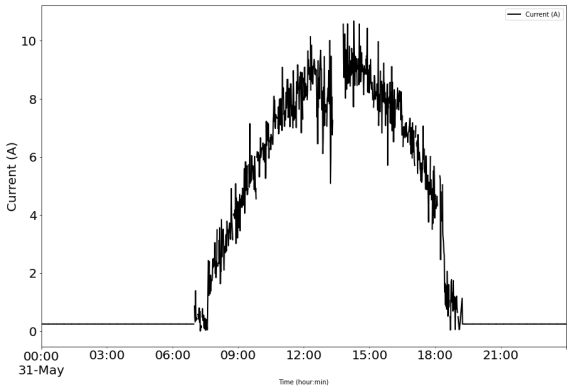

Figura 5.20: Datos de intensidad registrados sobre el modulo con el sistema propuesto

términos de datos eléctricos recopilados, la figura 5.20 muestran datos registrados de intensidad.

En cuanto a la calidad de comunicación de la solución propuesta, también se evalúan con las métricas utilizadas en trabajos anteriores [98] debido a que no se han encontrado datos de trabajos con sistemas similares para poder comparar los resultados. Estas métricas son la tasa de entrega de paquetes, definida como la proporción entre los paquetes recibidos con éxito y el total de paquetes de datos enviados por los nodos finales, y los intervalos de tiempo entre diferentes paquetes de datos (tiempo entre llegadas), que está determinado por el valor del intervalo de tiempo correspondiente a cada paquete recibido. En el trabajo anterior que usaba comunicaciones Lorawan [98], el payload tenía una longitud de 38 bytes, casi el mismo tamaño de este trabajo, donde el tamaño de la cadena enviada es de 37 bytes, 4×5 bytes flotantes (medidas de cada sensor) y 17 bytes de huella digital temporal.

Con estas condiciones similares, nuestro estudio revela que el sistema propuesto proporciona una conectividad fiable con un error de entrega de paquetes de alrededor del 4,6 % y un intervalo de tiempo estable entre paquetes de 60 segundos. Estos resultados validan la viabilidad y fiabilidad de nuestra propuesta mejorando los resultados obtenidos en trabajos anteriores superando las limitaciones relacionadas con la falta de paquetes de datos y la frecuencia de los datos recibidos.

5.5.4. Conclusiones y contribución

Este artículo describe una solución de monitorización apta para ser aplicada en instalaciones de autoconsumo o cualquier otra microgeneración, cubriendo las instalaciones de los denominados ‘prosumidores“ y con el objetivo de proporcionarles una herramienta que les informe sobre su autoconsumo local.

El sistema propuesto nos permite monitorizar variables tanto eléctricas como ambientales. Se calibró y evaluó con éxito un prototipo en una instalación de autoconsumo fotovoltaico real. Se calibraron los sensores de corriente y voltaje, determinando un error relativo de 3 % y 4 % respectivamente en condiciones de laboratorio. El sistema incluye un, panel solar fotovoltaico de 6,5W y una batería para los requerimientos de

energía. Los ciclos de carga y descarga de la batería también fueron monitorizados e incluidos en el documento.

Respecto a los datos recibidos a través de las comunicaciones NB-IoT versus los datos del inversor, la tensión y la corriente tienen una precisión suficiente, 2,45 % y 3,9 % respectivamente, para evaluar el funcionamiento de la planta con seguridad.

Además, el sistema propuesto proporciona una conectividad fiable con un error de entrega de paquetes del orden del 4,6 % y un intervalo de tiempo estable entre paquetes de 60 segundos por lo que esta solución también se puede implementar en grandes plantas de energía fotovoltaica, así como en otras instalaciones renovables alternativas.

CAPÍTULO 6

CONCLUSIONES Y LÍNEAS FUTURAS

En este capitulo se presentan las principales conclusiones obtenidas en el desarrollo de los trabajos expuestos y las lineas futuras de investigación que se abren con este trabajo.

6.1. Conclusiones

En los próximos años se prevé la implantación masiva de nueva generación renovable en el sistema eléctrico para alcanzar los objetivos previstos de descarbonización de la economía estando la tecnología fotovoltaica llamada a ser de las más implantadas debido a su flexibilidad modularidad y a la competitividad de sus coste. Este previsible aumento de potencia fotovoltaica no gestionable supone un desafío para el sistema eléctrico ya que debe el garantizar una integración segura de estas aportaciones provenientes de las fuentes de energía renovables (RES) que por su propia naturaleza son variables y distribuidas.

Para afrontar esta transición hacia un sistema energético en gran medida descentralizado y basado en las energías renovables exigirá un sistema más inteligente y flexible sustentado, entre otras, en la implicación de los consumidores, en una mayor interconectividad y en un mejor almacenamiento de energía desplegado y una respuesta del lado de la demanda gracias al desarrollo de nuevas soluciones la gestión a través de la digitalización.

En esta tesis nos hemos centrado en el desarrollo de una solución de digitalización del sistema eléctrico en cuanto a generación fotovoltaica en un rango de potencias que actualmente la legislación no obliga a su monitorización ni gestión, como son las instalaciones fotovoltaicas de autoconsumo con una potencia hasta 100 kW.

Este tipo de instalaciones ha experimentado un notable crecimiento impulsado por el nuevo marco normativo liberalizado, definido por el RD de Autoconsumo 244/2019 y el RDL 15/2018, que, además de eliminar las barreras económicas y administrativas, ha introducido la posibilidad de instalar autoconsumo compartido en bloques de viviendas y el mecanismo de compensación simplificada, a través del cual los autoconsumidores pueden recibir una compensación económica para los excedentes de energía que vierten a la red.

Hasta hace unos años, el coste y la complejidad de los sistemas de monitorización de las instalaciones fotovoltaicas limitaban su uso a las plantas fotovoltaicas de gran capacidad (a partir de 1 MW, tanto por motivos económicos como normativos), pero la rápida evolución del mercado de IoT ha causado una explosión en la cantidad y variedad de soluciones de IoT de bajo costo que podrían permitir la implementación a gran escala de los sistemas de monitorización de manera rentable.

La tesis ha trabajado en las tres capas que componen una aplicación y sistema IoT: capa de percepción, capa de red y capa de aplicaciones.

En la **capa de percepción o capa física**, se ha desarrollado un sistema de bajo coste que permite monitorizará las variables de operación de la instalación fotovoltaica bajo los requerimientos del estándar IEC–61724. Estos sistemas desarrollados a partir de plataformas de desarrollo abiertas y de bajo coste han sido testeados en laboratorio y en entornos reales presentando resultados de fiabilidad y precisión cercana a sistemas convencionales a un coste mucho más reducido.

En la **capa de comunicaciones**, se han implementado y evaluado dos principales nuevas tecnologías de comunicaciones LPWAN (Low Power Wide Area Network) .como son la tecnología LoRA y NB-IoT analizando sus prestaciones y limitaciones para su empleo en la aplicación propuesta.

En relación a la tecnología LoRA, se demuestra la influencia de aspectos como la distancia entre el origen y el destino, la línea de visión entre el origen y el destino y los problemas de propagación en el proceso adecuado de recepción de datos lo que obliga a trabajar con tiempos de de transmisión que limitan considerablemente el número de transmisiones. Para superar estas limitaciones se ha evaluado el empleo de la tecnología NB-IoT que al presentar licencia puede soportar conexiones masivas sin restricciones del ciclo de trabajo a un coste adecuado .

Por último, en relación a la **capa de aplicaciones** se ha trabajado para avanzar en algoritmos para la predicción a corto plazo de la generación fotovoltaica para mitigar el impacto negativo en las redes de la implantación masiva de este tipo de instalaciones no controlables.

Los trabajos realizados se han orientado en un primer lugar hacia una caracterización de métricas basada en una aplicación de análisis de componentes principales (PCA) para clasificar datos de irradiancia como principal variable de influencia en la generación, medidos en tierra y por satélite y explorar e identificar sus diferencias como base para el desarrollo de algoritmos de predicción.

Por otra parte, en previsión de la disponibilidad de datos de irradiancia medidos en tierra gracias al despliegue de la solución de monitorizaron propuesta, se ha realizado un análisis de la influencia en los resultados de las predicciones de GHI a corto plazo de la localización de los nodos, el intervalo de tiempo en su recepción y la posible pérdida de datos.

De este análisis se puede concluir que la presencia de nubes medida como índice de cielo claro (clear sky GHI ratio) tiene más influencia que otros parámetros como la pérdida de datos o la frecuencia de estos por lo que se deben considerar los días de relación Kt GHI bajos para estimar los errores potenciales permitidos de cara al diseño de la red.

6.2. Líneas futuras

Tras las contribuciones presentadas en esta tesis, se han identificado nuevas líneas de investigación para continuar avanzando en el desarrollo de este tipo de sistemas de monitorización para instalaciones de autoconsumo fotovoltaico cuyo importante despliegue es uno de los grandes retos a los que se va a enfrentar el sistema eléctrico en los próximos años. Partiendo de los sistemas desarrollados en esta tesis, las líneas futuras de esta investigación serían las siguientes:

- Despliegue del sistema de monitorización propuesto en un mayor número de instalaciones dispersas geográficamente y su monitorización a lo largo de varios meses con el fin de conocer la fiabilidad y precisión del sistema en ensayos a largo plazo. Durante este trabajo se han evaluado los sistemas a lo largo de varias semanas, pero es necesario disponer más experiencias y de mayor duración para analizar la influencia de variables como el envejecimiento y/o la degradación de algunos componentes en la fiabilidad del sistema.
- Partiendo de los datos recopilados con este despliegue el desarrollo de nuevos modelos de predicción de generación a corto plazo a partir de las series espacio temporales disponibles y comparar los resultados obtenidos frente a los sistemas actuales.

CAPÍTULO 7

FACTOR DE IMPACTO DE LAS PUBLICACIONES

En este capítulo se incluyen los resultados del cuartil e índice de impacto de las publicaciones incluidas en la tesis, del año de la publicación o último disponible.

- *"PV Module Monitoring System Based on Low-Cost Solutions: Wireless Raspberry Application and Assessment". Paredes-Parra, J.M., Mateo-Aroca, A., Silvente-Niñirola, G., Bueso, M.C., Molina-García, A. 2018. Energies 11, no. 11: 3051.*
  `https://doi.org/10.3390/en11113051`
  - Factor de impacto en el momento de la publicación: **2.707**
  - Cuartil: **Q3 in ENERGY & FUELS**
  - Citas: **38**
- *"An Alternative Internet-of-Things Solution Based on LoRa for PV Power Plants: Data Monitoring and Management". Paredes-Parra, J.M., García-Sánchez, A.J., Mateo-Aroca, A., Molina-García, A. 2019. Energies 12, no. 5: 881.*
  `https://doi.org/10.3390/en12050881`
  - Factor de impacto en el momento de la publicación: **2.702**
  - Cuartil: **Q3 in ENERGY & FUELS**
  - Citas: **37**
- *"A Characterization of Metrics for Comparing Satellite-Based and Ground-Measured Global Horizontal Irradiance Data: A Principal Component Analysis Application". Bueso, M.C., Paredes-Parra, J.M., Mateo-Aroca, A., Molina-García, A. 2020. Sustainability 12: 2454.*
  `https://doi.org/10.3390/su12062454`
  - Factor de impacto en el momento de la publicación: **3.251**
  - Cuartil: **Q2 in ENVIRONMENTAL SCIENCES**
  - Citas: **5**
- *"Sensitive Parameter Analysis for Solar Irradiance Short-Term Forecasting: Application to LoRa-Based Monitoring Technology". Bueso, M.C., Paredes-Parra, J.M., Mateo-Aroca, A., Molina-García, A. 2022. Sensors (Basel) 22, no. 4:1499.*
  `https://doi.org/10.3390/s22041499`
  - Factor de impacto en el momento de la publicación: **3.847**

  - Cuartil: **Q2 in ENGINEERING, ELECTRICAL & ELECTRONIC**
  - Citas: **3**

- *"Democratization of PV micro–generation system monitoring via an open source IoT gateway based on NB–IoT'. Paredes-Parra, J.M., Jiménez-Segura, R., Campos-Peñalver, D., Mateo-Aroca A., Ramallo-González, A.P., Molina-García, A. 2022. Sensors 22, no. 13: 4966.*
  `https://doi.org/10.3390/s22134966`
  - Factor de impacto en el momento de la publicación: **3.847**
  - Cuartil: **Q2 in ENGINEERING, ELECTRICAL & ELECTRONIC**
  - Citas: **0**

CAPÍTULO 8

GLOSARIO

Las siguientes abreviaciones se han usado en este documento:

ECMWF	The European Centre for Medium-Range Weather Forecasts
ESA	The European Space Agency
EU	The European Union
EUMETSAT	The European Organisation for the Exploitation of Meteorological Satellites
GHI	Global Horizontal Irradiance
GOES	Geostationary Operational Environmental Satellite
IMIDA	Murcian Institute of Agricultural and Food Research and Development
MODIS	Moderate Resolution Imaging Spectroradiometer
MSG	Meteosat Second Generation
PCA	Principal Component Analysis
PV	Photovoltaic
PVGIS	Photovoltaic Geographical Information System
SIAM	Agricultural Information System of Murcia
UTM	Universal Transverse Mercator

Symbols in metrics:

BW	Bandwidth
CSS	Chirp Spread Spectrum
DTW	Dynamic Time Warping
GHI	Global Horizontal Irradiance
GHI^{grd}	Ground-measured GHI
GHI^{sat}	Satellite-based GHI
gMBD	General Mean Bias Deviation
ITM	Irregular Terrain Model
LASSO	Least Absolute Shrinkage and Selection Operator
LoRa	Long Range
MAD	Mean Absolute Difference
MAE	Mean Absolute Error
MAPE	Mean Absolute Percentage Error
MBE	Mean Bias Error
MSE	Mean Square Error
NCC	Normalized Cross-Correlation
nMAE	Normalized Mean Absolute Error
nMBE	Normalized Mean Bias Error
nRMSE	Normalized Root Mean Square Error
r	Pearson Correlation Coefficient
PV	Photovoltaic
RF	Random Forest
rgMBD	Relative General Mean Bias Deviation
rMAE	Relative Mean Absolute Error
rMBE	Relative Mean Bias Error
RMSE	Root Mean Square Error
rRMSE	Relative Root Mean Square Error
R^2	Determination Coefficient
SBD	Shape Based Distance
SF	Spreading Factor
SD	Standard Deviation
SNR	Signal to noise ratio
vRES	Variable Renewable Energy Sources

BIBLIOGRAFÍA

[1] UNFCCC. «Nationally determined contributions under the Paris Agreement: Synthesis report by the secretariat». En: *English* September (2021), págs. 1-42.

[2] *Clean energy for all Europeans package*. URL: https://energy.ec.europa.eu/topics/energy-strategy/clean-energy-all-europeans-package_en (visitado 10-07-2022).

[3] Ministerio para la Transición Ecológica y el Reto Demográfico. «Plan Nacional Integrado de Energía y Clima 2021-2030». En: *Gobierno de España* (2020), pág. 25. URL: https://www.miteco.gob.es/es/prensa/pniec.aspx.

[4] Ministerio para la trnsición Ecológicagia y Reto Demográfico. «Real Decreto 1183/2020, de 29 de diciembre, de acceso y conexión a las redes de transporte y distribución de energía eléctrica.» En: *Boletín Oficial del Estado* 2014.51, 28 de febrero (2019), págs. 18987-19106. URL: https://www.miteco.gob.es/es/prensa/estrategiadealmacenamientoenergetico_tcm30-522655.pdf.

[5] *BOE.es - BOE-A-2019-5089 Real Decreto 244/2019, de 5 de abril, por el que se regulan las condiciones administrativas, técnicas y económicas del autoconsumo de energía eléctrica*. URL: https://www.boe.es/buscar/doc.php?id=BOE-A-2019-5089 (visitado 10-07-2022).

[6] *BOE.es - BOE-A-2018-13593 Real Decreto-ley 15/2018, de 5 de octubre, de medidas urgentes para la transición energética y la protección de los consumidores*. URL: https://www.boe.es/buscar/doc.php?id=BOE-A-2018-13593 (visitado 10-07-2022).

[7] D E L Autoconsumo, Marco Estratégico y D E Energía Y Clima. «Hoja de ruta del autoconsumo». En: *Ministerio para la Trnasición Ecológica y el Reto Demográfico* (2021), pág. 104.

[8] Gobierno de España. *Plan de Recuperación, Transformación y Resiliencia*. Inf. téc. 2. Gobierno de España, 2021, págs. 1-23. URL: https://www.mitma.gob.es/ministerio/proyectos-singulares/prtr.

[9] UNEF. *Energía Solar Fotovoltaica. Oportunidad para la Sostenibilidad*. 2021, pág. 73.

[10] Wolf-Peter Schill, Alexander Zerrahn y Friedrich Kunz. «Prosumage of solar electricity: pros, cons, and the system perspective». En: *Economics of Energy &amp Environmental Policy* 6.1 (ene. de 2017). DOI: 10.5547/2160-5890.6.1.wsch.

[11] Shadi Al-Sarawi y col. «Internet of Things Market Analysis Forecasts, 2020–2030». En: *2020 Fourth World Conference on Smart Trends in Systems, Security and Sustainability (WorldS4)*. IEEE, jul. de 2020, págs. 449-453. ISBN: 978-1-7281-6823-4. DOI: 10.1109/WorldS450073.2020.9210375.

[12] *The Internet of Things - An explosion of Connected Possibility*. Available On-line. https://docs.wixstatic.com/ugd/eccc1ade5fda268ed945e885a43a39b38752 (Last access November, 28, 2018): LoRa-Alliance, 2018.

[13] «IEEE Standard for an Architectural Framework for the Internet of Things (IoT)». En: *IEEE Std 2413-2019* (2020), págs. 1-269. DOI: 10.1109/IEEESTD.2020.9032420.

[14] J.A. Fuentes, A. Molina-García y E. Gómez. «A measurement approach for obtaining static load model parameters in real time at the distribution level». En: *European Transactions on Electrical Power* 17.2 (2007). ISSN: 1430144X. DOI: 10.1002/etep.135.

[15] Gökay Bayrak y Mehmet Cebeci. «Monitoring a grid connected PV power generation system with labview». En: *2013 International Conference on Renewable Energy Research and Applications (ICRERA)*. 2013, págs. 562-567. DOI: 10.1109/ICRERA.2013.6749819.

[16] Aissa Chouder y col. «Monitoring, modelling and simulation of PV systems using LabVIEW». En: *Solar Energy* 91 (2013), págs. 337-349. ISSN: 0038-092X. DOI: https://doi.org/10.1016/j.solener.2012.09.016. URL: http://www.sciencedirect.com/science/article/pii/S0038092X12003416.

[17] Bruno Ando y col. «Sentinella: Smart Monitoring of Photovoltaic Systems at Panel Level». En: *IEEE Transactions on Instrumentation and Measurement* 64 (ago. de 2015), págs. 1-1. DOI: 10.1109/TIM.2014.2386931.

[18] Miguel J. Prieto y col. «Development of a Wireless Sensor Network for Individual Monitoring of Panels in a Photovoltaic Plant». En: *Sensors (Basel, Switzerland)* 14 (feb. de 2014), págs. 2379-96. DOI: 10.3390/s140202379.

[19] P. Papageorgas y col. «Smart Solar Panels: In-situ Monitoring of Photovoltaic Panels based on Wired and Wireless Sensor Networks». En: *Energy Procedia* 36 (2013). TerraGreen 13 International Conference 2013 - Advancements in Renewable Energy and Clean Environment, págs. 535-545. ISSN: 1876-6102. DOI: https://doi.org/10.1016/j.egypro.2013.07.062. URL: http://www.sciencedirect.com/science/article/pii/S187661021301148X.

[20] I. M. Moreno-García y col. «Performance monitoring of a solar photovoltaic power plant using an advanced real-time system». En: *2016 IEEE 16th International Conference on Environment and Electrical Engineering (EEEIC)*. Jun. de 2016, págs. 1-6. DOI: 10.1109/EEEIC.2016.7555473.

[21] S Fanourakis y col. «Low-cost data acquisition systems for photovoltaic system monitoring and usage statistics». En: *IOP Conference Series: Earth and Environmental Science* 93 (nov. de 2017), pág. 012048. DOI: 10.1088/1755-1315/93/1/012048.

[22] M. Caruso y col. «A low-cost, real-time monitoring system for PV plants based on ATmega 328P-PU microcontroller». En: *INTELEC, International Telecommunications Energy Conference (Proceedings)*. Vol. 2016-September. Institute of Electrical y Electronics Engineers Inc., sep. de 2016. ISBN: 9781479965823. DOI: 10.1109/INTLEC.2015.7572270.

[23] F. P. Su y col. «A distributed monitoring system for photovoltaic arrays based on a two-level wireless sensor network». En: *IOP Conference Series: Earth and Environmental Science* 93.1 (2017). ISSN: 17551315. DOI: 10.1088/1755-1315/93/1/012077.

[24] Fawzi Al-Naima y Abdullah Hamad. «a Low-Cost Solar Farm Monitoring System Based on Cloud Database». En: *MEST Journal* 7.2 (2019), págs. 1-8. ISSN: 23347171. DOI: 10.12709/mest.07.07.02.01.

[25] Renata I.S. Pereira, Sandro C.S. Jucá y Paulo C.M. Carvalho. «IoT embedded systems network and sensors signal conditioning applied to decentralized photovoltaic plants». En: *Measurement* 142 (ago. de 2019), págs. 195-212. ISSN: 02632241. DOI: 10.1016/j.measurement.2019.04.085.

[26] Lawrence O. Aghenta y M. Tariq Iqbal. «Development of an IoT Based Open Source SCADA System for PV System Monitoring». En: *2019 IEEE Canadian Conference of Electrical and Computer Engineering, CCECE 2019*. Institute of Electrical y Electronics Engineers Inc., mayo de 2019. ISBN: 9781728103198. DOI: 10.1109/CCECE.2019.8861827.

[27] Ricardo Mazza Zago y Fabiano Fruett. «A low-cost solar generation monitoring system suitable for internet of things». En: *INSCIT 2017 - 2nd International Symposium on Instrumentation Systems, Circuits and Transducers: Chip on the Sands, Proceedings*. Institute of Electrical y Electronics Engineers Inc., nov. de 2017. ISBN: 9781538620212. DOI: 10.1109/INSCIT.2017.8103509.

[28] Nouredine Erraissi y col. «Implementation of a low-cost data acquisition system for "PROPRE.MA" project». En: *Measurement: Journal of the International Measurement Confederation* 117.March (2018), págs. 21-40. ISSN: 02632241. DOI: 10.1016/j.measurement.2017.11.058. URL: https://doi.org/10.1016/j.measurement.2017.11.058.

[29] Chaimae Zedak y col. «A proposed secure remote data acquisition architecture of photovoltaic systems based on the Internet of Things». En: *International Conference on Multimedia Computing and Systems -Proceedings*. Vol. 2018-May. IEEE Computer Society, nov. de 2018. ISBN: 9781538662205. DOI: 10.1109/ICMCS.2018.8525902.

[30] Kun Xia y col. «A real-time monitoring system based on ZigBee and 4G communications for photovoltaic generation». En: *CSEE Journal of Power and Energy Systems* 6.1 (2020), págs. 52-63. ISSN: 20960042. DOI: 10.17775/cseejpes.2019.01610.

[31] V. Katsioulis y col. «Wireless Monitoring and Remote Control of PV Systems Based on the ZigBee Protocol». En: *Technological Innovation for Sustainability*. Ed. por Luis M. Camarinha-Matos. Berlin, Heidelberg: Springer Berlin Heidelberg, 2011, págs. 297-304. ISBN: 978-3-642-19170-1.

[32] Oussama Ben Belghith y Sbita Lassaad. «Remote GSM module monitoring and Photovoltaic system control». En: mar. de 2014, págs. 188-192. ISBN: 978-1-4799-3602-1. DOI: 10.1109/ICGE.2014.6835420.

[33] S. Zahurul y col. «A novel Zigbee-based data acquisition system for distributed photovoltaic generation in smart grid». En: *2015 IEEE Innovative Smart Grid Technologies - Asia (ISGT ASIA)*. Nov. de 2015, págs. 1-6. DOI: 10.1109/ISGT-Asia.2015.7387097.

[34] Farihah Shariff, Nasrudin Abd Rahim y Wooi Ping Hew. «Zigbee-based data acquisition system for online monitoring of grid-connected photovoltaic system». En: *Expert Systems with Applications* 42.3 (2015), págs. 1730-1742. ISSN: 0957-4174. DOI: https://doi.org/10.1016/j.eswa.2014.10.007.

[35] Y F Li y col. «On-line monitoring system of PV array based on internet of things technology». En: *IOP Conference Series: Earth and Environmental Science* 93 (nov. de 2017), pág. 012078. DOI: 10.1088/1755-1315/93/1/012078.

[36] S. Adhya y col. «An IoT based smart solar photovoltaic remote monitoring and control unit». En: *2016 2nd International Conference on Control, Instrumentation, Energy Communication (CIEC)*. Ene. de 2016, págs. 432-436. DOI: 10.1109/CIEC.2016.7513793.

[37] Kai-Hsiang Ke y col. «A LoRa wireless mesh networking module for campus-scale monitoring». En: *Proceedings of the 16th ACM/IEEE International Conference on Information Processing in Sensor Networks - IPSN '17*. ACM Press, 2017. DOI: 10.1145/3055031.3055034.

[38] Ravi Tejwani, Girish Kumar y Chetan Solanki. «Remote Monitoring for Solar Photovoltaic Systems in Rural Application Using GSM Voice Channel». En: *Energy Procedia* 57 (2014). 2013 ISES Solar World Congress, págs. 1526-1535. ISSN: 1876-6102. DOI: https://doi.org/10.1016/j.egypro.2014.10.145. URL: http://www.sciencedirect.com/science/article/pii/S1876610214015124.

[39] Renata I.S. Pereira y col. «IoT embedded linux system based on Raspberry Pi applied to real-time cloud monitoring of a decentralized photovoltaic plant». En: *Measurement* 114 (2018), págs. 286-297. ISSN: 0263-2241. DOI: https://doi.org/10.1016/j.measurement.2017.09.033. URL: http://www.sciencedirect.com/science/article/pii/S026322411730605X.

[40] Nicolas Sornin y col. «LoRa Alliance, LPWA technologies unlock new IoT Market Potential». En: *LoRa alliance* (2015).

[41] Rashmi Sharan Sinha, Yiqiao Wei y Seung-Hoon Hwang. «A survey on LPWA technology: LoRa and NB-IoT». En: *ICT Express* 3.1 (mar. de 2017), págs. 14-21. ISSN: 24059595. DOI: 10.1016/j.icte.2017.03.004.

[42] J.M. Paredes-Parra y col. «An alternative internet-of-things solution based on LORa for PV power plants: Data monitoring and management». En: *Energies* 12.5 (2019). ISSN: 19961073. DOI: 10.3390/en12050881.

[43] José Miguel Paredes-Parra y col. «Democratization of PV Micro-Generation System Monitoring Based on Narrowband-IoT». En: *Sensors* 22.13 (jun. de 2022), pág. 4966. DOI: 10.3390/s22134966.

[44] J Shi y col. «Forecasting Power Output of Photovoltaic Systems Based on Weather Classification and Support Vector Machines». En: *IEEE Transactions on Industry Applications* 48.3 (mayo de 2012), págs. 1064-1069. ISSN: 0093-9994. DOI: 10.1109/TIA.2012.2190816.

[45] C. Yang, A. A. Thatte y L. Xie. «Multitime-scale data-driven spatio-temporal forecast of photovoltaic generation». En: *IEEE Transactions on Sustainable Energy* 6.1 (ene. de 2015), págs. 104-112. DOI: 10.1109/TSTE.2014.2359974.

[46] Adil Ahmed y Muhammad Khalid. «A review on the selected applications of forecasting models in renewable power systems». En: *Renewable and Sustainable Energy Reviews* 100 (2019), págs. 9-21. ISSN: 1364-0321. DOI: 10.1016/j.rser.2018.09.046.

[47] Gilles Notton y col. «Estimation of hourly global solar irradiation on tilted planes from horizontal one using artificial neural networks». En: *Energy* 39.1 (2012), págs. 166-179. ISSN: 0360-5442. DOI: 10.1016/j.energy.2012.01.038.

[48] C Manoel dos Santos y col. «Assessment of ANN and SVM models for estimating normal direct irradiation (Hb)». En: *Energy Conversion and Management* 126 (2016), págs. 826-836. ISSN: 0196-8904. DOI: 10.1016/j.enconman.2016.08.020.

[49] Kada Bouchouicha y col. «Estimating the global solar irradiation and optimizing the error estimates under Algerian desert climate». En: *Renewable Energy* 139 (2019), págs. 844-858. ISSN: 0960-1481. DOI: 10.1016/j.renene.2019.02.071.

[50] Ali Mohammad Noorian, Isaac Moradi y Gholam Ali Kamali. «Evaluation of 12 models to estimate hourly diffuse irradiation on inclined surfaces». En: *Renewable Energy* 33.6 (2008), págs. 1406-1412. ISSN: 0960-1481. DOI: 10.1016/j.renene.2007.06.027.

[51] Ahmet Teke, H Basak Yıldırım y Ozgor Celik. «Evaluation and performance comparison of different models for the estimation of solar radiation». En: *Renewable and Sustainable Energy Reviews* 50 (2015), págs. 1097-1107. ISSN: 1364-0321. DOI: 10.1016/j.rser.2015.05.049.

[52] A P Dobos. *PVWatts Version 5 Manual – National Renewable EnergyLaboratory (NREL)*. 2014. URL: https://www.nrel.gov/docs/fy14osti/62641.pdf.

[53] Marcel Uri, Thomas Huld y Ewan Dunlop. «PV-GIS: A web-based solar radiation database for the calculation of PV potential in Europe». En: *International Journal of Solar Energy* 24 (2005), págs. 55-67. DOI: 10.1080/14786450512331329556.

[54] International Renewable Energy Agency (IRENA). *Global atlas for renewable energy: Overview of solar and wind maps*. 2014. URL: https://www.irena.org/-/media/Files/IRENA/Agency/Publication/2014/GA_Booklet_Web.pdf.

[55] SOLARGIS. *Weather data and software for solar power investments*. 2019. URL: https://solargis.info/.

[56] Adam Piasecki, Jakub Jurasz y Alexander Kies. «Measurements and reanalysis data on wind speed and solar irradiation from energy generation perspectives at several locations in Poland». En: *SN Applied Sciences* 1.8 (jul. de 2019), pág. 865. ISSN: 2523-3971. DOI: 10.1007/s42452-019-0897-2.

[57] Katalin Bódis y col. «A high-resolution geospatial assessment of the rooftop solar photovoltaic potential in the European Union». En: *Renewable and Sustainable Energy Reviews* 114 (2019), pág. 109309. ISSN: 1364-0321. DOI: 10.1016/j.rser.2019.109309.

[58] B E Psiloglou y col. «Comparison between MRM simulations, CAMS and PVGIS databases with measured solar radiation components at the Methoni station, Greece». En: *Renewable Energy* 146 (2020), págs. 1372-1391. ISSN: 0960-1481. DOI: 10.1016/j.renene.2019.07.064.

[59] Alberto Bocca y col. «Multiple-regression method for fast estimation of solar irradiation and photovoltaic energy potentials over Europe and Africa». En: *Energies* 11.12 (2018). ISSN: 1996-1073. DOI: 10.3390/en11123477.

[60] Jiaojiao Feng, Weizhen Wang y Jing Li. «An LM–BP neural network approach to estimate monthly-mean daily global solar radiation using MODIS atmospheric products». En: *Energies* 11.12 (2018). DOI: 10.3390/en11123510.

[61] Ana Maria Gracia Amillo y col. «Application of satellite-based spectrally-resolved solar radiation data to PV performance studies». En: *Energies* 8.5 (2015), págs. 3455-3488. DOI: 10.3390/en8053455.

[62] Marco Pierro y col. «Data-driven upscaling methods for regional photovoltaic power estimation and forecast using satellite and numerical weather prediction data». En: *Solar Energy* 158 (2017), págs. 1026-1038. ISSN: 0038-092X. DOI: 10.1016/j.solener.2017.09.068.

[63] F Antonanzas-Torres, F Cañizares y O Perpiñán. «Comparative assessment of global irradiation from a satellite estimate model (CM SAF) and on-ground measurements (SIAR): A Spanish case study». En: *Renewable and Sustainable Energy Reviews* 21 (2013), págs. 248-261. ISSN: 1364–0321. DOI: 10.1016/j.rser.2012.12.033.

[64] René Buffat, Stefano Grassi y Martin Raubal. «A scalable method for estimating rooftop solar irradiation potential over large regions». En: *Applied Energy* 216 (2018), págs. 389-401. ISSN: 0306–2619. DOI: 10.1016/j.apenergy.2018.02.008.

[65] Anthony C S Porfirio y Juan C Ceballos. «A method for estimating direct normal irradiation from GOES geostationary satellite imagery: Validation and application over Northeast Brazil». En: *Solar Energy* 155 (2017), págs. 178-190. DOI: 10.1016/j.solener.2017.05.096.

[66] Stefan Pfenninger y Iain Staffell. «Long–term patterns of European PV output using 30 years of validated hourly reanalysis and satellite data». En: *Energy* 114 (2016), págs. 1251-1265. ISSN: 0360-5442. DOI: 10.1016/j.energy.2016.08.060.

[67] Marco Ernst y col. «Comparison of ground-based and satellite-based irradiance data for photovoltaic yield estimation». En: *Energy Procedia* 92 (2016), págs. 546-553. ISSN: 1876-6102. DOI: 10.1016/j.egypro.2016.07.139.

[68] Jamie M Bright. «Solcast: Validation of a satellite-derived solar irradiance dataset». En: *Solar Energy* 189 (2019), págs. 435-449. ISSN: 0038-092X. DOI: 10.1016/j.solener.2019.07.086.

[69] M.C. Bueso y col. «A characterization of metrics for comparing satellite-based and ground-measured global horizontal irradiance data: A principal component analysis application». En: *Sustainability (Switzerland)* 12.6 (2020). ISSN: 20711050. DOI: 10.3390/su12062454.

[70] Utpal Kumar Das y col. «Forecasting of photovoltaic power generation and model optimization: A review». En: *Renewable and Sustainable Energy Reviews* 81 (2018), págs. 912-928. ISSN: 1364-0321. DOI: 10.1016/j.rser.2017.08.017.

[71] Foad H Gandoman, Fatima Raeisi y Abdollah Ahmadi. «A literature review on estimating of PV–array hourly power under cloudy weather conditions». En: *Renewable and Sustainable Energy Reviews* 63 (2016), págs. 579-592. ISSN: 1364-0321. DOI: 10.1016/j.rser.2016.05.027.

[72] S Hamid Oudjana, A Hellal e I Hadj Mahamed. «Short term photovoltaic power generation forecasting using neural network». En: *2012 11th International Conference on Environment and Electrical Engineering*. 2012, págs. 706-711.

[73] Changsong Chen y col. «Online 24–h solar power forecasting based on weather type classification using artificial neural network». En: *Solar Energy* 85.11 (2011), págs. 2856-2870. ISSN: 0038-092X. DOI: 10.1016/j.solener.2011.08.027.

[74] M Rana, I Koprinska y V G Agelidis. «Forecasting solar power generated by grid connected PV systems using ensembles of neural networks». En: *2015 International Joint Conference on Neural Networks (IJCNN)*. 2015, págs. 1-8.

[75] Yinghao Chu y col. «Short-term reforecasting of power output from a 48 MWe solar PV plant». En: *Solar Energy* 112 (2015), págs. 68-77. ISSN: 0038-092X. DOI: 10.1016/j.solener.2014.11.017.

[76] Luyao Liu y col. «Forecasting Power Output of Photovoltaic System Using a BP Network Method». En: *Energy Procedia* 142 (2017), págs. 780-786. ISSN: 1876-6102. DOI: 10.1016/j.egypro.2017.12.126.

[77] G M d. Paiva y col. «Intra-day forecasting of building-integrated PV systems for power systems operation using ANN ensemble». En: *2019 IEEE Milan PowerTech*. 2019, págs. 1-5.

[78] Muhammad Naveed Akhter y col. «Review on forecasting of photovoltaic power generation based on machine learning and metaheuristic techniques». En: *IET Renewable Power Generation* 13.7 (mayo de 2019), 1009-1023(14).

[79] Manoja Kumar Behera, Irani Majumder y Niranjan Nayak. «Solar photovoltaic power forecasting using optimized modified extreme learning machine technique». En: *Engineering Science and Technology, an International Journal* 21.3 (2018), págs. 428-438. ISSN: 2215-0986. DOI: https://doi.org/10.1016/j.jestch.2018.04.013. URL: http://www.sciencedirect.com/science/article/pii/S2215098617316063.

[80] Dazhi Yang y col. «History and trends in solar irradiance and PV power forecasting: A preliminary assessment and review using text mining». En: *Solar Energy* 168 (2018), págs. 60-101. ISSN: 0038-092X. DOI: 10.1016/j.solener.2017.11.023.

[81] Florian Barbieri, Sumedha Rajakaruna y Arindam Ghosh. «Very short-term photovoltaic power forecasting with cloud modeling: A review». En: *Renewable and Sustainable Energy Reviews* 75 (2017), págs. 242-263. ISSN: 1364-0321. DOI: 10.1016/j.rser.2016.10.068.

[82] D W van der Meer, J Widén y J Munkhammar. «Review on probabilistic forecasting of photovoltaic power production and electricity consumption». En: *Renewable and Sustainable Energy Reviews* 81 (2018), págs. 1484-1512. ISSN: 1364-0321. DOI: 10.1016/j.rser.2017.05.212.

[83] Amanpreet Kaur y col. «Benefits of solar forecasting for energy imbalance markets». En: *Renewable Energy* 86 (2016), págs. 819-830. ISSN: 0960–1481. DOI: 10.1016/j.renene.2015.09.011.

[84] C Yang, A A Thatte y L Xie. «Multitime-scale data-driven spatio-temporal forecast of photovoltaic generation». En: *IEEE Transactions on Sustainable Energy* 6.1 (2015), págs. 104-112. DOI: 10.1109/TSTE.2014.2359974.

[85] Romain Dambreville y col. «Very short term forecasting of the Global Horizontal Irradiance using a spatio–temporal autoregressive model». En: *Renewable Energy* 72 (2014), págs. 291-300. ISSN: 0960-1481. DOI: https://doi.org/10.1016/j.renene.2014.07.012.

[86] Christian A Gueymard. «A review of validation methodologies and statistical performance indicators for modeled solar radiation data: Towards a better bankability of solar projects». En: *Renewable and Sustainable Energy Reviews* 39 (2014), págs. 1024-1034. ISSN: 1364-0321. DOI: 10.1016/j.rser.2014.07.117.

[87] Kejun Wang, Xiaoxia Qi y Hongda Liu. «A comparison of day-ahead photovoltaic power forecasting models based on deep learning neural network». En: *Applied Energy* 251 (2019), pág. 113315. ISSN: 0306-2619. DOI: 10.1016/j.apenergy.2019.113315.

[88] E G Kardakos y col. «Application of time series and artificial neural network models in short-term forecasting of PV power generation». En: *2013 48th International Universities' Power Engineering Conference (UPEC)*. 2013, págs. 1-6.

[89] Y Huang y col. «Comparative study of power forecasting methods for PV stations». En: *2010 International Conference on Power System Technology*. 2010, págs. 1-6.

[90] L Gigoni y col. «Day-Ahead Hourly Forecasting of Power Generation From Photovoltaic Plants». En: *IEEE Transactions on Sustainable Energy* 9.2 (2018), págs. 831-842.

[91] G Chaojun y col. «Spatial Load Forecasting With Communication Failure Using Time-Forward Kriging». En: *IEEE Transactions on Power Systems* 29.6 (2014), págs. 2875-2882.

[92] *IEC 61724-1 Photovoltaic System Performance Monitoring-Guidelines for Measurement, Data Exchange, and Analysis (Part 1)*. Inf. téc. 1. Switzerland, Geneva: International Electrotechnical Commission (IEC), 2017.

[93] *LPWAN: redes de baja potencia para el IoT*. URL: https://lpwan.es/ (visitado 12-05-2021).

[94] Frank Kraemer y col. «Solar Energy Prediction for Constrained IoT Nodes Based on Public Weather Forecasts». En: oct. de 2017. DOI: 10.1145/3131542.3131544.

[95] J.E. Shuda, A.J. Rix y M.J. Booysen. «Towards Module-Level Performance and Health Monitoring of Solar PV Plants Using LoRa Wireless Sensor Networks». En: *2018 IEEE PES/IAS PowerAfrica*. IEEE, jun. de 2018, págs. 172-177. ISBN: 978-1-5386-4163-7. DOI: 10.1109/PowerAfrica.2018.8521179.

[96] Chang-Sic Choi y col. «LoRa based renewable energy monitoring system with open IoT platform». En: *2018 International Conference on Electronics, Information, and Communication (ICEIC)*. IEEE, ene. de 2018, págs. 1-2. DOI: 10.23919/ELINFOCOM.2018.8330550.

[97] S Daliento y col. «Monitoring, Diagnosis, and Power Forecasting for Photovoltaic Fields: A Review». En: *International Journal of Photoenergy* (2017), págs. 1-13. DOI: https://doi.org/10.1155/2017/1356851.

[98] J.M. Paredes-Parra y col. «PV module monitoring system based on low-cost solutions: Wireless raspberry application and assessment». En: *Energies* 11.11 (2018). ISSN: 19961073. DOI: 10.3390/en11113051.

[99] María C. Bueso y col. «Sensitive Parameter Analysis for Solar Irradiance Short-Term Forecasting: Application to LoRa-Based Monitoring Technology». En: *Sensors* 22.4 (feb. de 2022), pág. 1499. DOI: 10.3390/s22041499.

[100] C Wan y col. «Photovoltaic and solar power forecasting for smart grid energy management». En: *CSEE Journal of Power and Energy Systems* 1.4 (2015), págs. 38-46. DOI: 10.17775/CSEEJPES.2015.00046.

[101] A Moreno y col. «Validation of daily global solar irradiation images from MSG over Spain». En: *Renewable Energy* 60 (2013), págs. 332-342. ISSN: 0960-1481. DOI: 10.1016/j.renene.2013.05.019.

[102] Liwei Yang y col. «Nowcasting of surface solar irradiance using FengYun-4 satellite observations over China». En: *Remote Sensing* 11.17 (2019). ISSN: 2072-4292. DOI: 10.3390/rs11171984. URL: https://www.mdpi.com/2072-4292/11/17/1984.

[103] John Paparrizos y Luis Gravano. «K-Shape: Efficient and accurate clustering of time series». En: *Proceedings of the 2015 ACM SIGMOD International Conference on Management of Data*. SIGMOD '15. New York, NY, USA: Association for Computing Machinery, 2015, págs. 1855-1870. ISBN: 9781450327589. DOI: 10.1145/2723372.2737793. URL: https://doi.org/10.1145/2723372.2737793.

[104] A Molina-Garć y col. «Vertical wind profile characterization and identification of patterns based on a shape clustering algorithm». En: *IEEE Access* 7 (2019), págs. 30890-30904. ISSN: 2169-3536. DOI: 10.1109/ACCESS.2019.2902242.

[105] E Keogh y C A Ratanamahatana. «Exact indexing of dynamic time warping». En: *Knowledge and Information Systems* 7.33 (2005), págs. 358-386. DOI: 10.1007/s10115-004-0154-9.

[106] *Online viewer of the Agricultural Information System of Murcia*. 2019. URL: https://geoportal.imida.es/siam/.

[107] *European Union's Earth Observation Programme*. 2019. URL: https://www.copernicus.eu/.

[108] R Core Team, R Core Team y col. «R: A language and environment for statistical computing». En: (2021). URL: https://www.r-project.org/.

[109] Matt Dowle y Arun Srinivasan. *data.table: Extension of 'data.frame'*. 2019. URL: https://cran.r-project.org/package=data.table%20(accessed%20on%2030%20November%202021).

[110] Marvin N Wright y Andreas Ziegler. «ranger: A Fast Implementation of Random Forests for High Dimensional Data in C++ and R». En: *Journal of Statistical Software* 77.1 (2017), págs. 1-17. DOI: 10.18637/jss.v077.i01.

[111] Alexis Sardá-Espinosa. «Comparing time-series clustering algorithms in r using the dtwclust package». En: *R package vignette* 12 (2017), pág. 41.